Stable isotope fractionation during diamond growth and the Earth's deep carbon cycle

Sami Mikhail

Department of Earth Sciences

A thesis submitted to University College London for the degree of

Doctor of Philosophy

2011

I, Sami Mikhail, confirm that the work presented in this thesis is my own. Where information has been derived from other sources, I confirm that this has been indicated in the thesis.

Sami Mikhail

Date

I have chosen a quote from a living scientist to break the usual status quo. This is a quote from Dr Adrian P Jones (principal supervisor to this project) that was said to me during my interview for the privilege of being the student to undertake this project:

''I must state that this study could produce profound results, but it may be technically impossible to achieve. Therefore, should that be the case, we may have to think on our feet to quickly devise a project that can actually get you a PhD as well as being technically and logistically feasible''

Dr Adrian P Jones, October 2007

Disclaimer

Several of the studies in this thesis form parts of wider collaborative studies; therefore here I detail the contributions of other workers to the data presented in the following chapters.

Chapter 3:

The analysis of the standards and initial calibrations such as the bleed rate were performed by Dr Alexander B Verchovsky at the Open University.

Chapter 5:

The major and trace element data from the syngenetic garnets and sample selection for the stable isotope analysis was undertaken by Dr Chris B Smith (project leader), Dr Galina P Bulanova, Prof Mike Walter, Dr Simon Kohn (Department of Earth Sciences, University of Bristol, UK), Dr Luis Gobbo (Rio Tinto, Brasilia, Brazil) and the Edinburgh Ion Microprobe Facility (School of Geosciences, Grant Institute at the University of Edinburgh, UK). The major and trace element data from the silicates inclusions (garnet) are cited from an ongoing study in this chapter with permission and cited as Smith et al (In Prep 2011).

Chapter 7:

The samples in this chapter were received polished with major element data provided and cited from the published extended abstract of Jones et al (2008). The samples were classified as type II using infra red absorption spectroscopy by Dr H. J. Milledge (Research School of Earth Sciences, University College and Birkbeck London, Gower Street, London WC1E 6BT, UK). The operation of the Cameca 50L nanoSIMS was the responsibility of Drs C. Guillermier and I.A. Franchi (Planetary and Space Science Research Institute, the Open University, UK, Open University, Walton Hall, Milton Keynes, MK7 6AA, UK) with my assistance.

Chapter 8:

In this chapter two of the 4 experimental samples were synthesized at other institutes by my collaborators. Experiment AS1 was conducted by Dr Anat Shahar at the Geophysical Laboratory (Carnegie Institution of Washington, Broad Branch road, Washington DC, 20015, USA) and experiment CO#8 by Dr Simon A Hunt at the Mineral Physics Institute (Department of Geoscience, Stony Brook University, NY, USA, current address; Department of Earth Sciences, UCL, Gower Street, London, WC1E 6BT, UK). I have also been given access to unpublished and theoretically calculated equilibrium fractionation factors in the iron-carbon system to assist my endeavour. This was previously presented at the American Geophysical Union Fall Meeting, San Francisco, California, USA in 2009 and is cited as Schauble (2009) and personal communication 2011.

Abstract

The flux of carbon between the mantle and crustal reservoirs can have a large impact on the melting of mantle rocks, the long and short term stability of the climate, and the growth of a very precious mineral; diamond. Diamond can be as young as 200 Ma and as old as > 4000 Ma, which is most of Earth's entire 4500 Ma history and can also contain samples of the Earth's mantle over a depth range of > 600 km, from the base of the crust and into the lower mantle. This spatial and temporal sampling of the Earth is unrivalled; therefore the study of mantle diamond is the best way to place constraints on the geodynamic carbon cycle over geological time.

This study has used the stable isotopes of carbon and nitrogen in natural diamond of three groups and found that monocrystalline diamonds from Dachine, French Guyana have carbon and nitrogen isotopic compositions consistent with a crustal origin, inferring Phanerozoic type subduction > 2 Ga. The same is true for the source for the same isotopic systems in diamondites; however they appear to be evidence of mobilised subducted fluids that metasomatise primary mantle peridotites and induced melting and contemporaneous diamond formation. This study has also explored the potential effects of isotopic fractionation during diamond growth, y quantifying the magnitude and direction of carbon isotope fractionation between diamond and Fe-carbide in natural and experimental samples. This has shown that carbon isotope fractionation in the lower mantle should be larger than in the upper mantle, despite the higher temperatures.

The implications for this new data are discussed in light of terrestrial and extraterrestrial geodynamic carbon cycling.

Acknowledgements

There are a lot of people I am grateful to for helping me produce this thesis. I would like to start with Prof Peter J Treloar from Kingston University where I achieved my BSc Hons degree reading Geology. During a field trip at the start of my 3rd year in Santorini (Greece) and after several large brandies Peter said the following to me 'stop talking about a PhD, with your current grades you will get a 2.2 at the very most, you've not achieved your potential and probably never will, I wouldn't piss on you for a masters let alone a PhD', I replied and said 'I can get a 2.1 and I will do a PhD' he replied 'I have been teaching as long as you have been alive, I know what I am talking about, so prove me wrong'. I got a 2.1 honours degree and we are still friends.

I would like to direct my gratitude to those who have been on hand over the last 3.5 years. Firstly the Diamond Trading Company in the form of Drs Simon Lawson, Philip Martineau and Bob Caveney for making me feel welcome with the DeBeers 'family' of scientists, as well as for their child-like enthusiasm for geology, from the stance of solid state physicists.

The team at the OU, practically all of the stable isotope data in this thesis is from the OU- and this PhD uses stable isotope geochemistry as the tool to derive the conclusions. Dr Ian A Franchi is especially thanked for his ruthless approach to data acquisition, analysis and interpretation, which I share and have enjoyed his and the OU's support both scientifically and financially.

My supervisory team: Dr Adrian P Jones (principal supervisor) for his enthusiasm for carbon in general, trust in my ability and for supporting me to set up collaborations and conduct research on projects that I have devised (chapters 3-6). My subsidiary supervisor Stuart Robinson who has probably never seen a diamond before putting one on Jen's finger, but throughout the course of this PhD was on hand to answer any questions, provide assistance, review presentations and anything else I requested on demand as well as for being a good sport when being totally outclassed by me on the football pitch; this is greatly appreciated. Finally, no words can describe the gratitude I have to

Dr Sasha Verchovsky of the PSSRI, OU. Without Sasha's expertise in the field of stable isotope mass spectrometry and dedication to keeping the Finesse machine alive even coming in at 2 am after a balls up, this PhD would not have been possible.

Dr Galina Bulanova for supplying samples for this PhD and other projects that are currently in progress. As well as support and guidance throughout, as well as teaching me to polish diamonds. Dr Judith 'the diamond queen' Milledge for being a role model; good science and good drinking make for a happy life; 'nuff said about that really.

My family have always supported my love of rocks and without that support I'd be lost. My Mum for bailing me out whenever she could, my dad for teaching me that a degree is even better than a passport from a very young age and both for installing undoubting belief in myself. My Nan Rose 'super-gran' Douglas for housing me in her flat for the final 8 months for free! And for washing my cloths, ironing my shirts, making me packed lunches and hot dinners, and for being a good laugh and good company to watch any level of football any day (and WWII documentaries). And my brother for reasons only we both need to know. I am also lucky to have grown up the best mates ever (fact) who need not be named, but are seen to me as family and not as friends. I have also met some real characters at UCL, the OU, the Geophysical lab and at MANY meetings overseas during this time and they are also thanked.

Finally, Dr Claire Cousins (my woman) is thanked for being a mate and a party buddy over the last few years (even before we were together) and for reviewing the grammar, scientific arguments and grammar again in every chapter of this thesis in GODSPEED.

P.S. My examiners, Profs Hilary Downes (internal) and Monica M Grady (external) are thanked for a thorough and enjoyable viva.

Table of contents

List of figures

List of tables

Chapter 1

Synopsis

Carbon is the 4th most abundant element in the cosmos, yet it is found on the surface of the Earth as a trace element in terms of the bulk geochemistry. This means that the Earth has either lost a substantial amount of carbon at some stage, the Earth accreted from unusually C-poor solar system materials, or, that the bulk of the carbon is stored in the interior of the planet. Using geophysical and geochemical studies of the deep Earth and samples of the Earth's interior (mantle rocks), the latter is the agreed consensus (Deines, 2002). In the Earth's atmosphere, lithosphere and biosphere carbon forms fundamental atmospheric compounds which can affect global climate, and are essential in key biochemical reactions. Therefore it is an essential ingredient for a habitable environment (Hayes and Waldbauer, 2006). This means that understanding the cycles and fluxes within and between reservoirs, as well as the relative sizes of these reservoirs, is fundamental to understanding the future of our planets biosphere. When modelling carbon flux, the reservoir sizes and the input and output parameters are paramount. Arguably the most important geological flux for carbon is between the crust/atmosphere and silicate mantle, i.e. volcanism and subduction zone plate tectonics, which represent the total input and output of the atmospheric/crustal reservoirs (Dasgupta and Hirschmann, 2010).

To study these fluxes in the present, geoscientists use a variety of methods such as deep sea drilling to determine the amount of carbon sequenced by pelagic sediments in the oceans (i.e. Strasser et al., 2006), and by monitoring active volcanoes at different tectonic settings to measure and compare the volatile releases between arc and intra-plate oceanic volcanoes (Oppenheimer et al., 2010). However to study these fluxes in the past one must use geochemical studies of the rock record where samples permit. Some workers study basaltic samples to estimate the carbon concentration of the ambient upper mantle (Saal et al., 2002), and use this data to model the potential impact that

carbon degassing could have had on ancient mass extinction events, for example during short periods of large scale volcanic activity (Self et al., 2006). Others determine the isotopic compositions of volcanic gasses to estimate the fluxes of carbon between the mantle and crust/atmosphere system during subduction zone processes using mixing relationships and mass balance calculations, relative to other volatile systems such as argon, nitrogen and helium (Wallace, 2005). However, when considering the Pre-Cambrian and/or the deeper Earth, these methods fall short in providing credible information on the subject of volatile cycling and fluxing. This is where studies of mantle diamond can provide an unparalleled wealth of information for geochemists; by enabling them to probe trapped ancient volatiles and directly examine fluxing and cycling. The age of mantle diamond spans a time period of from 4000 to 200 Ma (Gurney et al., 2010), which is most of Earth's entire 4500 Ma history. Diamond can also contain samples of the Earth's mantle over a depth range of > 600 km, from the base of the crust to the lower mantle (Hayman et al., 2005). Mantle diamond commonly contains microscopic mineral inclusions that are akin to either a peridotite (normal mantle) or an eclogite (subducted oceanic crust). One can use the coupled systematics between the carbon and nitrogen stable isotope compositions of the diamonds themselves to address the origin of the carbon, and therefore study the cycling of important volatiles through geological time (Boyd and Pillinger, 1994). There are isotopic differences for peridotitic and eclogitic diamonds. In simple terms, the eclogitic diamonds can show isotopic ^{13}C depletion that is similar to pelagic organic carbon (Pearson et al., 2003).

To understand the stable isotope data acquired from natural mantle diamond there are two main sources of information that must be available to the isotope geochemist; a database with which to compare the measured values, and an understanding of stable isotope fractionation under mantle conditions. This thesis addresses both of these sources of information to understand the source of carbon which has formed diamond in the Earth's mantle.

I begin this thesis by introducing key concepts related to diamond formation in the mantle, such as the origins of terrestrial carbon, the speciation of carbon with depth, and a background on the formation of terrestrial mantle diamonds (chapter 2). I then provide a description of a novel, custom-built and fully automated analytical facility which can determine the carbon and nitrogen isotopes of very small samples (< 0.1 mg) with lower nitrogen concentrations than previously possibly (chapter 3). This is followed by a demonstration of the accuracy and precision for the determination of the coupled carbon and nitrogen isotopes, using natural samples of diamond that have very low nitrogen concentrations (chapter 4). These diamonds with low nitrogen concentrations form a comparative data set to the isotopically unique samples in chapter 5; because no comparable data exists in the literature owing to the extremely low nitrogen concentrations for both sample sets. I then use the coupled carbon and nitrogen isotope values of the diamond to constrain the origin of the diamond-forming carbon for two diamond populations which both have anomalous ^{13}C concentrations. The first has no statistical value representative of the average mean mantle and overlaps almost entirely with crustal organic carbon, contrary to most mantle diamond populations (chapter 5). The second diamond samples contain intergrown silicates representative of peridotite, but exhibit ^{13}C depletion more commonly seen in eclogite, contrary to peridotitic diamond populations globally (chapter 6). These studies are followed up by expanding the understanding of stable isotope fractionation under mantle conditions by determining the isotopic fractionation factors in a newly quantified natural system, diamond coexisting with iron carbide. This is achieved using two extremely rare natural diamond samples from South Africa (chapter 7). I then test for the temperature and pressure dependence of isotopic fractionation in this system by using high pressure and high temperature experiments which simulate mantle conditions (chapter 8).

The thesis is concluded by a broad discussion which this new data can provide to current views on mantle geodynamics, volatile cycling through time, the mantle carbon cycle in the uppermost Martian mantle, the role of carbon during large-scale volcanism (and its potential relation to mass extinction events) and to the relative mass proportions between the likely major interior carbon

reservoirs in the Earth, the mantle and core (chapter 9). This chapter also identifies potential further research which will be required in order to answer the scientific questions that have been raised by the work presented here, but are beyond the scope of this thesis.

Chapter 2

An introduction to diamond-forming carbon in the terrestrial mantle

Nomenclature

Within this thesis, the term "mantle carbon" refers to carbon from the mantle without having been involved in crustal processes, i.e. indigenous mantle carbon. The term crustal carbon shall be used to refer to carbon that has been out-gassed from the mantle into the hydrosphere, biosphere and atmosphere, and re-deposited into the lithosphere. Once this out-gassed carbon has been recycled back into the mantle via subduction zone tectonics, it becomes relevant to this thesis. So before discussing the stable isotope geochemistry of mantle diamond and the distribution and speciation of carbon in the terrestrial mantle, I must first outline the origin of terrestrial carbon.

2.1 Formation of the Earth and primordial carbon

In the beginning there was a proto-planetary disk surrounding a young Sun. This was made up of residual gas from the formation of the Sun which began to condense, forming proto-planetary dust (i.e. calcium-aluminium Inclusions) < 4,568 Ma (BOUVIER and WADHWA, 2010). Eventually, these accreted to form the chondritic meteorites (ALEXANDER et al., 2008), which themselves accreted to form planetesimals, that in turn formed proto-planets and so on, until a stratified solar system with rocky interior planets and gaseous outer planets existed (WOOD et al., 2006). In between the gaseous and rocky planets resides an orbiting array of planetesimals that either failed to form planets or are the result of two proto-planets destroying each other through low angle collisions.

This raises the question; what is the definition of primordial in geochemistry? Primordial means *existing at or from the beginning of time*. For the context of this thesis, the beginning of time is regarded as the formation of the solar system, therefore in the field of mantle geochemistry this means upon the Earth's accretion. It is impossible for chondritic material within the Earth to have not melted since the Earth's formation, either during accretion itself or via incubation in the terrestrial magma ocean at temperatures between 2000 and 3000 °C (LEE et al., 2010). The only exception to this would be pure carbon, diamond and graphite at temperatures > 50,000 K and > pressures >1.1 TPa (Eggert et al., 2010). However, there are no diamonds with inclusions older than the Earth (Gurney et al., 2010), therefore as feasible as the existence of mantle diamonds older than the Earth may be in the physical sense, this notion is not considered here. Therefore, the actual primordial chondritic material is homogenised through melting and mixing via mantle thermo-chemical convection (JACKSON et al., 2011; PEARSON et al., 2003). However, there is another use of the term primordial in mantle geochemistry: isotopic primordiality. If one observes an isotope ratio that is chondritic in mantle-derived samples, it can be called primordial. This is not to say that the material has remained static through time in the physical sense, but it can be assumed that the isotopic ratio has remained as it was pre-accretion (CARTIGNY et al., 1997; JAVOY et al., 1986; RUMBLE et al., 2011).

To identify the primordial carbon isotope composition of the Earth one must first identify the building blocks of the bulk Earth. There are differing models as to what chondrite group formed the bulk Earth and therefore provided the bulk of the carbon. Some workers invoke enstatite chondrites using stable isotope constraints (JAVOY et al., 2009) and other workers invoke carbonaceous chondrites based on the relative abundances of major and trace elements (MCDONOUGH and SUN, 1995). Some models propose a late veneer dominated by carbonaceous chondrites to explain the siderophile enrichment of the mantle with the bulk Earth being made of chondrites (HOLZHEID et al., 2000). Some also propose a late veneer, but suggest that enstatite chondrites make up the bulk of the planet (JAVOY, 1995). There are strong arguments for both, but regarding the primordial isotopic

composition of carbon, both chondritic groups can explain the mean mantle $\delta^{13}C$ value of -5 ± 3 ‰ (DEINES and WICKMAN, 1985; GRADY and WRIGHT, 2003). The $\Delta^{13}C$ for the mantle and chondrites is effectively 0 ‰, because the bulk $\delta^{13}C$ values for both chondrite classes mention is around -5 ‰ (GRADY and WRIGHT, 2003), where $\Delta^{13}C$ is the mean $\delta^{13}C$ value for the bulk silicate earth - the mean $\delta^{13}C$ value for chondrites. This is contrary to some other systems; for example there is a $\Delta^{56}Fe$ and $\Delta^{30}Si$ for Earth vs. chondrites. They can be explained by isotopic fractionation during the Moon-forming impact for Fe and core formation for Si (for a discussion see RUMBLE et al., 2011). Therefore it can be stated that the observed modal $\delta^{13}C$ value of -5 ‰ is primordial in composition and has not been significantly fractionated during the Moon-forming impact, core formation, crustal growth or formation of the atmosphere; in the simplest sense. This observation is imperative to the scope of the research presented in chapters 4, 5, 6, 7 and 8. The next questions to address are what and where are the terrestrial deep carbon reservoirs? And what are their sizes?

2.2 Terrestrial deep carbon reservoirs

The late Professor Victor Goldschmidt first classified carbon as an atmophile element, being depleted in the silicate proportion of the Earth relative to the gaseous atmosphere, due to carbon being a volatile element (GOLDSCHMIDT, 1954). But in fact, carbon can also be described as a siderophile element. Carbon readily dissolves into iron liquids and forms carbides and iron alloys, such as industrial steel and cementite (LORD et al., 2009). However, if one was so inclined, carbon could also be described as a lithophile element. Carbon forms stable rock forming carbonate minerals in the crust that in turn form massive sedimentary beds such as limestone and chalk (MACKENZIE and MORSE, 1992) and mantle carbonates such as carbonatites (STAGNO and FROST, 2011). Carbon is also fundamental is biochemistry, forming the basis of organic compounds that sustain life though fuel (food) and the building block of life itself, (amino acids). In short, carbon can and does exist on Earth in every environment, under all pressure, temperature and redox conditions (figure

2.1). This figure outlines the main sub-sections of the mantle, however one can think of them collectively as 3 main regions, crustal (lithosphere), mantle (cratonic lithospheric mantle to D'') and the core (inner and outer). The dashed line at circa 250 km is taken from Rohrbach et al (2007). This illustrates the transition in the redox state of the mantle from relatively oxidising (carbonate stable) to relatively reducing (methane stable), this is discussed in full from section 2.3 to 2.4. D'' refers to the core mantle boundary layer made of a mix of Mg-Si perovskite and Mg-Si post-perovskite (MURAKAMI et al., 2004; OGANOV and ONO, 2004). The figure illustrates that carbon phases are either known to be stable (depths < 660 km) or predicted to be stable and expected to be present (depths > 660 km) in the Earth. For discussions regarding the speciation of carbon in the mantle during subduction of pelagic carbonate see Rohrbach and Schmidt (2011), carbon in the core see Nakajima et al., (2009), the occurrence of diamond see Stachel et al., (2005), mantle fluid speciation see Stagno and Frost (2011) and for the crustal carbon system in the biosphere through time see Horita (2005), for the sedimentary carbon cycle in the pre-Cambrian see Shields and Veizer (2002), for the sedimentary carbon cycle in the Phanerozoic see Mackenzie and Morse (1992) and for the lithospheric and atmospheric carbon cycle in general see Hayes and Waldbauer (2006).

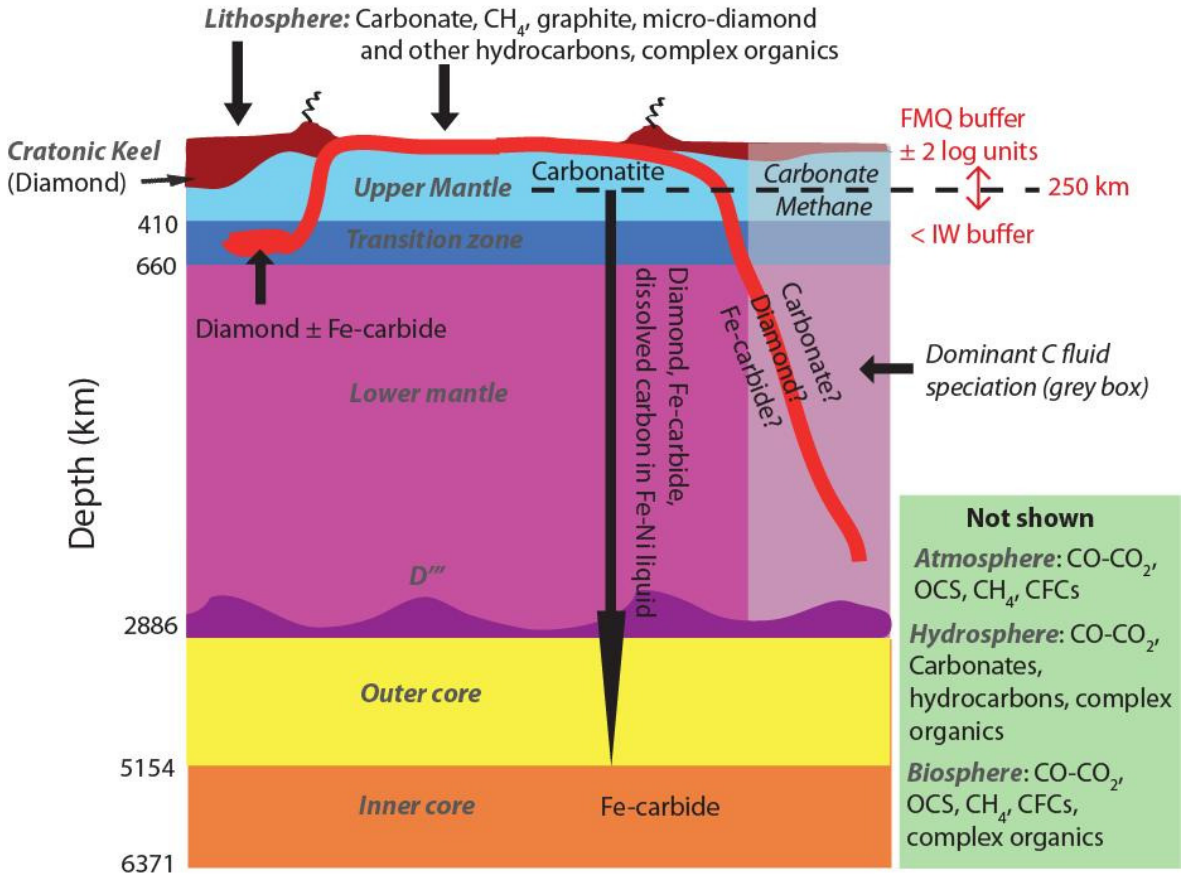

Figure 2.1. This cartoon details both the known and hypothetical deep carbon reservoirs with no estimates of mass or relative proportions. Italics in grey bold font are used for terrestrial layers and black text is for carbon species and depth and the redox state is in red text.

The sizes of these deep terrestrial reservoirs are poorly constrained. Estimates vary across several orders of magnitude using empirical data from MORB, OIB and mantle xenoliths analyses (DEINES, 2002). However there is a consensus that of the three main reservoirs, the crustal system is the smallest (see DASGUPTA and HIRSCHMANN, 2010 for a discussion). Most studies based on geophysical constraints (experimental petrology and theoretical thermodynamics) predict that the core is the largest reservoir of carbon (DASGUPTA and HIRSCHMANN, 2010; DASGUPTA and WALKER, 2008; LORD et al., 2009; NAKAJIMA et al., 2009; VOCADLO and GERALD, 2007; WOOD, 1993), but the ratio between the mantle and core or the sizes of either reservoir are not constrained (DASGUPTA and HIRSCHMANN, 2010). This topic is addressed in the discussion section of chapter 8 using new data from natural

(chapter 7) and experimental (chapter 8) samples that place an isotopic constraint to this problem for the first time.

2.3 Mantle redox conditions

Unlike the silicate minerals, carbon speciation is primarily controlled by the redox state of the environment (shown in brief in figure 2.1), even more so than the direct effects of pressure and temperature (STAGNO and FROST, 2011). However, the redox state of the ambient pyrolitic mantle is directly influenced by pressure and temperature (FROST and MCCAMMON, 2008; MCCAMMON, 2005; WADE and WOOD, 2005; WOOD et al., 2006). In the field of mantle geochemistry and petrology the mantle redox state is expressed as the oxygen fugacity, which is expressed on a log scale relative to a buffer reaction defining the stable assemblage (figure 2.2). Oxygen fugacity (fO_2) is a thermodynamic constraint that describes the measure of available oxygen to react in a given system. The fO_2 of the bulk silicate Earth (BSE) is buffered by reactions that are referred to as redox buffers. These are reactions (assemblages of phases) that control the oxygen fugacity as a function of temperature (figure 2.2).

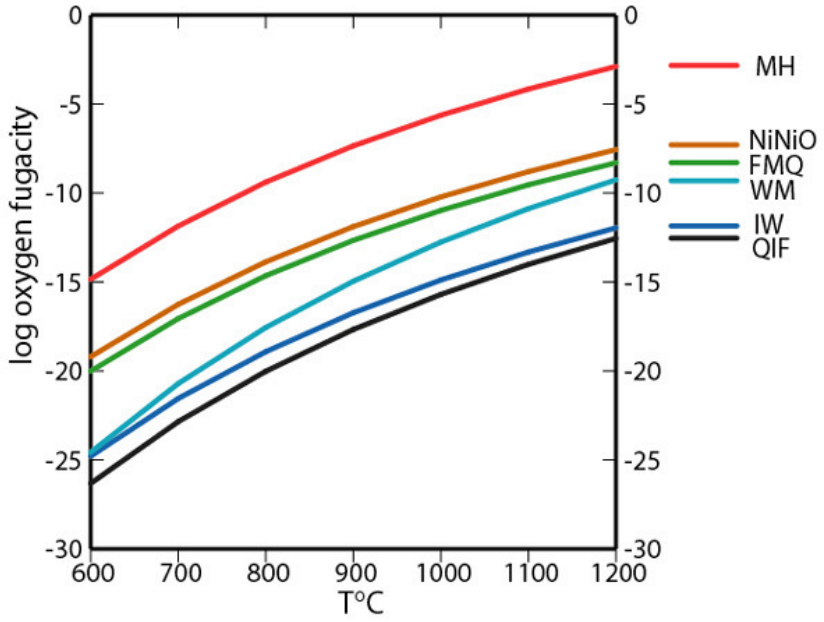

Figure 2.2 Log oxygen fugacity vs. temperature (for 0.0001 GPa) for common buffer assemblages and expressed using algorithms compiled by Frost (1991). Where MH, magnetite-hematite; NiNiO, Nickel-nickel oxide; FMQ, fayalite-magnetite-quartz; WM, wustite-magnetite; IW, iron-wustite; QIF, quartz-iron-fayalite.

This requires an understanding of the redox state of the mantle as a function of depth to be a constrained parameter in order to understand the speciation of carbon throughout the deep Earth and during subduction of carbon into the mantle. The redox state for both the upper mantle and the deeper Earth is described below.

2.3.1 Upper mantle

The magnitude of variation for the uppermost mantle redox state is based on samples from the upper mantle in arc, rift and hotspot tectonic settings. They yield a near constant range for the 'uppermost mantle' (herein referred to as the 'volcanic sampling field') where the fO_2 is buffered in by the reaction Fayalite-magnetite-quartz (FMQ) ± 2 (log units) and is consistent through time. This

range is mostly based on the $Fe^{3+}/\sum Fe$ system (reviewed by FROST and MCCAMMON, 2008; and shown in figure 2.3).

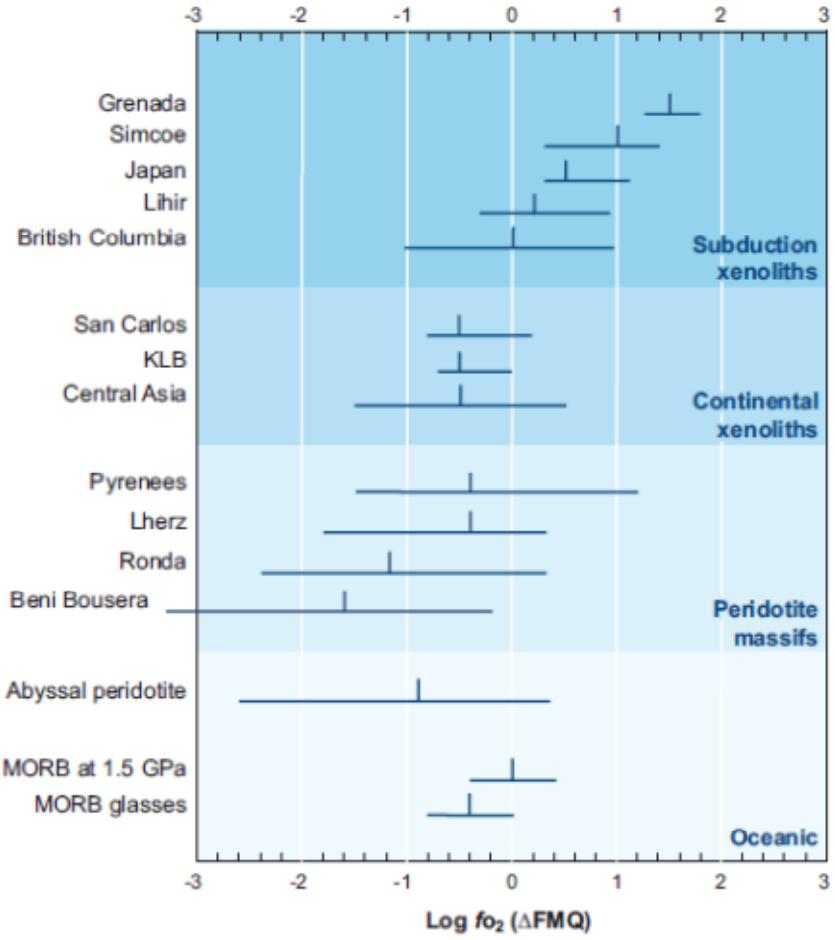

Figure 2.3 The Log fO_2 relative to FMQ for samples of mantle origin. This figure demonstrates the range for the typical volcanic sampling field of 0 ± 2 Log units relative to FMQ using the $Fe^{3+}/\sum Fe$ redox indicator system from silicate mineral separates (from FROST and MCCAMMON, 2008).

2.3.2 The deeper Earth

The depth of our understanding for the mantle fO_2 as a function of depth is restricted to the depth of volcanic sampling. This leads to the question of the greater relationship between fO_2 and depth regarding the 'poorly sampled' (transition zone and uppermost lower mantle) and the 'un-sampled' Earth (~70 % of the lower mantle; > 700 km depth) as a function of increasing temperature and also

pressure. Spinel peridotites originating closer to the asthenosphere have lower fO_2 values than their shallower counterparts (FROST et al., 2004; FROST et al., 2008; FROST and MCCAMMON, 2008). This trend for decreasing fO_2 with increasing depth is also reflected in garnet peridotites, which are attributed to the effect of pressure on the controlling Fe^{3+}/Fe^{2+} equilibria in garnets (FROST and MCCAMMON, 2008 and shown in figure 2.4).

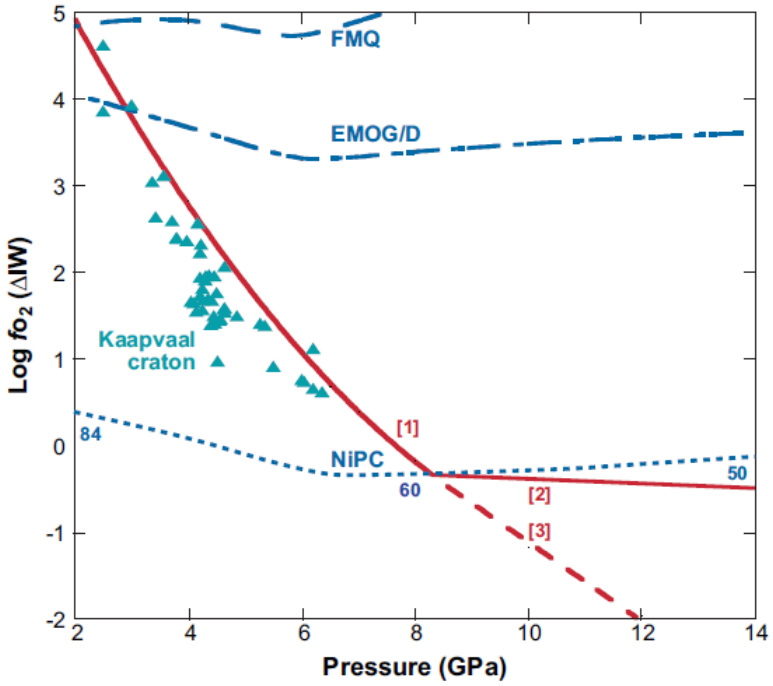

Figure 2.4 Oxygen of a four phase garnet peridotite assemblage as a function of pressure from Frost and McCammon (2008). The fO_2 is shown relative to the iron-wustite (IW) buffer, along a cratonic geotherm (red line [1]). Blue triangles shows the fO_2 calculated for xenoliths from the Kaapvaal craton for comparison. The dashed line marked `NiPC' is the nickel precipitation curve, below which Ni metal will precipitate from olivine. Red line [2] shows the fO_2 of the garnet peridotite after it begins to exsolve Ni-Fe metal. EMOG/D is the reaction Enstatite + Magnesite = Olivine + Graphite/Diamond + O_2 (LUTH, 1993), which controls the stability of diamond versus carbonate under more oxidizing conditions. The Fayalite = Magnetite + Quartz buffer is also shown for reference, marked FMQ.

Below the volcanic sampling field there are only thermodynamic models available to determine the fO_2. Frost et al. (2004) provided experimental evidence for the stability of Fe^0 with magnesium silicate perovskite (Mg-pv) and ferropericlase (Fp) in the Earth's lower mantle which led to the notion of a relative shift in fO_2 between the upper mantle to lower mantle, where the conditions become vastly more reducing across the 660 km seismic discontinuity. This has been tested at lower pressures and more recently (Rohrbach et al 2007; 2010). These studies demonstrated that from depths as shallow as 250 km, the upper mantle can also host stable Fe^0 with subcalcic pyroxene and majoritic garnet. This would mean that any assumptions for the fO_2 of the entire upper mantle using the $Fe^{3+}/\sum Fe$ system are incorrect. It would merely mean that the uppermost part of the planet, the volcanic sampling field, is an anomalously oxidising environment.

According to recent models based on experimental constraints (ROHRBACH et al., 2010; STAGNO and FROST, 2011), the majority of the BSE should be buffered below iron-iron wustite (IW) by the co-existence of Fe^0 in equilibrium with mantle silicates (circa >250 km). The importance of these works for this thesis is that the existence of Fe^0 in the deep Earth could have significant effects on the speciation of carbon and is considered herein. But first I shall outline the speciation of carbon in the mantle as a function of the pressure, temperature and fO_2.

2.4 Carbon speciation in the mantle

Carbon exists in the mantle as both solid state phases such as diamond, and fluid phases such as C-O-H-N fluids (NAVON et al., 1988). The term *fluid* is not adequately defined in the literature; some studies use it to describe volatiles in the system C-O-H-S-N (NAVON et al., 1988); while others include all non-solid phases such as carbonates and dissolved oxides (PEARSON et al., 2003). One reason for this is that at high pressure water-rich fluids and hydrous-silicate melts show increasing convergence toward the second critical end point, where the univariant melting curve ends in a divariant field. In

this thesis, I have used the definition from Tomlinson (2005), where a fluid is defined as being a liquid phase consisting chiefly of volatiles, with some dissolved solutes (oxides, halides, sulfates, nitrates, and carbonates).

2.4.1 Fluid speciation

The speciation of mantle fluids both controls, and is controlled by, the mantle fO_2 (FROST and MCCAMMON, 2008). This may sound oxymoronic, but simply reflects that the systems are coupled. In the simplest of senses; if one observes the carbon-carbon dioxide reaction (CCO), which is $C + O_2 \leftrightarrow CO_2$ then it can be stated that carbon can be stable as C^0 (Gr-Dia) in the presence of O_2 through the reduction of CO_2, therefore the reduction of CO_2 can form diamond (LUTH, 1993). In the reverse, diamond can be oxidised to CO_2 in the mantle, this can have dramatic effects for deep mantle melting because CO_2 can lowers the solidus of mantle peridotite to below the ambient geotherm (for a discussion see DASGUPTA and HIRSCHMANN, 2010). So it can also be stated that C^0 can buffer the fO_2 by removing oxygen from the system (BLUNDY et al., 1991). In the ambient pyrolitic mantle (shown in figure 2.5), the dominant fluids that are stable in equilibrium with Gr-Dia are as follows; $H_2O > CO_2$ at depths above 250 km and $CH_4 > H_2O$ at depths below 250 km (FROST et al., 2004; ROHRBACH et al., 2007).

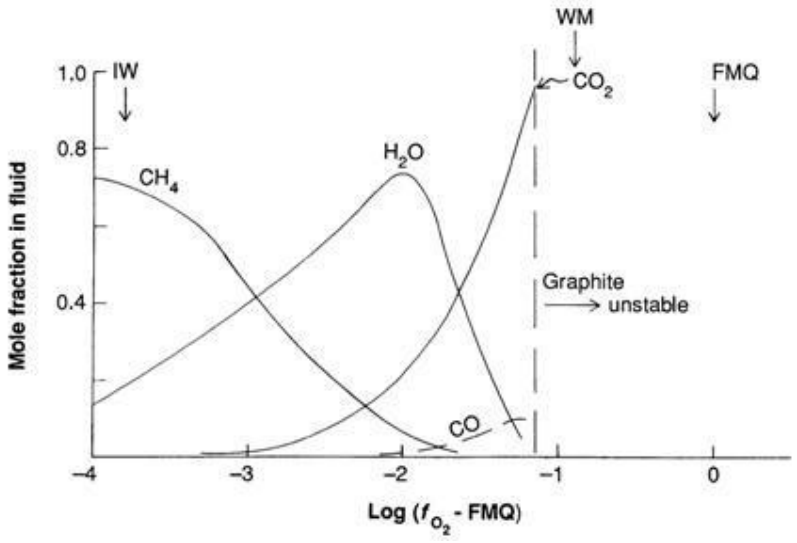

Figure 2.5. The relative proportions of the dominant mantle fluids in equilibrium with graphite at 1 GPa as a function of the fO_2 (from WOOD et al., 1990). It is worth stating that this relationship is consistent at pressures up to 30 GPa and under mantle temperature regimes of 1100-1600 °C (FROST and MCCAMMON, 2008); illustrating the dependence of carbon speciation of fO_2. The following buffering reactions are also shown; IW refers to Iron-Iron Wustite ($Fe^0 + {}^1/_2O_2 \leftrightarrow FeO$), WM refers to Wustite-Magnesite ($3FeO + {}^1/_2O_2 \leftrightarrow Fe_3O_4$) and FMQ refers to Fayalite-magnesite-quartz ($3Fe_2SiO_4 + O_2 \leftrightarrow 2Fe_2O_3 + 3SiO_2$).

2.4.2 Solids speciation

The speciation of solid carbon in the ambient pyrolitic mantle is summarised in figure 2.6 as a function of pressure and temperature and therefore depth. The dominance of carbonates, such as carbonatites, in the volcanic sampling field is restricted to the shallowest parts of the mantle (STAGNO and FROST, 2011). Whereas the overall dominant solid phase of carbon in the BSE should be as reduced phases; namely diamond and iron carbide based on the fO_2 constraints (this is the focus of chapters 7 and 8). The next topic to review is the geochemical information about the mantle carbon cycle that can be derived from studies of mantle diamonds, but first I must discuss the formation and distribution of diamond, potentially the most abundant terrestrial carbon reservoir.

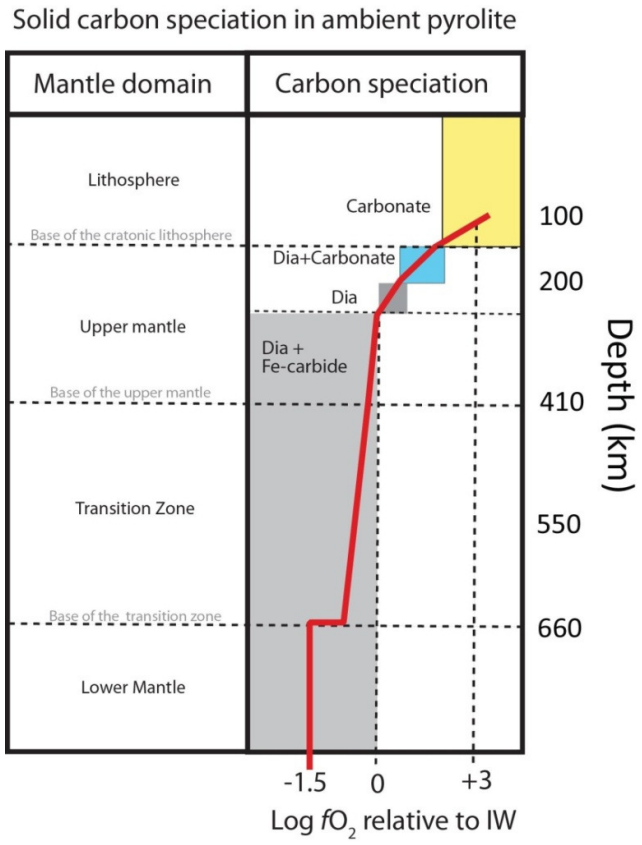

Figure 2.6 The speciation of solid carbon as a function of the fO_2 with depth in an ambient pyrolitic mantle (modified from ROHRBACH and SCHMIDT, 2011; and using data from STAGNO and FROST, 2011). Note the dominance in the terrestrial mantle for reduced carbon species relative to carbonate.

2.5 Mantle diamond

Diamond is a cubic form of carbon that typically contains trace amounts of nitrogen as a lattice-bound impurity; it is effectively a mono-elemental mineral. It is the first high pressure polymorph of graphite before lonsdaleite (BRETT and HIGGINS, 1969; HARLOW and DAVIES, 2005). Diamond is one of the hardest materials known with a Moh's hardness of 10, the hardest naturally occurring mineral (HARLOW and DAVIES, 2005). It is also one of the best thermal conductors known with a conductivity of 5 to 25 watts centimeter^{-1} °C^{-1} at 300K, which is 4 times greater than copper (HARLOW and DAVIES, 2005). It is a mineral that may receive a long string of superlatives to describe its physical and

gemmological properties, as well as the commercial importance diamond has to several economies and industries around the world (HARLOW and DAVIES, 2005).

From a geological point of view, the above properties are somewhat trivial. What is more important is the information about the Earth and its interior that can be derived by the petrological and geochemical study of mantle diamonds and their associated inclusions. This information covers a large range of geosciences, such as our understanding of crustal formation events and craton evolution (SHIREY et al., 2003), the onset of plate tectonics (SHIREY and RICHARDSON, 2011), the cycling of carbon during subduction (WALTER et al., 2008) and physical exchange of material between the upper and lower mantle thus demonstrating, possibly only on a local scale, whole mantle convective processes (SCOTT-SMITH et al., 1984). Mantle diamonds have been observed in minerals older than 4000 Ma (MENNEKEN et al., 2007) and can contain material as young as < 200 Ma (BULANOVA et al., 2010); this age range is only ~ 700 Ma short of Earth's entire 4500 Ma history. Diamonds can contain samples of the Earth from the upper to the otherwise inaccessible transition zone and lower mantle (the latter two referred to as sublithospheric diamonds; see HAYMAN et al., 2005) as well as trapping fluid inclusions that enable direct sampling of mantle metasomatic agents (TOMLINSON, 2005). One can also use coupled systematics between the carbon and nitrogen isotope compositions of the diamonds themselves to address the origin of the carbon, and therefore study the cycling of important atmospheric volatiles through geological time (BOYD and PILLINGER, 1994). Geochemical information from their associated (and syngenetic) silicate inclusions can enable the diamonds to be used as tracers of the interactions (or lack of) between the mantle and the crustal carbon reservoirs through time via plate tectonic processes (the scope of chapters 4, 5 and 6). Alternatively one can use the carbon isotope compositions of the diamond and rare syngenetic carbon-bearing inclusions to constrain the degree of isotopic fractionation in a system. This information to place constraints on the relative sizes of the terrestrial carbon reservoirs using isotopic mass balance calculations can also apply to other sampled celestial bodies, such as Mars (the scope of chapter 8).

Before briefly divulging into a review of relevant information for this thesis in the scientific literature, I must first address where on Earth are diamonds primarily sourced and where in Earth are they formed?

2.5.1 Diamond formation in the terrestrial mantle

The vast majority of known mantle diamonds have their origins in the cratonic lithosphere, which has roots that extend into the diamond stability field, roughly below 140 km (GURNEY et al., 2010). One reason for this is due to the cratonic keel acting as a reduced and cold diamond-forming 'sponge' (HAGGERTY, 1986). As has been outlined in section 2.4, the ambient upper mantle is too oxidising for diamond to be a stable phase, carbonates should dominate (STAGNO and FROST, 2011). However, the cratonic keel is colder and more reducing than the ambient mantle and thus provides the conditions appropriate for diamond formation (figure 2.7). Regarding sublithospheric diamonds, one model proposed it that the diamonds form in and around subducted oceanic crust that has buckled in the transition zone to form a megalith (for a review see STACHEL et al., 2005), this model is consistent with the eclogitic paragenesis of sublithospheric diamonds (BULANOVA et al., 2010; KAMINSKY et al., 2009; STACHEL et al., 2005; TAPPERT, 2005; TAPPERT et al., 2009; 2005; WALTER et al., 2008). However, because of the fO_2 in the ambient mantle < 250 km being below the IW buffer (ROHRBACH et al., 2007), one would expect diamond in the ambient mantle and a subducted megalith is not required to explain the occurrence of sublithospheric diamonds.

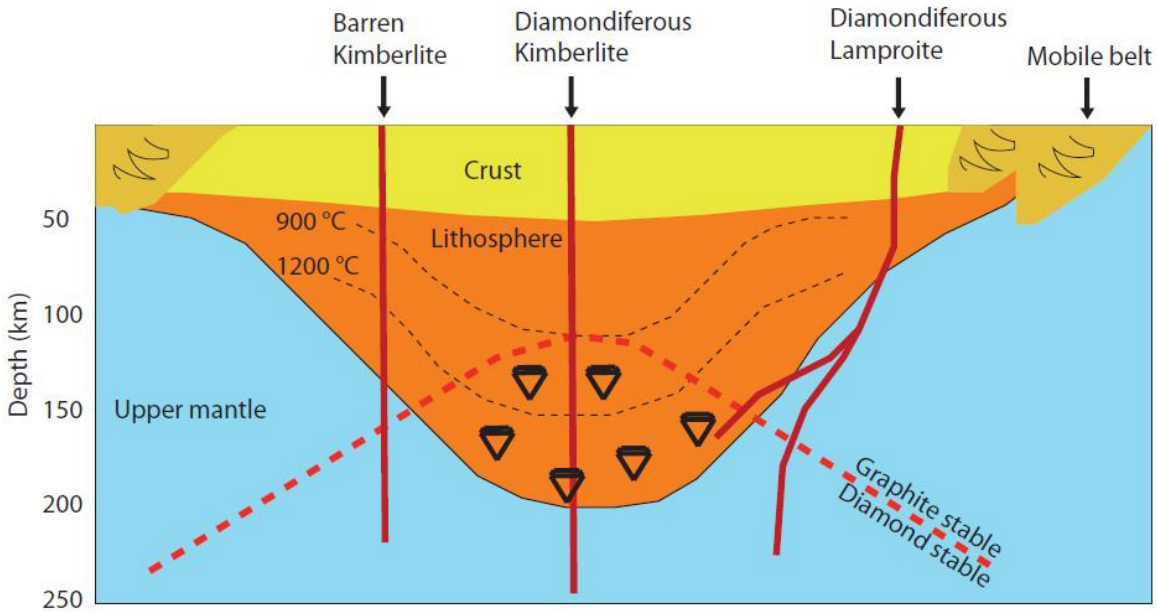

Figure 2.7 A schematic cross section of a sub-continental, sub-cratonic keel showing the diamond-graphite inversion curve (dashed red line). This is convex due to the concave isotherms (black dashed lines) through the craton relative to the ambient mantle, enabling diamond to be stable in the reducing cratonic keel(modified from HAGGERTY, 1986). The barren kimberlite can source material from the same depths as a diamondiferous kimberlite, but if it does not pass through the diamondiferous base of the keel, one will only find carbonated mantle xenoliths and not diamond (PEARSON et al., 2003).

The generally accepted model is that the cratonic keel was created in the Archean, at around 3200 - 3300 Ma, by high degree melting of mantle lherzolite, forming harzburgite (SHIREY et al., 2002). This coincided with diamond growth from indigenous mantle carbon forming peridotitic diamonds (SHIREY and RICHARDSON, 2011). Also subsequent subduction of basaltic oceanic crust resulted in some portions adhering to the base of the continental keel; this explains the eclogites (SHIREY and RICHARDSON, 2011). It is argued that the subducting slab provided the source of some diamond-forming carbon based on the carbon isotope values (KIRKLEY et al., 1991a; 1991b). More recently (between 50 and 1600 Ma), heating and/or fluid infiltration of the keel caused kimberlite (and related lamproite) melts to form and ascend to the surface carrying mantle xenoliths and xenocrysts, including diamond (HAGGERTY, 1999). These magmas are outlined below.

2.5.2 Primary sources of mantle diamond

Primary diamond source rocks are volcanic and exclusively located on stable and ancient cratons (figure 2.8). These melts must be generated deep enough to pick up diamond (> 140 km) and transport them to the surface fast enough to inhibit retrograde reactions to occur (diamond ↔ graphite). These volcanic rocks are from two groups of highly volatile-rich magmas called kimberlites and lamproite (SMITH and SKINNER, 1984; SMITH, 1983).

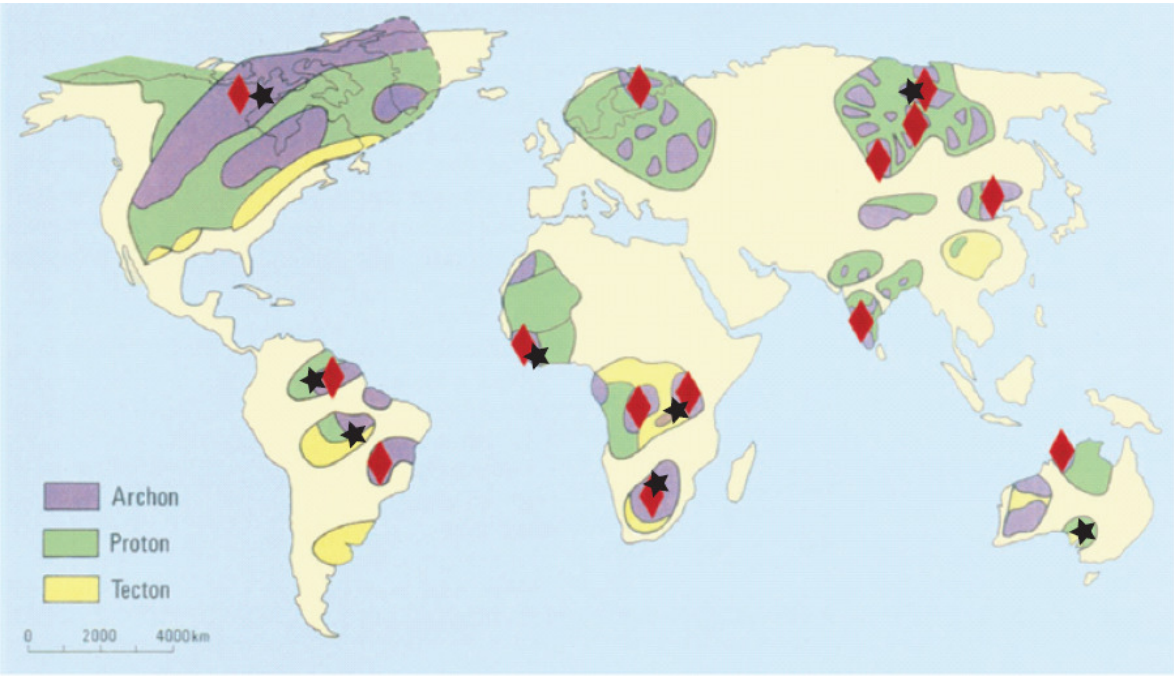

Figure 2.8 The geographical distribution of primary diamond deposits (HAGGERTY, 1999). Note the relationship to cratonic lithosphere. The red diamonds represent cratonic (upper mantle) diamonds and the black stars represent deep (sublithospheric) diamonds (MCCAMMON, 2001).

(a) Kimberlite

Kimberlite is the most important diamond-bearing source rock. Kimberlite is a volatile-rich potassic silica undersaturated ultramafic igneous rock, and is a hybrid of magma, xenocrysts and xenoliths (BEST, 2003). Smith (1983) recognised two compositional groups based on chemistry and mineralogy: Group I (basaltic) contain ilmenite macrocrysts and lack groundmass phlogopite; they are CO_2-rich, have a low K/Ti ratio and lie within the OIB field on a Sr and Nd isotope plot. Group II (micaceous) kimberlites are more H_2O-rich, have a high K/Ti ratio and contain groundmass phlogopite and clinopyroxene, they fall within the 'enriched' quadrant on a Sr and Nd isotope plot (SMITH, 1983). Kimberlites occur in cratons and stable platforms; diamondiferous kimberlites are confined to Archean and Proterozoic cratons (HAGGERTY, 1986). Kimberlite is usually found in diatremes and often forms dykes and sills. The exact locations are often controlled by faults and kimberlite pipes often occur in clusters.

(b) Lamproite

Mantle diamonds are also mined from lamproite. Lamproite is an ultrapotassic, typically peralkaline mafic rock. Lamproites are characterized by the presence of forsterite, phlogopite, leucite, richterite, diopside and sanidine (PELL, 1998). They differ from kimberlites because they are richer in SiO_2 and contain groundmass glass and alkali feldspar (BEST, 2003). Lamproites commonly occur in dykes and flows but also in diatremes or pipes on cratonic margins. Diamonds are found in pyroclastic rocks within shallow maartype craters, while magmatic lamproites are generally barren (PELL, 1998). Most olivine lamproites are post-tectonic and occur close to the margins of Archean cratons, either within the craton or in adjacent accreted Proterozoic mobile belts (PELL, 1998) e.g. at Argyle, Western Australia.

(c) Diamonds from kimberlites and lamproites

There is no difference in the geochemistry, morphology or diamond grade of the diamonds or their associated inclusions that are transported to the surface by either of these volcanic rocks (GURNEY et al., 2010). These volcanic rocks can be viewed simply as a 'carrier' for the diamonds to be emplaced in the lithosphere as mantle xenocrysts (BOYD et al., 1994). The magma's ascent is fast, relative to conventional volcanism (basalt), and thus inhibit retrograde reactions to occur, because at temperatures akin to the crust and atmosphere (< 600 °C) diamond is a metastable phase (HAGGERTY, 1986). The kinetics of the retrograde reaction diamond → graphite, at low temperatures, is so slow that the DeBeers® slogan *'a diamond is forever'* is true for the timescales experienced by humanity as a species thus far and for the next few billion years.

2.6 Subdivisions of mantle diamonds

Within this thesis I present work on diamonds subdivided by different means. Mantle diamonds are commonly subdivided based on several different criterions; such as their morphology, paragenesis and the concentration and nature of lattice-bound impurities which are discussed below.

2.6.1 Diamond morphology

Terrestrial mantle-derived diamonds can be divided into three main morphological groups: polycrystalline, monocrystalline and the fluid-rich group termed 'coated or fibrous' diamonds (figure 2.9). The latter two groups have received the most attention with regard to petrological studies for the several reasons. Monocrystalline diamonds are the group to which gem-quality diamonds belong, thus they are of unquestionable socio-economic importance. Coated diamonds in contrast contain an array of nano to macro fluid and solid silicate, carbonate and sulphide inclusions as well

as elemental carbon (graphite and amorphous carbon), making them the best tool to study (in situ) the chemical composition of fluids that metasomatise the crust-mantle interface (KLEIN-BENDAVID et al., 2004; KLEIN-BENDAVID et al., 2007; NAVON et al., 1988; TOMLINSON et al., 2005; 2009). Noteworthy is that fibrous diamonds are only known from group I kimberlites, where they can be a significant proportion of the diamond production e.g. Jwaneng, Botswana; Mbuji Mayi DR Congo; Koidu, Sierra Leone; Yakutia, Russia and Ekati, Canada (BOYD et al., 1994; TOMLINSON, 2005).

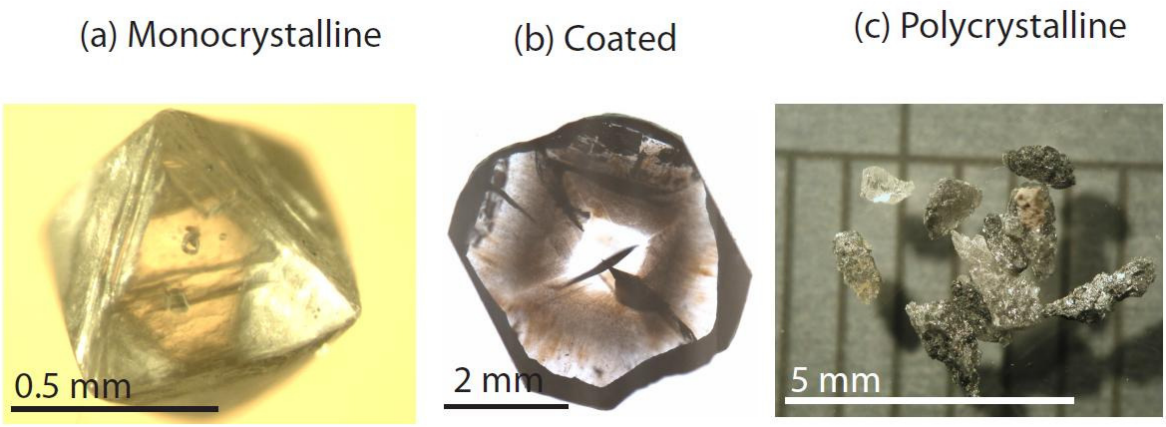

Figure 2.9. The three main morphologies of mantle diamond (a) monocrystalline (single crystal), (b) coated, sometimes referred to as fibrous due to the fibrous textures in the growth dark growth zone (BOYD et al., 1992), but they are not always fibrous (TOMLINSON et al., 2005), therefore I prefer the term coated. The photomicrograph is a cross section along the [110] crystallographic plane and (c) polycrystalline diamond. The monocrystalline sample is Prem22e (from chapter 4), the coated sample is Congo7 and the polycrystalline sample is sample Dia061 fragmented prior to analysis (from chapter 5).

Polycrystalline diamonds (diamondite- the focus of chapter 6) make for good abrasive material as the polycrystalline nature allows for less fracturing along cleavage planes under pressure. Despite this economic value, they have been relatively overlooked from a geochemical point of view (HEANEY et al., 2005). This is despite making up a substantial percentage of some diamond mines overall yield, up to 50% in Southern African diamond mines such as Orapa (Botswana), the world's most productive diamond mine (DEINES et al., 1993; HEANEY et al., 2005). Noteworthy is that coated and

polycrystalline diamonds are always from upper mantle depths (< 200 km), based on their syngenetic silicate inclusions and intergrowths (HEANEY et al., 2005; TOMLINSON, 2005). This is contrary to the monocrystalline diamonds that can be from > 660 km depth (STACHEL et al., 2005). There is a common feature of all three diamond morphological groups, they all have two main geochemical types of mantle minerals (silicate inclusions), which are discussed below.

2.6.2 Silicate paragenesis

Diamonds are also subdivided based on the chemistry of their associated silicate inclusions (this is termed *paragenesis*). Mineral inclusions in natural mantle diamond are routinely used to identify the nature of the host rock where the diamond formed; this is not necessarily the same as the source of the diamond-forming carbon (*discussed in section 2.8.1*). Commonly, these inclusions are ultramafic with an eclogitic or peridotitic affinity based on their major element geochemistry (AULBACH et al., 2008; SOBOLEV, 1977). These parageneses can be simplified into three main upper mantle groups; peridotitic and eclogitic with a small amount of intermediate groups such as websteritic. Their relative global abundances are roughly 65, 33 and 2 % respectively (STACHEL and HARRIS, 2009). Some studies describe sublithospheric inclusions (from depths > 200 km), such as majoritic garnet or retrograde Ca-Si perovskite as a paragenesis (BULANOVA et al., 2010; HUTCHISON et al., 1997; KAMINSKY et al., 2001). However, strictly speaking, this is not a paragenesis but a depth of origin. It is worth noting that almost all sublithospheric inclusions are eclogitic in composition (BULANOVA et al., 2010; KAMINSKY et al., 2009; STACHEL et al., 2005; TAPPERT, 2005; TAPPERT et al., 2009; 2005; WALTER et al., 2008).

Besides the geochemistry, there is an important point to note regarding the geochronology for the two main paragenesis; eclogitic inclusions are never older than 2900 Ma, whereas peridotitic inclusions can be > 3500 Ma (for a review see GURNEY et al., 2010). The importance of this

observation is out of the scope of this thesis. However there is an important model published recently that postulates a date for the onset of Phanerozoic type subduction zone tectonics (the Wilson cycle), so for a detailed discussion I direct the reader to a recent review by Shirey and Richardson (2011).

2.7 Lattice-bound impurities in diamond

Diamonds can also be sub-divided based on their particular lattice-bound impurity and the bonding of that impurity to the carbon atoms and each other. There are two main lattice-bound impurities in mantle diamonds: boron and nitrogen. The main focus of this section is on the more common of the two, which is nitrogen (MILLEDGE and MEYER, 1962). Nitrogen atoms are similar in ionic radius and charge to carbon atoms and therefore can substitute in the diamond lattice for carbon atoms during diamond formation. The range in concentrations for mantle diamonds is from less than 20 ppm to more than 2500 ppm (CARTIGNY, 2005). Nitrogen is present in almost all natural diamonds and occurs in several different aggregation states, which has led to a classification scheme with two main groups: type I and type II. This classification scheme uses non-destructive, in situ analyses (infra red absorption spectroscopy) and makes it possible to classify diamonds according to the principal features of their infrared spectra.

Type I diamonds are subdivided based on the degree of nitrogen aggregation in the diamond lattice. The nitrogen atoms are substitutionally trapped in the diamond lattice at high pressures and temperatures during diamond growth, but are meta-stable (see TAYLOR et al., 1996). Under mantle temperatures these atoms migrate along the crystalline lattice, towards other nitrogen atoms and form aggregates according to a second order kinetic law as a function of temperature (EVANS and QI, 1982; MENDELSSOHN and MILLEDGE, 1995; TAYLOR et al., 1996). Such atomic migration can only occur whilst diamond is in the Earth's mantle as high temperatures are required. At low pressure and high

temperature retrograde reactions would proceed and convert the diamond to graphite. This has been confirmed by high pressure-temperature experiments that induced nitrogen aggregation in synthetic diamonds (EVANS and HARRIS, 1989; TAYLOR et al., 1996).

Type II diamonds are identified as having no detectable nitrogen using infra red absorption spectroscopy. These can be subdivided on the basis of their electrical conductivity, Type IIa being non-conducting and Type IIb having semiconducting properties due to presence of substitutional boron as the major impurity (CHRENKO, 1973), The amount of boron present in Type IIb diamonds is between 0.02 and 0.26 ppm (BIBBY, 1982).

In the above I have discussed, in brief, the cosmochemical origin of terrestrial carbon, the nature of carbon in the terrestrial reservoirs as a function of the redox state of the environment under mantle conditions, the geographical distribution of diamond source rocks through geologic time, diamond formation and the various sub-divisions of mantle diamond. It is now that the topic of carbon isotopes in mantle diamonds should be introduced.

2.8 Carbon isotopes in mantle diamond

Carbon has two stable isotopes of interest to mantle geochemistry (^{13}C and ^{12}C). The isotopic ratio (^{13}C /^{12}C) is expressed as a part per thousand (‰) deviation to an internationally recognised standard called the Pee Dee Belemnite (CRAIG, 1953). The stable isotope ratios of carbon are commonly used as source indicators in various fields of the geo-sciences. Contrasting examples that exhibit the usefulness of this system can be taken from several studies, such as tracing the geographical origins of illicit heroin and cocaine (EHLERINGER et al., 1999), explaining the origins of the elevated CO_2 emissions from arc volcanoes relative to MORB and OIB coming from the decomposition of sedimentary carbonates (WALLACE, 2005), a tentative use to date the origins of life on Earth (ROSING, 1999), and even to argue for the existence of life on Mars (WRIGHT et al., 1989). Trying to trace the

origins of diamond-forming carbon in the mantle is no exception. There is a multitude of work where the stable isotopes of carbon relative to silicate inclusion geochemistry have been used to identify the origin of diamond-forming carbon in the terrestrial mantle (BULANOVA et al., 2010; CAPDEVILA et al., 1999; DE STEFANO et al., 2009; DEINES, 1980; DEINES and HARRIS, 2004; DEINES et al., 1987; 1991a; 1993; 1991b; 1989; 2001; FITZSIMONS et al., 1999; GALIMOV, 1984; HUTCHISON et al., 1997; KAMINSKY et al., 2001; 2000; MCCANDLESS et al., 1999). The first point to make about this work is that if one grouped all terrestrial mantle diamonds of both paragenesis, they exhibit a well defined mean $\delta^{13}C$ value of -5 ± 3 ‰ representative of the mean mantle as defined by studies of diamond, MORB, OIB, carbonatites and kimberlites (CARTIGNY, 2005). This was originally seen in the first study of the $\delta^{13}C$ value of 5 individual mantle diamonds by Craig (1953) and remains true today after > 5000 individual analyses of both silicate paragenesis (reviewed by STACHEL et al., 2009 and shown in figure 2.10).

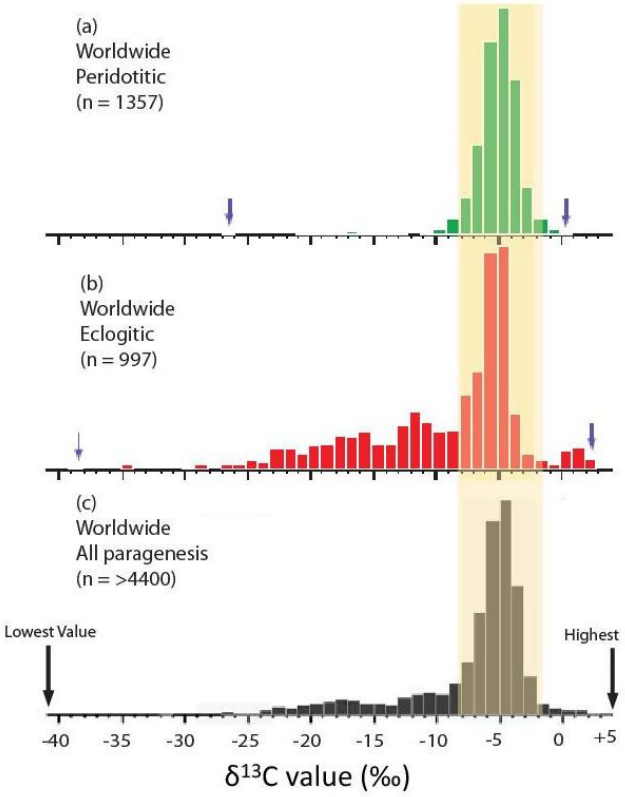

Figure 2.10. Histograms showing the $\delta^{13}C$ values for monocrystalline inclusions bearing diamonds of (a) peridotitic, (b) eclogitic and (c) all paragenesis from Cartigny (2005). The blue arrows in a & b represent the lowest and highest values as do the black arrows in c. The orange band at -5 ± 3 ‰ represents the mean mantle range.

It has long been known that monocrystalline mantle diamonds with peridotitic inclusions display a more narrow range and well defined mean $\delta^{13}C$ value relative to their eclogitic counterparts (for a review see CARTIGNY, 2005 and shown in figure 2.10). However this is not the case for coated diamonds (Boyd et al., 1994) or polycrystalline diamonds (Maruoka et al., 2004) as shown in figure 2.11. The coated diamonds exhibit a narrow range in $\delta^{13}C$ values and this is irrespective of the silicate paragenesis of the coated diamonds. Diamondites that also show no discrimination for their silicate paragenesis vs. $\delta^{13}C$ values; whereas they are globally bi-modal for $\delta^{13}C$ values with peaks at -20 and -5 ‰ (Maruoka et al., 2004). A detailed study on the $\delta^{13}C$ values for diamondites from several kimberlites is lacking (HEANEY et al., 2005) but is the focus of chapter 6.

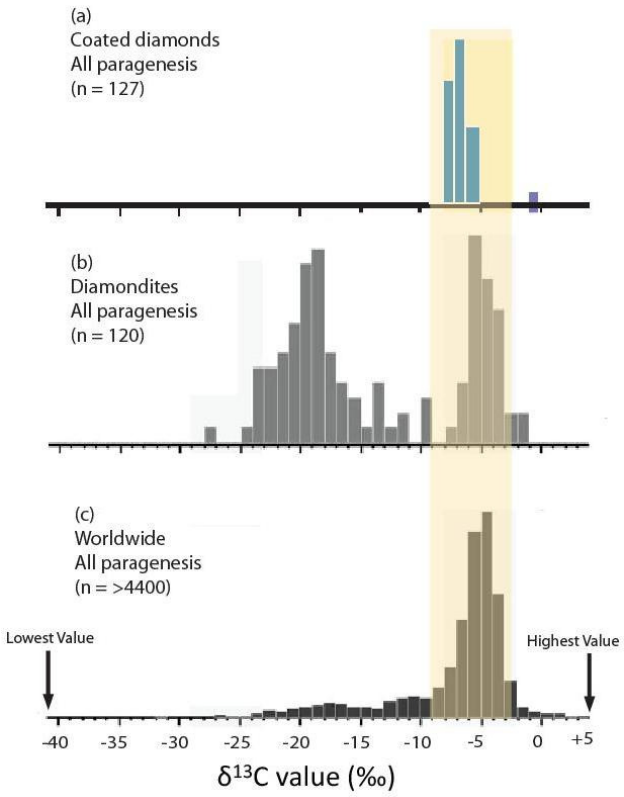

Figure 2.11. Histograms showing the $\delta^{13}C$ values for (a) coated diamonds, (b) polycrystalline (diamondites) and (c) monocrystalline inclusions bearing diamonds of both eclogitic and peridotitic paragenesis. The data for a & c are from Cartigny (2005) and the data for b are from Maruoka et al (2004). The orange band at -5 ± 3 ‰ represents the mean mantle range.

The origins of low $\delta^{13}C$ values exhibited by some diamonds with eclogitic inclusions and by some diamondites are difficult to decipher without a secondary indicator for the source. Any conclusions regarding the origin of diamond-forming carbon solely based on the carbon isotope ratios are ambiguous. This is for two reasons: firstly because there is no other proxy secondary indicator with which to *confirm* the concluding model (Boyd and Pillinger, 1994); this relates to the second reason where the geochemistry of the associated inclusions are not necessarily relevant, as diamond inclusions can be older than their diamond hosts (Viljoen et al., 2004). However, some inclusions can be syngenetic. This is determined using the morphology of a given silicate/sulphide inclusions should one observe an octahedral morphology, this is an imposed feature caused by the host diamond

(Meyer, 1987; as is the case for the diamonds in chapters 5 of this thesis). Below I will give an example as a case study from the Jwaneng kimberlite in Botswana, this case study illustrates the need for a secondary indicator, in form of nitrogen isotopes, to understand the origin of low $\delta^{13}C$ values exhibited by some diamonds with eclogitic inclusions.

2.8.1 Eclogitic diamonds from Jwaneng: the need for nitrogen isotopic complements

Deines et al (1997) published the $\delta^{13}C$ values for 75 inclusions bearing diamonds from Jwaneng, Botswana (figure 2.12) and found that some eclogitic diamonds, predictably, exhibited low $\delta^{13}C$ values, whereas the 16 peridotitic diamonds exhibited a range of $\delta^{13}C$ values from -2 to -9 ‰. It is very difficult to establish a conclusion from this data; in fact Deines et al (1997) made no conclusions regarding the origins of the low $\delta^{13}C$ values in the eclogitic diamonds. The link with eclogitic inclusions, and not peridotitic, will always raise the question that a crustal source could be involved (BULANOVA et al., 2010; CARTIGNY et al., 1998a; GALIMOV, 1984; KIRKLEY M B and DANIELS, 1991). This is because crustal organic compounds exhibit $\delta^{13}C$ values between -15 and -40 ‰ with a peak around -25 ‰ (HOEFS, 2009; SHIELDS and VEIZER, 2002; THOMAZO et al., 2009). However, with only low $\delta^{13}C$ values as evidence, this argument would be weak.

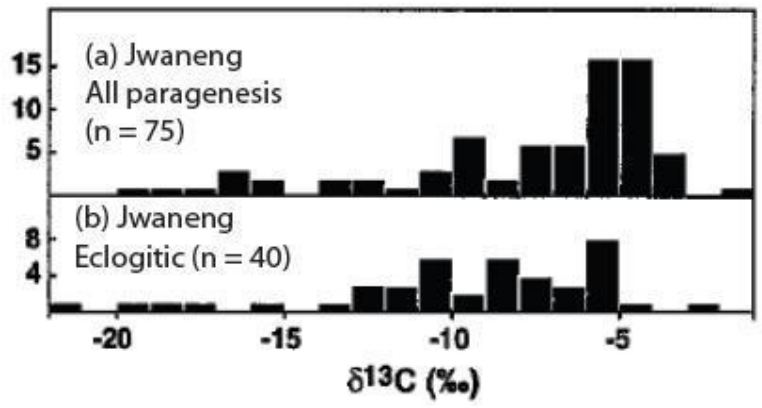

Figure 2.12. Histograms showing the $\delta^{13}C$ values for diamonds from Jwaneng, Botswana. (a) is for all paragenesis from Deines et al (1997) and (b) is for eclogitic diamonds from Cartigny et al (1998a).

This is where the use of nitrogen isotopes can provide a secondary insight, because the nitrogen partitions into the diamond during diamond formation from the same diamond-forming medium. Therefore should the carbon be sourced from a crustal reservoir, one would expect the nitrogen to also be from such a reservoir. Nitrogen has two stable isotopes of interest to mantle geochemistry ($^{15}N/^{14}N$). These are expressed as a part per thousand (‰) deviation AIR (Cartigny, 2005). There exists a stark contrast for mantle and crustal reservoirs; the mantle materials have mostly negative (70 %) and the crustal materials mostly positive (>80 %) $\delta^{15}N$ values which is consistent through time (BOYD and PILLINGER, 1994; CARTIGNY, 2005; THOMAZO et al., 2009 and shown in figure 2.13).

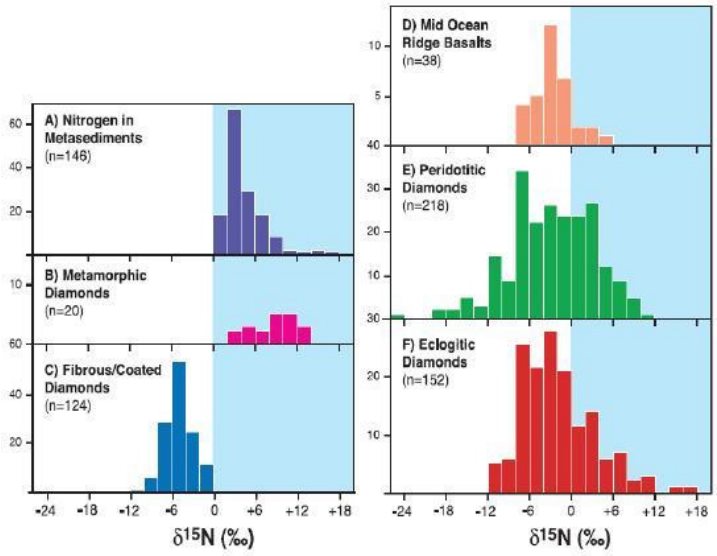

Figure 2.13. Histograms showing the $\delta^{15}N$ values for major mantle reservoirs (from CARTIGNY, 2005). The blue band represents positive values.

Cartigny et al (1998a) revisited the Jwaneng diamonds and determined the $\delta^{13}C$ values coupled with N concentrations and $\delta^{15}N$ values for 39 eclogitic diamonds and made the following observations;

- Decreasing $\delta^{13}C$ values correlates with and decreasing N concentrations and increasing $\delta^{15}N$ values;
- All of the eclogitic diamonds in their sample set exhibited mantle-like *negative* $\delta^{15}N$ values.

The authors used these trends to provide a model that explains the generation of low $\delta^{13}C$ values in the eclogitic diamonds from Jwaneng and predicts that eclogitic diamonds can exhibit low $\delta^{13}C$ values, whereas peridotitic diamonds should not. This model proposes that diamond formation is occurring in an open system where diamond and ^{13}C rich CO_2 are in isotopic equilibrium (by roughly +3.5 ‰ at 1200 °C according to the calculations of RICHET et al., 1977). The CO_2 is lost from the system in progressive stages, i.e. Rayleigh distillation (RAYLEIGH, 1902). This can only occur in an eclogite, because diamond and CO_2 cannot co-exist in a peridotite. The CO_2 would/could react with olivine to form carbonates and pyroxene (Luth, 1993). These carbonates (as the model requires) would later contribute to more diamond formation thus not fractionating the $^{13}C/^{12}C$ ratio (CARTIGNY

et al., 1998a). The reason for the N concentration decreasing and the $\delta^{15}N$ values increasing is that this model requires nitrogen to be an incompatible element in diamonds relative to the fluid, therefore during progressive diamond growth with carbon loss (as CO_2) there must be even more nitrogen loss (^{14}N enriched). This can cause the observed trends (shown graphically in figure 2.14). Therefore, the carbon isotope distributions the eclogitic diamonds from Jwaneng can be explained using a mantle carbon source with a homogeneous $\delta^{13}C$ value of -5 ‰ (CARTIGNY et al., 1998a).

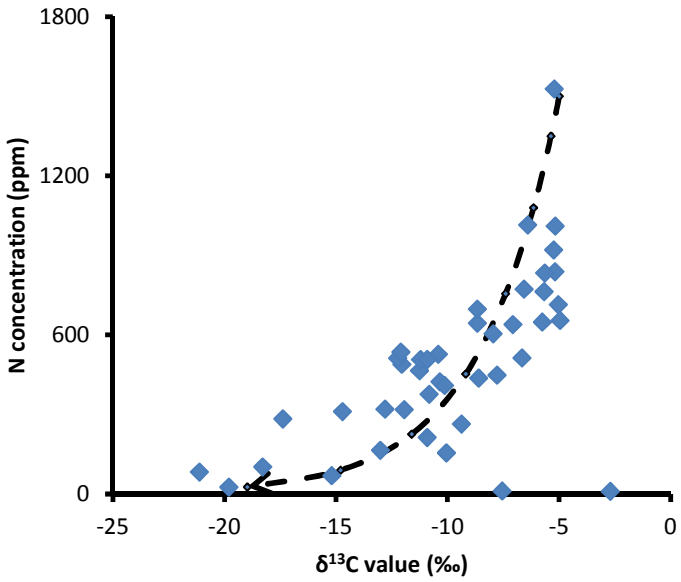

Figure 2.14. A variation diagram for $\delta^{13}C$ vs. N concentration. The blue diamond symbols represent data from eclogitic diamond samples from Jwaneng (CARTIGNY et al., 1998a) and the black dashed line is the model of Cartigny et al (1998a), discussed in the text.

2.8.2 Unexplained data

The above model can be applied to several data sets to either explain low $\delta^{13}C$ values in several eclogitic diamond populations (CARTIGNY et al., 1998a; 1999; 1998b) or small co-variations for $\delta^{13}C$-$\delta^{15}N$- and N concentrations (THOMASSOT et al., 2007) in single diamond populations. There are a few observations that this model cannot explain; such as bi-modality and a well defined peak for a given population of samples that is distinct from the mean mantle range, using the shape and distribution of the $\delta^{13}C$ values (figure 2.15). However, the use of a diagram for $\delta^{15}N$ vs. $\delta^{13}C$ can enable a good distinction between the crustal organic carbon and mantle sources as shown in figure 2.16.

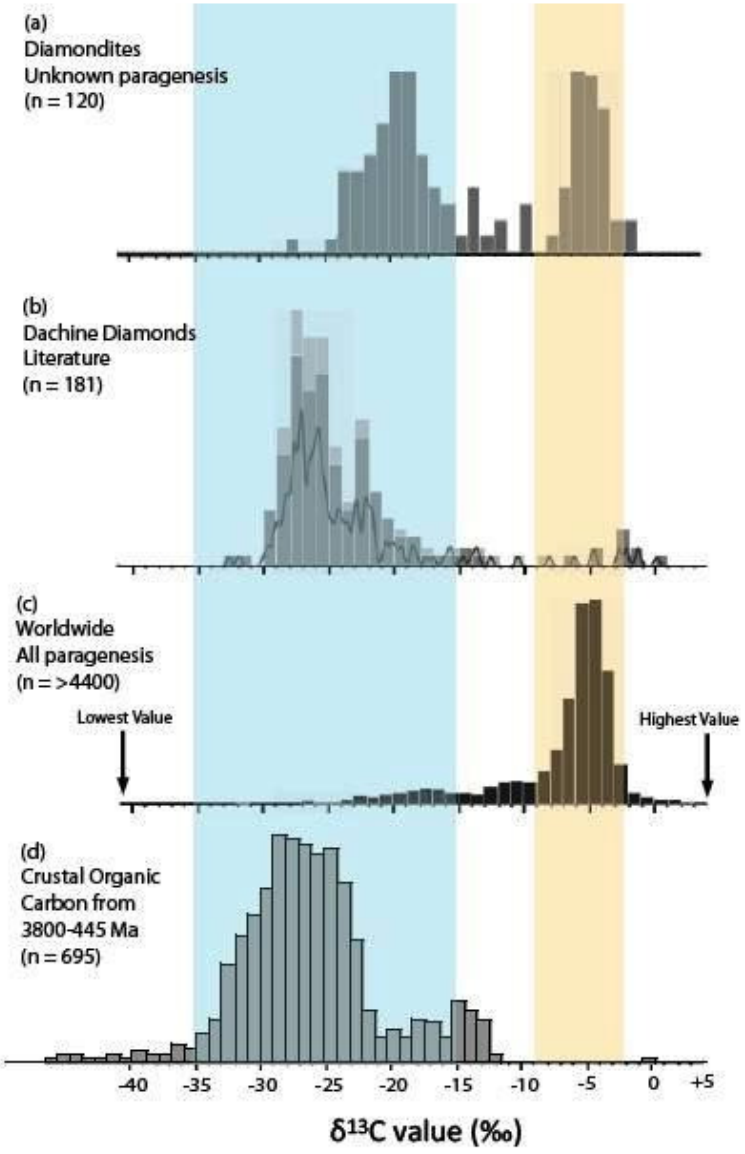

Figure 2.15. Histograms showing the $\delta^{13}C$ values for (a) polycrystalline (diamondites- from Maruoka et al., 2004), (b) diamonds from Dachine, French Guyana (from Cartigny 2010), (c) monocrystalline inclusion-bearing diamonds of both eclogitic and peridotitic paragenesis (from Cartigny 2005) and (d) and pre-Cambrian crustal organic carbon (compiled by Shields and Veizer, 2002). The orange band at $\delta^{13}C$ -5 ± 3 ‰ represents the mean mantle $\delta^{13}C$ range (from Cartigny, 2005) and the blue band represents the main range for the $\delta^{13}C$ values of the organic carbon.

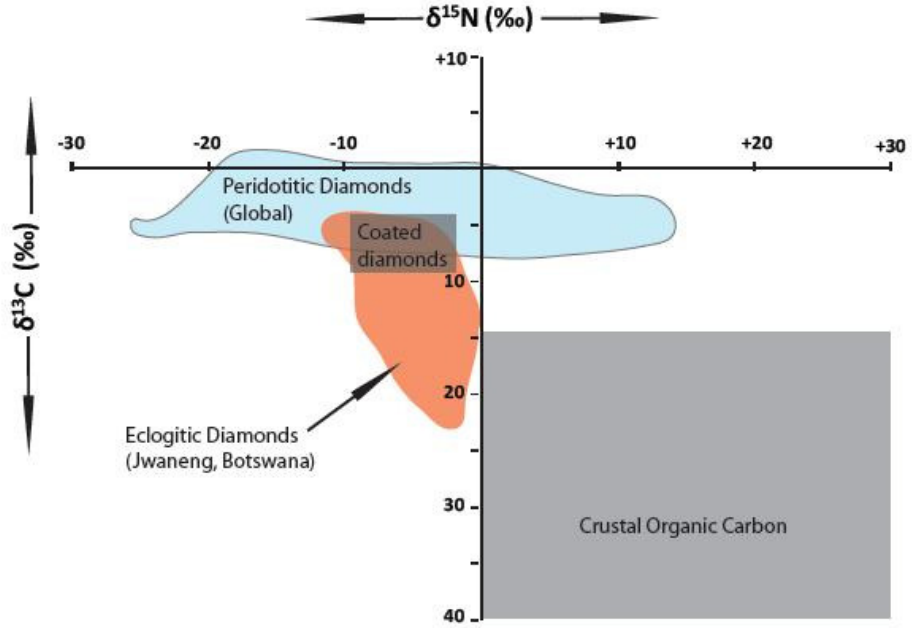

Figure 2.16. A variation diagram for $\delta^{15}N$ vs. $\delta^{13}C$ for mantle and crustal material. This illustrates the potential for coupled $\delta^{15}N$-$\delta^{13}C$ values from mantle materials to be used to discriminate mantle from organic crustal reservoirs. The data for eclogitic diamonds from Jwaneng is from Cartigny et al (1998a), coated diamonds is from Boyd and Pillinger (1994), peridotitic diamonds is made up of a compilation of Namibian (CARTIGNY et al., 2004) and Chinese (CARTIGNY et al., 1997) diamonds, crustal organic carbon is from (THOMAZO et al., 2009).

2.8.3 The main hypothesis

The models provided in the literature that attempt to explain low $\delta^{13}C$ values from mantle materials and are tested in this thesis using coupled determinations for $\delta^{13}C$- $\delta^{15}N$- and N concentrations (chapters 4, 5, 6), and are as follows:

(1) The existence of undefined primordial heterogeneities;

(2) Subduction of crustal organic carbon;

(3) Mass dependant stable isotope fractionation in the mantle before diamond formation.

I discuss all three of these models in detail in chapter 5 and 6 using new data. However, I shall briefly outline each below.

1) Primordial heterogeneities

Deines (2002) published a detailed review of the carbon isotope geochemistry of mantle xenoliths and argued that the shape and regularity of a peak at -20 ‰ for the high temperature carbon releases (by stepped heated mass spectrometry) in mantle silicates is evidence for an indigenous mantle component and attributed this to a relic and minor isotopic heterogeneity in the mantle that has not been homogenised since accretion. This is as opposed to a subducted component that he argued should be a flat peak, and high temperature isotopic fractionation that should be a gradual trend from the initial mean mantle $\delta^{13}C$ value of -5 ‰ (as is seen for the Jwaneng eclogitic diamonds in figure 2.11). However the meteoritic origins of this low $\delta^{13}C$ component are not defined and nor is any mention of $\delta^{15}N$ in this model.

2) Subduction

The fact that low $\delta^{13}C$ values for diamonds with eclogitic inclusions are more prevalent than for diamonds with peridotitic inclusions (figure 2.10), and sometimes from the same kimberlite pipe (as in the kimberlite in Jwaneng, Botswana see section 2.8.1), suggests that subducted crustal organics may explain the low $\delta^{13}C$ values for eclogitic diamonds (figure 2.15). Because eclogite is the high pressure metamorphic equivalent of basalts, i.e. the top layer of the oceanic crust (Best, 2003), it is not inconceivable to envisage that there may be a link. The model of Cartigny et al. (1998a) (summarised in section 2.8.1) cannot explain distributions in $\delta^{13}C$ for the diamonds from Dachine and diamondites (shown in figure 2.15). However use of nitrogen isotopes would enable the

question of primordial heterogeneities to be discussed as is provided in chapter 5 for Dachine diamonds and chapter 6 for diamondites according to the fields shown in figure 2.16.

3) Mass dependant stable isotope fractionation

Mass dependant equilibrium stable isotope fractionation at high temperature between different carbon phases has long been proposed as a viable mechanism to explain the isotopic variability observed in mantle xenoliths (DEINES, 2002), xenocrysts (CARTIGNY, 2005; CARTIGNY et al., 1998a; 2001; GALIMOV, 1991; JAVOY et al., 1986; MARUOKA et al., 2004; THOMASSOT et al., 2008; 2009; 2007) and for Martian magmatic carbon (Grady et al., 2004). An example of this has already been discussed in section 2.8.1 regarding the data from eclogitic diamonds from Jwaneng. There is a fundamental issue to raise that is addressed in chapter 8; the issue is with the lack of work regarding the role of pressure for stable isotope fractionation. There is a large body of thermodynamic work exploring theoretically calculated equilibrium fractionation factors for ^{13}C between diamond-CO_2/CH_4 (Bottinga, 1969; Horita, 2001; Richet et al., 1977). These thermodynamic calculations demonstrate that at high temperatures (circa. 1200 °C) there are significant fractionation factors directly applicable to diamond formation. For example;

- Diamond - CO_2 = -3 ‰ (Richet et al., 1977)
- Diamond - CH_4 = +1 ‰ (Bottinga, 1969)

What is evident here is that for a given temperature the speciation of carbon being removed from the system (CO_2- CH_4 relative to diamond) is the governing parameter and therefore the hydrogen fugacity (fH_2) and oxygen fugacity (fO_2) are fundamental, and require constraints to be placed before any modelling can be performed to explain empirical data. All of the above studies are theoretical calculations at 0 GPa, i.e. the effects of pressure are either assumed to be negligible or were not considered. These thermodynamic calculations use the vibrational frequencies between the ^{13}C

relative to ^{12}C atomic bonding based on the differences for the occupation sites for the two phases in the calculation. This is because sensitivities of vibrational frequencies to isotopic substitutions (Urey, 1947). Pressure can decrease the volume of compressible phases and therefore alter the vibrational frequencies of the site of occupation for the carbon atoms. Regarding diamond, the compressibility at pressures akin to the Earth's mantle (2-135 GPa) is negligible (HARLOW and DAVIES, 2005), but most other known carbon phases in the mantle (carbonate and carbides) do show compressibility and therefore could affect the magnitude of the fractionation factors calculated thermodynamically at 0 GPa. This is revisited and fully introduced in chapter 8.

2.9 Aims of this thesis

The overall aim of this thesis is to apply new constraints on the origins of low $\delta^{13}C$ values in mantle diamond. This could enable a better understand for the use of the stable isotopes of carbon and nitrogen to trace carbon cycling in the deep Earth over geologic time. I aim to achieve this using two main methods that contain the several studies (chapters) outlined below;

(1) Determining the coupled $\delta^{13}C$- $\delta^{15}N$- and N concentrations from diamond known to exhibit low $\delta^{13}C$ values. The diamond populations available to me are diamondites of unknown geographical origins (chapter 6) and diamonds from Dachine, French Guyana (chapter 5). Data from the literature for both sample sets are shown in figure 2.15. Before determining the coupled $\delta^{13}C$- $\delta^{15}N$- and N concentrations in diamonds from Dachine, French Guyana (chapter 5) I must develop a technique that enables accurate $\delta^{15}N$ determinations in type II diamonds (chapter 3). This is because 97 % of Dachine diamonds (n = 181) studied prior to my work are type II (Cartigny, 2010). Another unknown that needs to be investigated is determining the $\delta^{15}N$ values for type II diamonds with mean mantle $\delta^{13}C$ values (chapter 4). This will enable a comparison to be made. This is because my $\delta^{15}N$ data for

diamonds from Dachine are mostly type II, whereas all of the literature for the $\delta^{15}N$ values for mantle diamond are type I.

(2) To place new constraints on the magnitude and direction of $^{13}C/^{12}C$ fractionation relative to diamond in an iron-rich system that is potentially indicative of the deep Earth carbon reservoir based on the fO_2 constraints outlined in section 2.3. This will be achieved by determining the $\delta^{13}C$ values of co-existing Fe carbide inclusions and their host diamond using rare diamonds available to this project (chapter 7), the effects of pressure and temperature in this system will be tested experimentally by high pressure and high temperature experiments (chapter 8).

Chapter 3

A fully automated technique to determine the $\delta^{13}C$, $\delta^{15}N$ and the N concentration simultaneously in mantle diamonds

3.1 Introduction

Diamond is a precious and rare commodity. Therefore people who possess samples do not like to destroy large amounts of them to acquire data; acquiring C and N isotopes by gas sourced mass spectrometry leaves no residual sample. Therefore one must find a way of analysing small fragments and producing getting good data. In order to measure nitrogen isotopes in very small samples (< 0.1 mg) or in samples where nitrogen concentration is extremely low (< 30 ppm), considerable time was spent developing and improving cutting -edge techniques to extend their capability. This was required both for analysis of small synthesised run products and for type II natural diamond, where nitrogen is very low (< 30 ppm). The techniques extend methods previously developed at the OU for meteoritic nanodiamond (see BOYD et al., 1998 and VERCHOVSKY et al., 1998), and so a natural collaboration was developed to pursue this analytical methodology. This chapter described in detail that work, and is placed here rather than in an appendix, since this formed an integral and formative part of the research.

Herein I describe the automation and calibration of the Finesse machine housed at the Planetary and Space Science Research Institute, The Open University, UK. The Finesse machine is a custom built, computer automated facility that utilises three static mode mass spectrometers fed from a common extraction system under high vacuum. Operating in static mode enables the analysis of smaller aliquots of sample gas to determine the isotopic ratios relative to continuous flow facilities, albeit

with less precision (BOYD et al., 1988; GARDINER and PILLINGER, 1979; WRIGHT et al., 1988). However, the precision is still good enough to study mantle geochemical systems because typical errors are optimally circa ± 0.5 ‰ for carbon and nitrogen, and the terrestrial range for mantle samples is > 40 ‰ for both systems (CARTIGNY, 2005). Operating under high vacuum, with stainless steel pipework, and by using copper valve tips for the nitrogen section of the facility enables this facility to operate with extremely low nitrogen blanks. I will finish this chapter by outlining the superior blank levels and stability that this facility has provided to the studies in my thesis.

3.2 Overview of the Finesse machine

The majority of the mechanical components that make up the Finesse machine have previously been outlined in detail (Shelkov, 1997), and so this information is not repeated here. What I detail here is an update to the systems automated analytical procedure for the automation and simultaneous determinations of $^{15}N/^{14}N$, $^{13}C/^{12}C$ ratios and the nitrogen and carbon concentrations from a single sample source, using mass spectrometry operated in static mode under vacuum.

Figure 3.1 shows a simplified 2D schematic diagram of the Finesse machine and identifies all of the components referred to in the subsequent sub-sections. The machine has several components:

- Pumping system (4 Ion pumps, 1 turbo pump)
- Quartz combustion furnace
- O_2 supply (CuO) and O_2 clean up (CuOcl)
- Capacitance manometer (baratron)
- 2 static multi-collector mass spectrometers
- Quadrupole mass spectrometer
- Molecular sieve
- 3 ‘cold fingers’
- 3 reference gas sources (Air, CO_2 and N_2)

The components are all connected by steel piping with several manual and computer controlled valves. The liquid nitrogen (LN) supply and the manual valves (not used during sample analysis) are the only item that is not fully automated. Topping up the supply is a manual task; however administration of LN to the cooling devices is automated.

All of the analysis is performed at high vacuum. With the exception of the loading chamber and furnace vacuum tube there are two main vacuum systems for the inlet section of the Finesse. The inlet system is maintained at circa 10^{-8} mbars. Each section (C and N) and each mass spectrometer (C, N and quadrupole) have one dedicated ion pump that is required to maintain this high vacuum.

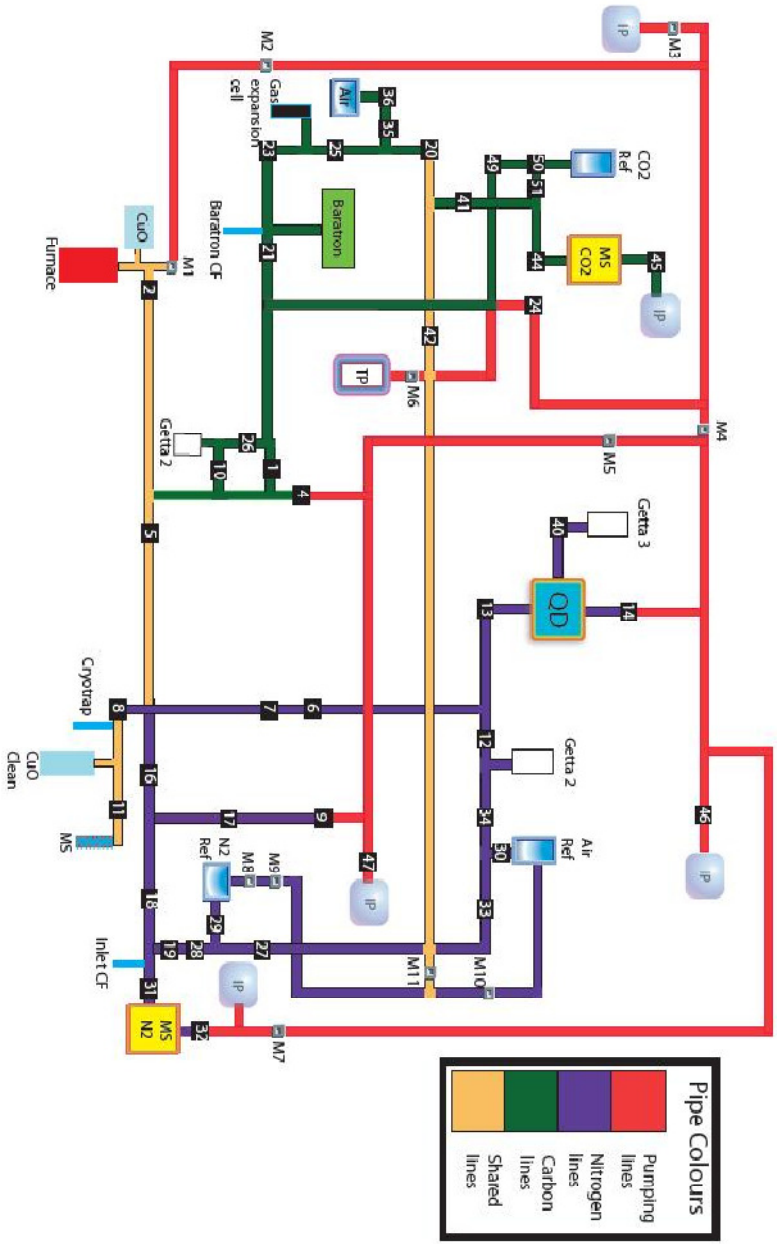

Figure 3.1. A schematic layout of the Finesse machine. M1-9 refers to a manual valve, black boxes with white numbers refers to a pneumatic (automated) valve, IP is an Ion Pump, TP is the turbo pump, AIR and Air Ref refer to air standards, N2 ref refers to the N_2 reference gas, CO2 ref is the CO_2 reference gas, Inlet and Baratron CF are the Inlet and Baratron cold traps, Getta 2-3 are nitrogen gettas (heated Ti powder), CuO and CuOcl are the O_2 source and sink, QD is the quadrupole mass spectrometer and MS N2 and MS CO2 are the mass spectrometers for nitrogen and carbon isotopic determinations respectively.

3.2 Automation

Once the sample is loaded into the furnace the whole procedure is fully automated and controlled using LabView software. This enables the following parameters to be controlled by the operator prior to an experiment: the number of analyses (set by numbering the temperature steps), combustion or pyrolysis heating for a given step, duration of each step, the temperature of the CuO and CuOcl for O_2 removal and addition and the temperature range used by the cryotrap, molecular sieve (MS), baratron cold finger and the inlet cold finger during gas transfer and separation (all shown and labelled in figure 3.1).

A notable exception to the automated procedure is the amount of LN in the source, which needs to be periodically added by the operator. This is used for the variable temperature traps (cryotrap, MS and baratron CF) and the inlet cold trap. The 25 L Dewar flask can last a 7 stage combustion sequence for carbon and nitrogen analysis. If any more steps are required then the operator must add more liquid nitrogen to the Dewar flask. Should the liquid nitrogen source become exhausted then the system produces an error message on the computer console and pauses indefinitely until restarted by the operator. This is also a failsafe so as not to perform any analysis without liquid nitrogen, which would result in a complete fail.

3.2.1 Temperature controls

Furnace, CuO and CuOcl

All of the temperature controls are controlled by Eurotherm microprocessors that feedback to the computer. Should the temperature (measured using a thermocouple) in the component (Furnace, CuO or CuOcl) be above the target temperature then the power supply is reduced in the component and it is allowed to equilibrate down to the desired temperature. If it is too low then the power supply is increased automatically with the desired temperatures set by the operator.

The thermocouple and heating system for the quartz combustion furnace is sensitive enough to confidently achieve temperature increments of about 25 °C from 200 – 1400 °C (A.B. Verchovsky pers comm. 2008). In this thesis the smallest increment was 50 °C (chapter 8), and the furnace was operated between 200 and 1400 °C. The furnace is doubly insulated as shown in figure 3.2 with the quartz tube in a vacuum tube that provides two benefits to single insulation. One is to stabilise the quartz tube (mechanically) at high temperatures (circa >1100 °C) because at high temperatures the quartz weakens and atmospheric pressure would cause collapse. Therefore the vacuum seal and pump reduce the external confining pressure and enable higher temperatures to be attained. Secondly it reduces the amount of atmosphere to be in contact with the quartz at high temperatures which reduces the amount of diffusion of atmospheric gasses. The CuO and CuOcl are similar in design, with a notable exception being the gap in the insulation that allows the furnace to cool rapidly, thus saving time. Such a rapid cooling down time is required as the desired temperature gradient is >500 °C in 20 minutes (figure 3.3). However, this is not the only difference. The extraction furnace heater is made of SiC and the CuO and CuOcl furnaces use a high-resistance alloy wire. Also, the CuOcl is a single-wall furnace.

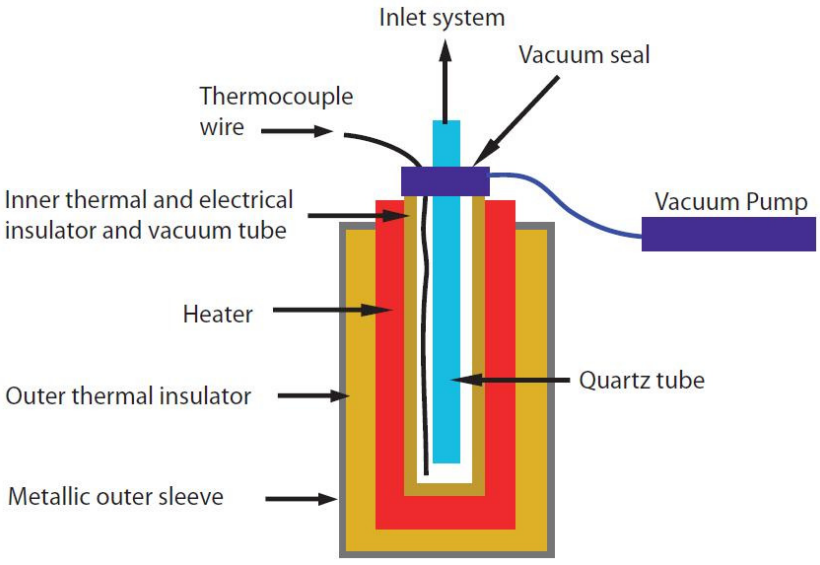

Figure 3.2 Furnace assembly with all the components labelled (not to scale).

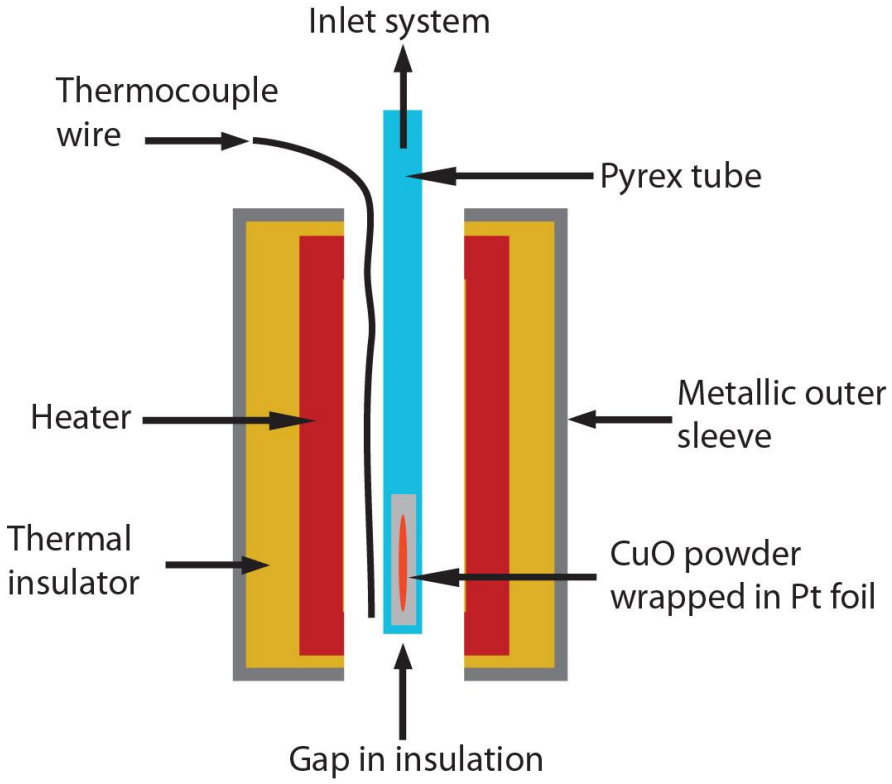

Figure 3.3 CuO and CuOcl assembly with all the components labelled (not to scale). Note the gap in the insulation (see text).

Cryotrap, MS, Baratron and inlet cold fingers

These components are Pyrex tubes doubly encased in metallic sleeves where liquid N_2 can be pumped (using rotary pumps) around the inner sleeve to cool the pyrex tube to low temperatures where the thermocouple is located (figure 3.4). The outer sleeve of the baratron cold finger has a thermal wire (electrical insulator) wrapped around it to allow rapid heating once the rotary pumps are turned off to reach high temperatures. The cryotrap and molecular sieve have the inner heater as shown in fig. 3.4. They can be heated above the evaporation temperature of H_2O (circa 60 °C for the cryotrap) and higher (250 °C for the MS to purify it and keep the N blank low) and cooled below the condensation point of CO_2 (< -160 °C for the cryotrap and baratron cold fingers) and N_2 (< -190 °C for the MS and inlet cold fingers). There is no need in the analytical procedure to heat the inlet cold finger in a rapid manner and it therefore does not have a heating system.

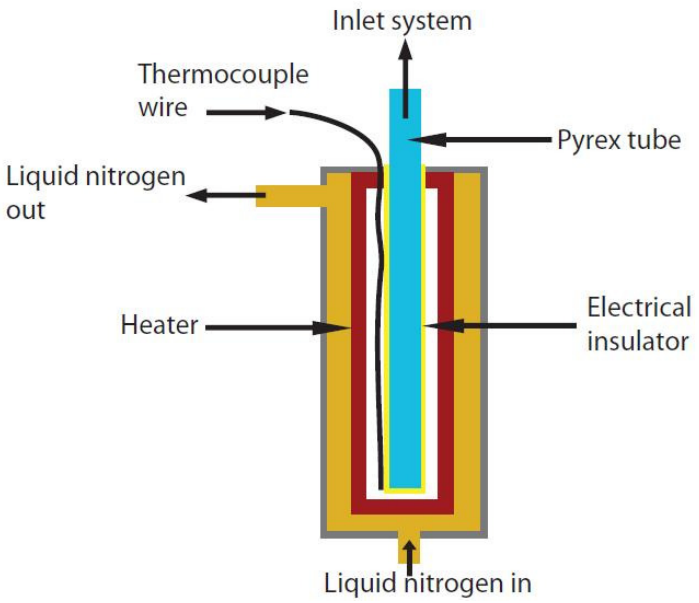

Figure 3.4 Typical design of a variable temperature trap (not to scale). This is the design for the CO_2 cryotrap. The MS varies slightly as the molecular sieve is contained within the Pyrex tube. The heated is not in physical contact with the liquid nitrogen. The inlet cold-finger trap differs as it does not have a heat source. All of the components are labelled.

3.2.2 Pneumatics valves

The valves labelled and detailed in figure 3.1 are computer controlled valves operated using a pneumatic system (compressed air) controlled through solenoid valves using the LabView software. The valves that function for the nitrogen analysis use copper tips as opposed to rubber or plastic so as to keep the nitrogen blank levels low. The valves used solely for carbon are plastic as they are cheaper and justified because the blank needs not be as low.

3.2.3 Reference gas aliquots

To automate the amount of reference gas that is used for carbon and nitrogen isotope analyses, quadrupole mass spectrometers, baratron concentration analysis, and during calibrations, the bleed time technique is implemented (SHELKOV et al., 1997). This is where the reference gas is bled through a capillary gas pipette (between the reference gas cylinders and valve 50 for carbon and 28 for nitrogen; see figure 3.1). This technique is capable of delivering nanograms of reference gas with a reproducibility of 0.5 % (PILLINGER, 1992), which is important for the static mode measurements where the sample and reference gases are analysed in sequence. It is required that there are equal amounts of sample and reference gases to be present in the mass spectrometer during the analysis. The amount of reference gas administered is computer-controlled by the 'bleed time' (SHELKOV et al., 1997).

The baratron is calibrated by combusting a diamond or graphite sample of known size and measuring the CO_2 mass in the baratron (figure 3.5). Once calibrated the baratron can be used to determine the mass of N_2 or CO_2 vs. the bleed time of the reference gas. The bleed rate for the CO_2 reference is calibrated by comparing the mass of CO_2 gas taken during a certain amount of time and then measured on the baratron.

Nitrogen bleed rate is calibrated using fixed volume aliquots of air. It is much bigger in volume than the nitrogen reference gas accumulated for a reasonable time, and therefore enables a more precise

baratron measurement of the mass. First the O_2 is removed using the CuOcl, and then the mass is measured on the baratron. Finally it is analysed on the mass spectrometer in the same manner as a sample. It produces a signal in volts that corresponds to a known mass of nitrogen. Analysis of reference gas aliquots at the same time gives volts vs. bleed time (figure 3.7). The quadrupole MS is calibrated using the reference N gas when its bleed rate is determined (figure 3.8). The fixed-volume air is also used to calibrate the isotopic composition of the reference nitrogen gas.

This fixed-volume air is processed using the same analytical procedure as a sample gas, where the mass of the gas is measured using the mass spectrometer and is calibrated against another aliquot of the reference gas. The baratron is calibrated by combusting a diamond or graphite sample of known size and measuring the CO_2 mass in the baratron (figure 3.5). Once the baratron is calibrated the mass of N_2 or CO_2 vs. the bleed time can be determined using the baratron. The calibration of the baratron for bleed time also enables the calibration of the quadrupole in measuring the mass of nitrogen using the intensity of mass 14 (^{14}N; see figure 3.6) as well as more precise measurements of N_2 gas vs. time by using the calibration of the reference gas (figure 3.7). Knowing the $^{15}N/^{14}N$ ratio of the reference gas enables the conversion of the intensity of mass 28 ($^{14}N_2$) into the mass of nitrogen (as for the sample post $^{15}N/^{14}N$ ratio determination). The mass of nitrogen is determined using the relationship of grams and volts measured for mass 28 ($^{14}N_2$) where:

$$k3 = \frac{N\ ng}{Volts} = \frac{K2}{K1}$$

The value for K_1 is determined using the linear array of int28 vs. time (s^{-1}) for the sample where:

$$K1 = \frac{Intensity\ of\ mass28\ (volts)}{Time\ (seconds)}$$

And K_2 is for the reference gas where the mass of N is known from the bleed time calibration where:

$$K2 = \frac{N\ ng}{Time\ (seconds)}$$

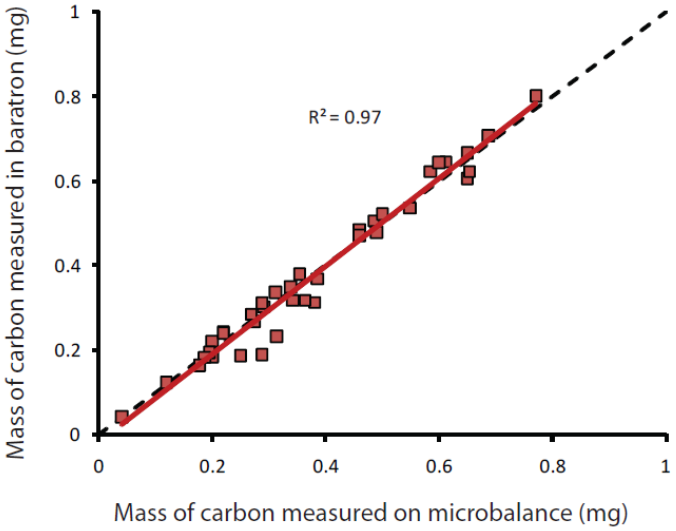

Figure 3.5. The correlation for the mass of all monocrystalline diamonds (n = 38) in this thesis weighed using a microbalance and determined using the baratron for samples in this study in 2009 and 2010. The average difference is 0.001 mg with a standard deviation of 0.041 mg (appendix table A1).

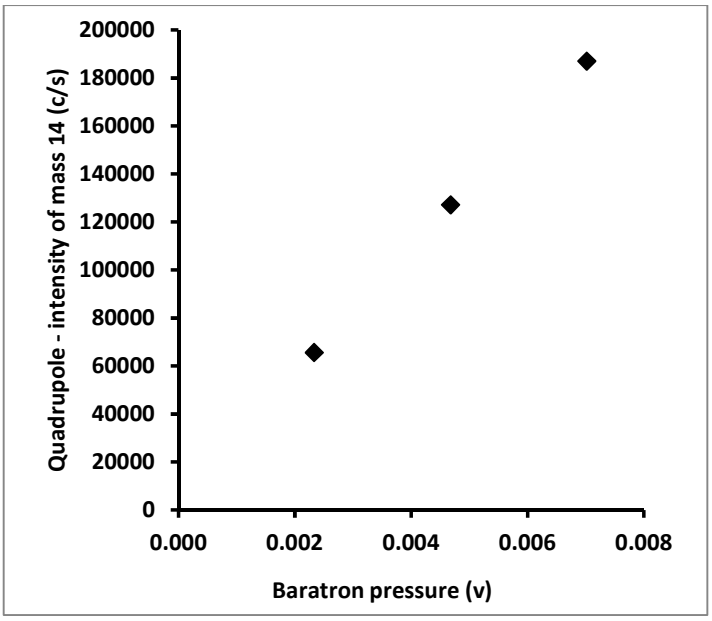

Figure 3.6. The correlation between the measured voltage in the baratron (pressure) vs. the intensity of mass 14 (^{14}N) in the quadrupole (appendix table A2).

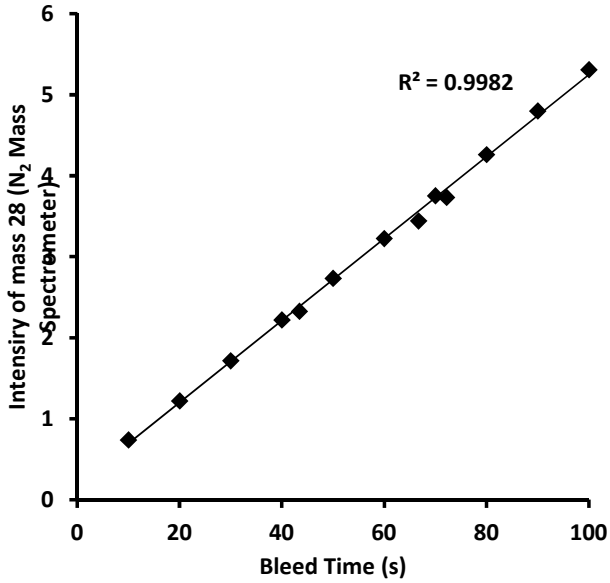

Figure 3.7. The correlation for the bleed time of N_2 vs. the measured intensity of mass 28 ($^{14}N_2$) in the N MS for the N_2 reference gas used to calibrate the bleed time for the N_2 reference gas (appendix table A3).

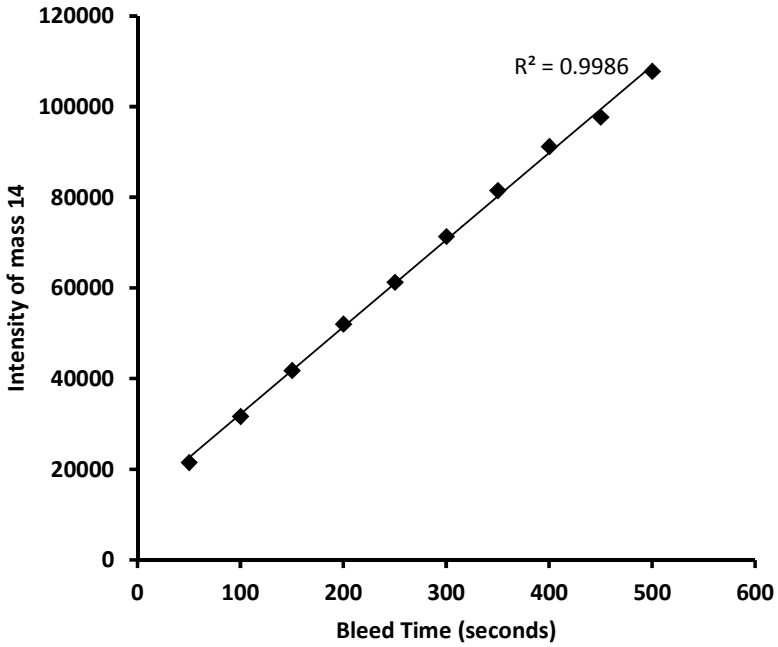

Figure 3.8. The correlation for the bleed time of air (post O_2 and noble gas removal) vs. the measured intensity of mass 14 (^{14}N) in the quadrupole MS for the Air reference gas used to calibrate the bleed time (appendix table A3).

3.3 Experimental procedure

3.3.1 Sample preparation, cleaning and loading

Samples (0.2-0.6 mg) are crushed into small pieces, weighed, and wrapped in Pt foil. The Pt foil is twice cleaned prior to use. It is placed into a quartz tube with CuO and heated to ~900 °C for 24 hours to oxidise contaminants. Then it is placed into a pure O_3 environment and treated with UV light in the UV-O_3 chamber to further purify for 24 hours prior to use. The samples are wrapped in Pt because it expedites the combustion of CH_4 and CO to CO_2 as well as catalysing the decomposition of nitrous oxides to N_2 (Boyd et al., 1988) that would otherwise lead to low temperature mass dependant stable isotopic fractionation (i.e. ^{15}N fractionation between nitrous oxides and N_2) as well as produce isotopologues that would interfere with analysis (i.e. both CO and N_2 have a mass of 28).

The diamonds are placed into a clean glass beaker and filled with ultra clean propanol and incubated in an ultrasonic bath for 40 mins. The samples are then weighed (to ensure 100 % yield is achieved during combustion) and wrapped in Pt foil. The Pt foil bearing diamond is then wrapped in Al foil for transport from the clean room to the Finesse machine.

Figure 3.8 displays the schematic layout of the sample loading system. Firstly one must ensure that glass valve 2 is securely sealed as to not expose the system to the open atmosphere, before removing glass valve 1. Due to the time taken to pump down the sample loading section (1 hour) it is advised that more than one sample is loaded at a time. The last sample that is to be analysed is placed in the sample loading section first and moved to the storage sub-section (see figure 3.9), this is done by moving the metal pusher from outside the loading chamber using a magnet. Once all of the samples are loaded (the maximum advised is 3) the sample loading chamber is pumped down using the turbo pump connected to manual valve 6 (figure 3.1). Once the turbo pump has evacuated the majority of the atmosphere from the loading section, manual valve 3 is opened to allow the system to be pumped back to the acceptable baseline through the back line (circa 10^{-8} mbars) so as

not to contaminate the main line or trip the Ion pumps. The gate valve, which separates the high-vacuum combustion section from the loading section, is a unique valve for the Finesse assembly in that it opens up to a size large enough for a sample to be passed through (roughly 5 mm)- the thickness of the quartz tube) and provide a high-vacuum seal during pumping of air from the loading system (figure 3.9).

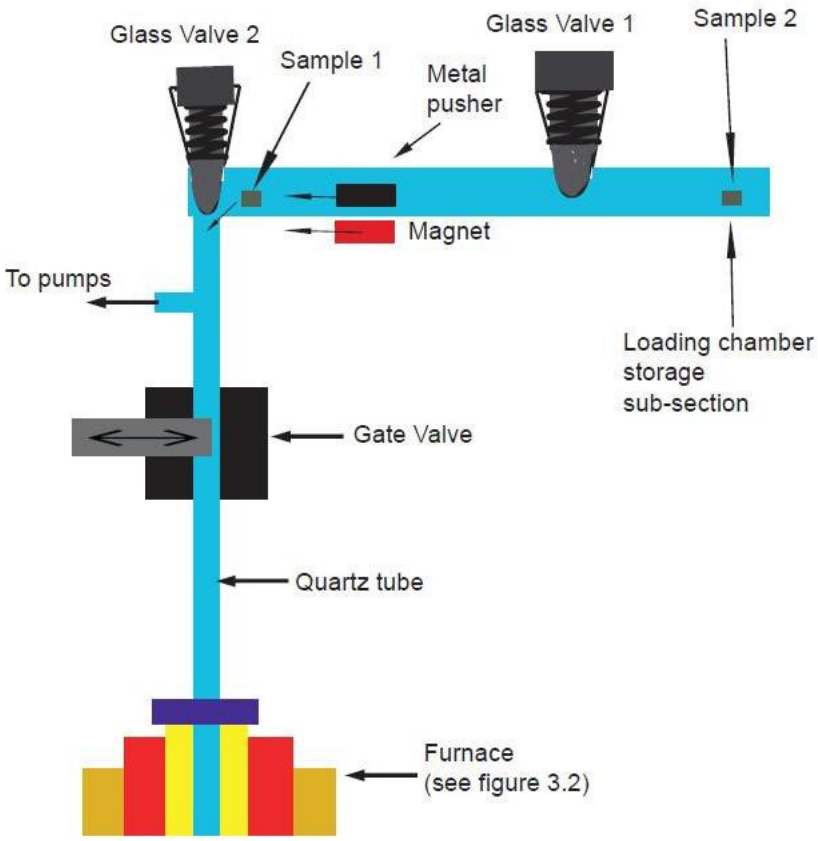

Figure 3.9. Sample loading assembly (not to scale).

3.3.2 Combustion sequence

The samples are combusted at the required temperatures (usually between 800-1400 °C for diamond) in a pure O_2 environment. The O_2 is generated by heating a CuO powder to >850 °C

(maximum 920 °C depending on the pO_2 generated by the CuO at 850 °C). Once combustion is complete, that is reached the allocated amount of time specified by the operator, excess O_2 is removed by cooling the CuO powder to 600 °C for 20 mins and then to 450 °C.

3.3.3 Gas purification (CO_2 and N_2 separation)

This section comprises of a molecular sieve variable temperature trap (MS), CuOcl finger and a cryogenic trap (figure 3.10). Once combustion has ceased and the CuO is <500 °C (not releasing O_2) the cryotrap begins cooling to -160 °C, once this is achieved valves 4 and 16 are closed and 2, 5 and 8 are opened and the CO_2 gas is transferred into the CO_2/H_2O cryotrap in the gas separation/purification unit. Nitrogen is not condensed on the cryotrap. The next step is to collect nitrogen on the molecular sieve at LN temperature. For that the valve 11 is opened when the transferring of CO_2 is completed and the temperature of the cryotrap is kept low to prevent CO_2 from being released. All non-condensable gases are pumped away from the combustion and cleanup sections trough valve 4. (see Fig 3.1 and 3.10). Then, valves 2, 8 and 11 are closed, the combustion section is set for the next temperature step and the CO_2 and N_2 are ready for further processing.

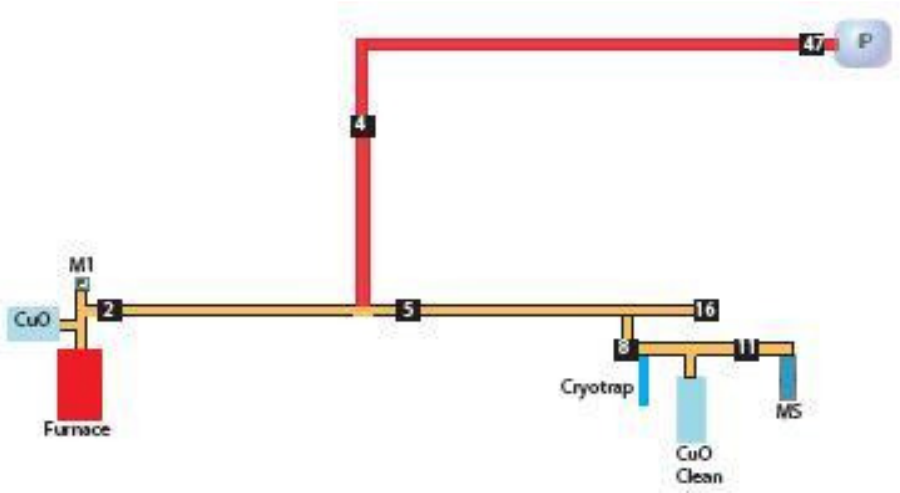

Figure 3.10. The gas separation/purification unit. Components as in figure 3.1.

3.3.4 Carbon measurements

The sections of the Finesse machine used for C measurements are shown in figure 3.11. The technique for analysis is detailed in the forthcoming sub-sections.

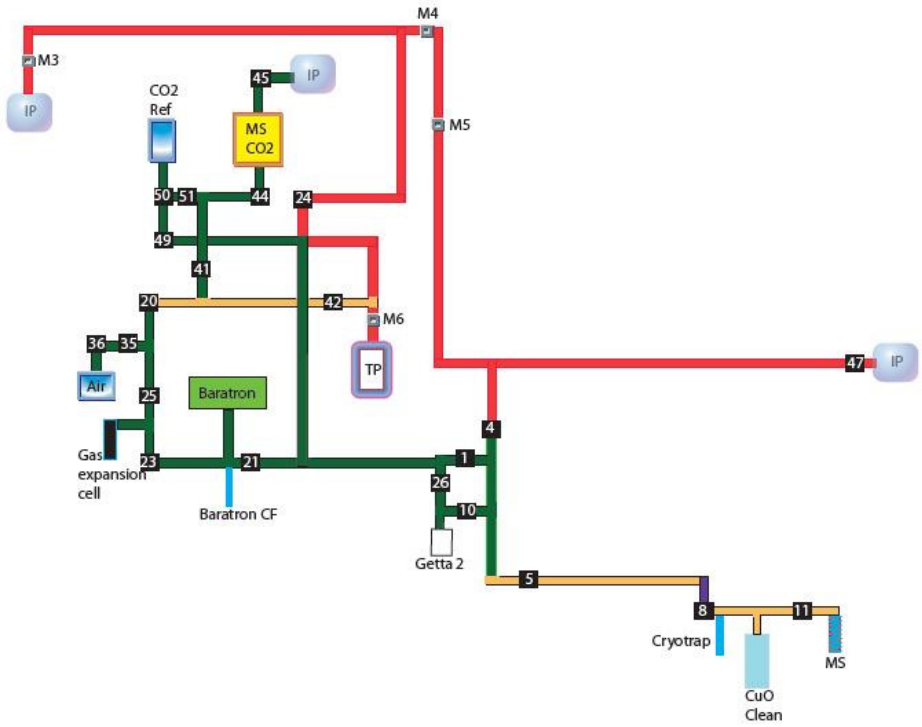

Figure 3.11. The sections used for C measurements (colours as in figure 3.1).

3.3.4.1 Gas abundance

By this point CO_2 and N_2 are duly separated and stored in different sections (section 3.3.3). Valve 11 remains sealed to the MS isolating the N_2 gas. The next stage is to determine the C abundance and isotopic composition. Determining the amount of C is achieved using the baratron. To do this the cryotrap is heated to -60 °C to transfer the gas to the baratron cold finger which is cooled to liquid nitrogen temperature. The transfer is achieved by opening valves 8, 5, 1 and 21 and closing valves 24, 20, 23, 4 and 42. This allows for the transfer of the CO_2 gas to the baratron section whilst retaining the H_2O, which is later removed and pumped away by heating the cryotrap to +60 °C and opening the line up to the main line ion pump via valve 4. The CO_2 is transferred into the baratron and the abundance determined with an accuracy of ± 1 % (figure 3.5) using the calibrated capacitance manometer.

The CO_2 gas is 'split' into smaller aliquots to avoid saturation of the mass spectrometer. This is achieved by gas expansion chamber between valves 25 and 23, piping between valves 25 and 20, and the baratron section itself. Once the CO_2 gas has an appropriate volume (1 ng CO_2) it is expanded and stored between valves 55, 44 and 41 (see figure 3.11). During analysis some CO_2 is stored in these sections just in case the analysis fails (mechanical or computational), this gas can then be analysed by performing the analysis in manual mode as an insurance policy. The final aliquot to be analysed on the mass spectrometer is held in the section between valves 41, 44 and 51.

3.3.4.2 Carbon isotopic determination

The $^{13}C/^{12}C$ ratio is not determined directly as it is impossible to have elemental C as a gas or liquid for any length of time longer than 1 nanosecond, as the temperatures required exceed 50,000 K (Eggert et al., 2010). Instead, these determinations can be performed with great accuracy and

simplicity by measuring the mass of CO_2 gas (Craig, 1953). The isotopologues of importance for CO_2 are $^{13}C^{16}O_2$, $^{12}C^{16}O^{17}O$, $^{12}C^{16}O_2$, $^{12}C^{16}O^{18}O$, $^{12}C^{18}O^{17}O$ that correspond to masses 45, 44 and 46. Therefore the ratio of masses 45/44 and 46/44 are measured using a triple collector mass spectrometer.

The C mass spectrometer then performs a 'zero' measurement to subtract the background from the sample and reference gas. The sample CO_2 gas is transferred to the C mass spectrometer by a simple expansion via valve 44 (when valve 45 is shut) and the ratio of masses 45/44 and 46/44 are measured. Once this is completed and the sample gas is pumped away from the MS to the Ion pump (IP) an aliquot (similar amount to the sample gas) of the reference gas is fed into the C mass spectrometer. The size of the reference gas aliquot is achieved by using the technique outlined in section 3.2.3. If the size of the reference aliquot does not match that for the sample gas within 5%, a new aliquot is taken with a corrected size. The isotopic composition ($^{13}C/^{12}C$) is determined relative to the reference gas corrected using international standards (appendix Table A4) then normalised to $\delta^{13}C$ relative to the Pee Dee Belemnite (where PDB $\delta^{13}C$ = 0 ‰).

3.3.5 Nitrogen measurements

The sections of the Finesse machine used for N measurements are shown in figure 3.12.

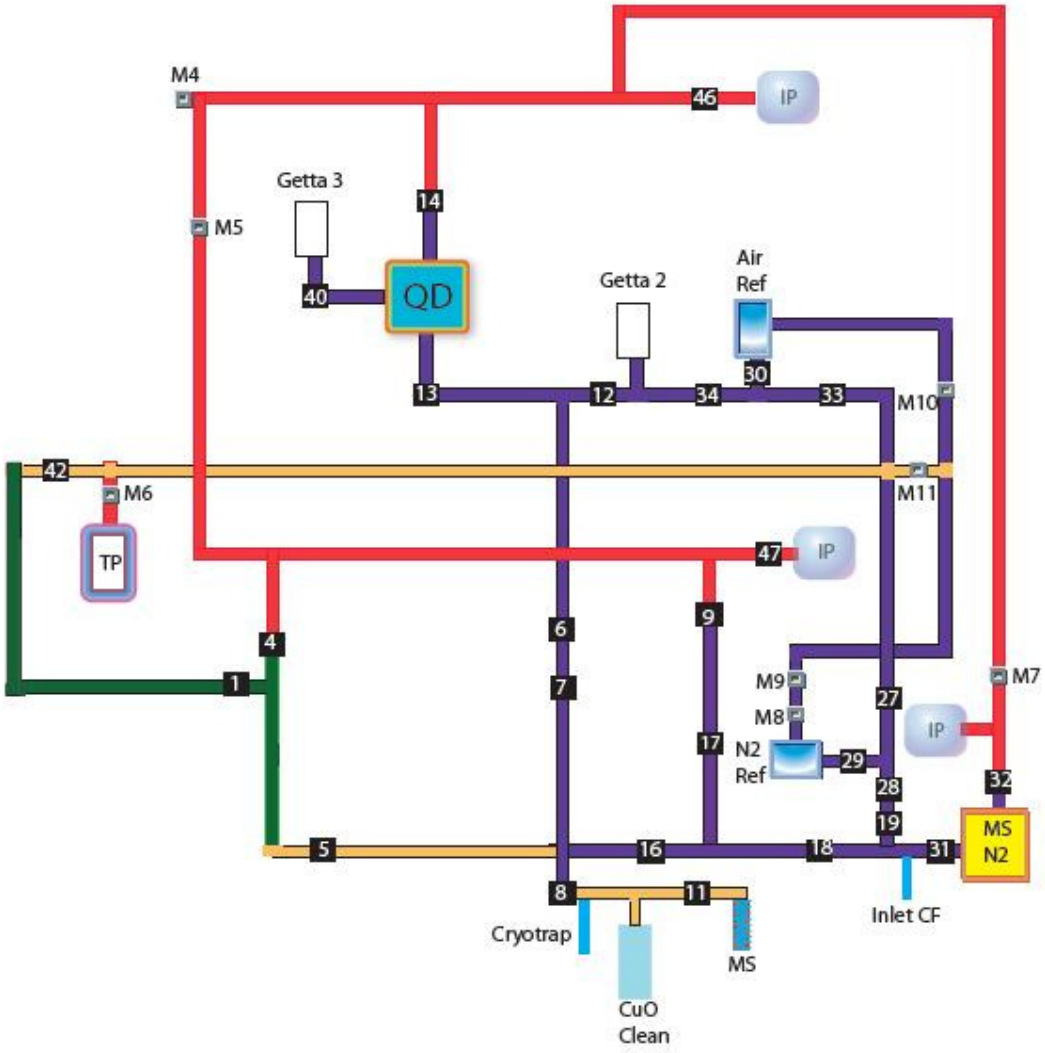

Figure 3.12. The sections used for N measurements (colours as in figure 3.1).

3.3.5.1 Gas abundance

Once the CO_2 + H_2O is removed from the cryotrap the MS begins heating to 250 °C to liberate the N_2 (+ CO and noble gases) and the CuOcl is heated to 800°C to oxidise CO to CO_2 and remove any residual O_2. After cooling the CuOcl to 450 °C and the cryotrap to -140 °C (to keep CO_2 level as low as possible), nitrogen abundances are first measured using the quadrupole mass spectrometer. This is achieved using the intensity of mass 14 (^{14}N) because the background for this mass is extremely low and not affected by $^{12}C^{16}O$ (mass 28). The aliquot of gas is of a known volume (~5% of the total) by using the piping space between valves 6 and 7 calibrated using the reference gas according to bleed time (section 3.2.3). This is not a very accurate determination of the mass of nitrogen and is solely used to gauge the rough amount of gas. This enables the correct amount of splitting to be performed.

The mass of nitrogen (ng) is determined in the N MS (figure 3.12) and calibrated against the reference gas. Once split a fraction of gas is always stored in a cleanup section, as with carbon, just in case the analysis fails (mechanical or computational), this gas can then be analysed by performing the analysis in manual mode as an insurance policy. The nitrogen gas to be analysed is usually stored in between valves 19, 18 and 31 where the inlet finger is cooled to liquid nitrogen temperature to condense any condensable gases and further purify the N_2 to be analysed (however this can vary depending upon the amount of N_2 from the sample but need not be discussed further here). The N MS performs a '0' measurement (empty mass spectrometer) to subtract the background from the sample and reference gas.

3.3.5.2 Nitrogen isotopic determination

The carbon and nitrogen mass spectrometers process the data using the same multichannel digital multimeter and therefore the carbon measurements must be finished before the nitrogen measurements can begin. Having two multimeters would avoid this time consuming factor.

The $^{15}N/^{14}N$ ratio is determined using the same principles and procedures as for C isotopes but with a different mass ratio (29/28 that corresponds to N_2 as $^{14}N/^{14}N$ and $^{15}N/^{14}N$) intensities calibrated against the reference gas, and corrected using the reference gas (AIR) as a standard, then expressed as $\delta^{15}N$ relative to AIR on a different mass spectrometer. The inlet cold finger is also cooled to the LN temperature during reference gas measurement as a means to remove condensable species.

The fixed-volume air standard used for the calibration of nitrogen sensitivity (see section 3.2.3) is used to calibrate the reference gas $^{15}N/^{14}N$ composition (figure 3.8). The reference gas $^{15}N/^{14}N$ composition is originally the same as air ($\delta^{15}N$ = 0 ‰). However owing to the long-term continuous bleeding over time, the reference gas becomes fractionated (^{15}N rich). This is taken into account by running regular calibrations with the air reference gas. The reference gas is of a similar aliquot size to that of the sample gas.

3.4 Blank levels in the inlet system and furnace

Having the system fully automated with metallic piping for the nitrogen section enables the blank levels to be extremely low, and importantly, stable. When quantifying the blank levels in the system the procedure is identical to that of a sample run with the only exception being that no sample is used. The Pt foil is treated the same and the entire pyrolysis/combustion sequence (temperature steps and duration) is mirrored.

The majority of diamonds in this thesis have low nitrogen concentrations and are termed type II (having no detectable N using FTIR). The effects of the nitrogen blank for samples with a mean nitrogen concentration of circa 500 ppm (polycrystalline diamonds in chapter 6 and analysed in 2009) is not an issue, whereas it is a defining issue for those with mean nitrogen concentrations of 15 ppm (Dachine in chapter 5 and octahedral type II's in chapter 4 that were analysed in 2010). Therefore the focus on the blank discussion uses the blanks from 2010.

3.4.1 Carbon

The contribution of the $^{13}C/^{12}C$ ratio from the blank to the sample CO_2 gas is negligible for this PhD thesis. This is because the blank levels for carbon are always <50 ng. The stepped combustion data *in this thesis* mainly discusses the analysis of diamond where the minimum amount of carbon released from diamond combustion is 25,500 ng (maximum percentage of CO_2 analysed being blank = 0.39 %; average amount of carbon released 156,000 ng with σ of 71,000 ng where n = 76 analyses). Therefore, irrespective of the blank $^{13}C/^{12}C$ ratio, the measured CO_2 gas will reflect the $^{13}C/^{12}C$ ratio of the diamond and requires no secondary corrections for blank contribution with regard to the analysis of diamonds.

3.4.2 Nitrogen

Two different procedures were tested in this study. One (March-April 2010) used a stepped combustion sequence where diamond samples were combusted from 700-1400 °C with 100°C increments and run blanks accordingly. In the second session (August 2010) I tested the feasibility of performing multiple steps at 1100 °C for the following two reasons. 1- The majority of diamond combustion occurs >1000 °C thus this approach may save time; 2- keeping the furnace at a set temperature that is not too high increases the lifespan of the furnace (by reducing the temperature gradient during a run) as well as reducing the diffusion of atmospheric N_2 (relative to temperatures between 1200-1400 °C). This may reduce the blank increase (in grams) over time and increase isotopic stability as a function of the reduced diffusion of atmospheric N_2 into the furnace at high temperatures. Noteworthy is that the blank has several sources, not only originate from the furnace. Over time the pipework, CuO/CuOcl, MS, cryotrap and inlet CF can all contribute nitrogen to the blank. Also there may be leaks of various degrees; a small enough leak could go un-noticed for some time as the pumping system may not produce a pressure increase. This would add atmosphere into

the system (>78 % N_2) which would contribute to a higher blank. The full data set for the blanks are shown in the appendix (Table A5).

3.4.2.1 Blank stability vs. time

During these two time periods I measured the blank every two sample runs. The data for low nitrogen diamonds in this study was accumulated in two separate lab session separated by 3 months in March-April and August 2010. During March-April 2010 the mean mass of the nitrogen blank was 0.44 ng (σ = 0.24 with n = 54 individual combustion steps see figure 3.13) and during August 2010 the mean mass of the nitrogen blank was 0.61 ng (σ = 0.23 with n = 24 individual combustion steps see figure 3.13). The increase on the mass of the blank with time is not strongly reflected in the period of analysis (circa 1 month) (figure 3.13). What is consistent is that the blanks during this time period were always <1 ng of nitrogen with no obvious increase during the periods of data acquisition. This is required for the determination of the $^{15}N/^{14}N$ ratios of type II diamonds where a sample of diamond with 10 ppm and weighing 0.2 mg will only contain 2 ng of nitrogen.

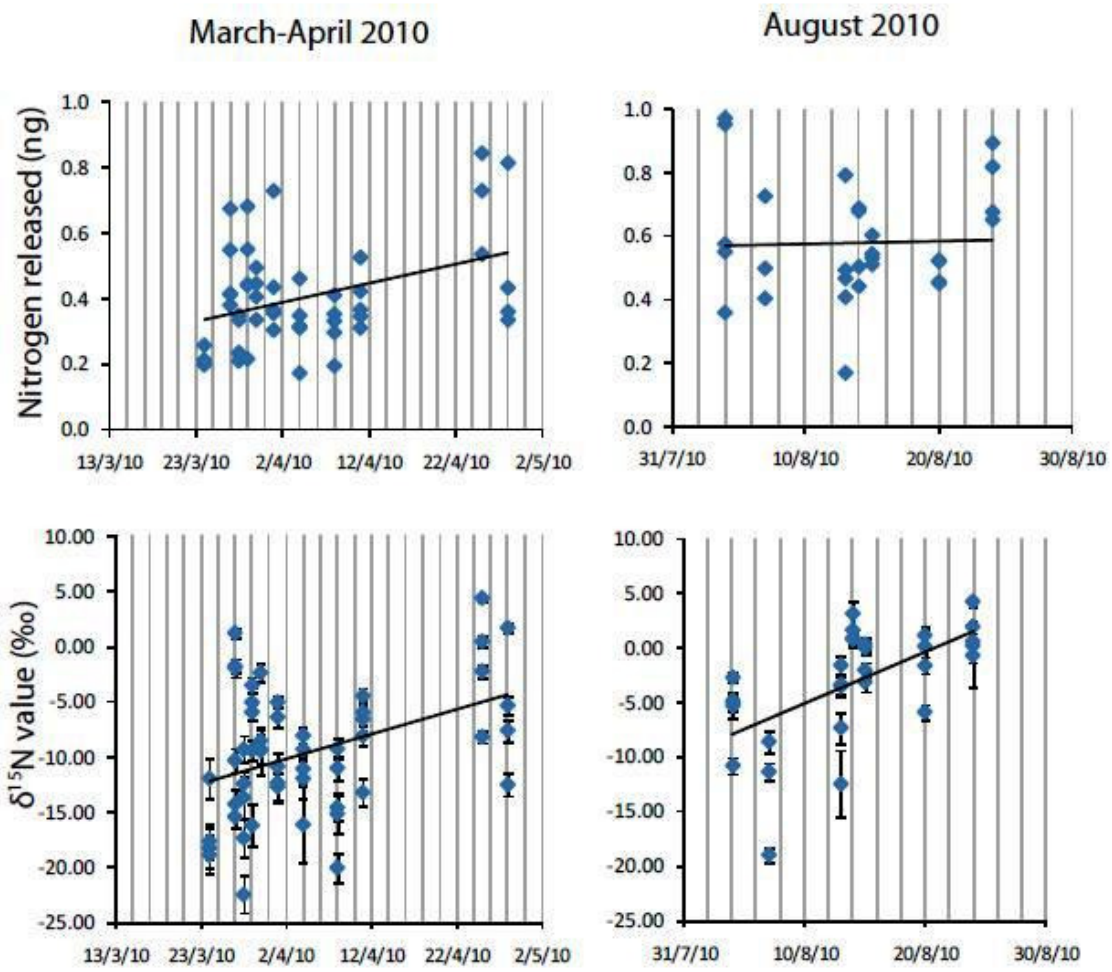

Figure 3.13. Left is for March-April 2010 and right is for August 2010. All of the X axes are labelled with dates using the system Day/Month/Year. The graphs on the top show the variability for the mass of N (ng) for multiple steps on the same day. The graphs on the bottom show the variability for $\delta^{15}N$ values (‰) for multiple steps on the same day.

3.4.2.2 Blank stability (isotopic) vs. time

Despite the lack of a blank level increase due to diffusion of atmospheric N_2 through the quartz furnace over the analytical time period (figure 3.13 top), there is tentative evidence of atmospheric N_2 gas diffusing into the furnace over time (see Fig 3.13 for August 2010). This is because the pyrolysis step employed to clean the sample (see chapter 4) also cleans the furnace and restores the low blank. The blank is typically negative in its $\delta^{15}N$ value, because of the diffusion of atmospheric N_2 into the quartz furnace the blank $\delta^{15}N$ value is a variable and in August tended to get heavier with

time (figure 3.13 August 2010). If this function is ignored and not monitored and implemented into the blank correction procedure, the removal of the blank $\delta^{15}N$ value would be incorrect and therefore the final blank-corrected $\delta^{15}N$ value of the sample would also be false (see chapter 4 section 4.4.2).

3.4.2.3 Blank stability vs. temperature

Figure 3.14 demonstrates that the neither the $\delta^{15}N$ value nor the nitrogen mass (ng) is strongly influenced or affected by the combustion temperature used during March-April 2010. Therefore any potential effect that the temperature of the combustion step may have with blank concentration or $^{15}N/^{14}N$ value can be ruled out.

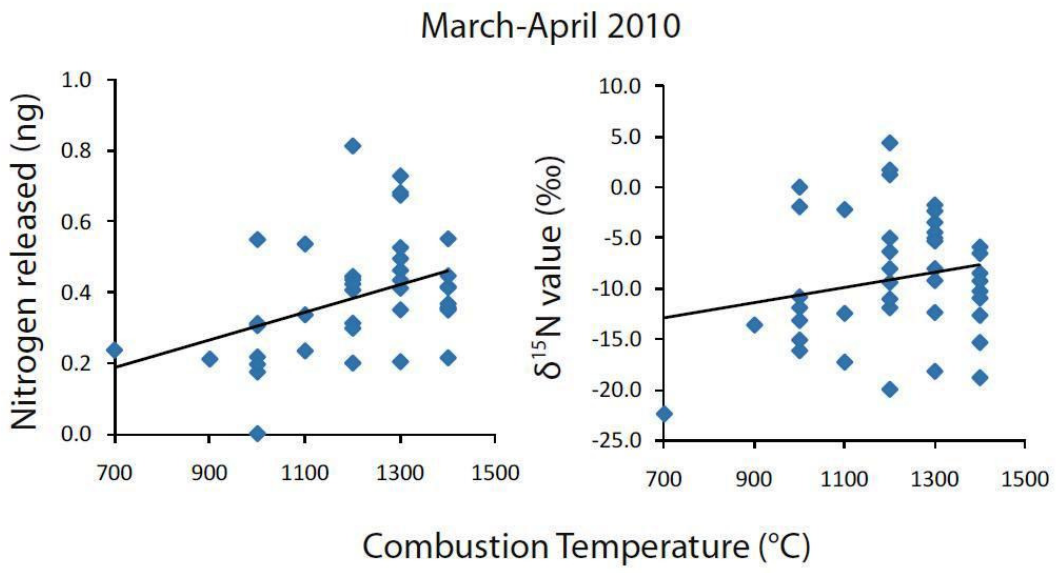

Figure 3.14. These graphs show the lack of any notable correlations for combustion temperature and mass of N (left) and $\delta^{15}N$ value (right).

3.4.2.3 Collector sensitivity vs. error

Having low blanks also has a negative effect. As figure 3.15 demonstrates, the lower the amount of N_2 (in ng), the larger the standard error becomes on the blank due to the sensitivity of the faraday cups (collectors).

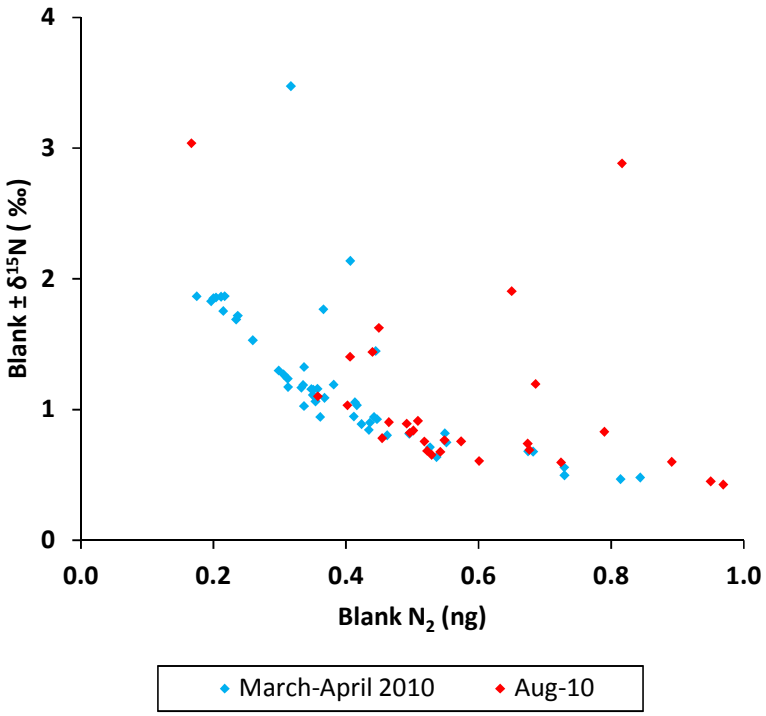

Figure 3.15. The correlations between the mass of the N blank and the precisions on the $\delta^{15}N$ (± ‰) for the measured N blank. Noteworthy is the increase in the uncertainties relative to the reference gas with decreasing amount of gas.

3.5 Concluding remarks

This facility is capable of analysing both reduced (by combustion) and oxidised (by thermal decomposition) samples in a fully automated mode where the operator needs only to tend to the LN Dewar, should the analysis require more combustion/pyrolysis steps that a filled Dewar can

accommodate. This is dependent upon the volume of the Dewar and/or the amount of individual analytical steps for the analysis, which can be a function of sample size of the nature of the analysis.

This makes the determination of the carbon and nitrogen isotope values in natural and synthetic diamonds less time consuming (about 12 hours for a type II sample of 0.5 mg) than an un-automated facility where a single sample of comparable size (0.5 mg) will require about 24 hours to run with an operator present *at all times* (see BOYD et al., 1998 for a discussion). This facility can perform these analyses in 12 hours for 7 stages of combustion and requires no operator assistance. However, regular checks by the operator are advised. This is because malfunctions can arise, typically freezing of water in the LN pipework. This results in the analysis being paused by the computer controller and the potential for 7 hours to pass by with no data being acquired, which does happen.

Upon noticing the consistency of these low blanks for nitrogen in the Finesse and the definition of type II diamonds being 'no *detectable* nitrogen using FTIR', I proposed the following question 'can I determine the $\delta^{15}N$ values of type II diamonds with a reasonable error?' The scientific importance of this question and the results of this question/endeavour are presented in the following chapter.

Chapter 4

Determining the $\delta^{15}N$ values in spectral type II diamonds

The work in this chapter was inspired by the first lesson taught to me by Prof Matthew Thirlwall during my M.Sc at Royal Holloway between September 2006 and September 2007, this can be summed up in a quote from himself:

'There are no zeros in geochemistry; there are merely limits of detection and quantification'

4.1 Introduction

Mantle diamond is sub-divided using various criteria such as inclusion geochemistry, morphology, and the presence, absence and state of lattice-bound nitrogen and boron (chapter 2, section 2.6). The classification using lattice-bound nitrogen can be over-simplified into two groups that are commonly (and wrongly) described as nitrogen-bearing and nitrogen-free: Type I and Type II respectively. Specifically, Type II is defined as *no detectable nitrogen using FTIR spectroscopy* (PEARSON et al., 2003), and not nitrogen-free (as it was in recent works such as BULANOVA et al., 2010; CARTIGNY, 2010). FTIR, in general, cannot detect nitrogen where the concentrations fall below about 30 ppm on average (MENDELSSOHN and MILLEDGE, 1995a).

The aim of this chapter is to detail the precision on blank-corrected $\delta^{15}N$ determinations for small (< 0.5 mg) samples of Type II diamonds using the Finesse machine at the PSSRI, Open University (discussed in chapter 3). This enables me to compare the range of $\delta^{15}N$ values for low $\delta^{13}C$ Type II diamonds with Type I diamonds from the literature that exhibit mean mantle $\delta^{13}C$ values (circa -5 ± 3 ‰; shown in figure 4.1). In the next chapter I use the $\delta^{15}N$-$\delta^{13}C$ systematics for monocrystalline diamond from the Dachine volcaniclastic deposit in French Guyana as a means to understand the origin of the diamond-forming carbon. Specifically as their mean $\delta^{13}C$ values are circa -24 ‰ (and the

mean mantle value is -5 ‰) with 97 % of the diamonds classified as Type II (Cartigny, 2010). Therefore, before attempting to determine the $\delta^{15}N$ values of type II diamonds with low $\delta^{13}C$ values (i.e. Dachine), I need to know the range of $\delta^{15}N$ shown from spectral type II diamonds with mean mantle $\delta^{13}C$ values. To do this I have used several octahedral mantle diamonds determined as type II using the FTIR facility at the department of Earth Sciences, UCL.

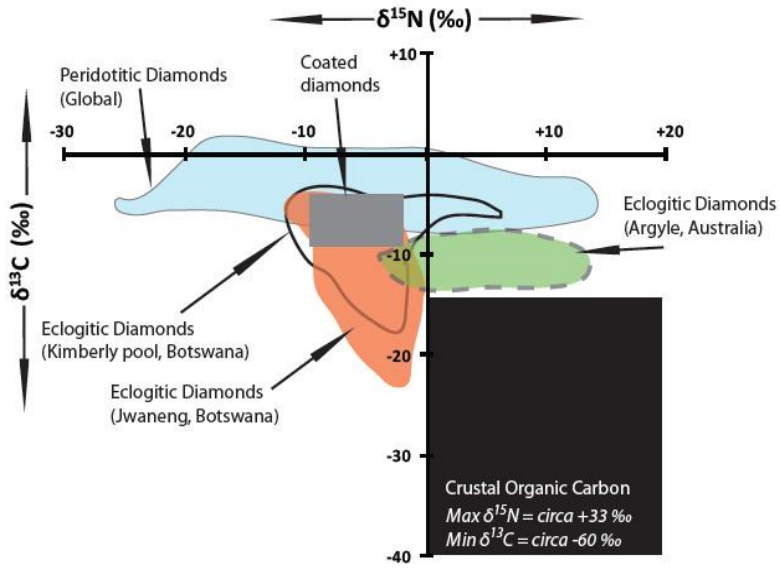

Figure 4.1. This variation diagram illustrates the fields occupied in coupled $\delta^{15}N$ vs. $\delta^{13}C$ space for various diamonds groups; Peridotitic (CARTIGNY et al., 1997; CARTIGNY et al., 2004), coated (BOYD et al., 1994), eclogitic (CARTIGNY et al., 1998a; CARTIGNY et al., 1998b) and the range for crustal organic carbon which extends to +30 for $\delta^{15}N$ (HOEFS, 2009; THOMAZO et al., 2011; 2009).

4.2 Samples

The samples used in this chapter are from several localities (4 cratons) and are shown in table 4.1. These samples are as follows: 5 are from the Cullinan mine, Kaapvaal craton South Africa; 3 are from Mir pipe, Siberian Craton, Russia, and 2 are from West Africa, Sierra Leone. All of these samples are from the personal collection of Dr H Judith Milledge (emeritus reader of Crystallography UCL). I have also acquired 7 sublithospheric samples from Juina, Brazil, Amazonia from Dr Mark Hutchison, Trigon GeoServices.

The full set of results for the diamonds from Dachine are presented and discussed in the next chapter of this thesis (chapter 5). Some data from the diamonds from Dachine are also used here to demonstrate the process of blank correction and the error propagation as a measure to expand the sample set in the discussion of errors (blank-corrected per mil precision on $\delta^{15}N$ values and their associated nitrogen concentrations).

Name	Juina 5	Cullinan	Mir	WestAf	Dachine
Amount	7	5	2	3	20
Craton	Amazon	Kaapvaal	Yakutia	West Africa	Amazon
Source rock	Alluvial	Kimberlite	Kimberlite	Ukn	Talc schist
Age of deposit	Mesozoic	Proterozoic	Proterozoic	Ukn	Proterozoic

Table 4.1. Details of type II diamonds used in this chapter. The information for the Juina samples comes from Hutchison et al (1997); the information regarding the Dachine samples is from Smith et al (SMITH et al., In Prep 2011) and the remaining information is from Dr H.J Milledge pers comm. (2009).

4.3 Analytical techniques

This chapter utilises two analytical techniques; FTIR and gas sourced mass spectrometry (the Finesse machine- chapter 3). Type II diamonds are commonly indistinguishable from type I diamonds in optical appearance. However, nitrogen is a lattice-bound impurity in natural diamond and is easily detected using Infra red absorption spectroscopy (FTIR); therefore an absence of detectable nitrogen is also easy to observe. I use FTIR absorption spectroscopy to identify the type II diamonds and characterise the sample suites, I then determine their $\delta^{15}N$-$\delta^{13}C$ values and nitrogen concentrations of the samples simultaneously using the Finesse machine.

4.3.1 Infra red absorption spectroscopy

Infrared absorption spectra were collected using a Vector22 Fourier Transform Infrared (FTIR) spectrometer at University College London (MENDELSSOHN and MILLEDGE, 1995a; 1995b). The spectrometer is equipped with a HeNe laser (633 nm) a KBr beam splitter, and a Brukker IR Scope-1 microscope. Absorption spectra were recorded in transmission with a resolution of 2 cm^{-1} in the range 4000 to 670 cm^{-1} with one spectrum being the average obtained from 200 scans with a spot size of 16 µm.

4.3.2 Identifying type II diamonds

To determine a diamond as type II no standards are required to correct the data. All that is required is an absence of any absorption between wave numbers 1000-1400 cm^{-1} with the characteristic absorption peaks and trough for diamonds being displayed between wave numbers 1400-2500 cm^{-1} (see figure 4.2).

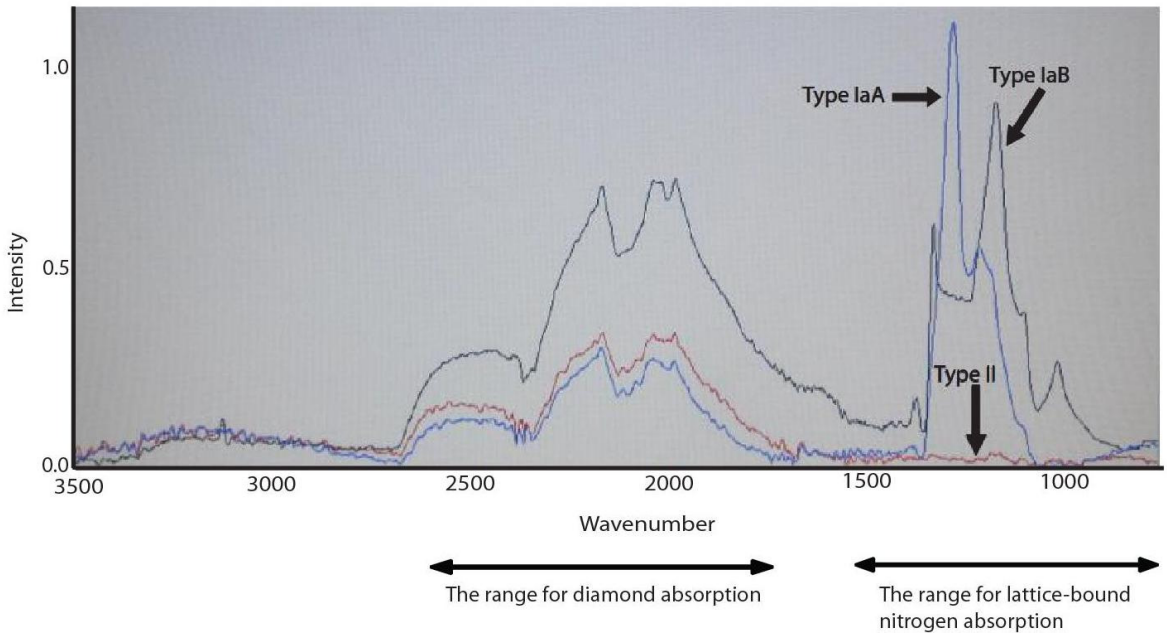

Figure 4.2 Baseline-corrected IR absorption spectra for lattice-bound nitrogen in diamond showing the different spectra relating to the different types of nitrogen bonding within diamonds. Also shown is the shape of a type II spectra (for a detailed discussion on the diffusion of nitrogen in diamonds and the speciation within mantle diamonds see MENDELSSOHN and MILLEDGE, 1995a; 1995b).

4.4 Results

Nitrogen is a trace element in diamond and therefore one must question the origin of the N_2 gas measured at the collectors post-combustion and purification. There are 3 possible sources: contaminant, blank, and sample. If I can rule out a significant contribution of $^{15}N/^{14}N$ from the contaminant and blank, then I can determine the $^{15}N/^{14}N$ of the sample. Therefore the following sub-sections address the removal of the contaminant and blank nitrogen from the sample data.

4.4.1 Removing N contaminants using pyrolysis

The first step in determining the nitrogen concentration and $^{15}N/^{14}N$ composition in diamonds is to remove the contaminants from both the diamond and the Pt foil. The samples are cleaned in propanol prior to weighing and wrapping in Pt foil. Then once the samples are loaded I further reduce the amount of contaminants in the analysis by employing a pyrolysis step at 1100 °C prior to the combustion sequence. This is employed to de-volatilise any non-lattice-bound nitrogen (ammonia and ammonium) into $4H_2$ and N_2 (Shelkov, 1997). Table 4.2 gives an example of the amount of N_2 produced during pyrolysis and the subsequent N_2 produced by combustion of the Pt foil and type II diamond that outlines the amount of contaminant on the clean Pt foil. This demonstrates, without this secondary cleaning step the N_2 signal received by the mass spectrometer would be heavily dominated by a contaminant. Once this step is finished a second pyrolysis step is employed at 500 °C to allow the furnace to re-equilibrate before the main combustion sequence begins.

Sample	DAC 45-6 Diamond		DAC 105 Diamond		Blank Pt Foil		Blank Pt Foil	
	Temp °C	N ng	Temp °C	N ng	Temp °C	N ng	Temp °C	N ng
Pyrolysis (cleaning)	1100	10.82	1100	28.30	1100	3.76	1100	11.98
Combustion (analysis)	800	1.23	800	1.52	800	0.44	800	0.17
	1200	9.75	1000	1.49	1200	0.63	1000	0.31
	1400	3.52	1200	2.34	1400	0.76	1200	0.46
	1400	0.82	1250	0.35			1300	0.35

Table 4.2. Results of two diamonds and two Pt foil blank runs where pyrolysis was performed. Note the 'relatively' large release of N_2 during pyrolysis compared to the samples concentrations and blanks. The two samples from Dachine (DAC 45-6 and DAC 105) have N concentrations of 34 and 8 ppm respectively.

4.5 Blank contributions and corrections

4.5.1 Blank corrections

The measured $\delta^{15}N$ value and nitrogen mass is inclusive of the blank ($^{15}N/^{14}N$ for the sample + blank N_2). Therefore one must correct the data for blank contribution and to quantify the $\delta^{15}N$ value and N/C ratio (N ppm) of the sample. The precision for $\delta^{15}N$ calculated using the reference gas correction is not applicable post-blank correction because those errors are inclusive of the blank ($^{15}N/^{14}N$ for the sample + blank). To calculate the precision on the blank-corrected isotopic values of a sample one must know the blank levels, isotopic composition and both the abundance and isotopic variability of the blank over the time period of data acquisition. To measure the $^{15}N/^{14}N$ ratio of a diamond of 0.2 mg mass with 10 ppm N only 2 ng of N_2 is sourced from the sample. Due to this, any blank > 1 ng results in a system bake-out to reduce the blank level. Removal of a known blank $^{15}N/^{14}N$ ratio where the blank mass is less than the sample mass is not a problematic task, so long as the blank is monitored regularly (i.e. the blank being a well constrained variable/parameter). The

blank levels and stabilities are discussed in chapter 3 section 3.4. Herein I discuss and demonstrate the consequences of such mathematical manipulation to the data regarding the uncertainties (in ‰).

4.5.2 Blank correction and errors

The precision on the measured $\delta^{13}C$ value is determined using the reference gas measurements after each sample analysis. For $\delta^{13}C$ there is no need to correct for blank contribution (discussed in chapter 3 section 3.4.1). The precision of the measured $^{15}N/^{14}N$ ratio is achieved using the reference gas and is typically 0.5 ‰. The precision (referred to herein as the error) of the samples $^{15}N/^{14}N$ ratio is greater after the blank correction. There are several reasons for this with one of which being the blank stability (discussed in chapter 3 sections 3.4.2.1 through to 3.4.2.3). Also owing to the low amounts of nitrogen in the samples there is always a high percentage of blank N_2 in the measured gas, given that the blank does not have a constant $^{15}N/^{14}N$ ratio or mass, the deviation of each factor for the blank used to apply the correction will contribute to the propagated error using the following relationships:

1. Blank Correction for Mass (sample N ng) = $N\,ng_m + N\,ng_{bk}$
2. Blank correction for $\delta^{15}N = \frac{((N\,ng_m \times \delta^{15}N_m) - (N\,ng_{bk} \times \delta^{15}N_{bk})) = A}{(N\,ng_m - N\,ng_{bk}) = B}$
3. Therefore $\delta^{15}N = \frac{A \pm \Delta A}{B \pm \Delta B}$
4. $\Delta A = \Delta(N\,ng_m \times \delta^{15}N_m) + \Delta(N\,ng_{bk} \times \delta^{15}N_{bk})$
5. $\Delta B = \Delta N\,ng_m + \Delta N\,ng_{bk}$
6. $\Delta\delta^{15}N = \delta^{15}N_{corr} \times \sqrt{\left(\frac{\Delta A}{A}\right)^2 + \left(\frac{\Delta B}{B}\right)^2}$

Where N ng_m and N ng_{bk} refers to the mass of nitrogen in the measured gas and blank, $\delta^{15}N_m$ and $\delta^{15}N_{bk}$ refers to the $\delta^{15}N$ value of the measured gas and blank, $\Delta\delta^{15}N_m$ refers to the measured error in per mil, $\Delta\delta^{15}N_{bk}$ and $\Delta N\ ng_{bk}$ refers to the standard deviation for the multiple blank analyses.

For the mass and $\delta^{15}N$ value of the blank I use mean values when calculating the size of the uncertainties for the $\delta^{15}N$ value of the sample post-blank correction. This is because of the variability of both parameters during a blank run, as in from step to step and for multiple runs at a constant temperature (chapter 3 figure 3.12). Therefore instead of using the per mil precision of any particular blank determination (± ‰) I used the standard deviation on the mean value of the precision to represent and account for the deviation shown in chapter 3 (figure 3.12). This is because it is non-linear and unpredictable. The measure used to counter this non-linear and unpredictable behaviour was to run a blank every 2 sample runs and calculate the mean values and standard deviations from 2 blank runs for every sample correction.

4.5.3 Percentage of measured N_2 as blank

The less sample N_2 gas generated the more the blank N_2 gas there is measured relative to the sample (blank percentage). This increases the errors post-blank correction according to equation 6 (and precursor equations 1-5). The average blank percentage in this study for March-April 2010 is 25.74 % (σ = 18.82 ‰ where n = 54) and for August 2010 is 33.54 % (σ = 20.91 ‰ where n = 20). The relationship between the blank percentage and the error (‰) is clear and demonstrated Figure 4.3, whereas there is no correlation between the blank percentage and the corrected $\delta^{15}N$ value or the amount of diamond combusted (figure 4.4) or for the blank-corrected $\delta^{15}N$ values vs. N concentrations in these samples (figure 4.5). This gives confidence that despite the relationship between the increase in the error and the percentage blank in Figure 4.3, the mathematical

approach used to remove the isotopic signature of the blank allows for the isotopic signature of the sample to be deduced. Otherwise one should observe a relationship between the amount of N_2 gas measured being blank and the blank-corrected $\delta^{15}N$ values. The blank has a negative $\delta^{15}N$ value (< 0 ‰) whereas the vast majority of the data points from Dachine (figure 4.4) exhibit blank-corrected $\delta^{15}N$ values that are positive, irrespective of the percentage blank.

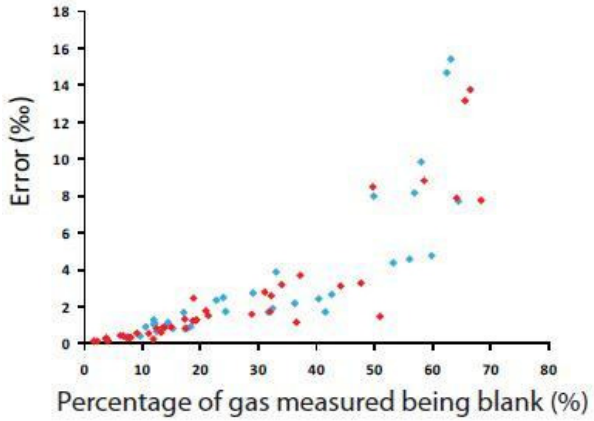

Figure 4.3. The results of the blank-corrected errors vs. the percentage of the measured gas being the blank. The blue data points are for the samples in this chapter and the red data points are for the Dachine samples (discussed in chapter 5). These data are not bulk values, they are the values determined for individual combustion steps as a measure to assess the internal variability for these samples.

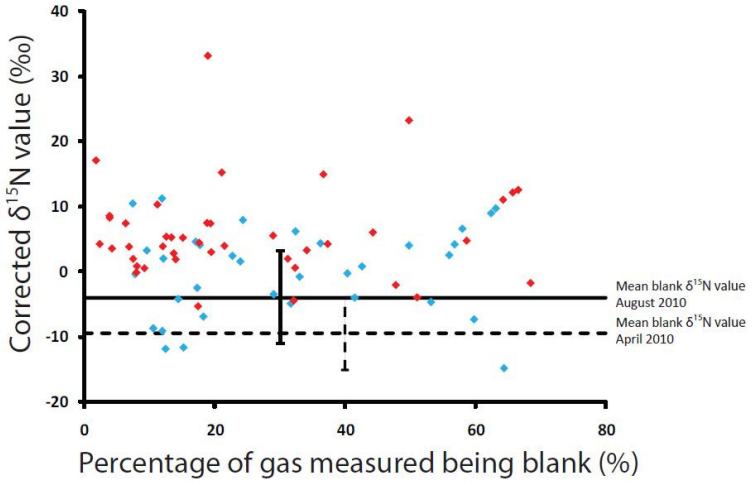

Figure 4.4 blank-corrected $\delta^{15}N$ values vs. the percentage of the measured gas being the blank. The blue data points are for the samples in this chapter and the red data points are for the Dachine samples (discussed in chapter 5). Note the dissimilarity between the mean blank $\delta^{15}N$ values (labelled solid and dashed lines) with the sample values. These data are not bulk values, they are the values determined for individual combustion steps as a measure to assess the internal variability for these samples.

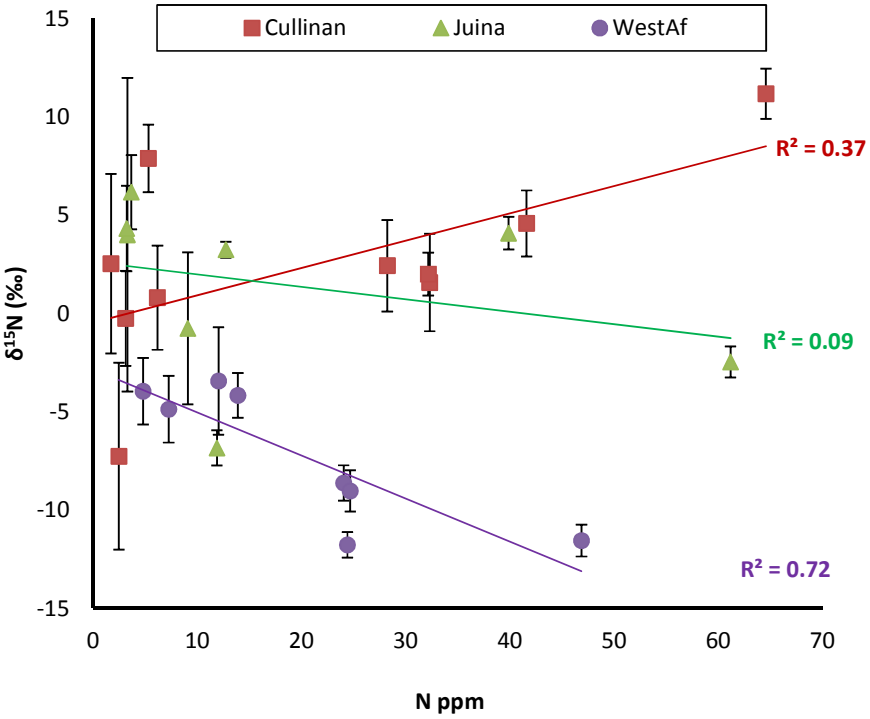

Figure 4.5. This plot presents the blank-corrected $\delta^{15}N$ values vs. the blank-corrected nitrogen concentrations (in ppm) for the samples from Juina, Cullinan and WestAf. Note the lack of any relationship for the 3 populations as a whole; i.e. no linear relationship for blank-corrected ^{15}N values vs. the blank-corrected nitrogen concentrations for the 3 populations collectively. These data are not bulk values, they are the values determined for individual combustion steps as a measure to assess the internal variability for these samples.

4.5.4 N concentrations

There is a direct relationship between the N concentration of the diamonds and the magnitude of the per mil error. The magnitude of the error is controlled by the isotopic stability of the blank and the percentage of the measured gas being blank N_2 acting as the controlling factors.

Post-blank correction I observe a clear and predicable power law relationship between the nitrogen concentration and the size of the errors in parts per thousand (figure 4.6). This is mainly due to the function in figure 4.5 where blank percentage increases the uncertainties in the sample $\delta^{15}N$ value increase owing to removal of a blank with a variable isotopic composition (considered and accounted for by using the standard deviation of the $\delta^{15}N$ value of the blanks).

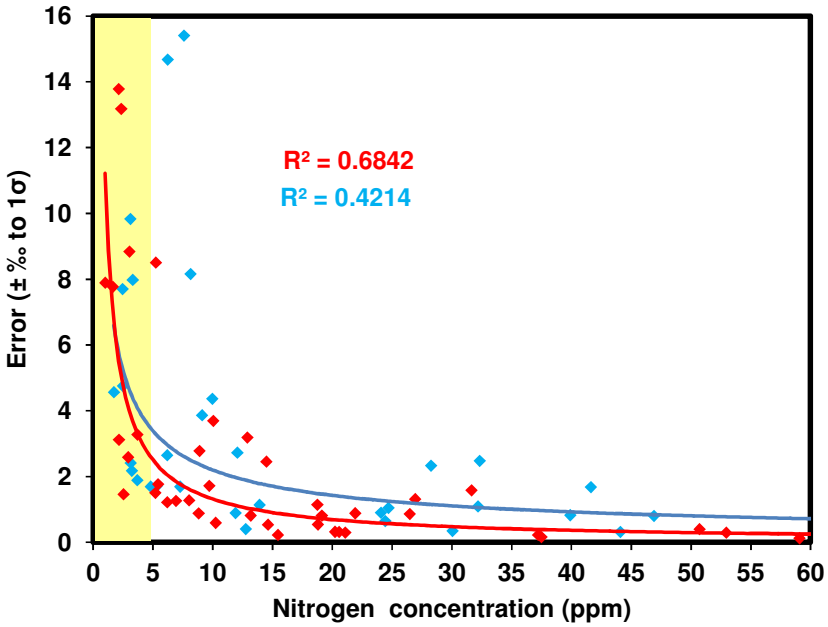

Figure 4.6. This plot demonstrates the power law relationship between the per mil errors vs. The nitrogen concentration of the samples. This figure demonstrates that above 10 ppm the errors are generally < 3 ‰ and < 5 ppm the errors are considerably varied exceed 10 ‰. These data are not bulk values, they are the values determined for individual combustion steps as a measure to assess the internal variability for these samples.

4.6 Discussion

5.6.1 Sample size constraints

Nitrogen concentrations are a dimensionless parameter. Therefore, the mass of nitrogen for a given concentration (in ppm) within a diamond is not constant and varies depending upon the mass of the diamond. A sample of 0.2 mg in mass with 10 ppm nitrogen contains 2 ng of nitrogen, whereas a sample of 1 mg in mass with 10 ppm nitrogen contains 10 ng. The maximum sample size constraints are governed by the volume of the furnace, because this controls the equilibrium state for diamond combustion (the maximum amount of C that can be oxidised to CO_2). A larger furnace has the potential to oxidise more diamond than a smaller furnace because of this function. But as outlined in chapter 3 (section 3.4.2), the furnace is the source for the majority of the blank N_2 gas. Therefore

increasing the furnace volume (size) to enable the combustion of larger samples, may improve the errors on samples with low nitrogen concentrations by increasing the mass of nitrogen analysed for low concentrations. However, this would also increase the blank levels for N_2 and therefore may prove to be counter intuitive, but to what degree remains to be tested. One possibility considered to reduce the blank levels of nitrogen and enable more accurate determination of < 5 ppm in sample sizes, would be to use a furnace made of a material with a higher melting point. This may reduce diffusive processes of atmospheric N_2 simply by being more physically robust between 1000 and 1400 °C relative to SiO_2, for example Al_2O_3.

The sample sizes used to determine the coupled $\delta^{15}N$-$\delta^{13}C$ values ranged from 0.03 to 0.67 mg with an average size of 0.35 ± 0.16 mg (see appendix). The small sample size requirements enable the analysis of very small fragments of rare and therefore scientifically precious diamonds, such as sublithospheric diamonds. The analysis can be achieved using < 0.1 mg of sample, such as 'cut-offs' from diamonds that are laser sectioned to produce windows to their inclusions. This was the case with the Juina samples in this study and several other sublithospheric samples that have been acquired for future analysis as an ongoing project. The next question is what is a reasonable error to resolve terrestrial mantle components?

4.6.2 A reasonable error

A reasonable error is defined by the objective and governed by the range for $\delta^{15}N$ in the system under scrutiny. As discussed in detail in chapter 2 section 2.8.1 (and repeated in brief in figure 4.1) the terrestrial discrepancy for crustal vs. mantle $\delta^{15}N$ is not unequivocal. Despite this the range shown for mantle and crustal reservoirs is such that an error of up to ± 3 ‰ for $\delta^{15}N$ can be sufficient in coupled isotope space (with $\delta^{13}C$) to make a distinction. As well as the distinction between mantle and crustal C and N is the question of primordial $\delta^{15}N$. Javoy et al (1986) postulated that the

primordial $\delta^{15}N$ value should be circa -27 ‰, based on a model of the bulk Earth (BE) being dominated by enstatite chondrite. Values this low have been documented in mantle diamonds from Fuxian, China (Cartigny et al., 1997). Such low $\delta^{15}N$ values can be distinguished from the mean mantle and crustal reservoirs with an error as large as ± 5 ‰.

4.6.3 Type II diamonds as a sub-population?

There is no discrepancy between Type I and Type II diamonds in terms of coupled $\delta^{15}N$ and $\delta^{13}C$ values, i.e. they both seem to fit the mantle range as defined by peridotitic monocrystalline Type I diamonds (figure 4.7). This is contrary to predictions of Moore (2009), which predicted Type II diamonds, as a whole, to be megacryst suites with distinct isotopic values based on a study of Type II diamonds from Cullinan by Milledge et al (1983). Milledge et al (1983) presented multiple $\delta^{13}C$ analyses from 6 Type II diamonds where the majority of the samples had low $\delta^{13}C$ values. The data presented here clearly demonstrates that Type II diamonds from Cullinan can have mean mantle $\delta^{13}C$ values with $\delta^{15}N$ values within the mantle range, thus discrediting the earlier argument of Moore (2009). However, accessing Type II samples from the Cullinan mine that exhibit the low $\delta^{13}C$ values and determining the $\delta^{15}N$ values of said samples would be an interesting study for the future.

Noteworthy is that megacryst diamonds do tend to be Type II dominated (MOORE, 2009), and polishing of diamond (from rough to gem quality) results in the loss of more than double the original mass (Dr G Bulanova pers comm. 2009). Therefore, a detailed study of the coupled $\delta^{13}C$-$\delta^{15}N$ values in megacryst samples from a given mine where the macro diamonds have been studied for coupled $\delta^{13}C$-$\delta^{15}N$ values (i.e. several southern African mines including Orapa- the world's most productive diamond mine) is overdue from an exploration point of view. Especially as this study demonstrates that the amount of sample required to determine the coupled $\delta^{13}C$-$\delta^{15}N$ values in Type II diamonds can be < 0.1 mg.

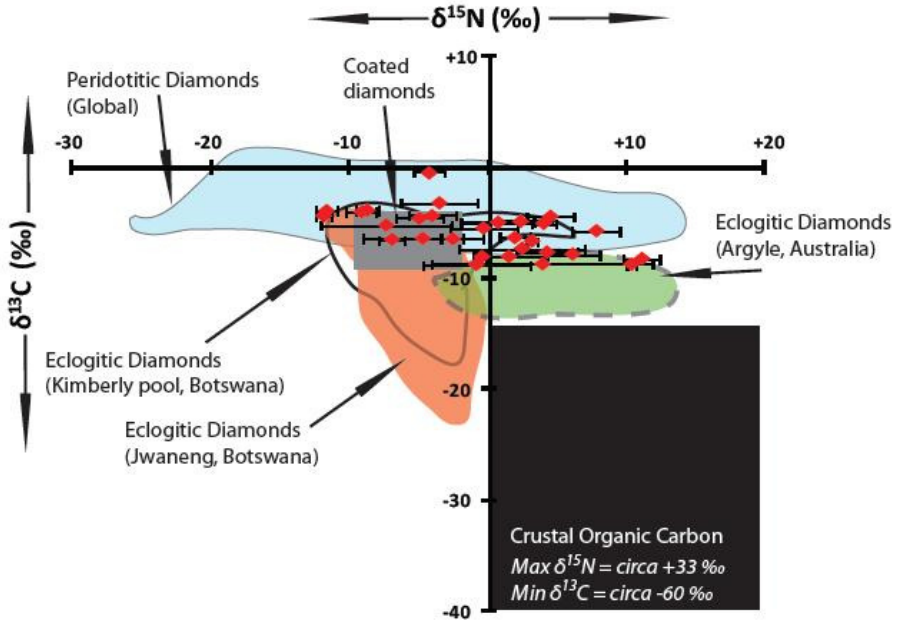

Figure 4.7. This plot compares the coupled $\delta^{13}C$ vs. $\delta^{15}N$ values for the type II samples in this chapter (Dachine excluded) with various types of type I diamonds and crustal organic carbon (references the same as figure 4.1). These data are not bulk values, they are the values determined for individual combustion steps as a measure to assess the internal variability for these samples.

4.7 Concluding remarks

This study demonstrates that the Finesse machine can determine the coupled $\delta^{15}N$-$\delta^{13}C$ values for small Type II diamonds with an average size of 0.35 mg with reasonable errors, routinely.

This opens up several possibilities for future studies such as;

- A full study to determine the coupled $\delta^{15}N$-$\delta^{13}C$ values on a significant number of diamonds originating from the deep upper mantle, transition zone and lower mantle where the abundance of type II diamonds increases. The available data for the N concentration for lower mantle and transition zone diamonds from São Luiz (HUTCHINSON et al., 1997) (alluvial) and Collier 4 (BULANOVA et al., 2010; WALTER et al., 2008) (kimberlitic), both from Brazil as well as alluvial diamonds from Kankan (STACHEL et al., 2002) (Guinea, West Africa) exhibits an

interesting distribution; 88.99 % (n = 109) of the lower mantle diamonds and 50 % (n = 26) of the transition zone (majoritic) are type II. This is in contrast to diamonds from the upper mantle (globally) where type I diamonds dominate (98%, where n = >2500) (CARTIGNY, 2005).

- The low and stable nitrogen blanks enable an evaluation of the coupled $\delta^{15}N$-$\delta^{13}C$ values of mantle peridotite xenoliths, akin to a similar study on the $\delta^{18}O$ values (MATTEY et al., 1994). This would use a well constrained parameter in their $\delta^{13}C$ values (see DEINES, 2002 for a review) to assess the heterogeneity or homogeneity of mantle peridotite $\delta^{15}N$ values to compliment the data base which is mainly comprised of studies of mantle diamond.
- There are also diamonds from Dachine, French Guyana, Amazonian craton that exhibit a high proportion of type II diamonds (97 %) and a mean $\delta^{13}C$ values of -24 ‰ with > 180 analyses (CARTIGNY, 2010). Their paragenesis and the source of their low $\delta^{13}C$ values remain enigmatic. The following chapter presents the coupled $\delta^{15}N$-$\delta^{13}C$ values and nitrogen concentrations of 20 samples of these Dachine diamonds.

Chapter 5

Origin of the diamond-forming carbon in the mantle beneath Dachine, French Guiana: A stable isotope approach

5.1 Introduction

The objective of this chapter is to determine and detail the $\delta^{15}N$-$\delta^{13}C$ values and N concentrations from 1 Type I and 19 Type II diamond samples from the Dachine region of French Guyana (Amazonian craton). I use these constraints to discuss the source of the anomalously low 'organic carbon like' $\delta^{13}C$ values and unusually low nitrogen concentrations exhibited by the Dachine diamond population. The methods for determining the $\delta^{15}N$-$\delta^{13}C$ values and N concentrations has been given in chapter 3 (facility and techniques of acquisition) and chapter 4 (data processing and associated errors for type II diamonds post-blank correction). To begin I shall discuss the diamonds from Dachine in light of their several geochemical characteristics that are un-common for mantle diamonds and highlight the importance of this diamond population for understanding mantle geodynamics.

5.1.1 Unusual characteristics

(A) Host rock

The first un-common characteristic to mention is the nature and geochemistry of the host rock. The diamondiferous Dachine ultramafic deposit is located in an arc-type setting and forms part of the 2.11 Ga Lower Paramaca greenstone belt in southern French Guiana (Bailey, 1999; Capdevila et al., 1999) (shown in figure 5.1).

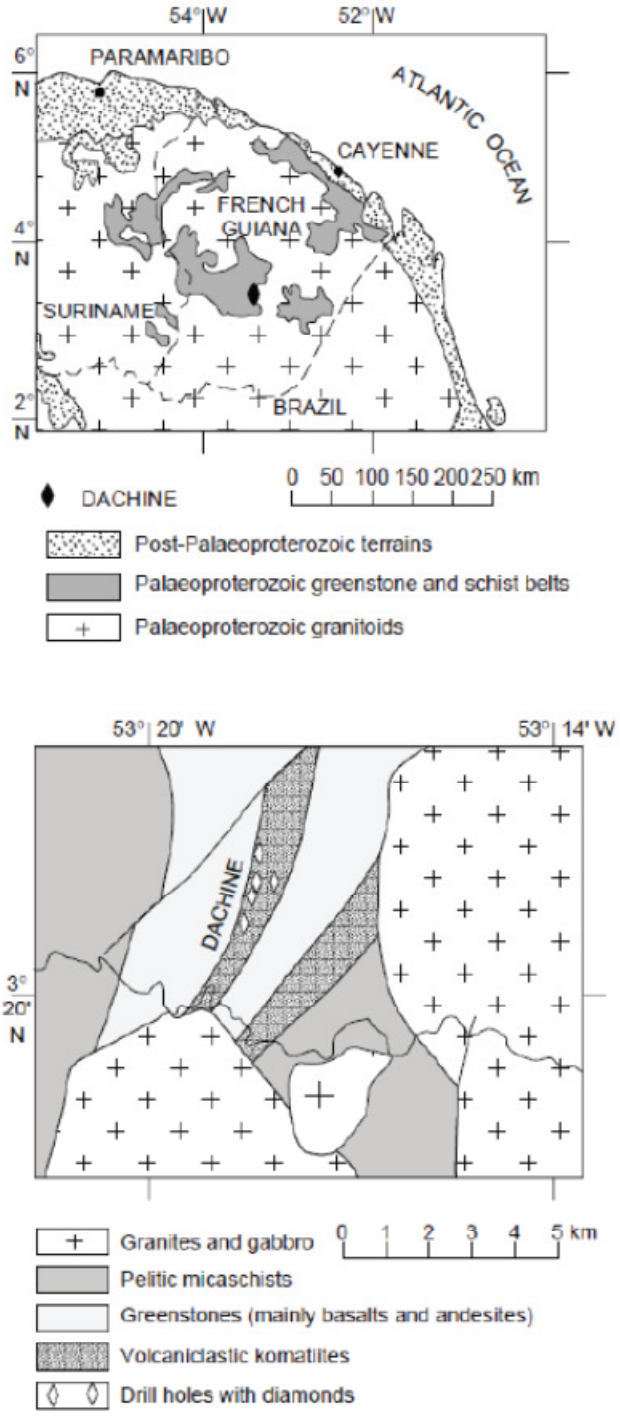

Figure 5.1. Geological maps. Shown are the location of the Dachine region and the local geology (top), and the distribution of diamond-bearing ultramafic rocks (bottom) from CAPDEVILA et al. (1999).

The Paramaca series consists mainly of metabasalts and overlying felsic gneisses derived from volcanic sediments, dacite and rhyolite tuffs and lavas. The diamondiferous ultramafic unit has been metamorphosed to a talc schist with volcaniclastic textures preserved (Bailey, 1999). This host rock has been described as a komatiite based on its major, trace, and rare Earth element chemistry (Bailey, 1999; Capdevila et al., 1999), not a kimberlite or lamproite host with which diamonds are normally associated (HAGGERTY, 1986). However, komatiites are generally held to have been generated from mantle melting at temperatures of circa 1700 °C (JONES, 2002), which might be expected to threaten diamond preservation during upward transport to surface as retrograde reactions should convert the diamonds to graphite. Magee and Taylor (1999) and Magee (2001) used compositions of contained chromite to suggest the source rock is a picritic shoshonite. Wyman et al. (2008), based on a comparison with the properties of diamondiferous lamprophyres in Canada, have likewise suggested the host rock may be an adakitic lamprophyre similar to those hosting diamonds at Wawa in Quebec (Wyman et al., 2006). The host rock also contains mantle xenoliths with garnet populations from both lherzolite and eclogites (BAILEY, 1999), which has never been reported from Komatiites and must preclude anomalously high temperatures in the mantle (JONES, 2002). Because the occurrence of komatiite would require melting close to the mantle liquidus, which certainly therefore cannot have preserved mantle xenoliths. In short, the nature of the host rock is intriguing and requires further studies. One reason for the lack of detailed studies in the literature may be due to the entire deposit being submersed by the North Eastern section of the Amazon rain forest, therefore making sampling only possible via bore hole drilling.

(B) Mantle residence time

The second un-common characteristic within the Dachine diamond suite is apparent evidence for a short residence time in the mantle. The Dachine diamond suite exhibits low degrees of nitrogen aggregation where the nitrogen substituting for carbon is present exclusively as a mixture of single

and pairs of N-atoms ranging from 2 to 76% of N-pairs (type 1b-1aA). Conversely, the vast majority (> 90 %) of kimberlitic diamonds exhibit far more advanced N aggregation in the 1aA-1aB type (CARTIGNY, 2010). This low degree of aggregation is either indicative of very short residence times at mantle temperatures, or prolonged periods at anomalously low temperatures < 1000 °C (TAYLOR et al., 1996). This means that the diamonds were formed, transported and subsequently emplaced in the crust within a time period of 100 yrs to 7 Ma, depending on the activation energy for the conversion, which incidentally is poorly constrained for diamonds with low N concentrations (CARTIGNY, 2010; TAYLOR et al., 1996).

(C) Carbon isotope geochemistry and nitrogen concentrations

The final un-common characteristic (that is the focus of this chapter) is the carbon isotope geochemistry and nitrogen concentrations of the Dachine diamonds. These samples exhibit anomalously low $\delta^{13}C$ values and N concentrations. The mean mantle $\delta^{13}C$ value is -5 ± 3 ‰ and the mean $\delta^{13}C$ value for the diamonds from Dachine is -23 ± 6 ‰ (figure 5.2 and caption). The distribution and position of the peak agrees incredibly well with pre-Cambrian crustal organic carbon, and is clearly distinct from primary mantle carbon (represented by mantle diamonds in figure 5.2). The N concentrations are also unique for upper mantle diamonds, with 97 % of the diamonds containing no detectable N using FTIR (type II) (CAPDEVILA et al., 1999; CARTIGNY, 2010; MCCANDLESS et al., 1999), whereas upper mantle diamonds usually exhibit a range of type II diamonds from 2 to 55% globally (CARTIGNY et al., 2009).

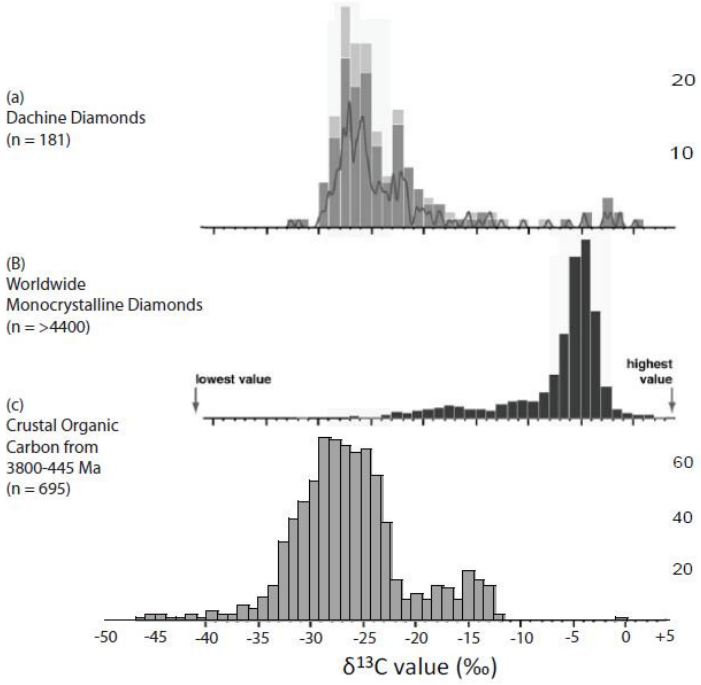

Figure 5.2 The $\delta^{13}C$ values for (a) diamonds from Dachine (compiled by CARTIGNY, 2010), worldwide monocrystalline mantle diamonds (compiled by CARTIGNY, 2005) and pre-Cambrian crustal organic carbon (compiled by SHIELDS and VEIZER, 2002).

I have determined the $\delta^{15}N$ and $\delta^{13}C$ values and the N concentrations of 18 diamonds from Dachine as a measure to place constraints on the origin of the carbon by simultaneously investigating the origin of the nitrogen. This is because as Figure 5.3 demonstrates, the majority of monocrystalline diamonds and other mantle samples have negative $\delta^{15}N$ values, whereas crustal $\delta^{15}N$ values are intrinsically positive. Therefore, coupled nitrogen and carbon isotopic discrimination can enable a better understanding of the origin of the anomalously low $\delta^{13}C$ values seen in the Dachine diamonds.

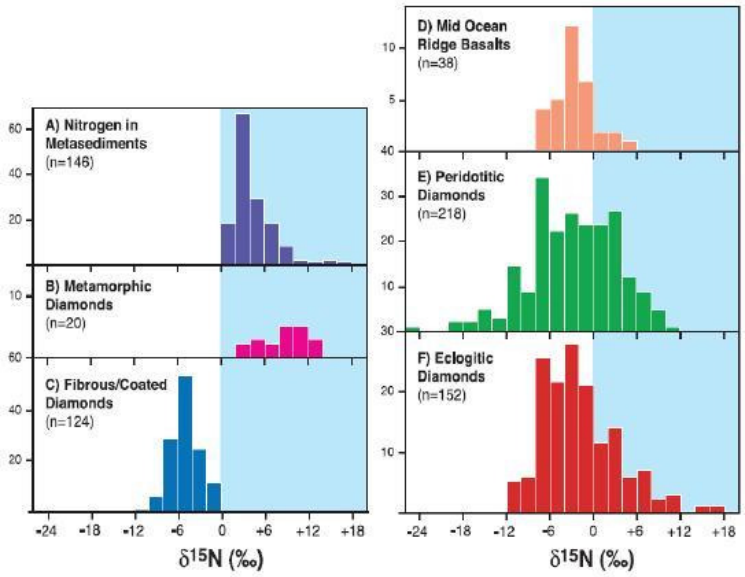

Figure 5.3 The $\delta^{15}N$ values for various terrestrial reservoirs (compiled by CARTIGNY, 2005).

I use major and trace element concentrations from syngenetic garnet inclusions from within 3 of the Dachine diamonds (not analysed for isotopic values) to place tentative constraints on the paragenesis of the diamonds. I use this *as a secondary proxy* to determine the origin of the low $\delta^{13}C$ carbon as opposed to investigating the host rock. As stated above, this is because these samples could be 7 Ma older than their host rock and therefore could be geochemically unrelated. This silicate data was sourced from the ongoing collaborative study detailed at the beginning of this thesis (see disclaimer). Before discussing my data I must address a recent study (CARTIGNY, 2010) that postulated a link between Dachine monocrystalline diamonds, Komatiites and polycrystalline carbonado diamonds.

5.1.2 Polycrystalline carbonado diamonds and Komatiites: The tentative 'link' with Dachine monocrystalline diamonds

Cartigny (2010) observed that the unusual geochemical characteristics exhibited by the Dachine diamond population are akin to carbonado diamond (for a review of the geochemical properties of carbonado diamonds see HEANEY et al., 2005) and proposed that both populations of diamonds are sourced from a komatiite. This model did not address the high proportion of type II diamonds from Dachine relative to the low proportion of type II diamonds in the carbonado group. The geochemical similarities are the distribution of $\delta^{13}C$ values (figure 5.4) and the low degree of N aggregation (1b-1aA and shown in figure 5.5).

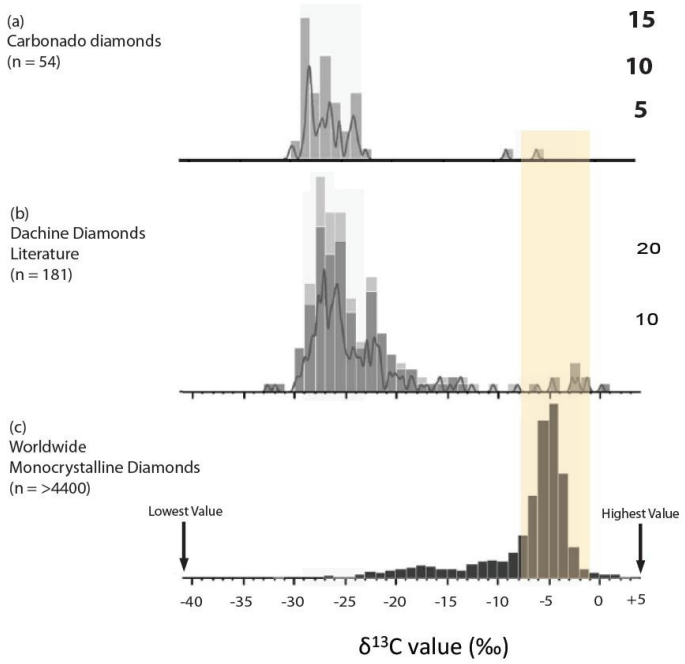

Figure 5.4 The $\delta^{13}C$ values for (a) Carbonado diamonds (b) diamonds from Dachine (both compiled by CARTIGNY, 2010) and (c) worldwide monocrystalline mantle diamonds (compiled by Cartigny, 2005). The orange band at $\delta^{13}C$ -5 ± 3 ‰ represents the mean mantle $\delta^{13}C$ range (from CARTIGNY, 2005).

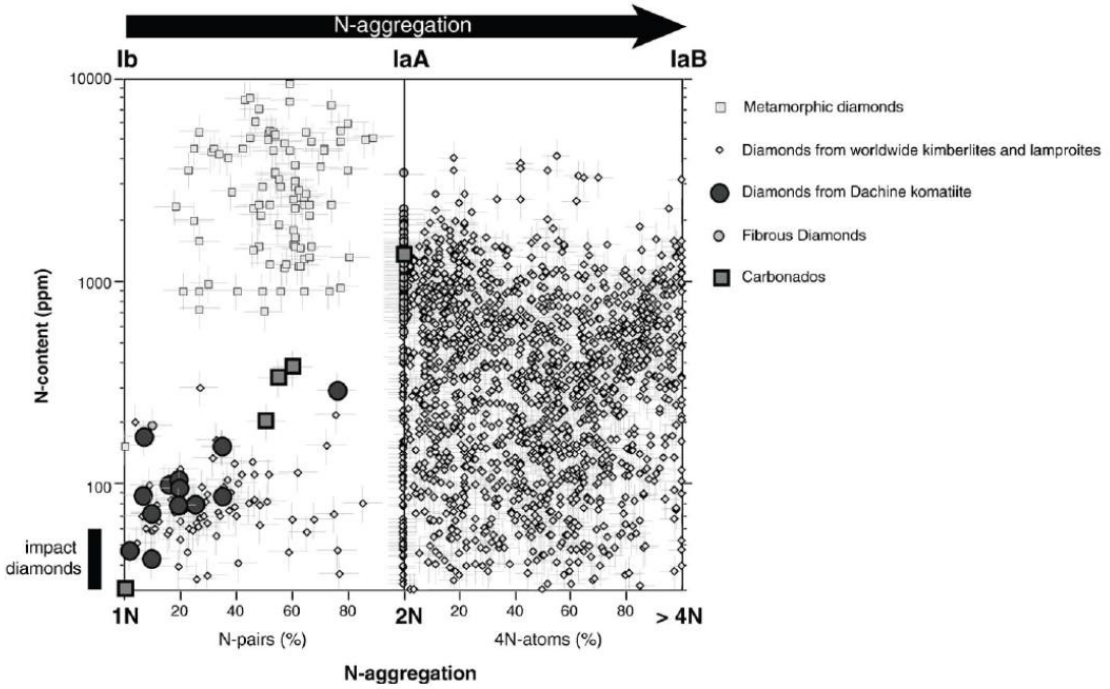

Figure 5.4 The degree of N aggregation in groups of terrestrial monocrystalline and fibrous diamonds, metamorphic, carbonado and impact diamonds (taken from CARTIGNY, 2010).

These similarities do prove that the peak at circa -27 ‰ for the $\delta^{13}C$ values and the 1b-1aA state of N aggregation in carbonado diamonds can be derived from mantle samples as opposed to other sources originally proposed, such as an extraterrestrial origin (GARAI et al., 2006; HAGGERTY, 1998; 1999). The argument of Garai et al (2006) that the 1b-1aA dominance in carbonado diamonds proves an extraterrestrial origin is now disproved, because the Dachine diamonds are certainly of mantle origins (CARTIGNY, 2010). Also, as demonstrated in figure 5.5, rare kimberlitic diamonds (un-questionably mantle-derived) do have comparably low degrees of N aggregation to carbonado diamonds.

In light of new data I disagree that there is a link to suggest that carbonado diamonds should be found in a komatiite, specifically Dachine. Cartigny (2010) made some predictions that are self-admittedly 'speculative' but does state that carbonado still remains to be observed in a primary host

rock (volcanic or plutonic) and therefore its origins remain enigmatic. The first prediction is that some mantle-related silicate inclusions will be found within micrometer-sized carbonado crystallites, and secondly that some monocrystalline diamonds with low $\delta^{13}C$ values and little advanced N-aggregation are associated with carbonados in Meso-Proterozoic alluvial deposits. The final prediction is that several of these monocrystalline diamonds will contain reduced types of inclusions. This rationale is based on data from Brazilian carbonado diamonds that contain 3 previously un-described nitride phases (JONES et al., 2006). However carbonado diamonds tend to also contain inclusions that are akin to crustal rocks such as kaolinite, quartz, orthoclase and zircons (Heaney et al., 2005), whereas Dachine diamonds contain inclusions that are akin to an upper mantle assemblage (eclogitic; see section 5.3). Since the publication of Cartigny (2010) the study highlighted in the disclaimer at the start of this chapter has identified 19 sulphides (pyrrhotite-pentlandite with minor chalcopyrite), 3 garnets, 2 clinopyroxenes and one SiO_2 phase (probably coesite) (SMITH et al., In Prep 2011). There is nothing striking about this assemblage being found in mantle diamonds (for example see a description and detail of the geochemistry of some diamonds from Juina that are sourced from the lithosphere, asthenosphere and possibly the transition zone in BULANOVA et al., 2010). Despite the reducing nature of sulphides in general, they are not as reducing as the nitrides observed in carbonado (JONES et al., 2006). The actual quantification for the thermodynamic equilibrium (i.e. in log units relative to a mineral system buffer vs. temperature) of sulphide-nitride stability is currently unknown (WATENPHUL et al., 2010). The only observed speciation of N observed in or from the mantle is N substituting for C in diamonds, N_2 in volcanic vents and fluid inclusions of xenocrysts (DAUPHAS and MARTY, 1999), NH_4^{3+} in micas (BOYD, 2001) and nitride phases of a potential mantle origin found in Tibetan ophiolites (DOBRZHINETSKAYA et al., 2009). Also noteworthy is that of >300 samples from Dachine recovered and documented, none are polycrystalline (a total of 181 in CARTIGNY, 2010; and a total of 131 SMITH et al., In preparation) whereas carbonado diamonds are a sub-set of the polycrystalline group of diamond and are also porous (HAGGERTY, 1998), whereas the Dachine diamonds are not (MCCANDLESS et al., 1999).

Regarding a komatiite as the source rock, it is worth noting that there are no characteristic spinifex textures observed, and owing to the extensive rainforest (the Amazon rainforest) that overlies the deposit , together with its old age (>2 Ga), it is highly altered both the physically and geochemically. The deposit is part of a greenschist to amphibolite facies metamorphosed pyroclastic ultramafic unit, intercalated within the 2.11 Ga Lower Paramaca meta-volcanics (palaeo-Proterozoic in age) located in the southern greenstone belt of the French Guianan shield (BAILEY, 1999; CAPDEVILA et al., 1999). This is an island arc setting. Relict primary olivine crystals and chromite are recognisable, as are volcaniclastic features, but other primary mineralogy and textures have been destroyed during the metamorphism. A variety of host rocks have been suggested for Dachine, based on whole rock/trace element patterns, ranging from komatiite (BAILEY, 1999; CAPDEVILA et al., 1999) to boninite to adakitic lamprophyre (MAGEE and TAYLOR, 1999; SMITH et al., In preparation). Due to element mobility during weathering and metamorphism, the primary rock chemistry is not definitive. But the very high temperatures (circa 1700 °C eruption temperature) and lack of volatiles associated with komatiite (BERRY et al., 2008) make it unlikely that diamond would survive during transport to surface in such a host rock without being fully converted to graphite or oxidised to CO_2, therefore a lamprophyric host is favoured here.

5.2 Samples

A total of 131 diamonds recovered from bulk samples and drill cores during prospecting operations on the Dachine ultramafic body were made available to Dr Chris B Smith (Rio Tinto Diamonds pc, UK) and Dr Galina P Bulanova (University of Bristol, UK). They made available (to me) a total of 20 samples for the C and N isotopic determinations, the results of which form the core of this chapter.

Of the samples (for which inclusion chemistry has been determined) an eclogitic affinity has been observed (SMITH et al., In preparation; see section 5.3). This is in agreement with the macroscopic

heavy mineral suite dominated by common eclogitic garnet, but also including lherzolitic and harzburgitic G10 kimberlite/diamond indicators (BAILEY, 1999). External morphologies for 464 alluvial and alluvial stones nearby to Dachine have also been described in detail and illustrated in McCandless et al (1999). Regarding their textures, the samples are not uncommon or unique relative to various kimberlitic diamonds (MCCANDLESS et al., 1999). They are mostly small (typically ≤ 1 mm), anhedral and irregular octahedra (71% of stones examined) with minor cubo-octahedra faces being present (15%), and are highly fractured with step-layering as a common surface texture (SMITH et al., In preparation). What is unusual is their colour. They range from pale greyish yellow to pale brown, which is rare for type II diamonds (CAPDEVILA et al., 1999). Cathodoluminescence studies of polished plates of the Dachine diamonds reveal complex polycentric internal structures (figure 5.6 a,b) with blocky growth and very intensive plastic deformation in the form of linear dislocations, often giving rise to tatami (figure 5.6, d) or granular effects (figure 5.6 a,b). Etched out cracks are common around the crystal margins; the cracks usually follow structural dislocations, but occasionally are curved. In one case where cuboid features were discernable, fibrous growth at the rim was observed, which would imply some local carbon oversaturation in the diamond-forming fluid (Figure 5.6, c) (SMITH et al., In preparation). Again, these are not unique relative to kimberlitic mantle diamonds (BULANOVA, 1995).

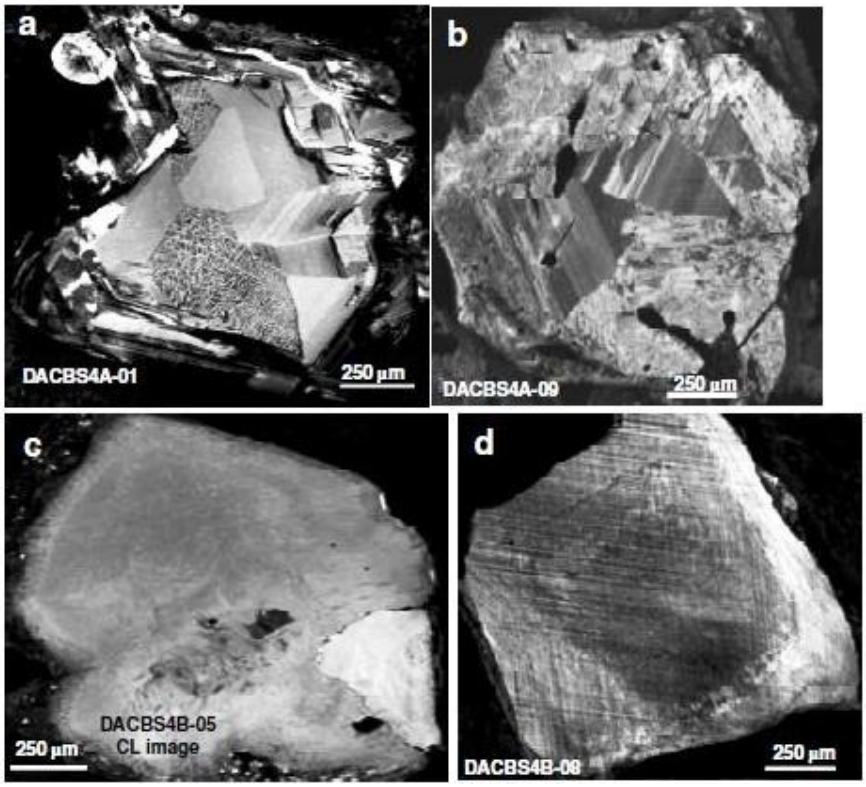

Figure 5.6. Cathodoluminescence images of four Dachine diamonds showing representative internal structures (from SMITH et al., In preparation). a) Irregular octahedral aggregate external form, this internally shows polycentric cubo-octahedral blocky sectorial growth centres and in part showing vermiform granular texture due to intense plastic deformation dislocations; b) Irregular octahedral diamond with blocky polycentric internal structure and strong plastic deformation in rim areas giving granular effect with etched-out cracks being prominent; c) Cubo-octahedron growth sectors with weak internal zonation. The rim of this sample shows fibrous growth, demonstrating at least one stage of C oversaturation. d) This shows cuboid zoning and intensive plastic deformation ("tatami" structure).

The following investigations were carried out for these diamonds:

- Inclusion geochemistry;
- Diamond nitrogen concentration determinations;
- Diamond carbon and nitrogen stable isotope determinations.

The results of these investigations are presented below.

5.3 Diamond Mineral Inclusion Geochemistry

Inclusion geochemistry has been obtained to identify the paragenesis of the Dachine diamonds. There is no published data so far regarding the inclusion paragenesis of the Dachine diamonds. Therefore I detail here syngenetic garnet geochemistry undertaken by Smith et al (In Preparation) that provides the first investigation into the paragenesis of these diamonds. Smith et al (In preparation) has determined the major and trace element compositions of 3 syngenetic garnet inclusions from 3 individual Dachine diamonds. These were analysed by electron microprobe and ion-microprobe (the results are given in appendix tables A10 and A11). Electron microprobe analyses of exposed and polished garnet inclusions were made at the University of Bristol using a Cameca SX100 using a beam current of 20 nA at 15 kV voltage, and a spot size of ~1 micron at the surface.

The identification of syngenesis is based on these inclusions not being associated with cracks, and on their having octahedral morphology imposed on them by the diamond host (MEYER, 1987). The common hexagonal inclusion shapes are off-centre dodecahedral plane cross sections of octahedral crystal, demonstrating their imposed morphology as shown in figure 5.7. Three Dachine garnets were used to determine the silicate paragenesis of the growth environment using the Cr_2O_3 vs. CaO discrimination diagram of Aulbach et al (2002) (figure 5.8), and chondrite-normalised REE patterns (figure 5.9). It is evident that these syngenetic inclusions are distinctively eclogitic.

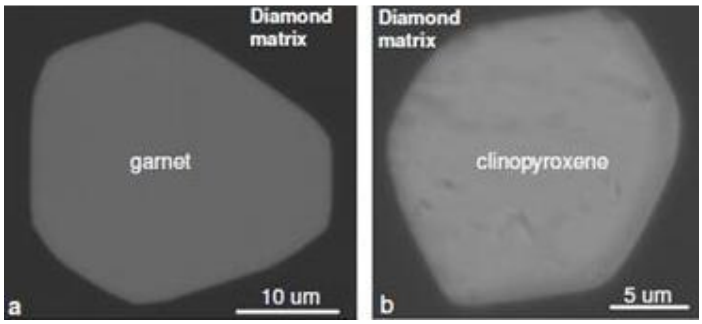

Figure 5.7. Back-scattered SEM imagery of syngenetic mineral inclusions in Dachine diamonds: a) Mn-rich garnet in diamond DACBS 4A-11., b) clinopyroxene from DACBS 4B-07Note also the frequent hexagonal shaped morphology imposed on the inclusions by the diamonds.

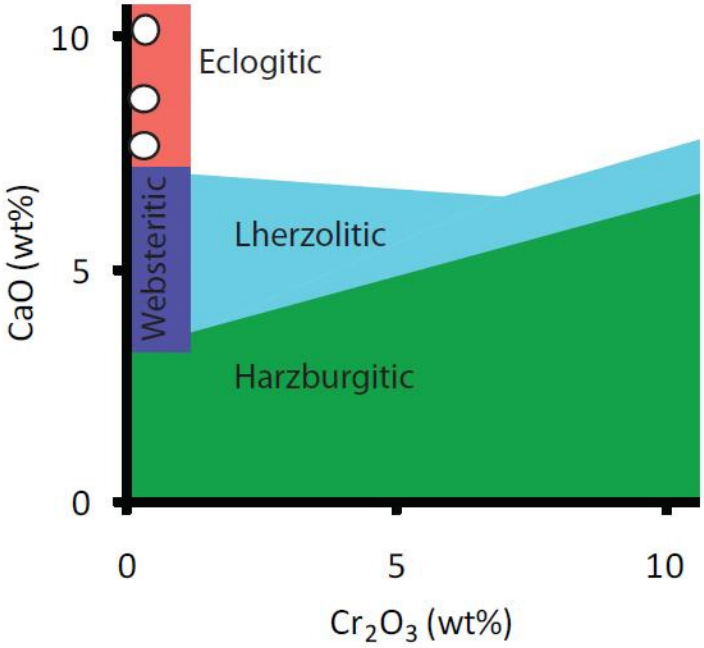

Figure 5.8. A Cr_2O_3 vs. CaO discrimination diagram after Aulbach et al (2002). The garnet data is from Smith et al (In preparation) and demonstrates the eclogitic nature of the garnets as seen in the host rocks at Dachine (BAILEY, 1999).

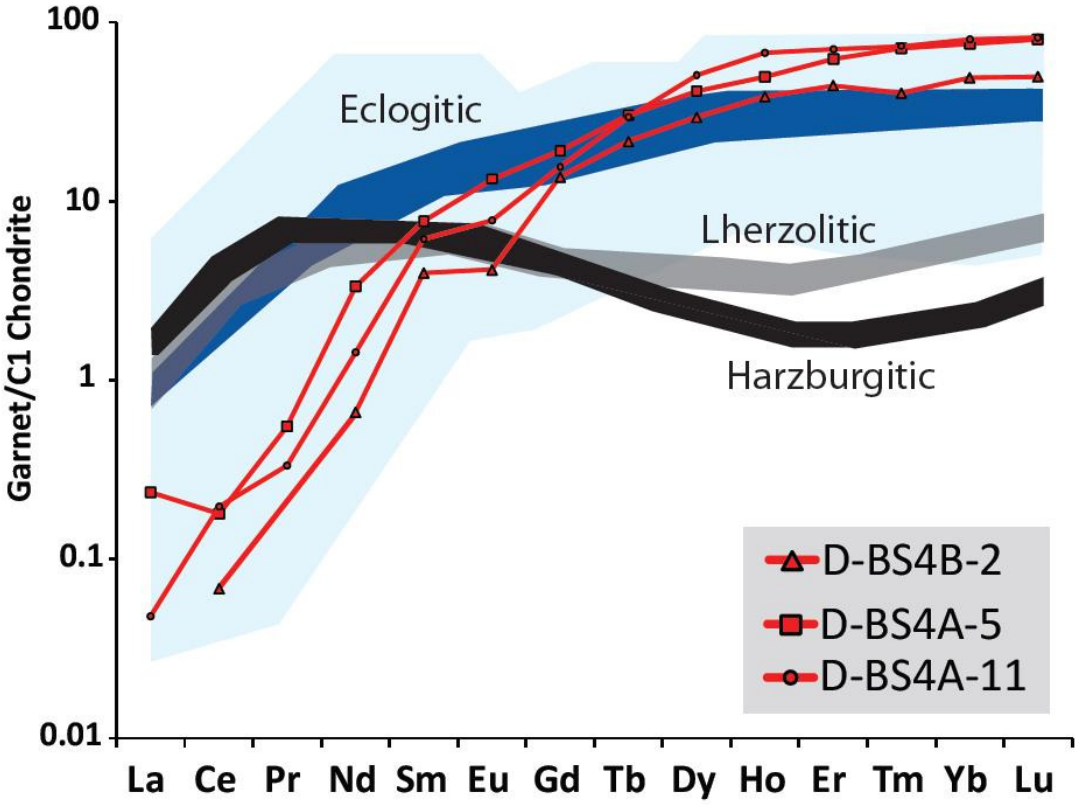

Figure 5.9. REE concentrations for Dachine diamond inclusion garnets normalised against C1 chondrite, compared to mean trends for world-wide eclogitic and peridotitic (lherzolitic and harzburgitic) garnet data from diamond inclusions (STACHEL et al., 2004); this confirms the eclogitic nature of the garnet inclusions within Dachine diamond.

5.4 Diamond Geochemistry

The Dachine diamonds were analysed for C-N isotope compositions and N concentrations using the Finesse machine at the Open University. The data was processed (see chapters 3 and 4), and the full data set is given in the appendix (stepped data in table A8 and bulk data in A9). The new data are presented here, and then their interpretation is discussed.

5.4.1 Nitrogen concentrations

None of the (20) diamonds in this study demonstrated transmission spectroscopic N absorption identifiable with FTIR implying very low N contents. However, some diamond samples were difficult to observe the dominant characteristic diamond absorption band, owing to either the sample thickness or internal deformation within the sample. Chapter 4 demonstrates that the FTIR facility at the department of Earth sciences (UCL) has a detection limit of ~60 ppm for samples 1 mm thick (see chapter 4 section 4.3.1). I have chosen to use a more universally accepted concentration of < 30 ppm (PEARSON et al., 2003) to class the samples as Type II using the N concentrations derived using the data derived from combustion analysis (chapters 3 and 4). The proportion of designated Type II diamonds in this sample set (with < 30 ppm N) is 78 %, (determined by mass spectrometry). This is less than the 97 % determined in Cartigny (2010), but still high relative to upper mantle diamonds in general, where the proportion of type II diamonds in upper mantle populations is between 2 and 55% worldwide (see CARTIGNY et al., 2009).

Overall the N concentrations (determined by mass spectrometry) in this sample population are low when compared to other upper mantle diamonds (figure 5.10). The total range for the samples in this study is from 110 ppm to unquantifiable (circa <2 ppm for mass of 0.2 mg of diamond). The individual samples display a consistent range in N concentration for multiple combustion stages, with a mean standard deviation of 8.11 ppm, and a mean error of 0.89 ± 1.03 ppm for 3 or more combustion steps (≈ individual analyses). This demonstrates that the individual samples exhibit homogeneous N concentrations (appendix table A8) and would not be expected to show zonation using in situ high resolution techniques such as FTIR and SIMS.

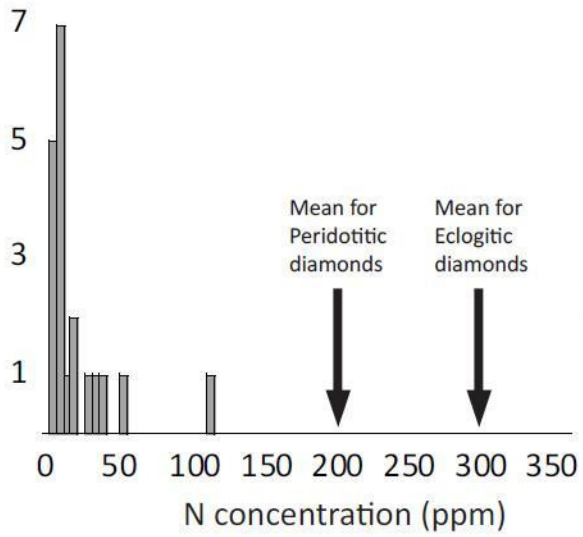

Figure 5.10 The N concentration for the Dachine diamonds in this study (n = 19). The bin size used was 5 ppm. The mean values for eclogitic and peridotitic diamonds is from Cartigny (2005).

5.4.2 Carbon isotopes

The range for $\delta^{13}C$ values in this study (n = 19) is comparable to the range shown in the published literature (where n = ~ 180; see CARTIGNY, 2010 and shown in figure 5.11). The bulk sample range for $\delta^{13}C$ values range from -0.04 to -36.07 ‰ (figure 5.11). However the range for individual steps is larger for some samples, where the highest value is +2.89 and the lowest value is -36.44 ‰ (sample DAC101 y2 and DAC45-7 in appendix table A8). Most individual samples display a consistent range for their $\delta^{13}C$ values for multiple steps of combustion, with a mean standard deviation of 1.16 and a mean error of ± 0.53. Hence, the individual samples appear isotopically homogeneous for samples smaller than 0.6 mg and individual $\delta^{13}C$ determinations on 0.2 mg of CO_2. This is despite the large range shown for the whole population (appendix table A8), therefore a high resolution SIMS study would probably show little variation. The samples in this study and the literature are distinct from the mean mantle $\delta^{13}C$ value of -5 ± 3 ‰ (figure 5.11).

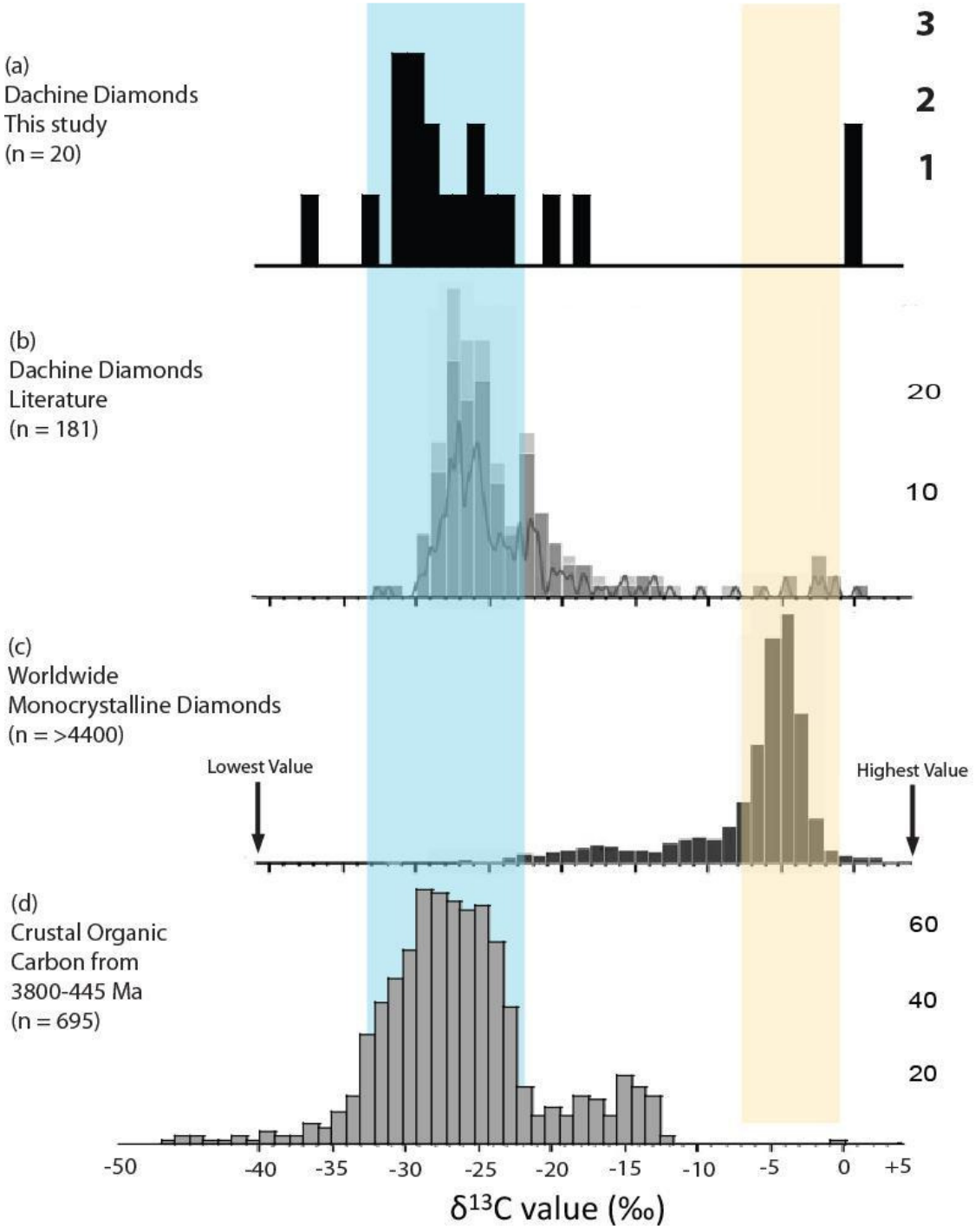

Figure 5.11 The $\delta^{13}C$ values for (a) Dachine diamonds in this study, (b) Dachine diamonds from the literature , (c) worldwide monocrystalline diamonds and (d) pre-Cambrian crustal organic carbon (reference are the same as figure 5.2). The bin size used was 1 ‰. The orange band at $\delta^{13}C$ -5 ± 3 ‰ represents the mean mantle $\delta^{13}C$ range (from Cartigny, 2005) and the blue band represents the main peak for pre-Cambrian organic carbon (SHIELDS and VEIZER, 2002).

5.4.3 Nitrogen isotopes

The range for $\delta^{15}N$ values in this study (n = 20) is comparable to the range shown in the published literature (where n = circa 12; see CARTIGNY, 2010 and shown in figure 5.14). The bulk range is from -3.94 to +21.93 ‰ (figure 5.12), however the range for individual steps is larger where the highest value is +33.27 and the lowest value is -5.32 ‰ (appendix table A8). Most samples display a larger range for their $\delta^{15}N$ values for multiple steps of combustion with a mean standard deviation of 5.16 ‰ and a mean blank-corrected precision of ± 2.65 (σ = 3.45 ‰).

However given the larger errors it can be stated that (within error) the individual samples exhibit isotopic homogeneity, despite the large range shown for the whole population (appendix table A8 with the range shown in figure 5.12). The model peak overall is similar for Dachine and the Type II diamonds from chapter 4, but the rarity of peaks in the mantle range is a striking feature, as well as the high $\delta^{15}N$ values (> +10 ‰) when compared to both Type I and Type II monocrystalline mantle diamonds (figures 5.12 and 5.13). Therefore I deduce that the $\delta^{15}N$ values of > +10 ‰ shown for the Dachine diamonds are source reflective.

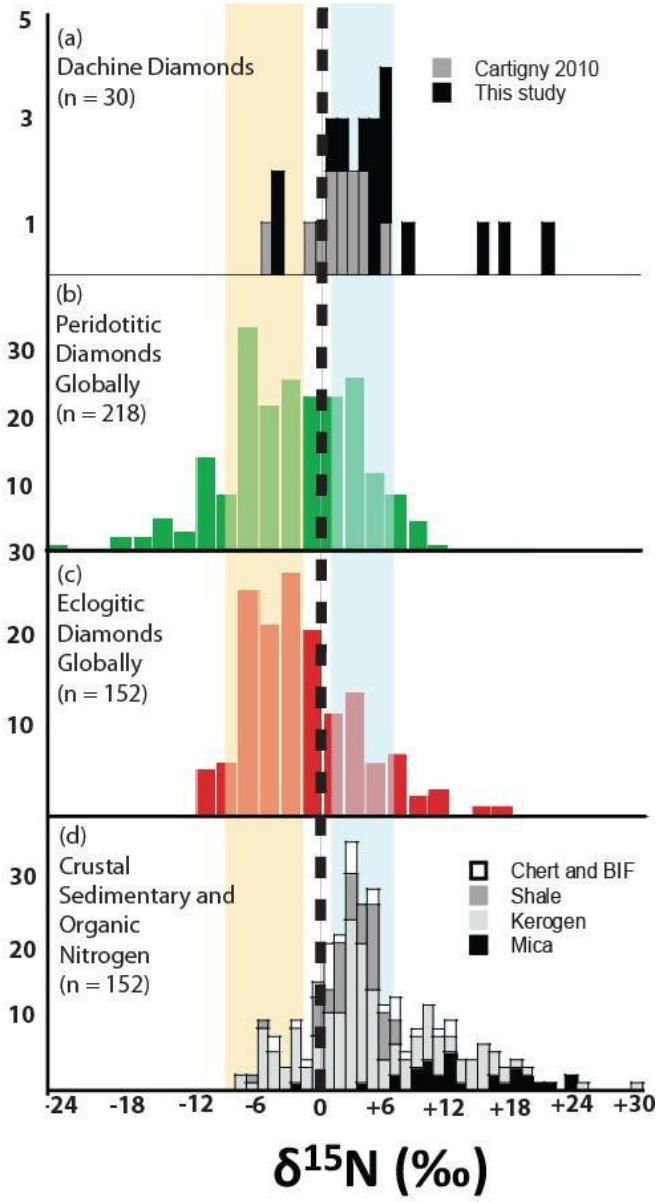

Figure 5.12. The $\delta^{15}N$ values for (a) diamonds from Dachine, (b) worldwide peridotitic monocrystalline diamonds and (c) worldwide eclogitic monocrystalline diamonds (sourced from CARTIGNY, 2005) with (d) the N isotopic values for pre-Cambrian chert, banded Iron formations (BIF), shale, Kerogen and micas (taken from THOMAZO et al., 2009). The bin size used was 1 ‰. The orange band at $\delta^{15}N$ -5 ± 3 ‰ represents the mean mantle $\delta^{15}N$ range (from Cartigny, 2005).

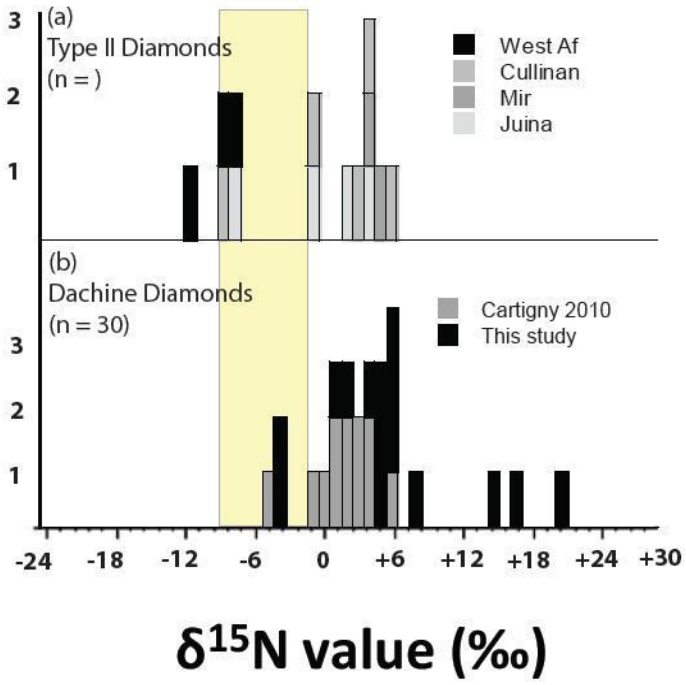

Figure 5.13. The $\delta^{15}N$ values for (a) various spectral type II diamonds from chapter 4 and (b) diamonds from Dachine. Note the lack of both the lack of $\delta^{15}N$ values > +10 ‰ for the various spectral type II diamonds and the low abundance of negative $\delta^{15}N$ values from Dachine. The abbreviations in (a) are as follows; West Af = West African diamonds (exact country unknown), Cullinan = diamonds from the Cullinan mine, SA (formerly the Premier mine), Mir = diamonds from the Mir pipe in, Eastern Siberia, Russia and Juina = sublithospheric alluvial diamonds from the Juina Region, Brazil (as described in chapter 4).

5.5 Are these samples representative of Dachine diamonds?

Before discussing the characteristics and origin of the Dachine diamond-forming carbon, I must demonstrate that the samples in this chapter are representative of the Dachine diamond population. To do this I compare the distribution of the nitrogen concentrations (figure 5.14) and $\delta^{13}C$ values where corresponding $\delta^{15}N$ values were also determined (figure 5.15) from this study and Cartigny (2010) to the distribution in $\delta^{13}C$ values from all 181 Dachine samples from the peer reviewed literature (figure 5.15). Noteworthy is the nitrogen concentration for the samples where $\delta^{15}N$ values were determined are representative of the Dachine diamond population. Figure 5.14 demonstrates that the majority of the $\delta^{15}N$ values from Cartigny (2010) were from samples with N concentrations

above 30 ppm, whereas 97 % of diamonds from Dachine have N concentrations < 30 ppm (spectral type II).

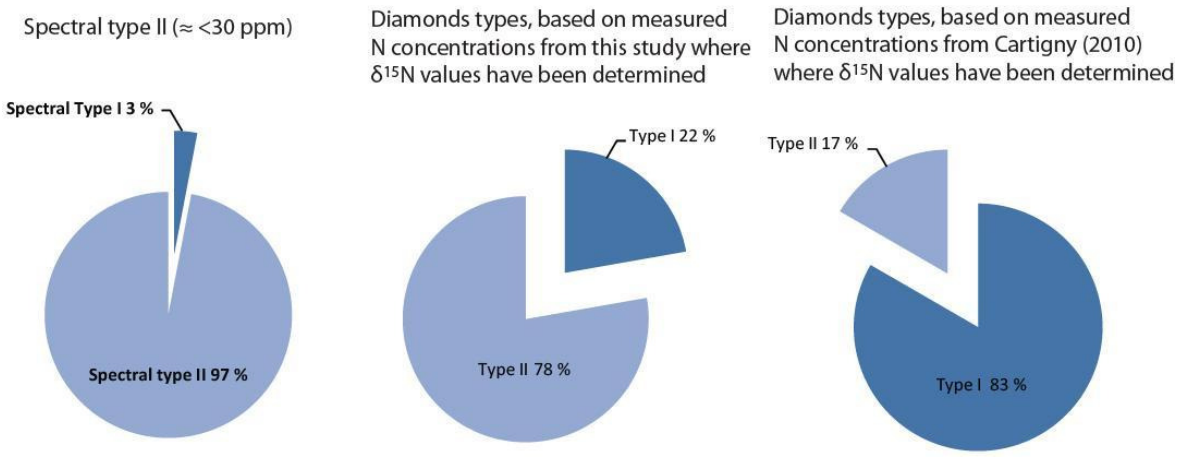

Figure 5.14. Pie charts demonstrating the relative proportions for type I and type II diamonds from Dachine. (a) is for all Dachine diamonds from the literature (Cartigny, 2010), (b) is this study where type II is defined as <30 ppm nitrogen and (c) is the proportion type I and II Dachine diamonds in Cartigny (2010) where corresponding $\delta^{15}N$ values were determined. Note the abundance of type I samples in C relative to (a) and (b).

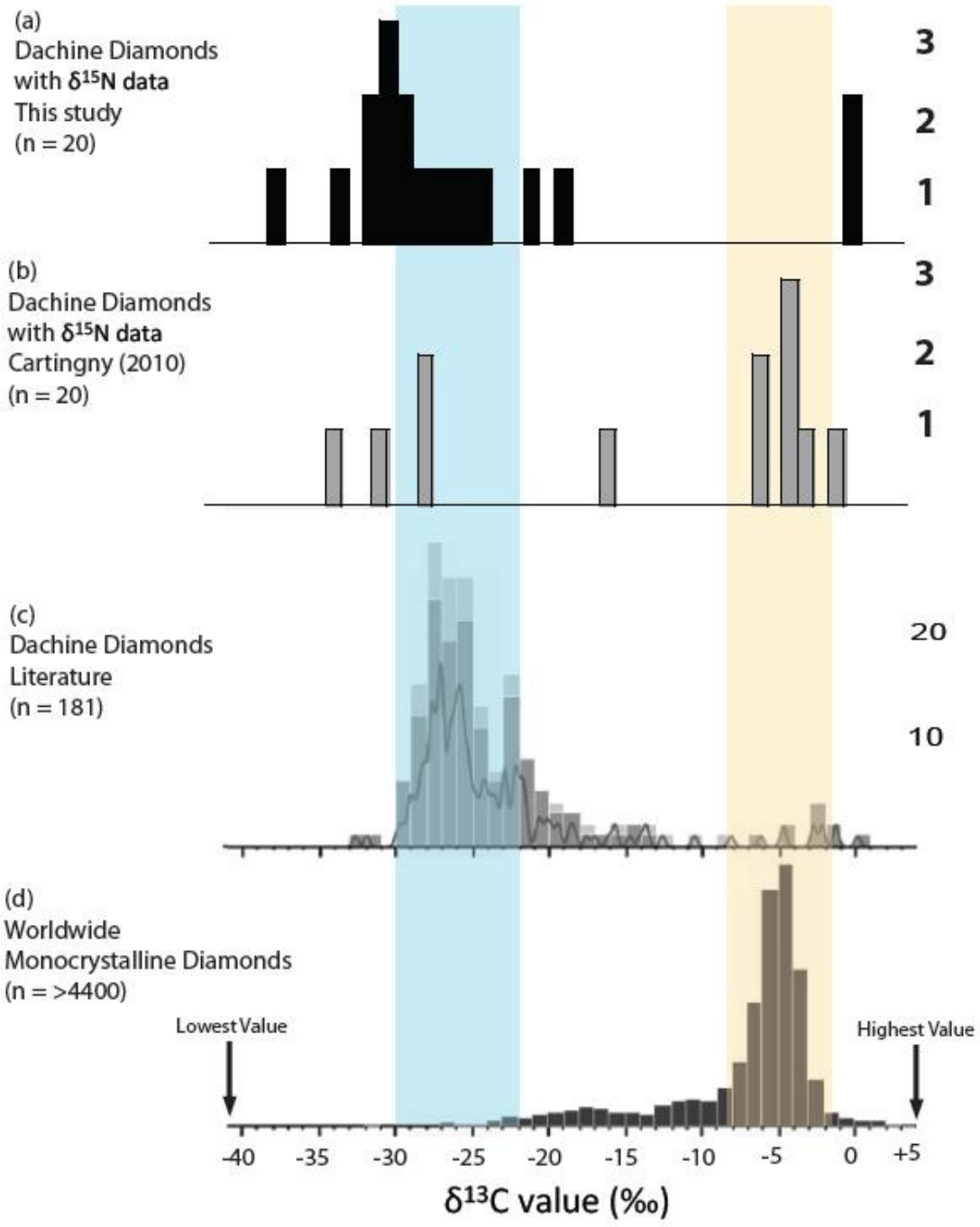

Figure 5.15. The $\delta^{13}C$ values for (a) Dachine diamonds in this study, (b) Dachine diamonds from the literature where corresponding $\delta^{15}N$ values were determined (see the supplementary material for CARTIGNY, 2010), (c) all Dachine $\delta^{13}C$ values from the literature and (d) worldwide monocrystalline diamonds (reference are the same as figure 5.2). The bin size used was 1 ‰. The orange band at $\delta^{13}C$ -5 ± 3 ‰ represents the mean mantle $\delta^{13}C$ range (from Cartigny, 2005) whereas the blue band at $\delta^{13}C$ -26 ± 4 represents the modal $\delta^{13}C$ values for Dachine as shown in the figure above.

The samples in this study have a range in bulk $\delta^{13}C$ values of -36.07 to -0.04 with a mean value of -24.94 ‰ (σ= 9.30). The mean value from the literature is -23.11 ‰ (σ= 6.24) (CARTIGNY, 2010; CARTIGNY et al., 2001b; MCCANDLESS et al., 1999). Figure 5.15 demonstrates that for the samples from Cartigny (2010) where the $\delta^{15}N$ values were determined, the mean $\delta^{13}C$ value is -12.9 ± 12.38 ‰ and are biased to mean mantle-like $\delta^{13}C$ values in their distribution. Therefore they do not represent the $\delta^{13}C$ distribution of the Dachine diamond population. However the samples in this study do (figure 5.15), thus making my discussion of the coupled $\delta^{13}C$-$\delta^{15}N$ systematics representative of the Dachine diamond population, albeit with a small sample set.

5.6 Co-variations of $\delta^{13}C$-$\delta^{15}N$ vs. N concentration?

Cartigny (2010) found that the samples with the highest N concentrations had mean mantle $\delta^{13}C$ values. This is not the case for the sample set presented here, where the highest N concentrations in this study have low $\delta^{13}C$ values (DAC45-3 and DAC45-9 with 53 and 110 ppm nitrogen have -28.12 and -24.06 ‰ respectively). Therefore, this rule cannot be applied to describe the Dachine diamond $\delta^{13}C$-N/C systematics (see figure 5.16). As shown in figure 5.16 (a-d), there are no systematic co-variations of either $\delta^{13}C$ or $\delta^{15}N$ vs. N concentration. Figures 5.16 a & c show a tentative trend for 5 samples from this study whereby $\delta^{13}C$ and $\delta^{15}N$ decrease with a decreasing N concentration, I interpret this to be a consequence of a very small sample set and is simply part of a larger scatter for $\delta^{13}C$ vs. N concentrations and no correlation at all for $\delta^{15}N$ vs. N concentrations (figure 5.16 b & d). The lack of correlations in figures 5.16 (a-d) is not surprising as the total range for N concentrations from this study and from Cartigny (2010) is from 171 to 2 ppm with a mean concentration of 41 ± 46 ppm from only a total of 31 determinations (where N concentration with $\delta^{13}C$ and $\delta^{15}N$ values were determined). This average and standard deviation is smaller than the usual bin size for histograms that contain N concentrations from mantle diamonds (usually 50 ppm) and cannot therefore be directly compared to Type I diamonds.

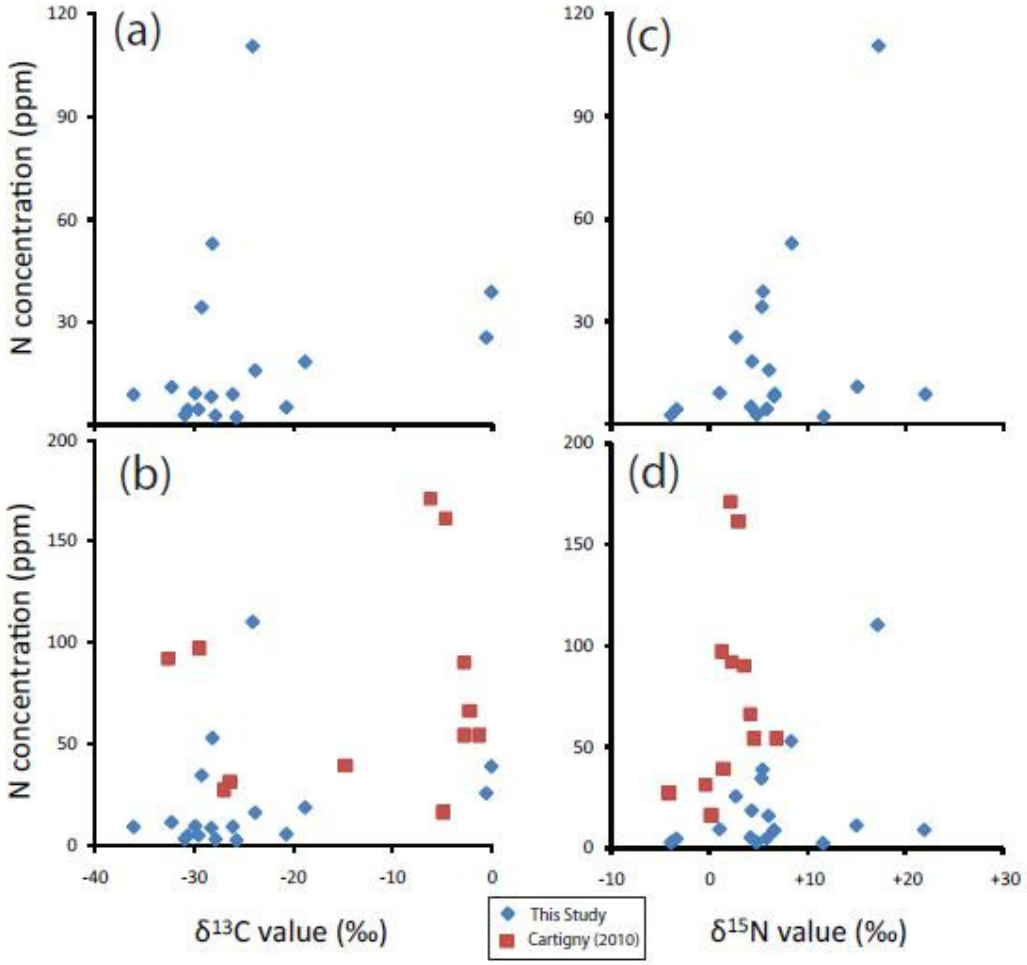

Figure 5.16. Variation diagrams for stable isotope δ values (‰) vs. N concentrations (ppm). (a) and (b) are for $\delta^{13}C$ values vs. N concentrations and (b) and (d) are for $\delta^{15}N$ values vs. N concentrations (the data from CARTIGNY, 2010 is sourced in the supplementary material). Note the lack of any distinct correlations.

5.7 Mantle or crustal Sources for N and C?

5.7.1 N concentrations

What is evident from this study and the literature is that the Dachine diamonds appear to have precipitated from a source fluid that was N depleted relative to the N concentrations inferred for fluids that precipitate upper mantle forming diamonds (figure 5.10).

There is only one type of diamond population where type II's are the dominating group - sublithospheric diamonds (DAVIS et al., 2003; KAMINSKY et al., 2001; STACHEL et al., 2002; TAPPERT et al., 2005). Sublithospheric diamonds do exhibit a large proportion of type II diamonds akin to the Dachine population. And there may be scope to use the overall low N concentrations from the Dachine diamonds to argue for a sublithospheric origin based on the correlation with depth of origin and N concentrations in diamonds, but this is inconsistent with the syngenetic silicate-sulphide inclusions (section 5.3) that cannot be argued to be retrograde LM or TZ phases i.e. show no evidence of exsolution and re-equilibration. However one cannot rule out the origin of the fluids being from anywhere in the bulk silicate Earth with the crystallisation of diamonds occurring in the lithospheric mantle, but the same can be said for any mantle fluid and should only be considered if all other feasible possibilities are exhausted and the data cannot be explained in a simpler and more concise manner. These other possibilities are explored below using carbon and nitrogen isotope compositions as constraints.

5.7.2 C and N isotopes

The overall distributions of $\delta^{13}C$ and $\delta^{15}N$ values observed in the Dachine diamonds are compared to various mantle and crustal reservoirs in figure 5.17. The source is evidently from a reservoir with a distinct $\delta^{13}C$ value of ~ -24.5 ‰ and positive $\delta^{15}N$ values centred at around +6.5 ‰. There are no monocrystalline diamond populations from the literature that match this coupled C-N isotopic

distributions (figure 5.17). The best match for the data in this study (low $\delta^{13}C$ and high $\delta^{15}N$ values) is pre-Cambrian crustal organic carbon (figure 5.17). This requires the crustal organic carbon to have been subducted into the mantle >2 Ga. This therefore is interpreted here as evidence for deep subduction zone tectonics (Phanerozoic-type) before the paleo-Proterozoic. This model is discussed further in Section 5.8.

The diamonds from Dachine are not the first population of mantle diamonds to be both eclogitic and demonstrate low modal $\delta^{13}C$ values and positive $\delta^{15}N$ values. There are others such as Guaniamo, Venezuela with a modal $\delta^{13}C$ value of circa -15 ‰ (KAMINSKY et al., 2000), and Jericho, NW Canada with a modal $\delta^{13}C$ value of circa -35 ‰ (DE STEFANO et al., 2009). However there are no published $\delta^{15}N$ values for either of these localities. Dachine is also the first whole population of monocrystalline diamonds to exhibit a domination of Type II diamonds, together with low $\delta^{13}C$ and high $\delta^{15}N$ values as a significant majority.

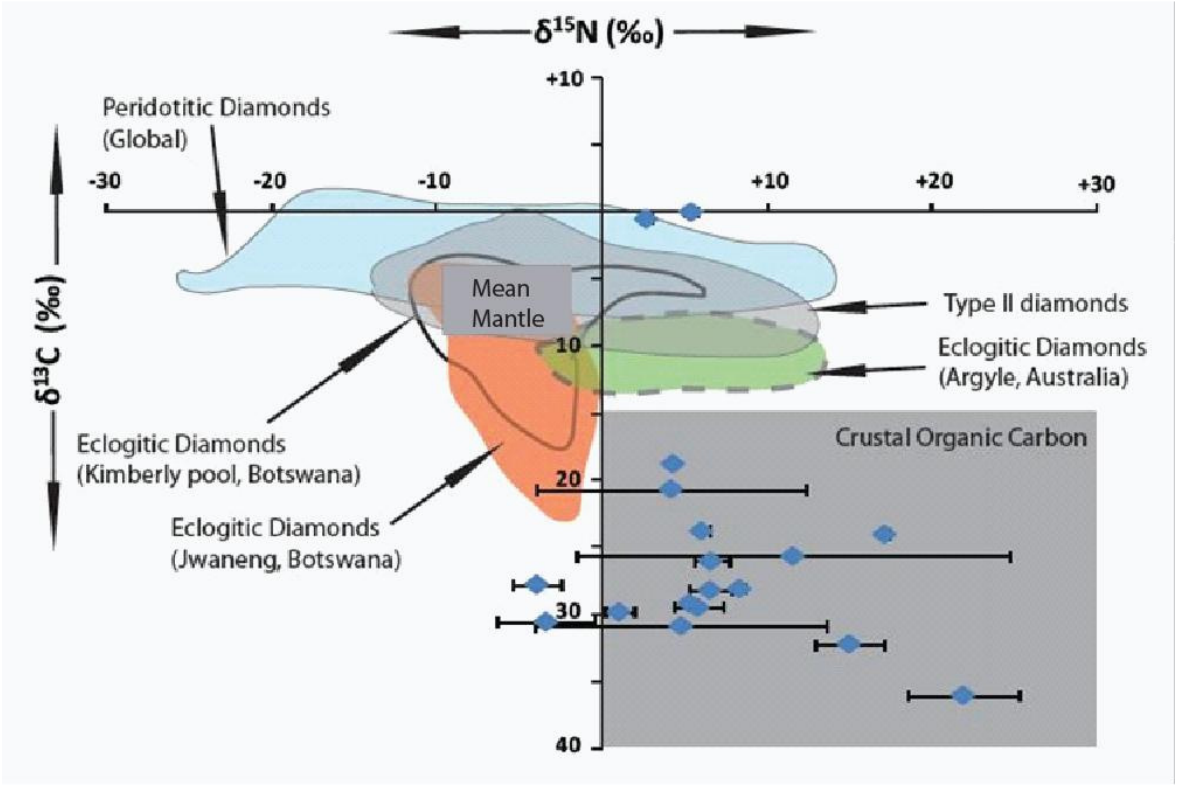

Figure 5.17. This plot illustrates the fields for coupled $\delta^{15}N$ vs. $\delta^{13}C$ values for various diamonds groups, the mean mantle range for MORB, OIB, carbonatite lavas and silicate xenoliths, pre-Cambrian crustal organic carbon and the diamonds from Dachine in this study (with blank-corrected precision to 1 σ is shown for $\delta^{15}N$, the errors for $\delta^{13}C$ are comparable to the symbol size). The data are sourced from the following studies: Peridotitic monocrystalline diamonds (P type diamonds from Fuxian China are from CARTIGNY et al., 1997; and P type diamonds from Namibia are from CARTIGNY et al., 2004b); Eclogitic monocrystalline diamonds from Kimberly pool, SA (CARTIGNY et al., 1998b), Jwaneng, Botswana (CARTIGNY et al., 1998a) and Argyle, Australia (BOYD and PILLINGER, 1994); the mean mantle range for MORB,OIB, carbonatite and silicate xenoliths (CARTIGNY, 2005); Type II diamonds (chapter 4) and pre-Cambrian crustal organic carbon (SHIELDS and VEIZER, 2002; THOMASSOT and VILJOEN, 2007; THOMAZO et al., 2011).

5.8 Possible origin(s) of the Dachine Diamonds

Before concluding that the source of the diamond-forming carbon is subducted organic carbon during the paleo-Proterozoic (as suggested using figure 5.17), alternative possibilities must be discussed. These alternate models are outlined below, and include the potential for mantle isotopic heterogeneities, both primordial and as a function of the layered earth and high temperature isotopic fractionation in the mantle. Additionally, there are also issues regarding the lack of pelagic

carbonate contribution to mantle mineral (with $\delta^{13}C$ roughly 0 ‰) globally (DEINES, 2002), and the low C/N of diamonds relative to crustal rocks and organic carbon.

5.8.1 Primordial mantle heterogeneities

Deines (2002) alluded to the possibility that some mantle-derived low $\delta^{13}C$ values may be a relic of undefined primordial heterogeneities. This is not applicable to the Dachine diamonds in light of their mean positive $\delta^{15}N$ values (range of -3.94 up to +21.93 with a mean of +6.5 ‰). This is because there does not seem a feasible meteorite class or a component of such a class that fits these characteristics. For example, C1 chondrites and Enstatite chondrites are commonly put forward as the building blocks of Earth (for the Enstatite chondrite model see JAVOY et al., 2009; and for the C1 chondrite model see MCDONOUGH and SUN, 1995), neither fit the model for coupled $\delta^{13}C$-$\delta^{15}N$ values (see table 1 in GRADY and WRIGHT, 2003 and figure 5.18). For example, the range for the C1 chondrites for $\delta^{13}C$ and $\delta^{15}N$ values range from -12 to -5 and +20 to +50 ‰ respectively. Enstatite chondrites exhibit negative $\delta^{15}N$ values (-30 to -10 ‰) and mean mantle-like $\delta^{13}C$ values (-9 to +4 ‰) (GRADY and WRIGHT, 2003). One may argue that some insoluble C in C1 chondrites does have lower than mantle $\delta^{13}C$ values (< -10 ‰), but this is coupled with extremely high $\delta^{15}N$ values (> +20 ‰) relative to terrestrial reservoirs and therefore do not fit the Dachine sample set (figure 5.18). It is difficult to argue that the coupled $\delta^{13}C$-$\delta^{15}N$ values observed in the Dachine diamonds are a relic of primordial heterogeneities, especially as there is not a meteorite class (or component of a class) to fit to the data (figure 5.18).

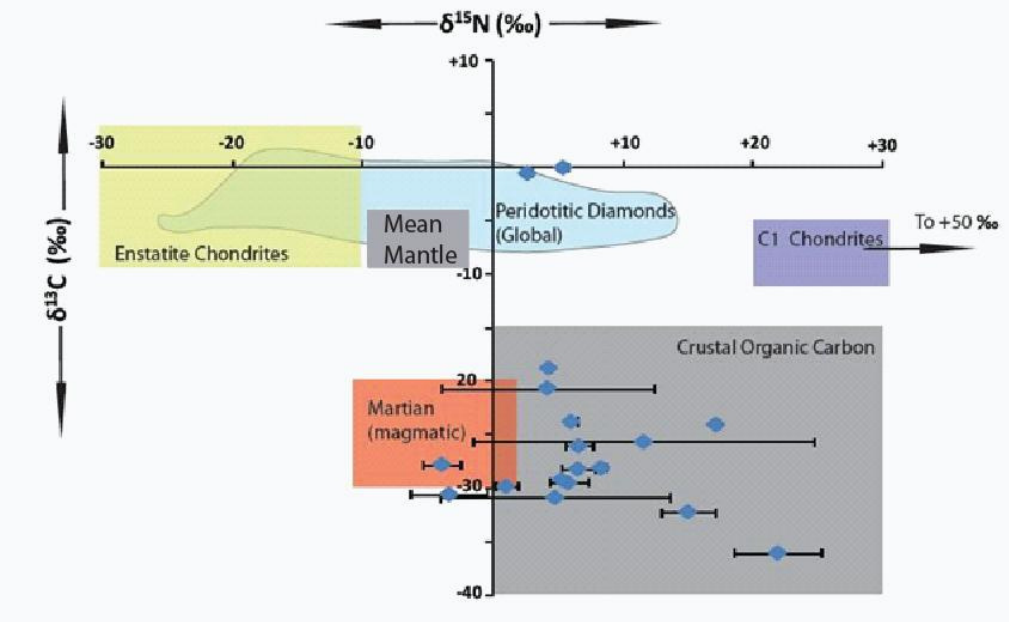

Figure 5.18. This plot illustrates the ranges and fields for coupled $\delta^{15}N$ vs. $\delta^{13}C$ values for the mean mantle and peridotitic monocrystalline diamonds (references as for figure 5.17), Enstatite and C1 chondritic meteorite groups, Martian magmatic C and N (from a review by GRADY and WRIGHT, 2003), pre-Cambrian crustal organic carbon (Shields and Veizer, 2002; Thomassot and Viljoen, 2007; Thomazo et al., 2011) and the diamonds from Dachine in this study (with blank-corrected precision to 1 σ is shown for $\delta^{15}N$, the errors for $\delta^{13}C$ are comparable to the symbol size).

5.8.2 Mantle layered heterogeneities

One model proposed to explain the low $\delta^{13}C$ values exhibited from the Dachine diamonds is that the carbon was derived from the transition zone (Cartigny, 2010). This is based, very tentatively, on the $\delta^{13}C$ values exhibited by TZ diamonds from the three studied occurrences: Juina in the Amazonian craton, and the Kankan and Jagersfontein from western and southern African cratons respectively. These exhibit (in order) modal $\delta^{13}C$ values of ∼-8, ∼ +1 and ∼-21 ‰ (± 2 ‰, see Stachel et al., 2005 for a review). The argument is that each geographical occurrence is distinct from one locality to the other, and different from the convecting upper mantle value known to have a $\delta^{13}C$ of -5 ± 3 ‰. I disagree that a mode at circa -8 ‰ (TZ samples from Juina) is significantly different from one at -5 ± 3 ‰ (terrestrial mantle). I also disagree that this is a feasible model as lower mantle diamonds exhibit a mean $\delta^{13}C$ value of -5 ‰ (for a review see Cartigny, 2005), therefore it is difficult to fathom

why the transition zone would be highly heterogeneous and the upper and lower mantle homogeneous. Additionally, all of the TZ samples from Juina, Kankan and Jagersfontein contain eclogitic majoritic garnets, and the Kankan and Jagersfontein $\delta^{13}C$ values fit well with sedimentary carbonate and organic carbon respectively, and therefore could be better explained using plate tectonics and reduction of sedimentary carbonates ($\delta^{13}C = 0 \pm 4$ ‰) or further reduction of already reduced organic carbon ($\delta^{13}C$ value = -10 to -40 with a mode at around -25 ‰). Since Cartigny (2010) went to print, Bulanova et al (2010) was published and documented majorite-bearing sublithospheric diamonds from Juina with $\delta^{13}C$ values ranging to circa -5.9 to -14.7 ‰, thus disagreeing with the previous observation of Stachel et al (2005). Therefore I do not feel the model of Cartigny (2010) is applicable for the diamonds from Dachine, especially as their syngenetic garnets are not majoritic.

5.8.3 Isotopic fractionation

The model whereby low $\delta^{13}C$ diamonds are produced from an initial mean mantle-like $\delta^{13}C$ value (circa -5 ‰) by isotopic fractionation of ^{13}C driven by the synchronous formation of diamond and CO_2 (where the CO_2 is removed in an open system- Rayleigh type) within an eclogitic host rock (CARTIGNY et al., 1998a) can perfectly explain some eclogitic monocrystalline diamond populations, such as Jwaneng (exemplified in figure 5.19). However it is not considered to apply to the Dachine diamond population for the following reason. This model requires a trend of decreasing $\delta^{13}C$ values for each stage in the progressive (Rayleigh type) fractionation process from a $\delta^{13}C$ value of circa -5 ‰ and N concentration that is akin to the mean mantle (> 300 ppm). This is not seen in the diamonds from Dachine (figure 5.19).

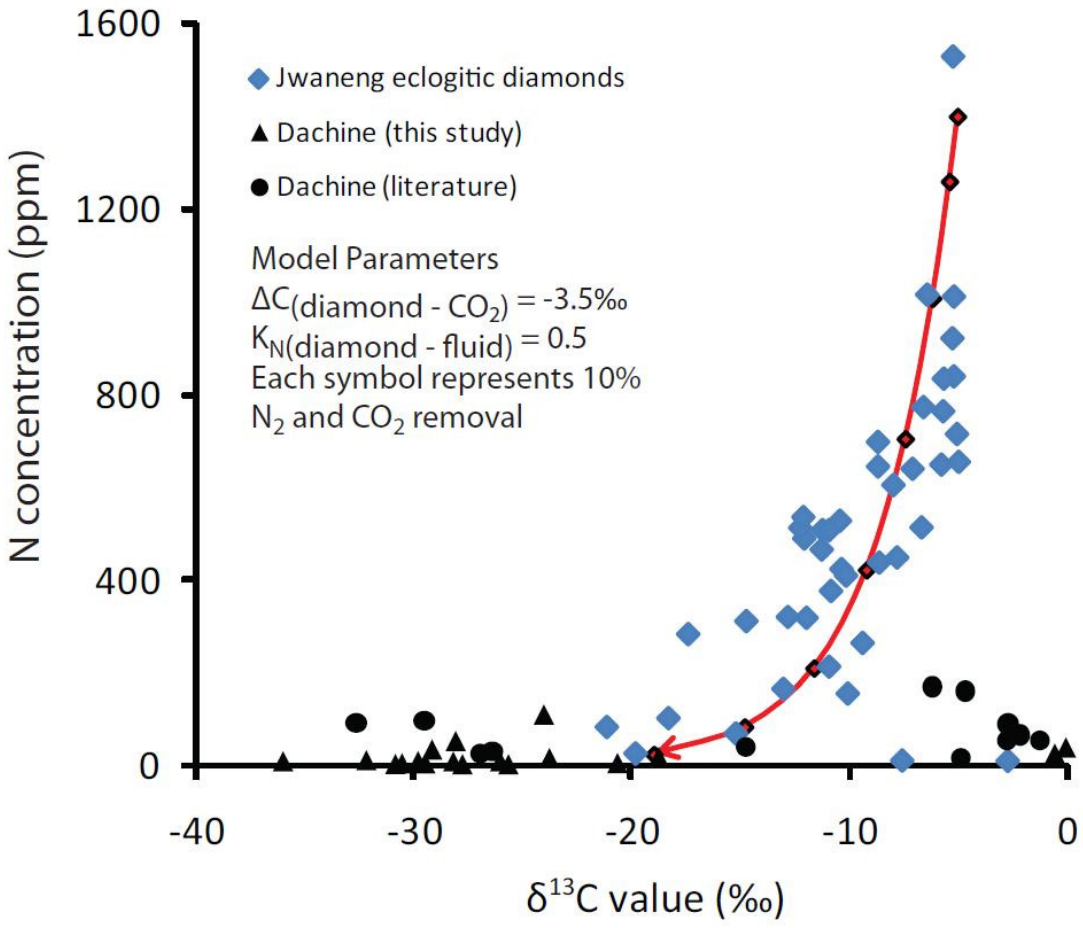

Figure 5.19. A variation diagram of $\delta^{13}C$ values vs. N concentrations (ppm) for eclogitic monocrystalline diamonds from Jwaneng (from CARTIGNY et al., 1998a), and Dachine diamonds from this study and the literature (CARTIGNY, 2010; CARTIGNY et al., 2001b; MCCANDLESS et al., 1999). The modelled trend (red line with red diamond symbols) is derived using the equations in Cartigny et al (2001b). Note the conspicuous absence of any Dachine samples plotting along this fractionation trend and the uniform low N concentrations for various $\delta^{13}C$ values in Dachine samples.

There is an alternative fractionation model that has been used to explain low $\delta^{13}C$ values exhibited by a population of garnet-bearing polycrystalline diamond nodules (diamondites) that was used to discuss the abundance of low $\delta^{13}C$ values (mean = -18 ‰) in diamondites and the intergrowths of peridotitic and websteritic garnets ± clinopyroxenes (silicate melts) with no olivine in diamondites (MARUOKA et al., 2004). This model is fully reviewed and tested using the same samples as said study by determining the coupled $\delta^{13}C$-$\delta^{15}N$ values and N/C ratios in the following chapter (chapter 6). I will briefly this model.

Diamond with anomalously low $\delta^{13}C$ values might be explained by Rayleigh fractionation from an isotopically homogeneous reservoir with an isotopic composition identical to that of the Earth's upper mantle (circa – 5 ‰). This fractionation model differs from Cartigny et al (1998) as the reaction governing the ^{13}C fractionation is CH_4-CO_2 as oppose to diamond-CO_2 (i.e. it precludes diamond formation as oppose to occurring simultaneously). The model assumes that the initial carbon source is CH_4 with a $\delta^{13}C$ value is circa -5 ‰. The separation of CO_2 is caused by removal of carbonates from the diamond-forming fluid that are generated by first oxidising some CH_4 to CO_2 (generating the isotopic fractionation according to HORITA, 2001). This CO_2 then reacts with silicates , namely olivine + CO_2 = enstatite and magnetite at 1200 °C with a fO_2 of FMQ ± 2 log units, and is required explain the lack of olivine in peridotitic diamondites. Maruoka et al (2004) argue that this process can cause C isotopic fractionation factors required to explain those observed in diamonds from diamondites ($\Delta C \approx$ -13 ‰). This process fractionates the $\delta^{13}C$ value from upper mantle values (circa -5 ‰) to the values actually observed in the population of diamondites in the following chapter (circa -18 ‰). Maruoka et al (2004) argue that total variation of $\delta^{13}C$ values in diamonds of diamondites can be explained by variable degrees of oxidation of the originally reduced fluid phase (only using $\delta^{13}C$ values as a proxy). The reason this model is not applicable to monocrystalline diamonds globally, and therefore Dachine, is the lack of abundant (or minor peaks) for low $\delta^{13}C$ values in peridotitic monocrystalline diamonds. Should this model operate in the mantle one must ask the question; *why do almost no peridotitic monocrystalline diamonds exhibit low $\delta^{13}C$ values?* Therefore it cannot apply to monocrystalline diamond formation as it predicts low $\delta^{13}C$ values for diamonds with peridotitic garnets which is not seen in monocrystalline diamonds (see CARTIGNY, 2005).

5.9 Subduction zone tectonics before the paleo-Proterozoic

There are various arguments against subducted crustal organic carbon as a source of ^{13}C depleted diamond-forming carbon (CARTIGNY, 2005; CARTIGNY et al., 1998a; 1999; 2001b; 1998b; 2004b; DE STEFANO et al., 2009; DEINES, 2002; GAUTHERON et al., 2005; 2006), and I have chosen to systematically test these below using my new data from the Dachine diamonds.

5.9.1 The $\delta^{15}N$ and modal $\delta^{13}C$ arguments

Two isotopic arguments are ruled out by the data in this chapter alone. These are that low $\delta^{13}C$ diamonds have mantle-like negative $\delta^{15}N$ values such as those shown in figure 5.17 for Jwaneng and Kimberly pool diamonds (CARTIGNY et al., 1998a; 1998b). The second is that low $\delta^{13}C$ diamonds are merely a sub-set of eclogitic populations and that the mode is still centred around -5 ± 3 ‰ (CARTIGNY, 2005; CARTIGNY et al., 1998a; 1999; 2001b; 1998b). To elaborate, most monocrystalline diamonds with coupled low $\delta^{13}C$ (-10 to -20 ‰) and high $\delta^{15}N$ (0 to < +20 ‰) values have previously been observed as sub-sets of several diamond populations, such as diamonds from Jagersfontein, Argyle, Arkansas (Boyd and Pillinger, 1994) and Namibia (CARTIGNY et al., 2004b). However these are minor sub-sets of populations that also exhibit modal peaks for $\delta^{13}C$ values at -5 ‰ (Cartigny, 2005; Cartigny et al., 1998a; 1999; 2001b; 1998b). This is not the case for diamonds from Dachine.

5.9.2 The lack of pelagic carbonate contribution

The lack of $\delta^{13}C$ values centred at around 0 ‰ (which represents the mean $\delta^{13}C$ value for pelagic carbonates) has been used to argue against the role of subduction in explaining the $\delta^{13}C$ values observed at Dachine (Cartigny, 2010), despite some Dachine diamonds exhibiting $\delta^{13}C$ values between -2 and +1 ‰ (figure 5.5). Despite this, Cartigny (2010) argued that there must still be an

explanation for the lack of a pronounced peak representing sedimentary carbonates. The argument is that '*if*' the subducted package contained carbonate rocks, they would dominate the majority of the subducted C by mass (> 80% relative to organic carbon). One argument against a large pelagic carbonate contribution is that carbonates (Ca and Mg types) have stable high pressure polymorphs (up to 130 GPa OGANOV et al., 2008). This could have inhibited the contribution of their carbon to the fluid that precipitated the diamonds.

Another argument against the role of subduction is that the subducted crustal carbon package was depleted in carbonates, which would be expected as it was > 2 Ga when pelagic carbonates were scarce. This is because the microorganisms that are known to produce the rock-forming carbonate in the oceans may not have existed before the Cambrian (Mackenzie and Morse, 1992). Also, should the carbon (and nitrogen) be sourced from subducted organic carbon, there is no reason to assume that the oceanic crust that was subducted was in an ocean where the depth of sedimentation was above the carbonate compensation depth (CCD) for the time in question (below the CCD, CO_2 is dissolved into the sea water and there is no solid carbonates precipitation). This is difficult to calculate for pre-Cambrian environments as there are no preserved pelagic carbonate sediments and uniformitarianism cannot be applied as the depth of the CCD varies as a function of pressure, temperature and the pCO_2 which is constantly changing with time. To complicate matters, oceanic pCO_2 is determined by the amount of dissolved CO_2 and H_2CO_3 in water (unknown for the paleo-Proterozoic). This variable is controlled by pH, depth, and temperature of the ocean/sea (also unknown for the paleo-Proterozoic). Another difficult issue is that biochemical processes in the ocean can also influence on the pCO_2 in the ocean. Interestingly, Proterozoic metamorphic diamonds that are directly converted crustal C do not display any $\delta^{13}C$ values centred around 0 ± 1 ‰ (CARTIGNY et al., 2001a) and have a similar modal value to eclogitic diamonds from Guaniamo, Venezuela of ~ -15 ‰ (KAMINSKY et al., 2000). Therefore the lack of a peak for $\delta^{13}C$ values centred on 0 ± 1 ‰ (the common composition for sedimentary carbonates through time- see SHIELDS and VEIZER 2002) in the Dachine diamonds may be a function of one or all of the reasons outlined above.

5.9.3 The low C/N ratio argument

A common argument implemented against low $\delta^{13}C$ values being derived from subducted crustal carbon is the relatively low C/N ratio of crustal material relative to mantle material (CARTIGNY et al., 1998a; 1999; 1998b). This is especially true of Dachine (crustal material C/N = 5-20 whereas Dachine C/N is >10,000). It is known that Proterozoic metamorphic microdiamonds in UHP metamorphic terrains have lower C/N ratios than mantle diamonds, and they are interpreted to have formed by the solid state conversion of crustal C to diamond (CARTIGNY et al., 2001a). Below I discuss the current understanding of the behaviour of N and C during subduction, and propose a model that generates high C/N ratios (akin to mantle diamonds from Dachine) from low C/N ratios (akin to crustal material).

The subducted 'package' (defined as an unknown mixture of pelagic sediments with an assumed isotopic and elemental C-N composition) may lose N in much greater proportions to C during subduction and therefore greatly fractionate its C/N ratio. This is based on the relative compatibilities of C and N in geological systems (WALLACE, 2005). Carbon is far more compatible in the residual (slab) than N, as it can form various solid species (mineral phases) under most terrestrial P-T-fO_2 conditions. This does depend on their respective compatibilities as a function of the phase equilibria in question, which requires better constraints. The behaviour of N relative to C in subduction zones is a non-uniform process and is heavily dependent upon the geothermal gradient (MITCHELL et al., 2010).

Fischer et al (2002) studied the N and He isotopic and relative abundance characteristics of volatiles emitted from two segments of the Central American volcanic arc, and postulated that on a global scale, sediments transport N during subduction to depths of arc magma generation only, and concluded that the recycling of subducted N to the surface via arc volcanism is an extremely efficient process. Therefore very little N will be subducted beyond the mantle wedge. The decrease in N with increasing metamorphic grade in sedimentary rocks has been observed and these rocks also show an

increase in $\delta^{15}N$ values with decreasing N concentrations (Bebout and Fogel, 1992; Haendel et al., 1986). However, the equilibrium fractionation factors for NH_3 decomposition to N_2 are low at high temperature, circa +0.7 and +2.7 ‰ for 800 and 600 °C (see LI et al., 2009) and would decrease as a function of increasing temperature (UREY, 1947). Therefore the degree of isotopic fractionation would depend upon the temperature of devolatilisation of N (possibly via decomposition of NH_3 to N_2). Applying a warmer mantle in the paleo-Proterozoic to the model of Fischer et al (2002) could explain why the $\delta^{15}N$ values for the Dachine diamonds are still centred on the model distribution for pre-Cambrian sedimentary and organic materials and not fractionated to heavier values (figure 5.12). The high $\delta^{15}N$ values (> +15 ‰) are consistent with high $\delta^{15}N$ values observed in pre-Cambrian kerogen and mica (THOMAZO et al., 2011; 2009).

This is not as simple as stated above because variations in the geothermal gradient between subduction zones can have a major effect on N degassing/devolatilisation. Busigny et al (2003) demonstrated that under cold slab environments N can be subducted to at least the depth of arc magmatism and cited the occurrence of microdiamonds with N concentrations as high as 11,000 ppm (CARTIGNY et al., 2001a) as evidence that N can be subducted beyond the depth of arc magmatism.

Therefore to summarise, N can be subducted below the depth of arc magmatism along cold slab environments as microdiamonds with high N concentrations testify (BOSTICK et al., 2003; CARTIGNY et al., 2004a; 2001a; DE CORTE et al., 1998; DOBRZHINETSKAYA et al., 2001; OGASAWARA, 2005), and is most likely highly depleted by devolatilisation reactions along warm-hot slab environments (FISCHER et al., 2002).

Regarding carbon it seems that less C is recycled back to the surface via arc magmatism than N (for a thorough review see WALLACE, 2005). The estimates of C recycling in subduction zones are mostly based on the C isotopic compositions of fumarolic gases to distinguish the relative proportions of different C sources (HILTON et al., 2002) assuming no significant ^{13}C fractionation during degassing

and/or melting. These estimates are sensitive to not only the assumption of minor ^{13}C fractionation, but also the values assumed for the mantle $CO_2/^3He$ ratio and the sedimentary $\delta^{13}C$ value, which may vary from arc to arc as well as from subducted package to subducted package (i.e. above or below the CCD). None the less there is a slight consensus that roughly 50 % of the subducted carbon is returned to the surface via arc magmatism (WALLACE, 2005).

What this means is that when C and N are not heavily degassed in cold slab, UHP environment microdiamonds with high N concentrations can form. When they are degassed (warm-hot slab environments) the loss of N >> C. Therefore there is no reason to assume that should subducted organic carbon surpass the depths of the mantle wedge (which is not a constant depth and is arc dependant) that the C/N ratio of the product will reflect the initial ratio. The C/N ratio will most likely be heavily fractionated towards higher values (low N concentrations). This subducted package need not form micro-diamonds as is the case for the solid state UHP metamorphic diamonds. The C and N might, for example, be locked up as NH_3 ions in amphiboles and C as deep hydrocarbons (SPANU et al., 2011). If the latter were to subsequently contribute to the diamond-forming fluids then diamond with low N concentrations and low (organic-like) $\delta^{13}C$ values may result, perhaps as the Dachine diamond population.

The trends in Figure 5.20 show the results of simple calculations to predict the N concentration of diamonds formed from subducted carbon with variable C/N ratios. The C/N ratio is calculated using the relative partitioning behaviours of C and N devolatilisation. In this model the amount of C loss is always 50 % (WALLACE, 2005) and the N loss varies from 90 to 99.8 % (FISCHER et al., 2002). This is plotted against the percentage of N devolatilisation from the subducting sediments (between 99 and 99.9 % according to FISCHER et al., 2002). This clearly demonstrates that if diamonds form from COHN fluids derived from subducted sediments along a warm-hot geotherm they should have high C/N ratios that do not reflect their crustal source and instead reflect eclogitic mantle diamonds.

To summarise, the low N concentrations in Dachine diamonds can be derived from sediments that had a much higher N concentration using the relative proportions of devolatilisation for C and N based on inferences made by interpreting empirical data. Another point is that should N be incompatible in diamond relative to the diamond-forming fluid (BOYD et al., 1994; CARTIGNY et al., 2001b) one can apply all of the trends for C/N ratios of 5-10 to generating the Dachine diamonds, as the subsequent diamond that precipitate should have less N than the fluid from which they precipitate.

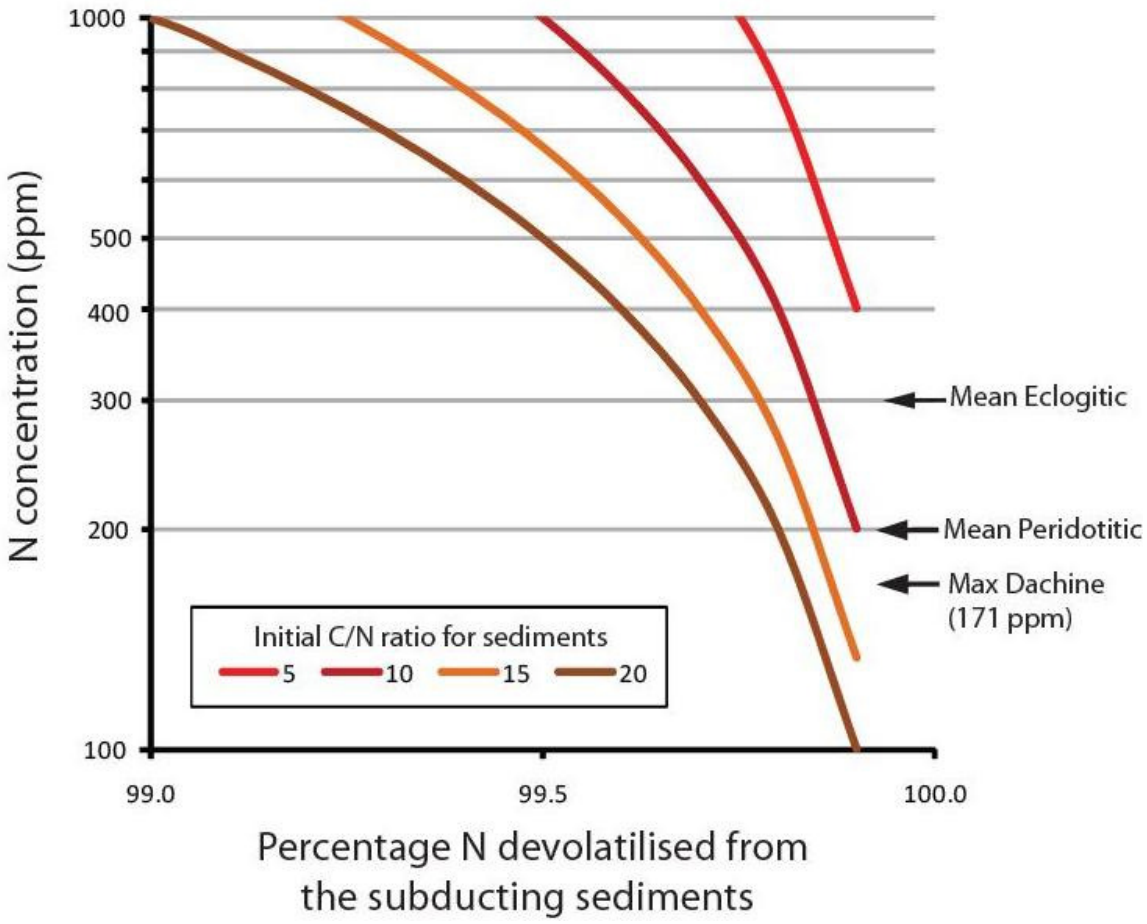

Figure 5.20. Fractionation trends for the percentage of N devolatilised vs. the resulting N concentration (ppm) expected in diamonds formed via subduction of crustal carbon (≈ N/C). The trends are all calculated using different initial C/N ratios (see key) where the degree of C loss is a constant set at 50 %.

What is also evident here is that more HPHT experimental and theoretical thermodynamic studies are required to better constrain the behaviour of C and N and other light volatile elements. These are required under various realistic P-T system(s) and will enable the K values, isotopic fractionation factors and equilibrium speciation as a function of fO_2 to be determined to better understand the fate of subducted volatiles though time.

5.10 Conclusion

This new data corroborates the pre-existing data that demonstrates Dachine diamonds to have low for $\delta^{13}C$ values and contain a high abundance of type II diamonds (> 90 %), relative the majority of mantle diamonds. I have demonstrated that the Dachine diamonds are of eclogitic paragenesis and characterised by positive $\delta^{15}N$ values.

Based on the carbon and nitrogen isotopic constraints the most likely origin of the diamond-forming carbon was from the subduction of crustal organic carbon (i.e. Kerogen). The low nitrogen concentrations can be formed by subducting sediments along a warm-hot geotherm where the nitrogen loss from the sediments is considerably greater than the carbon loss (this statement requires experimental constraints to test it, and quantify the K values). The decoupled nature of C and N removal by devolatilisation can strongly fractionate the C/N ratio from 5-20 in the sedimentary package to C/N > 10,000 as seen in the Dachine diamond population. This has produced diamonds with low nitrogen concentrations, positive $\delta^{15}N$ values and low organic-carbon like $\delta^{13}C$ values as observed at Dachine. The existence of a subduction zone before 2 Ga below the Dachine regions of the Guiana shield is also predicted based on the existence of the greenstone belt. This study does require, and may demonstrate, Phanerozoic-type subduction zone processes at least as deep as the top of the diamond stability field (~ 150 km) before the paleo-Proterozoic age of the

volcaniclastic host rock (2.11 Ga). This is based on the garnet paragenesis being eclogitic and the stable isotope constraints presented in this chapter.

Chapter 6

Origin of the diamond-forming carbon from diamondites: A stable isotope approach

Dedication:

This chapter is dedicated to Prof. Gero Kurat who passed away in December 2009. Gero had supplied the samples for this study after a conversation I had at the 9th International Kimberlite Conference in Frankfurt, Germany, August 2008. The conversation was with Dr. Gabor Dobosi regarding their work on these samples and the need for nitrogen isotope work that I was happy to perform. His reaction was to get the samples to me and for the data to be acquired with no hesitation or time wasting. I am also grateful for his hospitality during my visit to the Natural History Museum in Vienna (April 2008). I appreciated his harsh sense of humour that led to some banter regarding the abundance of other nations treasures in the museums of the British Empire compared to the Austro-Hungarian Empire. The last thing Gero said to me in an email (on Saturday, November the 21st, 2009 at 11:13am) regarding the data in this chapter reads as follows;

'I am very curious'

6.1 Introduction

The objective of this chapter is to determine the $\delta^{15}N$-$\delta^{13}C$ values and N concentrations from 13 websteritic and 8 peridotitic diamondites to place constraints upon the source of the anomalously low 'organic carbon-like' $\delta^{13}C$ values exhibited by a mostly peridotitic diamond population.

Diamondites are monomineralic mantle xenoliths made up predominantly of diamond with minor amounts of garnet and clinopyroxene (DOBOSI and KURAT, 2002; KURAT and DOBOSI, 2000). Very rarely trace amounts of metallic iron-carbides are present, which may explain some samples that have been observed to exhibit a subtle magnetisation (HEANEY et al., 2005; JACOB et al., 2004). Diamondites from different localities exhibit subtle variations in diamond textures and included assemblages in the polycrystalline mass, and unlike monocrystalline diamonds, several studies have revealed evidence for a mixed eclogitic (E-type) and peridotitic (P-type) paragenesis in the same sample (HEANEY et al., 2005). However, there are significant differences between the P and E type inclusions in monocrystalline diamonds, and the P and E type intergrowths in diamondites. Typical P type inclusion minerals such as olivine and orthopyroxene have not been found in P type diamondites thus far, and the typical E type inclusion mineral omphacitic clinopyroxene are very rare and not found in this sample suite (DOBOSI and KURAT, 2002; 2010; KURAT and DOBOSI, 2000). The compositional variation in certain mineral phases such as E garnets in diamondites is also different from E garnets within their single crystal diamond inclusion equivalents — they appear to have a restricted Ca variation (DOBOSI and KURAT, 2002; JACOB et al., 2000).

A rigorous study of the global range of diamond crystal size variations and geochemistry in diamondites is lacking (Heaney et al., 2005), despite the abundance of diamondites, they can make up to 50 % of a diamond mines total yield (DEINES et al., 1991; HEANEY et al., 2005). Also, the relative abundance of polycrystalline diamonds between kimberlites and lamproites is not known. It could be the case that the monocrystalline and polycrystalline diamonds represent different diamond-forming events at a given kimberlite pipe. This is known for coated diamonds, where they precipitate from

proto-kimberlite fluids and are kimberlitic phenocrysts that 'coat' around much older, pre-existing diamond cores which are therefore xenocrysts (BOYD et al., 1994). Another example that is unrelated to the proto-kimberlite melts are monocrystalline diamonds at the Udachnaya kimberlite in Yakutia, Siberia. Here, the monocrystalline diamonds represent 3 distinct diamond-forming events spanning a time frame >1.5 Ga. The harzburgitic diamond-forming event was 3.1-3.3 Ga, the eclogitic diamond-forming event was 2.9 ± 0.4 Ga and the final known diamond-forming event was lherzolitic and occurred at 2.01 ± 0.06 Ga (GURNEY et al., 2010). The spatial and temporal relationship for polycrystalline diamonds to their host kimberlites and monocrystalline counterparts at any kimberlite is also currently an unknown.

Regarding the stable isotope geochemistry of diamondites, they show a bimodal distribution for $\delta^{13}C$ values globally, again unlike monocrystalline diamonds (figure 6.1). Also unlike monocrystalline diamonds, the $\delta^{13}C$ values for diamonds within diamondites show no correlation with silicate paragenesis. Data for the $\delta^{15}N$ values for diamonds of diamondites is lacking relative to monocrystalline diamonds (figure 6.2 and caption). What can be stated is that the mean $\delta^{15}N$ values analysed from 20 samples are distinctively positive (+6.45 ± 4.49 ‰) with a large range for the N concentrations from 56 to 1973 ppm (GAUTHERON et al., 2005; SHELKOV, 1997), this is not typical for their monocrystalline counterparts.

In this chapter I present the $\delta^{15}N$-$\delta^{13}C$ values and N concentrations from 13 websteritic and 8 peridotitic diamondites to place constraints upon the source of the anomalously low 'organic carbon like' $\delta^{13}C$ values exhibited by both the peridotitic and websteritic populations. I use this data to question the similarities and differences for the petrogenesis of polycrystalline and monocrystalline diamonds in general, but I am not assuming that this study can explain the petrogenesis of all polycrystalline diamonds worldwide.

6.1.1 No constraints on the geographical origin

There is a problem with the samples in this study: their geographical origin, and therefore primary source rock is unknown (KURAT and DOBOSI, 2000). Despite this, I use the co-variations for $\delta^{15}N$-$\delta^{13}C$ values and N concentrations and test the model of Maruoka et al (2004 that is solely based on C isotope constraints for the samples in this chapter) and question why a mostly peridotitic sample set exhibits show ^{13}C depletion relative to the mantle.

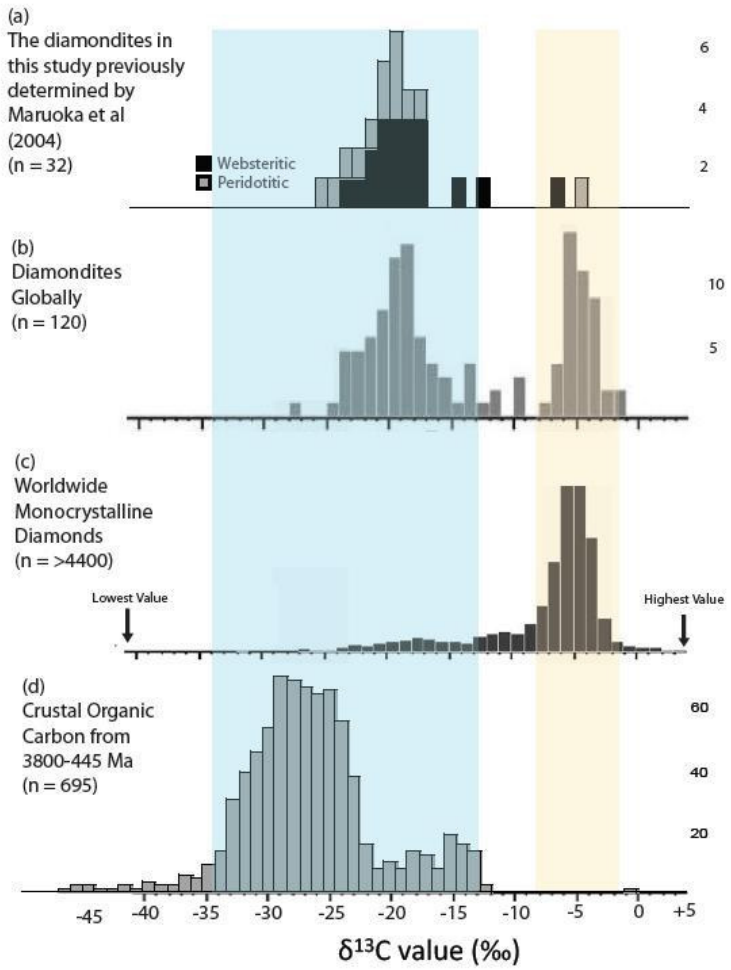

Figure 6.1. Histogram of the carbon isotope distribution of relevant diamond populations (a-c) and pelagic organic carbon (d). (a) Data for diamondites of which this chapters sample set are a sub-set (MARUOKA et al., 2004). (b) All diamondites globally (compiled in MARUOKA et al., 2004). (c) Worldwide monocrystalline mantle diamonds (compiled by Cartigny, 2005) and (d) pre-Cambrian crustal organic carbon (compiled by Shields and Veizer, 2002). The bin size used was 1 ‰. The orange band at $\delta^{13}C$ -5 ± 3 ‰ represents the mean mantle $\delta^{13}C$ range (from Cartigny, 2005) whereas the blue band at $\delta^{13}C$ -25 ± 10 represents the range for $\delta^{13}C$ values shown by pre-Cambrian crustal organic carbon (SHIELDS and VEIZER, 2002).

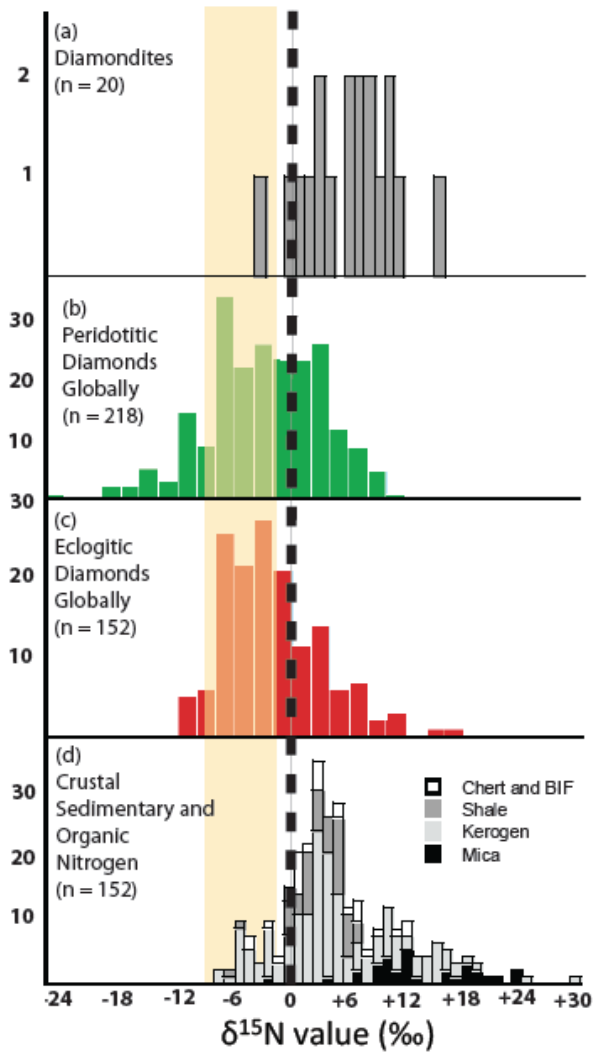

Figure 6.2. The $\delta^{15}N$ values for (a) diamonds of diamondites of unknown silicate paragenesis where Shelkov (Shelkov, 1997) and Shelkov et al (1997) documented the $\delta^{13}C$-$\delta^{15}N$ values and N concentrations for 12 samples and Gautheron et al (2006) produced data for 6 samples from Orapa, Botswana. There is no difference in distribution patterns for either study and therefore I have grouped them. (b) Worldwide peridotitic monocrystalline diamonds and (c) Worldwide eclogitic monocrystalline diamonds (compiled by CARTIGNY, 2005) and (d) the N isotopic values for pre-Cambrian chert, banded Iron formations (BIF), shale, Kerogen and micas (THOMAZO et al., 2011; 2009). The bin size used was 1 ‰. The orange band at $\delta^{15}N$ -5 ± 3 ‰ represents the mean mantle $\delta^{15}N$ range (from Cartigny, 2005).

6.2 Previous models for formation

Several models exist to explain the formation of diamondites and a summary is provided here. There are several opposing models to explain the origin of the carbon globally; however there is one definitive consensus. This is that the fine grain size and polycrystalline nature of diamondites is a function of carbon oversaturation and rapid nucleation and crystal growth (HEANEY et al., 2005) which has been demonstrated experimentally (LITVIN, 2006). The following summary with focus on the stable isotope models as these are the models being tested in this chapter. The only set of diamondites that have had their garnets studied in detail for major, trace and rare Earth element data with coupled stable isotope data are the samples in this study (DOBOSI and KURAT, 2009), which make detailed comparisons of other populations an impossible task.

6.2.1 Subduction of crustal organic carbon

Several studies have used C and noble gas isotope constraints to conclude a crustal origin for the diamond-forming Carbon (BURGESS et al., 1998; HONDA et al., 2004; SHELKOV, 1997), whilst others (GAUTHERON et al., 2005) have inferred a mantle origin. In fact, Mohapatra and Honda (2006) re-interpreted the data of Gautheron et al (2005) to conclude a crustal origin for the carbon based on the N and noble gas isotopes. They stated that the Xe, Ar and N isotopes are akin to subducted sea water and air. This was contested by Gautheron et al (2006) by arguing that the sea water and air compositions would be heavily fractionated during subduction and devolatilisation. Fundamentally, this is open to debate and more work is needed. However the model whereby diamondites are formed from subduction of crustal material may explain the mixed eclogitic and peridotitic chemical signatures imprinted within the syngenetic garnets (HEANEY et al., 2005), and the lack of a correlation between $\delta^{13}C$ values and garnet paragenesis (MARUOKA et al., 2004).

6.2.2 Mantle-derived carbon

Maruoka et al (2004) determined the $\delta^{13}C$ values for 13 peridotitic and 19 websteritic diamondites from the personal collection of Prof Gero Kurat housed at the Natural History Museum, Vienna, Austria, and their results are shown in figure 6.1a. Maruoka et al (2004) observed that the variations in the $\delta^{13}C$ values of diamonds from diamondites with peridotitic and websteritic garnet are almost identical and show maxima in their frequency distribution at about -18‰ (figure 6.1). They suggest that the difference between the peridotitic and websteritic garnets in the diamondites does not reflect different source rocks as may the case for monocrystalline diamonds (AULBACH et al., 2002). They accredited the modal $\delta^{13}C$ value at -18 ‰ and lack of paragenesis discretion to variable degrees of oxidation of an originally reduced fluid phase.

The model proposed by Maruoka et al (2004) explains the generation of low $\delta^{13}C$ values by Rayleigh fractionation from an isotopically homogeneous reservoir with an isotopic composition identical to that of the Earth's upper mantle (circa -5 ‰). The model (graphically shown in figure 6.3) assumes that the initial carbon source is CH_4 with a $\delta^{13}C$ value is circa -5 ‰. The separation of CO_2 is caused by removal of carbonates from the diamond-forming fluid that are generated by first oxidising some CH_4 to $H_2O + CO_2$ (generating the isotopic fractionation according to HORITA, 2001 and redox melting of peridotite). This CO_2 then reacts with silicates (namely olivine + CO_2 = enstatite and magnetite at 1200 °C with a fO_2 of FMQ ± 2 log units) and explains the lack of olivine in peridotitic diamondites. Maruoka et al (2004) argue that this process can cause carbon isotopic fractionation factors required to explain the observed in $\delta^{13}C$ values in diamonds from diamondites ($\Delta C \approx$ -13 ‰). This process fractionates the $\delta^{13}C$ value from upper mantle values (circa -5 ‰) to the values actually observed in the population of diamondites in this chapter (circa -18 ‰). Maruoka et al (2004) argue that total variation of $\delta^{13}C$ values in diamonds of diamondites can be explained by variable degrees of oxidation of the originally reduced fluid phase (only using $\delta^{13}C$ values as a proxy). They argue that this supports the model derived from trace element data, namely, that diamondites with peridotitic

and websteritic garnets were precipitated from carbonate- rich fluids that had a similar, peridotitic source (Dobosi and Kurat, 2002; Dobosi and Kurat, 2010; Kurat and Dobosi, 2000; 2008). This explains the limited CaO variations and large Cr_2O_3 variations that are a consequence of chromite removal from the melt (DOBOSI and KURAT, 2010). This causes the peridotitic garnets to plot in the websteritic field of the garnet discrimination diagram show in figure 6.4.

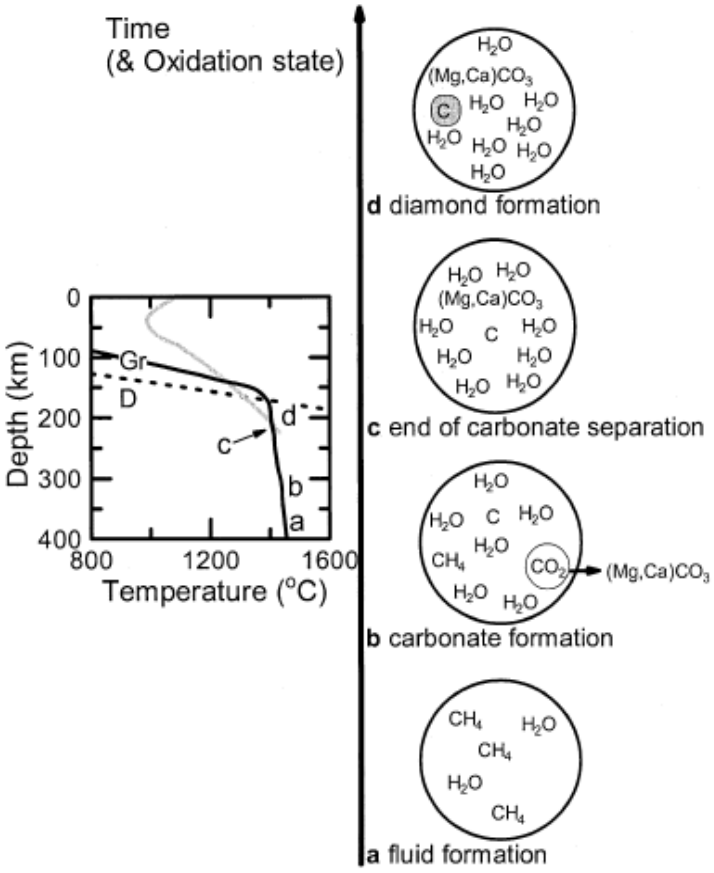

Figure 6.3. A cartoon illustrating the model from Maruoka et al (2004). See text for details.

6.2.3 Remobilised lithosphere forming young diamondites

Haggerty (1986) suggested that diamondites (globally) form in a similar manner to coated diamonds, whereby they represent C oversaturation from the proto-kimberlite fluid. One may argue that the textural (fibrous vs. polycrystalline) difference is due to the absence or presence of pre-existing diamonds to act as nucleation seeds that cause the extremely rapid growth rates that are required for coated diamond formation. One may then postulate that without 'seeds' acting as a growth nucleus, polycrystalline textures are more prevalent. Jacob et al (2000) also concluded that diamondites (from Venetia, SA) form synchronously with the kimberlite. They studied the trace element variations, $\delta^{18}O$ values, and radiogenic isotopic compositions (Nd and Sr) of 4 garnets, and the $\delta^{13}C$ values of the diamonds of 4 diamondites from the Venetia kimberlite, SA. The correlation between chemical variations from the garnets and the $\delta^{13}C$ values of the diamonds is interpreted as evidence of synchronous formation. They concluded that strontium zonation observed in the garnets would not be preserved for more than ~7000 years at 1000 °C, by assuming that the diffusion coefficients for Sr in eclogitic garnets (an unknown) may be comparable (within an order of magnitude) to the experimental values used for peridotitic garnet (SHIMIZU and SOBOLEV, 1995). Therefore the diamonds must have formed, in geological terms, synchronously with the kimberlite. This can be tested using the degree of nitrogen aggregation in diamondites, however there is no available data in the literature besides the extended abstract of Thomassot et al (2008). They cite B centres in diamondites from Orapa and Jwaneng (both Botswana) that require the diamonds to have been at mantle temperatures (~1100 to 1300 °C) on the Ga time scale.

6.2.4 Overall summary

I am unsure as to the applicability of these models above to the petrogenesis of diamondites on a global scale. An example of this is that for all of the models and contrasting views detailed above, the number of data points on the histogram for $\delta^{15}N$ values is > 350 for monocrystalline diamonds and only 20 for diamondites (figure 6.2). Therefore by detailing the nitrogen concentrations and doubling the amount of $\delta^{15}N$ data available for diamondites (in figure 6.2) where the garnets are well studied and $\delta^{13}C$ values are known for most of the samples and re-determined for clarity, should provide more of an insight into the population of diamondites in this study, and possibly globally.

6.3 Samples

The samples used in this investigation have been selected from a collection at the Museum of Natural History in Vienna by the now deceased Prof Gero Kurat. The exact locality of their source rock and therefore their geographical origins are not known, but according to the diamond dealer, the diamondites are of Southern African origin (KURAT and DOBOSI, 2000). Detailed descriptions of the samples are provided by Kurat and Dobosi (2000) and Dobosi and Kurat (2002). Therefore the size of the diamondites and diamond crystal size variations within the samples in this study are detailed, but not compared to any other diamondite populations, as this data is not available (HEANEY et al., 2005). The complete size of the diamondites varies from 1 to 2.5 cm with masses from 5 to 60 ct (Dia059 is exceptionally large, 103.5 ct). The samples used in this study are fragments of these Viennese diamondites, typically < 5 mm. Their colour varies from colourless (clear) through shades of grey to almost black, occasionally with a metallic lustre, which is common for diamondites (HEANEY et al., 2005). The sizes of individual diamond crystals vary among the samples from 50 µm (fine-grained samples) to > 1 mm (coarse-grained samples). The term “sample” may be misleading when discussing diamondites. As used in this chapter, ”sample” refers to a fragment of a diamondite

nodule that may contain many individual diamonds (as sizes range from 50 µm to 1 mm), which has been isolated after breaking the larger parent piece. This is opposed to monocrystalline diamonds where the term "sample" refers to a single crystal only.

The samples in this study have previously been studied for silicate geochemistry (Dobosi and Kurat, 2002; 2009; Kurat and Dobosi, 2000), diamond major and trace element geochemistry (REGE et al., 2008) and carbon isotope compositions (MARUOKA et al., 2004). The garnet paragenesis of all the samples in this study has previously been determined and is demonstrated in figure 6.4 (DOBOSI and KURAT, 2010). What is evident here is that unlike the Dachine garnets (chapter 5), the garnets in the diamondite samples are websteritic and cannot be defined as 'eclogitic'. There are 13 websteritic (previously defined as eclogitic by DOBOSI and KURAT, 2002; 2009; KURAT and DOBOSI, 2000; MARUOKA et al., 2004; REGE et al., 2008) and 8 peridotitic diamondites mostly of lherzolitic affinity.

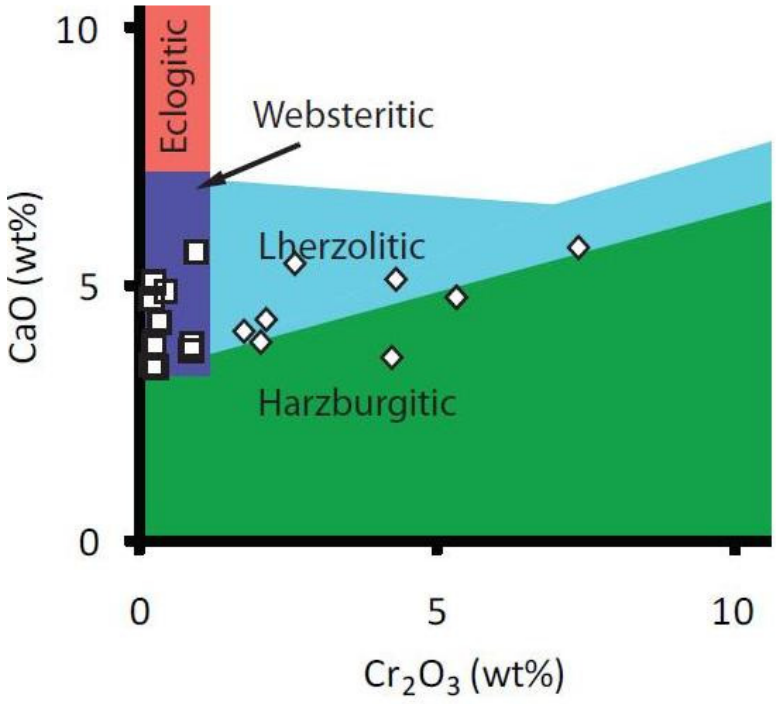

Figure 6.4. A Cr_2O_3 vs. CaO discrimination diagram after Aulbach et al (2002). The garnet data is from Dobosi and Kurat (2010). This demonstrates the websteritic nature of the samples termed eclogitic in previous works (DOBOSI and KURAT, 2002; DOBOSI and KURAT, 2010; KURAT and DOBOSI, 2000; MARUOKA et al., 2004; REGE et al., 2008).

6.4 Results

The full data table is given in the appendix (stepped data in table A12 and bulk data in table A13) and I present and discuss the data below in graphical form with comparative data. The selection of the Viennese samples for simultaneous $\delta^{13}C$, $\delta^{15}N$ and N/C (≈ N ppm) determinations was focused on samples where previous work has been published on the major and trace element concentrations of the silicates (DOBOSI and KURAT, 2002; DOBOSI and KURAT, 2009; KURAT and DOBOSI, 2000), and also $\delta^{13}C$ determinations in the diamonds (MARUOKA et al., 2004) to enable a comparison.

6.4.1 Carbon isotope values

The range for the $\delta^{13}C$ values in this study is -28.47 to -4.4 ‰ for diamondites with peridotitic garnets, and -22.85 to -5.49 for diamondites with websteritic garnets. As previously demonstrated by Maruoka et al (2004), there is no discrepancy between $\delta^{13}C$ values and garnet paragenesis (figure 6.1 a). There are 19 of the 20 samples in this study that are featured in Maruoka et al (2004), this provides a good opportunity to test the similarities in both sets of results. My carbon isotope data corroborate well with the previous study (MARUOKA et al., 2004) in terms of bulk $\delta^{13}C$ values and lack of any distinction between garnet paragenesis (figure 6.5 a & b). There is also a good agreement for the heterogeneity of the samples where multiple runs of the same sample in Maruoka et al (2004) and this study are comparable (maximum variation is 3 ‰ where the average standard deviation is < 1.2 ‰ with an average precision in this study of 0.33 ‰), this explains the deviation from a 1:1 trend in figure 6.6. The exception to this is sample Dia060 that exhibits a range for $\delta^{13}C$ values of 6 ‰ (n = 3).

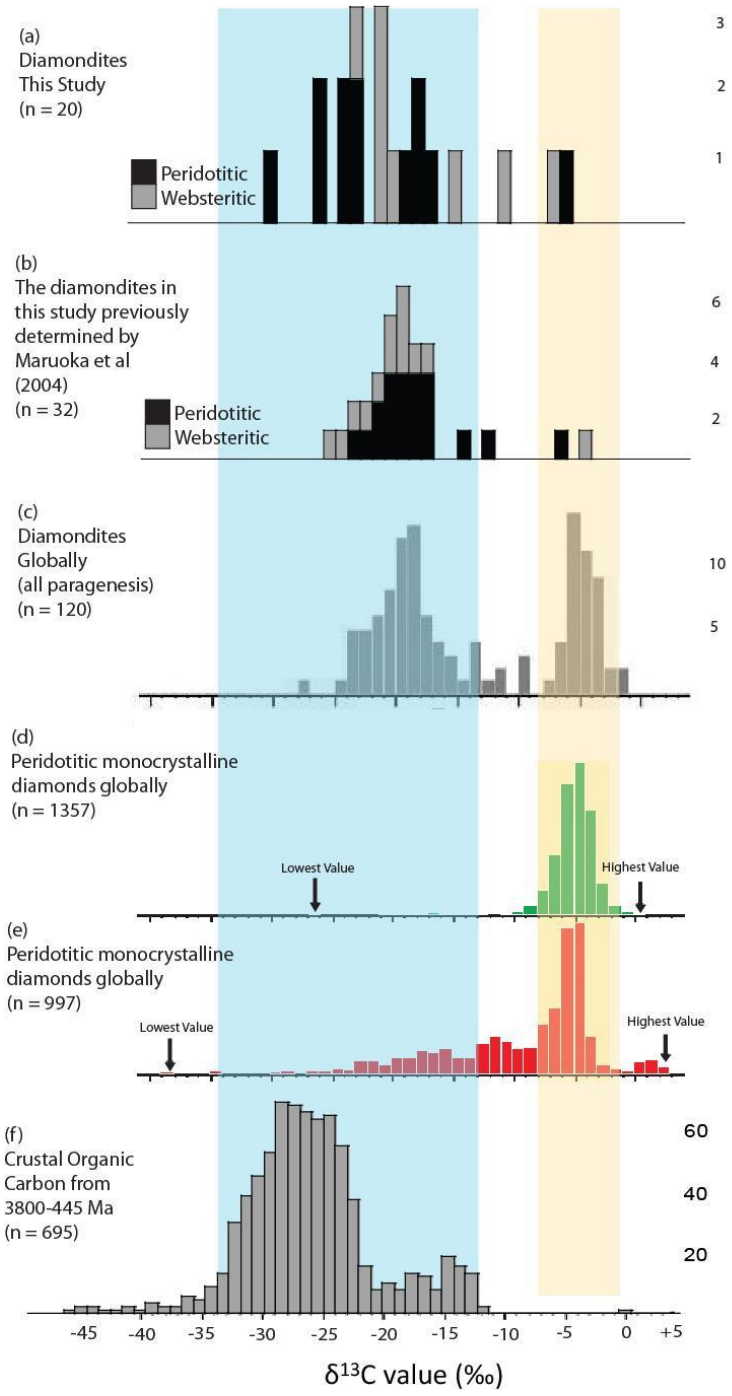

Figure 6.5: Comparative histograms for the $\delta^{13}C$ values for samples that feature in this study and in Maruoka et al., (2004) sub-divided by garnet paragenesis as determined by Dobosi and Kurat (2002; DOBOSI and KURAT, 2010). Note the lack of any correlation between garnet paragenesis and the $\delta^{13}C$ values as previously detailed by Maruoka et al (2004). The source of the data for b to f is the same as figure 6.1.

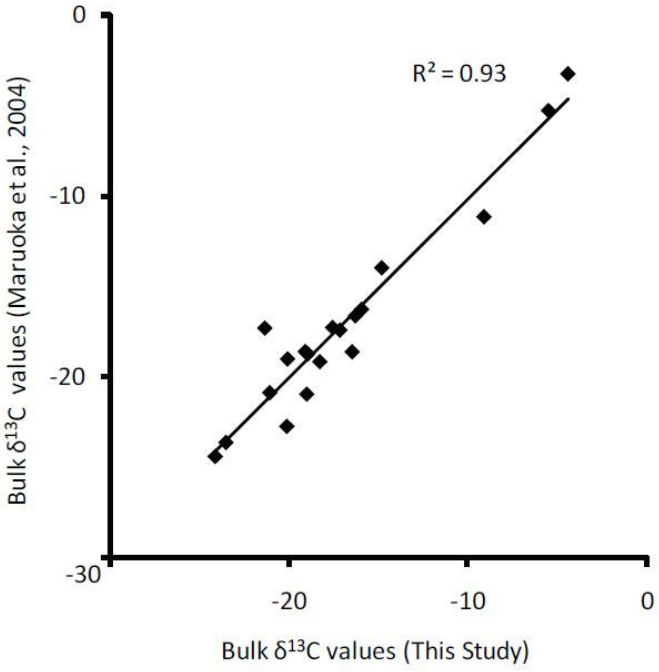

Figure 6.6: Comparative bulk (weighted mean) $\delta^{13}C$ values for samples that feature in this study and in Maruoka et al., (2004). The deviation away from a 1:1 trend is consistent with the deviation observed during multiple runs of samples from the same samples in Maruoka et al (2004) and by observing the deviation in $\delta^{13}C$ values at different stages of stepped combustion.

6.4.2 Nitrogen isotope values

The diamondites show a range in $\delta^{15}N$ values from -6.06 to +22.64 ‰ with a mean +8.68 ± 8.24 ‰ with the majority of the highest $\delta^{15}N$ values being of peridotitic paragenesis. This is however not a statistically significant observation (3 out of 5 samples with $\delta^{15}N$ values > +12 ‰ being of peridotitic paragenesis- see figure 6.7a). The mean value is not representative of the main peak centred at circa +3 ‰ owing to the large range in $\delta^{15}N$ values for this sample set (figure 6.7a). Data from the literature of diamondites with unknown silicate paragenesis exhibits a range of $\delta^{15}N$ values from -3 to +15 ‰ (figure 6.3b). The samples in this study extend the range for the $\delta^{15}N$ values of diamondites by almost +8 ‰ from circa +15 to +23 ‰ (figure 6.3). There is no observable peak in the literature data, possibly owing to several different sample populations and a small sample pool (see figure 6.3 and caption). What is evident is that neither the samples in this study nor the literature

plot with any clustering around a 'mantle' like $\delta^{15}N$ signature, nor are predominantly negative in value which is commonly argued to be a mantle characteristic shown in figure 6.2 . The websteritic samples display more variability than their peridotitic counterparts for multiple runs of the same sample with standard deviations of ± 6.18 and ± 2.38 ‰ respectively (with a mean precision of ± 0.55 ‰).

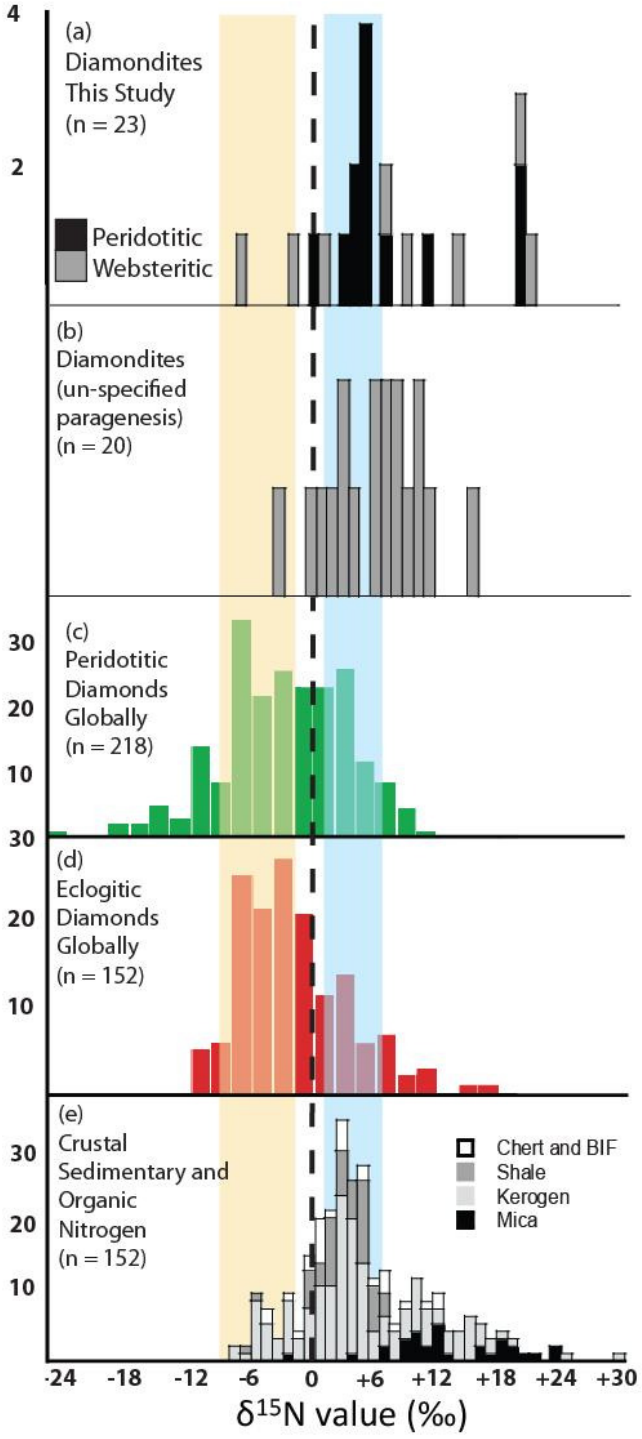

Figure 6.7: Histograms for the $\delta^{15}N$ values for samples that feature in this study and data from the literature. Comparative data and coloured bands are described in figure 6.2.

6.4.3 N concentrations

The mean N concentration for the diamondites in this study is 511 ppm; this is higher than the data sourced from the literature where the mean concentration is 331 ppm (GAUTHERON et al., 2005; SHELKOV et al., 1997). The distribution patterns for the N concentrations in this study and from the literature are comparable (figure 6.8). The N concentrations do show a discrepancy with garnet paragenesis that is again not statistically significant, in that the 3 samples with N concentrations > 500 ppm are websteritic (figure 6.8). The typical accuracy on the N concentrations is < 10 %.

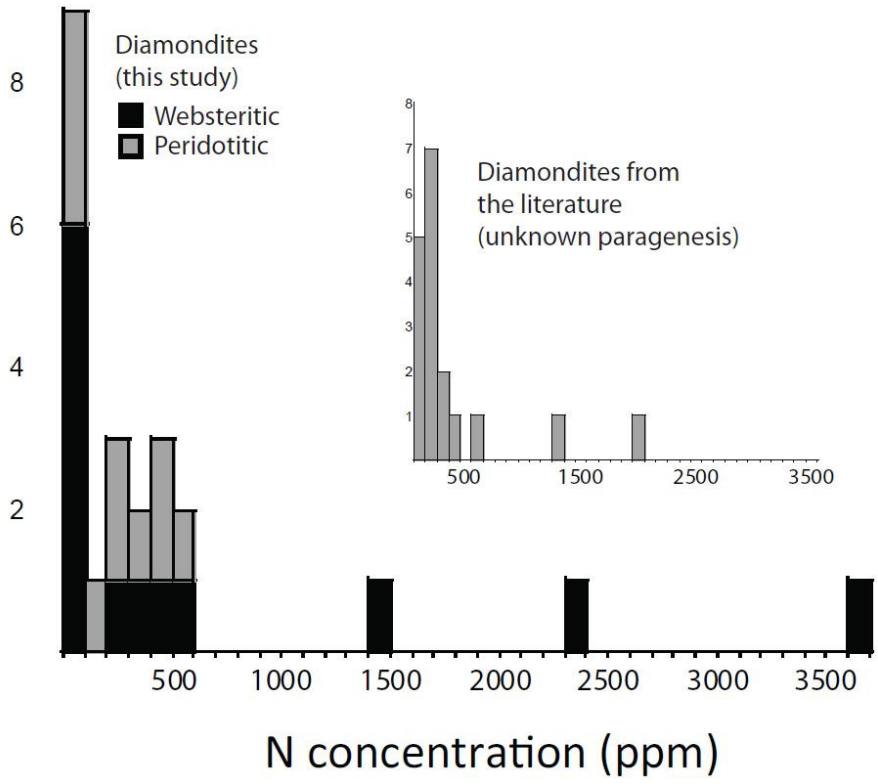

Figure 6.8. The nitrogen concentrations for this study and from the literature (sourced from GAUTHERON et al., 2005; SHELKOV et al., 1997). Note the similarity.

6.4.4 Co-variations of $\delta^{13}C$-$\delta^{15}N$ values vs. N concentrations

There is no discrepancy between $\delta^{13}C$, $\delta^{15}N$ values or N concentrations in the diamonds and the garnet paragenesis of the associated inclusions/intergrowths (detailed above). There is also no overall correlation for $\delta^{13}C$- $\delta^{15}N$ values vs. N concentrations for this sample set, as was the case for the samples in Shelkov (1997). There is no decrease in N concentration against decreasing $\delta^{13}C$ values or increasing $\delta^{15}N$ values for the sample set. Some samples plot distinctively in the mean mantle and pelagic organic fields for both C and N isotopes vs. N concentrations (figures 6.9 and 6.10). There is however, a positive trend for $\delta^{15}N$ vs. N concentration for the peridotitic suite. The linear nature could resemble a mixing line. For $\delta^{13}C$ vs. N concentration there is mostly scatter for the entire sample suite.

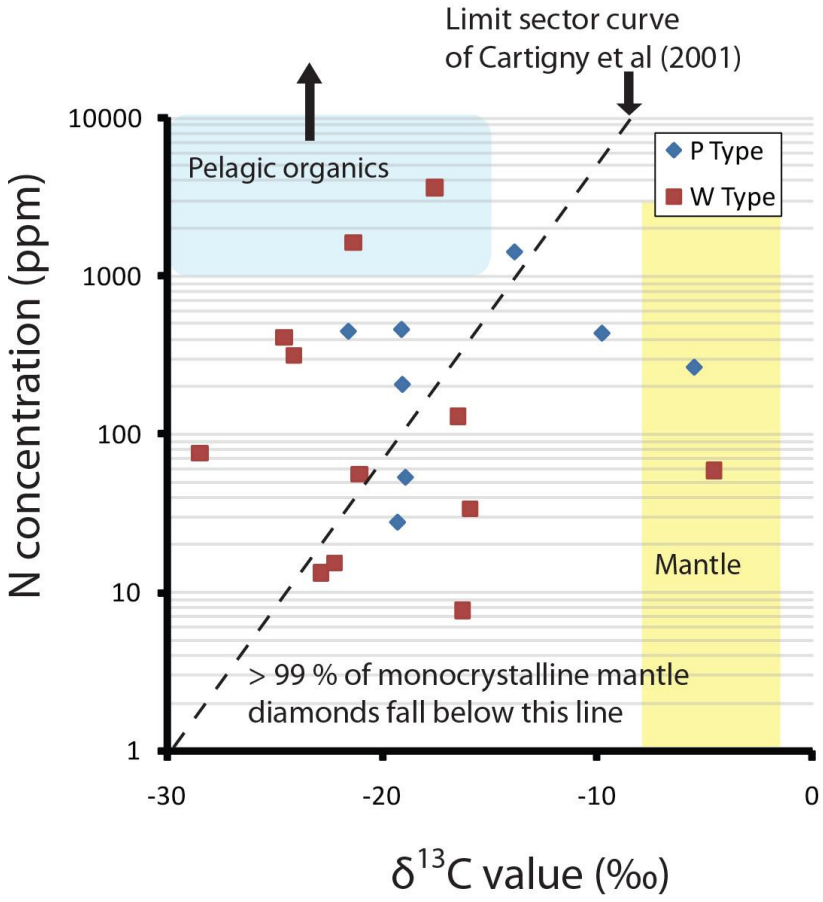

Figure 6.9: Variation diagram for $\delta^{13}C$ values (‰) vs. N concentrations (at.ppm) for the diamondites in this study. The dashed line labelled the limit sector curve and the yellow band that represents the mantle is from Cartigny et al (2001b) and the blue box that represents pelagic sediments and organic materials is from Hoefs (2009). About 90 % of monocrystalline mantle diamonds plot below the limit sector curve shown.

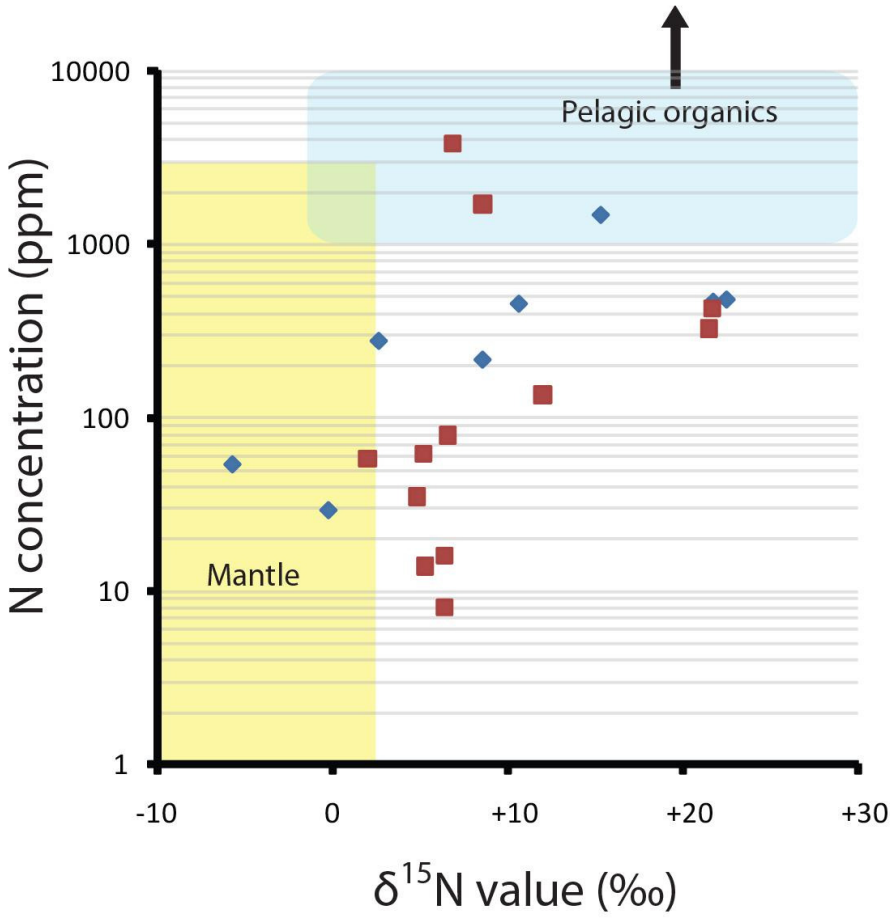

Figure 6.10: Variation diagram for $\delta^{15}N$ values (‰) vs. N concentrations (at.ppm) for the diamondites in this study. The yellow band that represents the mantle is from Cartigny et al (2001b) and the blue box that represents pelagic sediments and organic materials is from Thomazo et al (2009).

6.5 Source characteristics

6.5.1 N concentrations

The source for the diamonds in this chapter are characterised by a large range in N concentrations from < 10 to > 3000 ppm with a sample set that is only 20. This is larger than what has previously been seen in diamondites with a sample set of equal size (GAUTHERON et al., 2005; SHELKOV, 1997 and shown in figure 6.8). This range is as large as that for coated diamonds (n = 165) and larger than the range for monocrystalline diamonds of P and E types (where the sample set is 3 orders of magnitude larger; n = > 2500 as reviewed by Cartigny, 2005). The high N concentrations are consistent with

their rapid growth rate where nitrogen is incompatible in diamond (BOYD et al., 1994), but the low nitrogen concentrations in some samples (< 100 ppm) require a different explanation. It is either that they crystallised later and that the first diamondites fractionated the N/C ratio of the diamondite-forming fluid (N as a compatible element), or that the fluid was locally heterogeneous. I prefer the latter because such heterogeneity has been demonstrated with a minimum spatial resolution of only 27 cm^3 in diamond-bearing xenoliths. There are two studies of monocrystalline diamonds from single xenoliths: one a peridotite xenolith (59 diamonds in 27 cm^3) and one an eclogitic xenolith (35 diamonds with an unspecified volume). The N concentrations ranged from 40 to 1430 ppm in the peridotite (THOMASSOT et al., 2007) and 239 to 1272 ppm for the eclogite (PALOT et al., 2009), therefore such a large local heterogeneity could be predicted and is therefore the favoured explanation here.

6. 5.2 C and N isotopes

The source appears to have a high $\delta^{15}N$ value and a low $\delta^{13}C$ value with a minor component similar to the mean mantle. There is no definitive trend for this sample set in $\delta^{13}C$-$\delta^{15}N$ space (figure 6.11). The samples with low $\delta^{13}C$ values have $\delta^{15}N$ values that are distinctively positive and similar to some eclogitic diamonds from the literature. Where 7 out of 24 Namibian eclogitic diamonds exhibit low $\delta^{13}C$ values and high $\delta^{15}N$ values (Cartigny et al., 2004b), metamorphic diamonds in UHP terrains (CARTIGNY et al., 2004a 2001a), the low $\delta^{13}C$ group of Boyd and Pillinger (1994) and diamonds from Dachine (chapter 5). This is unlike eclogitic monocrystalline diamonds with low $\delta^{13}C$ values from Orapa (Cartigny et al., 1999), Jwaneng (Botswana) (Cartigny et al., 1998a) the majority of the Namibian diamonds (Cartigny et al., 2004b) and Kimberly pool (SA) (Cartigny et al., 1998b), where the majority of low $\delta^{13}C$ exhibit negative (mantle-like) $\delta^{15}N$ values. However, the samples with $\delta^{13}C$ values akin to the mean mantle also have positive $\delta^{15}N$ values which are contrary to > 70 % of monocrystalline P and E type diamonds (Cartigny, 2005).

The samples with mean mantle-like $\delta^{13}C$ values do not exhibit mean mantle $\delta^{15}N$ values and the same is true for the reciprocal. The samples have a strong similarity to the diamonds from Dachine in coupled C-N isotope space despite having an N/C ration that is several orders of magnitude higher, and mostly plot in the field that is characteristic for pelagic organic carbon (i.e. not mantle-derived; see figures 6.9 and 6.11).

There are geochemical and textural similarities for diamondites and coated diamonds; these are (a) a high mean N concentration, and (b) high nucleation and growth rate relative to monocrystalline diamonds. However in C- N isotope space, they are distinct. It can be stated that coated diamonds define the mean mantle C- N isotope space (figure 6.11- the black rectangle). The diamondites in this study and the literature do not have a single data point within the mean mantle field. It is assumed that coated diamonds crystallise so rapidly that they inhibit isotopic fractionation of ^{15}N and ^{13}C and their restricted C- N isotope values and low degree of N aggregation reflect the role of kimberlitic (mantle) precursor fluids (BOYD et al., 1994). A similar model was proposed for diamondites whereby they are the result re-mobilisation of ancient cratonic lithosphere (for the pyroxene and garnets) from mantle-derived kimberlite precursor CH- fluids with $\delta^{13}C$ values of -17 ‰ (for the diamonds) (see section 6.3.3 or JACOB et al., 2000) and this model shall be incorporated into the discussion below.

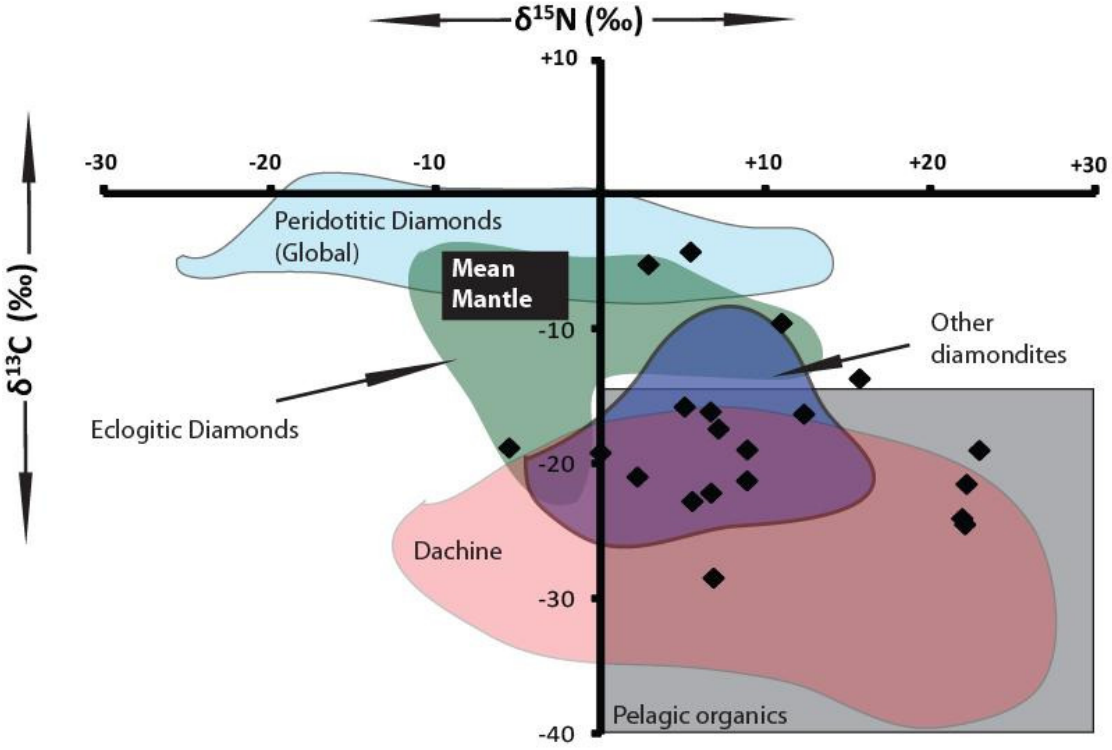

Figure 6.11. A variation diagram for various mantle and crustal reservoirs with the samples from this study. The fields are sourced from the following: mean mantle (CARTIGNY, 2005), eclogitic diamonds (Argyle, Australia BOYD and PILLINGER, 1994; Jwaneng, Botswana CARTIGNY et al., 1998a; Kimberly pool, South Africa CARTIGNY et al., 1999), Dachine (chapter 5), other diamondites (GAUTHERON et al., 2005; SHELKOV et al., 1997), peridotitic diamonds (Fuxian, China CARTIGNY et al., 1997; Orapa, Botswana CARTIGNY et al., 1999; Alluvial diamonds from Namibia CARTIGNY et al., 2004b) and pelagic organic materials (THOMAZO et al., 2009).

6.6 Discussion

This discussion focuses on determining the source of the carbon and proposes a model to explain the low $\delta^{13}C$ values, high $\delta^{15}N$ values, and variable N concentrations exhibited by this mostly peridotitic sample set. The high $\delta^{15}N$ values coupled with low $\delta^{13}C$ values do not fit a major meteorite class and therefore a model proposing primordial heterogeneity or layered heterogeneities cannot explain the data for the same reasons as chapter 5 (section 5.11.1 and figure 5.17). The data is compared to other diamond samples as well as crustal samples of pre-Cambrian age. Noteworthy is that modern systems and pre-Cambrian systems for C and N isotopes are

comparable. Therefore I have chosen pre-Cambrian sediments and organic components (i.e. Kerogen) as the comparative data as was done in the previous chapter.

6.7 Model of origin(s)

Before concluding that the source of the diamond-forming carbon is subducted organic carbon based on figure 6.11, I must first rule out the alternative possibilities as was done in chapter 5. In light of this new data from this sample population, I will first discuss models to discuss is the ones based on the syngenetic silicate geochemistry (DOBOSI and KURAT, 2002; DOBOSI and KURAT, 2010; KURAT and DOBOSI, 2000), diamond major and trace element geochemistry (REGE et al., 2008) and the $\delta^{13}C$ values (MARUOKA et al., 2004 or see section 6.3.2 and figure 6.3) of the diamondites analysed in this chapter.

6.7.1 Mantle-derived fluids

There have been several studies on the syngenetic silicate geochemistry (DOBOSI and KURAT, 2002; 2010; KURAT and DOBOSI, 2000) and one study that focused on the major and trace element geochemistry of the diamonds (Rege et al., 2008). These studies proposed that the intergrown nature of the garnets and diamonds, and the similarity in trace element patterns between the diamonds and the syngenetic garnets, are evidence of a shared source fluid (see REGE et al., 2008). The authors suggest that the diamondites, like many fibrous diamonds (NAVON et al., 1988; TOMLINSON, 2005) and monocrystalline diamonds (MCNEILL et al., 2009), crystallised from melts in the kimberlite–carbonatite geochemical spectrum. Should this be the case then the required starting composition of the kimberlitic-carbonatitic fluid would have to be anomalous to the mantle with respect to both the initial $\delta^{13}C$ and $\delta^{15}N$ values.

Maruoka et al (2004) proposed a model to explain the anomalous $\delta^{13}C$ values (section 6.3.2) that cannot be applied to this data. In the model by Maruoka et al. (2004), removal of 95-98 % of the C as CO_2 (^{13}C enriched) via the carbonation of olivines can cause an isotopic fractionation of $\Delta C_{diamond\text{-}carbonate}$ of -13 ‰ (open system Rayleigh type). This can explain the spread for $\delta^{13}C$ values exhibited by the diamonds as well as the absence of olivine in silicate-bearing diamondites that are geochemically consistent with a peridotitic source. This model assumes an initial $\delta^{13}C$ of -5 ‰, consistent with the convecting upper mantle (Cartigny, 2005; Deines, 2002; Stachel et al., 2009).

The model begins with a reduced metasomatic agent (i.e. CH_4) that is oxidised in a peridotite host to form CO by the reaction:

1- $CH_4 + O_2 = H_2O + CO$

This is followed by the reaction:

2- $2CO = CO_2 + C$

Elemental carbon can easily be dissolved into a carbonatitic melt which can be a precondition for diamond formation (Litvin, 2006; Litvin et al., 1997). The CO_2 created in the above reaction can react with the surrounding olivine in peridotite under sub-solidus conditions according to:

3- $Mg_2SiO_4 + CO_2 = MgCO_3 + MgSiO_3$

The above reaction would form solid carbonate and pyroxene, and explains the lack of olivine in a peridotitic assemblage. This process can also induce redox melting of peridotite to form carbonatitic/kimberlitic melts (DASGUPTA and HIRSCHMANN, 2010; MALKOVETS et al., 2007) and explains how the diamonds and silicates came to be intergrowths. Maruoka et al (2004) propose that the magnesite is removed but offer no mechanical explanation as to how. It would seem more feasible that the carbonatitic/kimberlitic carbon-saturated melts are mobile owing to their low viscosity (DOBSON et al., 1996), this causes migration into a more stable peridotite via grain boundary diffusion

and subsequently precipitates the diamondites. But this does not explain the mobility of the silicate melt.

Regarding the high N concentrations in these samples; the 95 % carbon loss (calculated by MARUOKA et al., 2004) coupled with nitrogen retention in the diamond-forming medium would increase the N/C ratio, thus producing diamonds in diamondites with $\delta^{13}C$ values lower than the initial value (assumed to be the mean mantle value of -5 ‰) and high N/C ratios (≈ ppm), as is the case for the samples in this chapter.

However, this model falls short in explaining the N- isotopes derived from mantle-like $\delta^{15}N$ values (< 0 ‰), as does the open system fractionation model of Cartigny et al (1998a) whereby diamond precipitates during isotopic fractionation (see chapter 2 section 2.8.1). The high $\delta^{15}N$ values (> 10 ‰) and large range (-5.7 to 22.53 ‰) cannot be realistically produced under mantle conditions (i.e. high temperatures) from a single, negative precursor (< 0 ‰) by open system Rayleigh fractionation of ^{15}N. This is because the fractionation factors are too small where the system in question is NH_3-N_2 or diamond-N_2. The method for quantifying the ΔN at 1200 °C for diamond-N_2 is based on empirical calculations using the slope derived from co-variations of $\delta^{15}N$ and $\delta^{13}C$ from a population of diamonds in a single peridotite xenolith, and therefore an assumed common source fluid (THOMASSOT et al., 2007). The temperature was determined using the relationship between N aggregation in the diamonds as a function of temperature (MENDELSSOHN and MILLEDGE, 1995). This ensures that the samples represent a single growth event from a single source fluid, and yields a ΔN of + 1.2 ‰ at 1150 °C (THOMASSOT et al., 2007). This corroborates well with theoretical predictions for NH_3-N_2; where ΔN is circa +1.4 ‰ at 1200 °C based on thermodynamic calculations (Richet et al., 1977). The reason for the comparison is that the nature of the bonding in diamond and NH_3 is very similar to nitrogen in diamond, where a single nitrogen atom is substituted for a carbon atom into the diamond, and bonded with 3 carbon atoms (the bonding of $NH_3 \approx NC_3$).

Noteworthy is the work of Boyd et al (1988) and Reutsky et al (2008). These studies documented a large kinetic isotope fractionation factor for ^{15}N (> 30 ‰) between cubic and octahedral growth sectors in synthetic HPHT diamonds. This is not seen in natural diamonds (BULANOVA et al., 2002; CARTIGNY et al., 2003; HAURI et al., 2002). It is therefore attributed to a kinetic isotope effect as a function of growth rate where HPHT samples in a high pressure device is much faster than in nature, therefore this is not considered.

6.7.2 Binary mixing

The $\delta^{15}N$-$\delta^{13}C$ range shown by this data set cannot be explained by high temperature fractionation processes from the known primary mantle reservoir (demonstrated in figure 6.12). This data requires more than one component as a source and involve mixing (disproportionally) with high and low $\delta^{15}N$-$\delta^{13}C$ values and variable N/C ratios. Regarding the low C/N ratios of organic carbon (5-20) relative to the mantle (>300), I have shown that the C/N ratios of organic carbon (5-20) can and should be devolatilised and therefore fractionated to values akin to what is seen in mantle diamonds-chapter 5 section 5.13. There is however, a question mark over the high $\delta^{15}N$ values exhibited by the samples in that they are considerably higher than the modal value (+6 ‰) for Pre-Cambrian oceanic nitrogen (up to +22.53 ‰- figure 6.7). However, this is not unusual for Pre-Cambrian micas and kerogen with a large range for $\delta^{15}N$ values from -2 to +24 ‰ and -6 to +30 ‰ (figure 6.7). The majority of the samples have $\delta^{15}N$ values centred around +4 ‰ which is consistent with pre-Cambrian shale, banded iron formations (BIFs) and kerogen. The large range for $\delta^{15}N$ values could be explained by multiple sources, where the majority of nitrogen being sourced from the pre-Cambrian kerogen and some samples from micas and possibly primary mantle nitrogen. This explains the range in $\delta^{13}C$ and $\delta^{15}N$ values and the variable nitrogen concentrations.

Figure 6.13 shows the results of a binary mixing model applied to this data set. This model keeps the mantle end member C/N ratio fixed to 300 (circa 3000 ppm nitrogen) and varies the C/N ratio of the subducted component. This could be a consequence of the different sources of nitrogen in the subducted package (i.e. mica vs. sedimentary and organic nitrogen; see figure 6.7). The $\delta^{15}N$ value of this end member is fixed as just above the highest $\delta^{15}N$ value observed in these samples (+ 25 ‰).

A binary mixing model also fails to fully explain all of this data due to the conspicuous absence of samples with coupled mantle carbon and nitrogen isotopic compositions and the clustering of the data within the field for pelagic organic material (figure 6.13). However there is evidence for a mixing event in some samples (mostly peridotitic samples). The samples that do not fit a mixing trend may well have simply crystallised without interacting with mantle-derived materials, the only exception being sample Dia001 ($\delta^{15}N$ = -5.7 ‰ and $\delta^{13}C$ -18.93 ‰).

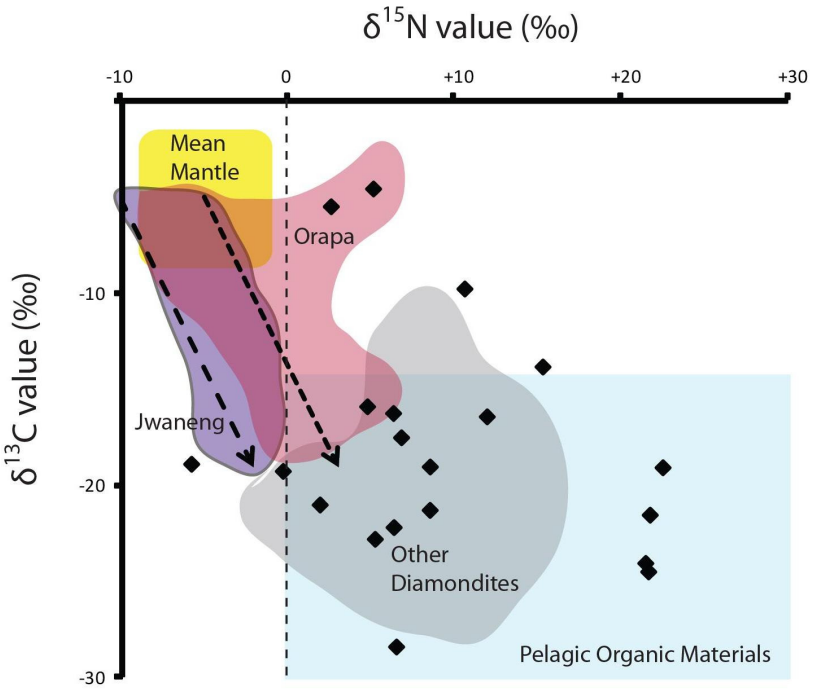

Figure 6.12. A variation diagram for various mantle and crustal reservoirs with the samples from this study and coupled isotopic fractionation modelled trends shown as dashed lines to fit the data of Jwaneng and Orapa. The fields are sourced from the following; mean mantle (Cartigny, 2005), Orapa eclogitic diamonds (CARTIGNY et al., 1999), Jwaneng (CARTIGNY et al., 1998a), other diamondites (Gautheron et al., 2005; Shelkov et al., 1997) and pelagic organic materials (Thomazo et al., 2009). The models are open system Rayleigh fractionation models using equations outlined in Cartigny et al (2001b) where $\Delta C \approx -3.5$ ‰ for diamond-CO_2 (calculated using chemical thermodynamics BOTTINGA, 1969) and $\Delta N \approx +2$ ‰ for diamond-N_2 (inferred using empirical data in THOMASSOT et al., 2007).

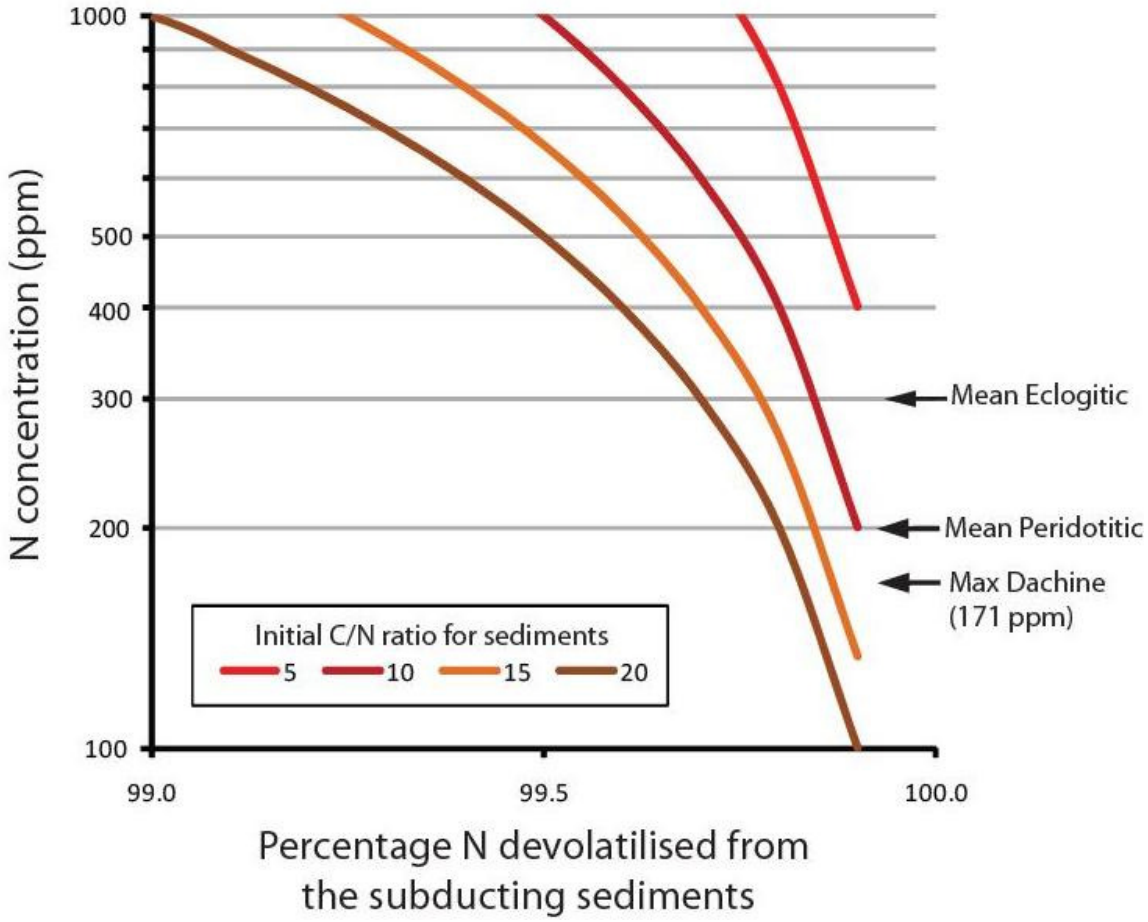

Figure 6.13. The results of a binary mixing model where the mantle end member C/N ratio fixed to 300 (circa 3000 ppm nitrogen) and varying the C/N ratio of the subducted component based on the calculations in figure 5.19 from chapter 5 for C/N fractionation during slab devolatilisation. The C and N isotope values are from the sample with the highest $\delta^{13}C$ value. The $\delta^{15}N$ value of this end member is fixed as just above the highest $\delta^{15}N$ value observed in these samples (+ 25 ‰). The field for pre-Cambrian mica and kerogen and pelagic organics are both from Thomazo et al (2009).

6.7.3 A unified model

The following and final part of this discussion aims to explain the diamondites in this study in terms of garnet geochemistry, diamond geochemistry and the intergrown nature of the two phases. To fully constrain this idea one requires thermodynamic data for carbon and nitrogen speciation and partition functions, under P-T-fO_2 conditions at each stage of subduction and under mantle conditions, but these are currently unavailable. However, I can use circular arguments. Metamorphic diamonds that form directly from reduction of crustal organic carbon contain up to 11,000 ppm

nitrogen (CARTIGNY et al., 2004a). None of the samples in this study have such high nitrogen concentrations. However micas can contain up to ~1800 ppm nitrogen as NH_3 (BUSIGNY et al., 2003), and this is comparable to the diamonds in diamondites (figure 6.8). Pelagic organic carbon that has $\delta^{13}C$ values overlapping the samples in this study (figure 6.9) exhibit C/N ratios much lower than the diamonds. Therefore, the C/N ratio of the organic carbon is required to have fractionated by de-volatilisation reactions during slab descent, as carbon loss is considerably less than nitrogen during devolatilisation. I have already demonstrated that calculations using the current understanding of the relative behaviour of carbon and nitrogen devolatilisation produce C/N ratios consistent with these samples (chapter 5, section 5.13, Figure 5.19).

This organic carbon and nitrogen will be in a reduced state during descent (CH_4 + NH_3). Not knowing the exact origin of these samples makes any model problematic as the age of the sub-continental mantle beneath cratons can vary in the order of several billions of years (GURNEY et al., 2010). However, the coupled $\delta^{13}C$ and $\delta^{15}N$ values can still be explained by addressing common geochemical features exhibited by the main reservoirs in question through geological time. For example;

- The volcanic sampling field has a fO_2 of FMQ ±2 log units through time that decreases with depth. This is consistent through geological time (FROST and MCCAMMON, 2008) where the only time in Earth's history that deviates from this 'constant' is during core formation in the Hadean (FROST et al., 2008)
- The mean mantle $\delta^{13}C$ and $\delta^{15}N$ values have remained relatively constant at -5 ± 3 ‰ through time (CARTIGNY, 2005; CARTIGNY et al., 2009)
- Crustal organic carbon has a mean $\delta^{13}C$ of -25 ± 8 ‰ through time (SHIELDS and VEIZER, 2002; THOMAZO et al., 2009)
- Crustal nitrogen reservoirs have intrinsically positive $\delta^{15}N$ values with a mean at +6 ‰ for organic + inorganic through time (THOMAZO et al., 2011; THOMAZO et al., 2009)

The reduced phases will be oxidised should they become mobile and leave their host slab and percolate through the mantle. This is because under upper mantle P-T-fO_2 conditions (>250 km) the equilibrium fluid phases are H_2O and CO_2 (FROST and MCCAMMON, 2008) which would, in theory, inhibit NH_3 survivability. Oxidising reduced organic carbon (i.e. CH_4) and nitrogen (NH_3) between 1000-1400 °C and between 4-8 GPa in a peridotite would therefore yield water, carbon dioxide and possibly N_2;

4- $CH_4 + NH_3 + O_2 \leftrightarrow H_2O + CO_2 + N_2$

This oxidation of reduced carbon and the subsequent addition of water can lower the solidus of dry pyrolitic mantle (peridotite) and induce redox melting (DASGUPTA and HIRSCHMANN, 2010; KESHAV et al., 2006; ROHRBACH and SCHMIDT, 2011). This could form a carbonatitic melt with geochemical affinities to the predicted fluids for these sample as previously proposed based on silicate and diamond trace element geochemistry (DOBOSI and KURAT, 2010). The diamond-forming COHN-rich fluids are mobile owing to the coupled high wetting properties (Hunter and McKenzie, 1989; Minarik and Watson, 1995) and low viscosities (Dobson et al., 1996) and could therefore be sourced from outside of the host peridotite. These are assumed to be derived from subducted pelagic sediments and enter a mantle peridotite as COHN-rich, oxidising carbonatitic metasomatic fluids based on their coupled $\delta^{13}C$ and $\delta^{15}N$ values. This induces local redox melting; with the resulting melt being garnet rich with carbon oversaturation. Garnet and pyroxene melt before olivine (Best, 2003), therefore the olivine could be a residual phase in this melting and extraction process producing a depleted harzburgite (Ol + minor Px) from a once fertile lherzolite (Ol + Px + minor Gnt). This would produce diamondites with no olivine and more garnet than pyroxene, as is the case for these samples. This would also explain why the diamonds and garnets have comparable trace element patterns (Dobosi and Kurat, 2010; Rege et al., 2008). The trace elements entrained within the diamonds are sourced from the silicate melt that was initially produced by redox melting of a mantle lherzolite, but initiated by metasomatic, subduction-derived COHN-rich fluids. Noteworthy is that the production of websteritic garnets do not require a subducted protolith and can be explained by the fluid evolving

from peridotitic to websteritic by the removal of chromite ± sulphide ± ilmenite (REGE et al., 2008). Subsequent reduction of the CO_2 + N_2 from reaction 4 in the sub-continental lithospheric mantle (SCLM) where the fO_2 is > FMQ and the fH_2 is low could produce reaction 5 where the CO_2 /N_2 ratio is larger than the C/N ratio of the samples in this study;

5- $nCO_2 + N_2 \leftrightarrow nC (+ 2N) + nO_2$

Where nC (+ N) is simply diamond with nitrogen as a lattice-bound impurity in thermodynamic equilibrium with oxygen according to the CCO reaction (see LUTH, 1993). The only subduction-derived component being present in the diamondites is the diamond-forming carbon (+ nitrogen) in this model.

6.8 Conclusions

The best explanation of the origin of the diamond-forming carbon in diamondites based on coupled carbon and nitrogen isotope constraints from the samples in this study is one of subducted organic carbon where the subducted packages is derived from below the CCD, and thus carbonate-poor. There is evidence of a mantle component in both carbon and nitrogen isotope space and some evidence for mixing. The most important observation that this study provides is that, as for monocrystalline diamonds, the diamonds and silicates can be completely un-related in terms of geochemical origins (CARTIGNY, 2005). In this case, the silicates are sourced from the mantle and the diamonds from subducted crustal pelagic (organic) carbon and nitrogen. This is opposed to several monocrystalline diamonds where the eclogitic inclusions are derived by subducting oceanic crust and the diamonds are from metasomatism of this material by mantle-derived carbon; where the generation of low $\delta^{13}C$ and higher than mantle $\delta^{15}N$ values is a function of high temperature isotopic fractionation (see CARTIGNY, 2005 for a review).

There is also the question as to why peridotitic monocrystalline diamonds almost never exhibit lower than mantle $\delta^{13}C$ values (Cartigny, 2005) whereas diamondites show no distinction for silicate paragenesis $\delta^{13}C$ values. Monocrystalline, low $\delta^{13}C$ eclogitic diamonds can be derived by subduction when the diamonds grow within the subducted material (chapter 5). Or by high temperature fractionation of $^{13}C/^{12}C$ when mantle carbon metasomatises an eclogite, because CO_2 can escape the system (LUTH, 1993) and cause ^{13}C loss (Cartigny et al., 1998a). This is because in a peridotite, CO_2 reacts with olivine to form magnesite + enstatite (reaction 3) which later contributes to diamond formation thus inhibiting ^{13}C fractionation.

The reason may be a function of carbon over-saturation induced by subducted carbon. The mantle is the a larger reservoir for carbon by several orders of magnitude dwarfing the crustal reservoir (DASGUPTA and HIRSCHMANN, 2010), however the carbon in the mantle may not be as concentrated, and subduction of pelagic organic carbon could be more concentrated. The reduced organic carbon (+ nitrogen), upon entering shallower mantle, would be oxidised producing a carbonatitic fluid with a $\delta^{13}C$ value of its source; in this case subducted organic carbon ($\delta^{13}C$ between -15 and -40 ‰). Once entering a host rock one could expect the induction of redox melting in both peridotites and eclogites (DASGUPTA and HIRSCHMANN, 2010) and produce diamondites with garnets > pyroxene and no olivine, not monocrystalline diamonds, due to carbon oversaturation leading to rapid nucleation (LITVIN, 2006). Without the fluid mobility, monocrystalline diamonds with low $\delta^{13}C$ values would grow in the host eclogite i.e. Dachine diamonds (chapter 5) or low $\delta^{13}C$ majorite-bearing, eclogitic monocrystalline diamonds (BULANOVA et al., 2010; TAPPERT et al., 2005). It may therefore be the case that a large proportion of subduction-derived diamonds in the SCLM are polycrystalline and not of gem quality monocrystalline morphology. This also explains the occurrence of low $\delta^{13}C$ peridotitic polycrystalline diamonds and the absence of low $\delta^{13}C$ peridotitic monocrystalline diamonds.

6.9 Un-answered issues

There are only 20 samples in this study and 20 from the literature that demonstrate distinctively low $\delta^{13}C$ and high $\delta^{15}N$ values akin to organic components and are distinct from the mean mantle. What is required to better understand the origin of diamondite-forming carbon is a detailed global study of the garnet and diamond geochemistry alongside monocrystalline diamonds from the same locality. Also required are time constraints such as; (1) direct dating of the syngenetic intergrowths and (2) the degree of nitrogen aggregation to address the amount of diamondite-forming events at a given locality and the relationship or lack of with proto-kimberlite fluids/melts (phenocrystic vs. xenocrystic). A detailed study for the $\delta^{15}N$ values for populations of diamondites that show bi-modal $\delta^{13}C$ values would also be required to test the above model further.

More work is also required to understand nitrogen speciation and isotope fractionation in mantle fluids, melts, or minerals as this remains poorly constrained at temperatures, pressures and oxygen fugacities under which diamond is stable (Roskosz et al., 2006; Watenphul et al., 2010). In fact, there are no experimental constraints or fractionation coefficients available for diamond and any other mantle phase/fluid. This requires several future studies. There is however, a substantial body of work that has focused on carbon isotope fractionation and speciation at HPHT as a function of P-T-fO_2.

The following chapter expands the data base for isotopic fractionation of carbon under mantle conditions by determining the fractionation factor of ^{13}C between diamond and Fe-carbide in two rare, natural mantle monocrystalline diamonds from Jagersfontein, SA. This work also goes on to add credibility to the model of Rohrbach and Schmidt (2011) for the existence of a fO_2 discontinuity at 250 km. This is achieved by observing the predicted carbon assemblage expected under their proposed P-T-fO_2 conditions in samples from a diamond mine known for sampling the transition zone, Jagersfontein, SA (chapter 7). I then use HPHT experiments to constrain a temperature of

diamond formation using stable isotope geothermometry based upon a mantle geothermal gradient (chapter 8).

Chapter 7

An in-situ determination of the fractionation factor of ^{13}C between diamond and iron carbide

7.1 Introduction

The aim of this chapter is to determine the $\delta^{13}C$ values for co-existing diamond and Fe-carbide in exceptional samples from the Jagersfontein diamond mine, Kaapvaal Craton, South Africa. These samples offers an opportunity to evaluate whether carbon isotopes are fractionated between coexisting deep carbon phases in the terrestrial mantle, where the grains are faithfully preserved due to rapid transport to the Earth's surface by kimberlite magma. Due to the complex textural relations and microscopic scale, carbon isotopic composition was determined by nanoSIMS to measure the isotopic compositions with high spatial resolution. Standarisation procedures had to be developed for carbon isotope analysis in carbides, which were known to form the major element chemistry of these natural mantle carbides based on prior electron microprobe data, which is also summarised. The phase relations and occurrence of iron carbide in the diamond, although extremely rare, is not unpredicted, and I review recent works which show from high pressure experiments that iron carbide should be expected deep in the mantle.

I compare these results to previous work for the $\delta^{13}C$ values for co-existing graphite and cohenite in iron meteorites where a near constant difference of circa +12 ‰ has been observed. This was concluded to be the consequence of equilibrium stable isotope fractionation, and not different carbon sources (Deines and Wickman, 1975). The subsequent chapter is a continuation of this study where I present experimental results for carbon isotope fractionation under mantle pressures and temperatures in the iron-carbon system. The overall objective of these studies combined is to quantify the $\delta^{13}C$ values from the diamond and Fe-carbide from two natural samples (this chapter)

and test the pressure and temperature effects using synthetic samples of graphite or diamond (herein Gr-Dia is used) and cementite to constrain the equilibration temperature, and therefore calculate the depth of origin for the two samples in this chapter (**chapter 8**).

7.2 The occurrence of terrestrial Fe-carbide from the mantle

The existence of Fe-carbide has been predicted in the Earth's mantle at depths >250 km based on the experimentally determined fO_2 conditions (FROST et al., 2004; FROST and MCCAMMON, 2008; ROHRBACH et al., 2007; 2010; ROHRBACH and SCHMIDT, 2011; STAGNO and FROST, 2011) and the reactivity of carbon and iron at high pressures and temperatures (LORD et al., 2009; ROUQUETTE et al., 2008). This is illustrated in figure 7.1 as a function of depth. However, in order for Fe carbide and diamond to co-exist in the terrestrial mantle one requires > 900 ppm of carbon assuming 1 wt % Fe^0 in the mantle < 250 km (Frost et al., 2004; Rohrbach et al., 2007) and illustrated in figure 7.2. The problem with modelling the occurrence of the two phases, and predicting the speciation of deep Earth carbon, is that the concentration and distribution of carbon in the mantle is very poorly constrained (DEINES, 2002). The carbon concentration of the mantle is only known to within 3 orders of magnitude (1 ppm to 1 wt %). This large range permits one to model various scenarios.

Despite the prediction for abundant Fe-carbides in the mantle, the observed occurrence is very rare, and almost always associated with diamond. Fe-carbides have been documented as inclusions within diamonds from Jagersfontein, South Africa (Sharp, 1966 and this study), Juina, Brazil (KAMINSKY and WIRTH, 2011) and the 23rd Party Congress Kimberlite, Russia (Bulanova and Zayakina, 1991). There is also an occurrence of inclusions of cohenite spherules within garnets that are intergrowths with polycrystalline diamonds (Jacob et al., 2004). Interestingly, two of the diamond populations that contain Fe-carbide as inclusions are also known to produce sub-lithospheric diamonds, which should in principle, be sampling the more reduced Fe^0 bearing deeper Earth (For Juina see KAMINSKY et al.,

2009; and for Jagersfontein see TAPPERT et al., 2005a). The only non-diamond related occurrence is the basalts emplaced on Disko Island, Greenland (GOODRICH and BIRD, 1985). These are known to contain cohenite; however their terrestrial origins are debated (JONES et al., 2005).

Two other studies have reported native iron as inclusions in diamond (Bulanova et al., 2010; Stachel et al., 1998). These are not a predicted to be an equilibrium assemblage (Lord et al., 2009) and may have been unrecognised Fe-carbide, since carbon in carbide can be difficult to analyse by EPMA when swamped by matrix diamond. Indeed, both authors did not measure the proposed native iron for carbon concentration (pers comms, G.D Bulanova and T Stachel, 2010).

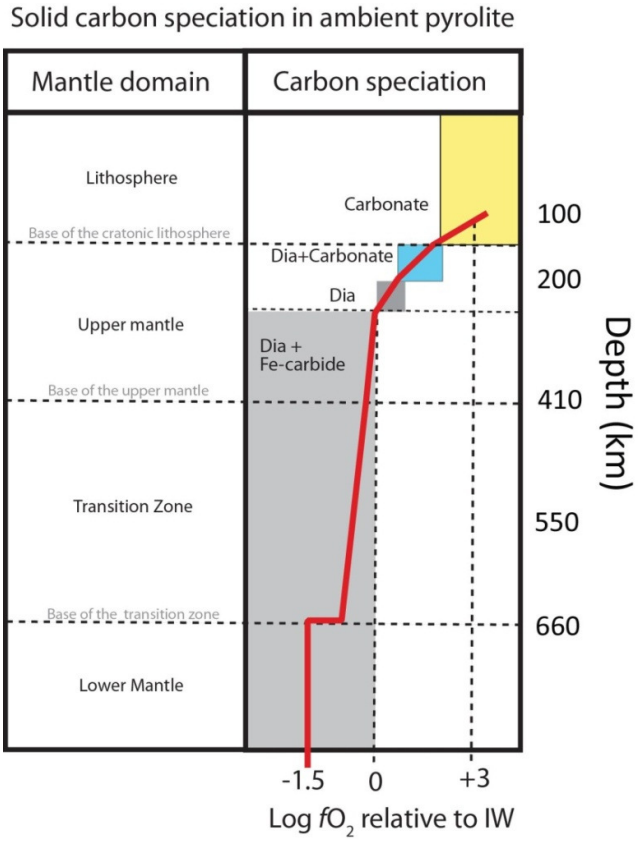

Figure 7.1 The speciation of carbon as a function of the fO_2 with depth in an ambient pyrolitic mantle (modified from ROHRBACH and SCHMIDT, 2011). Note the dominance in the terrestrial mantle for reduced carbon species relative to carbonate.

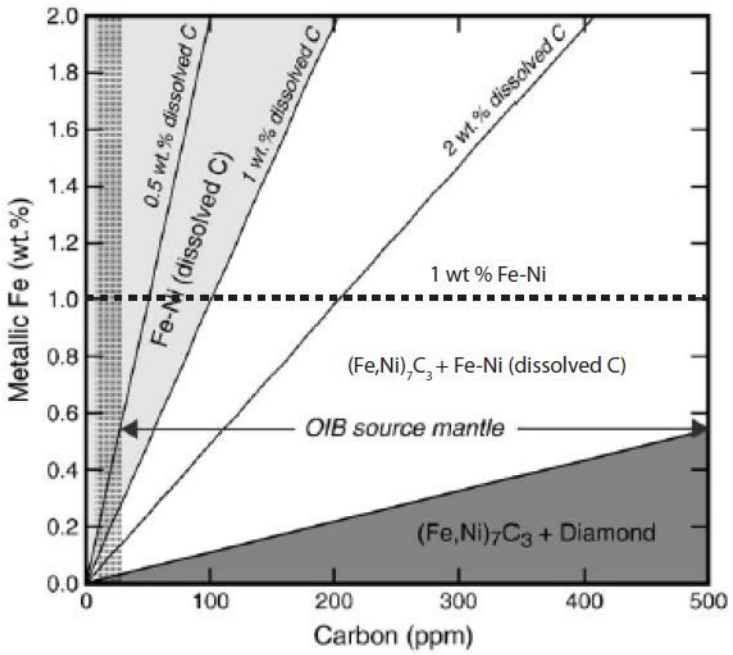

Figure 7.2 The speciation of carbon in the system iron-carbon as a function of relative concentrations of iron to carbon above 5 GPa and 1000 °C in the terrestrial mantle (Dasgupta and Hirschmann, 2010). Range for OIB source mantle is from observed concentrations of CO_2 in ocean island basalts (OIB) and the dashed grey line on the left is the observed CO_2 concentration in mid-ocean ridge basalts (MORB); also from Dasgupta and Hirschman (2010). The dashed black line at 1 wt % Fe-Ni is from Frost et al (2004).

The observed association of carbide with diamond may be due to preservation, and a function of diamond acting to contain and isolate the Fe-carbide from oxidation to carbonates in the more oxidising shallow mantle. Therefore, iron carbide may be common or even the dominant carbon store in the deep Earth (DASGUPTA and HIRSCHMANN, 2010) that simply does not manifest itself in emplaced magmatic rocks and mantle xenocrysts.

7.3 Carbon isotope fractionation in the iron-carbon system

I found no published carbon isotope data for co-existing mantle diamond and Fe-carbide. Some empirical work in this system was derived from analyses of extra-terrestrial samples sourced from two iron meteorites. Craig (1953) and Deines and Wickman (1975) determined the $\delta^{13}C$ values for mineral separates of co-existing cohenite and graphite from iron meteorites using gas sourced mass spectrometry. Both sets of authors obtained a similar fractionation factor of +12.3 to 13.2 ‰ with cohenite depleted in ^{13}C relative to graphite. This is shown in table 7.1.

Iron meteorite	Minimum ΔC	Maximum ΔC	Mean ΔC
Canyon Diablo	+9.32	+15.20	+12.26
Magura	+11.85	+16.82	+13.16

Table 7.1. The observed ΔC for graphite – cohenite determined from mineral separates of co-existing graphite and cohenite in two iron meteorites, Magura from Craig (1953) and Canyon Diablo from Deines and Wickman (1975). The minimum and maximums represent the smallest and largest difference for ΔC calculated from several individual analyses.

Regarding polymorphism of graphite-diamond (Gr-Dia) and Fe-carbide; Schauble (2009) performed electronic structure calculations to predict the equilibrium isotope fractionation of ^{13}C for Gr-Dia co-existing with Fe_3C and Fe_7C_3. His model used Density Functional Theory (DFT) and concluded as follows:

- Dissolution of light elements into an iron-rich metal phase is likely to cause pronounced isotopic fractionation, even at temperatures > 800 °C (unspecified);
- In all cases modelled (H, C, N, O, Si, S) the light isotopes preferentially partition into the metal phase;
- There is no predicted difference between $\Delta C_{Diamond\text{-}Fe3C}$ and $\Delta C_{Graphite\text{-}Fe3C}$ or between $\Delta C_{Diamond\text{-}Fe3C}$ and $\Delta C_{Diamond\text{-}Fe7C3}$ as a function of temperature. Therefore, polymorphism of the phases should have no predicted effect. As such, my new results for diamond – Fe-carbide might be

compared directly to graphite – Fe-carbide, assuming that impurities like Ni, have a minor role.

7.4 Samples

There are two samples in this study that were selected for isotopic analysis by Drs A.P. Jones and H.J Milledge from a suite of >70 inclusion-rich diamonds (~1-3 mm size) all from the Jagersfontein kimberlite, Kaapvaal craton, SA (JONES et al., 2008). These specimens were fragmented octahedral diamonds (pre-polishing), and show prominent dark metallic inclusions within 'cloudy' diamond cores surrounded by colorless optically transparent rims (figure 7.3). The samples in this study lack any nitrogen absorption bands in IR and were classified as type II (< 30 ppm nitrogen; Dr H. J Milledge pers comm. 2009). The samples are from the personal collection of Dr H. J Milledge housed in the Department of Earth sciences, University College London, UK, (now administered by Dr A.P. Jones).

Figure 7.3. Photomicrographs of the Jagersfontein diamond with metallic carbide inclusions, using transmitted light. Note the transparency of the Fe-carbide-free sections of the diamonds relative to the diamond surrounding the Fe-carbide.

7.5 Analytical techniques

The samples in this study have previously been polished (both sides) and analysed with WDS for major element compositions (JONES et al., 2008). Below I detail the analytical technique implemented for high spatial resolution in-situ carbon isotope determinations.

7.5.1 Ion microprobe analysis

The $^{13}C/^{12}C$ ratios were determined in collaboration with Christalle Guillermier and Ian A Franchi using a third-generation ion microprobe (Cameca nanoSIMS 50L) housed at the Planetary and Space Science Research Institute (PSSRI), Open University, Milton Keynes UK.

Prior to loading into the nanoSIMS, the samples were re-polished and cleaned before coating with a 40 nm thick layer of Au (99.99 % purity) to enable electrical conductivity between the sample and the indium into which they are pressed as a sample holder. Quantitative carbon isotope analyses and qualitative elemental analysis were performed using a Cs+ primary beam of ~30 pA with an accelerating voltage of 16 kV. Analyses were performed under ultra-high vacuum around 10^{-9} torr. For $^{13}C/^{12}C$ ratio determinations, the instrument was tuned for a mass-resolving power of 7000. For carbon isotope analyses, the primary beam was rastered over a 5 μm^2 region on each target (figure 7.4). Faraday cup collectors were used for both ^{12}C and ^{13}C. In general, isotope data acquisition was run as 10 blocks of 50 measurements and lasted for ~4 min per data point.

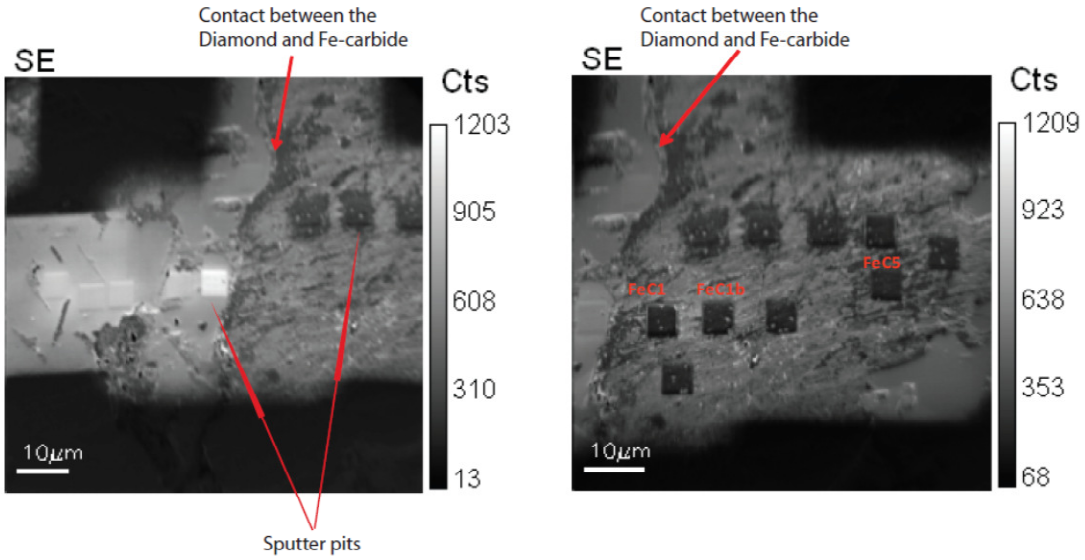

Figure 7.4 Sputter pits on the polished diamond/carbide surface are visible in secondary electron mode (SEM) resulting from analysis by nanoSIMS. The rough surfaces are Fe-carbide and the smooth surfaces are diamond.

7.5.2 Instrumental mass fractionation and Standard materials

Instrumental mass fractionation (IMF) was corrected using the analyses of standards. These were cohenite from basaltic rocks sourced from Disko Island for the Fe-carbide with $\delta^{13}C$ = -23.5 ‰, a large polished plate of homogeneous laser-sectioned diamond sourced from Drukkers diamond with $\delta^{13}C$ = -6 ‰ and synthetic diamond produced by chemical vapour deposition (CVD) with $\delta^{13}C$ = -62.44 ‰ (the diamonds were provided by H.J. Milledge and the Disko cohenite from Dr I .A Franchi). The $\delta^{13}C$ values of the standards and their derived errors (< 0.05 ‰) were determined by combustion gas-sourced mass spectrometry at the PSSRI (Open University, UK) by Dr Mabs Gilmore. The precision on the standards measured using the nanoSIMS was better than ± 0.88 ‰ for Disko cohenite, ± 1.88 ‰ for Drukkers diamond and ± 0.59 ‰ for a sample of diamond produced by CVD. For a full list of the standard data see the table 7.2. Equations and methods for counting statistics were used to calculate the per mil standard errors and $\delta^{13}C$ values were sourced from (Fitzsimons et al., 2000).

Cohenite	$\delta^{13}C_{PDB}$	Mean$\delta^{13}C_{PDB}$	σ (‰)	ΔSIMS-COMB (‰)
DISKO_DC6_30	-24.71	-24.92	0.38	-1.42
DISKO_DC6_31	-25.36			
DISKO_DC6_32	-24.71			
DISKO_DC6_1308_1	-20.96	-22.07	0.79	1.43
DISKO_DC6_1308_2	-22.07			
DISKO_DC6_1308_3	-22.73			
DISKO_DC6_1308_4	-22.54			
DISKO_DC6_1408_1	-22.76	-23.04	0.33	0.46
DISKO_DC6_1408_2	-23.41			
DISKO_DC6_1408_3	-22.94			
Disko_Shoe_29JUL10_1	-23.87	-23.94	0.48	-0.44
Disko_Shoe_29JUL10_2	-24.15			
Disko_Shoe_29JUL10_3	-23.31			
Disko_Shoe_29JUL10_4	-24.43			
Diamond	$\delta^{13}C_{PDB}$	Mean$\delta^{13}C_{PDB}$	± (‰)	ΔSIMS-COMB
DRUKER4_1809_run2_1	-4.95	-5.88	1.54	0.12
DRUKER4_1809_run2_2	-5.04			
DRUKER4_1809_run2_3	-7.65			
DRUKER4_1809_1	-7.23	-6.12	1.08	-0.12
DRUKER4_1809_2	-6.06			
DRUKER4_1809_3	-5.07			
CVD_Top_27JUL10_1	-62.60	-62.33	0.42	0.17
CVD_Top_27JUL10_2	-62.51			
CVD_Top_27JUL10_3	-61.87			
CVD_Top_27JUL10_4	-62.60			
CVD_Top_27JUL10_5	-63.05			

Table 7.2. Where the COMB refers to the $\delta^{13}C$ analysis by Dr Mabs Gilmore using continuous flow, dual inlet mass spectrometry. The $\delta^{13}C$ values for the Disko cohenite was -23.5 ‰; the diamonds were -6 ‰ for Drukker and -62.5 ‰ for CVD. The associated errors on these determinations were better than ± 0.05 ‰.

7.5.3 Matrix effects

The carbide standard was natural cohenite ($Fe[Ni,Co]_3C$), and the sample is a previously un-described Fe-carbide with minor to significant Si and O concentrations. Therefore, there may be a compositional matrix effect (Fitzsimons et al., 2000). I tested for matrix effects and isobaric interference on the obtained carbon isotope compositions. This was critically evaluated in 6 sputter

pits in Jag10, and achieved by producing elemental maps using the secondary ions generated to detect ^{16}O, ^{28}Si and $^{14}N^{12}C$ and plotting them against $^{13}C/^{12}C$ ratios (in collaboration with C Guillermier and I.A Franchi). We were satisfied that there was no correlation(s) or trend(s) for the intensities vs. $^{13}C/^{12}C$ ratios for the samples or standards and I therefore conclude no effect of their concentration on the presented $\delta^{13}C$ values in this chapter (see appendix graphs A1-A3).

These intensities are not quantitative because a suitable Fe-carbide standard with homogeneous O, Si and N abundances necessary to normalize actual atomic abundances of these elements was unavailable. Therefore the relative secondary ion counts do not reflect actual atomic ratios because the sputtered secondary ions have different ionization efficiencies. I cannot relate the intensities of O and Si acquired from the nanoSIMS to the WDS data in table 7.3 as a proxy as the homogeneity/heterogeneity at the scale of <5 μm of the unknowns (samples) are not constrained. This could is a target for future work.

7.6 Results

7.6.1. Major element chemistry

The WDS data presented in table 7.3 are from Jones et al (2008). The concentrations for Cr, Ni, Si and O vary considerably. The Fe-carbide in Jag5 and Jag10 is certainly not cohenite, because their low Ni contents are well below usual stoichiometric abundances with 1.13 to 2.21 wt% in mantle "cohenite", or 7-30 wt% Ni in meteoritic cohenite ($Fe_{1.8}Ni_{0.9}Co_{0.3}C$) and these samples have <0.33 wt % Ni (sample Jag1 has much more Ni, similar to cohenite, but is excluded from this discussion as this sample was not investigated in this study).

Jag5 has more Cr and Si but less O than Jag10, the concentrations of Si and O within some regions of the carbide could be due to a variety of sub-micron-sized phases; complete speculation suggesting minerals such as moissanite (SiC) + siderite ($FeCO_3$) or fayalite ($FeSiO_3$). Siderite is ruled out due to its

instability at temperature > 500 °C (FRENCH and ROSENBERG, 1965; KOZIOL, 2004), also I assume that there should be no CO_2^{3+} due to the low fO_2 in the source region that these samples are derived (FROST and MCCAMMON, 2008). This leaves fayalite (Fe_2SiO_4) as the most obvious host of the Si and O, being an end-member of the most common mantle mineral group this seems a feasible deduction (BEST, 2003).

The crystallography of the carbide is unknown, because the X-ray diffraction data is inconclusive (Dr I Wood, pers comm. 2010). This could be due to several micro-nano phases interfering with the diffraction and producing an abundance of 'noise' that results in a multi-component diffraction pattern of unknown phases in unknown proportions. Given the range in Cr, Ni, Si and O for 5 out of the 9 samples, and the potential for multiple phases at the sub-micron level, I propose a detailed re-examination of all samples utilising both WDS and TEM techniques to better constrain the phases present. This may yield information regarding their P-T conditions of formation and therefore the temperature conditions for the phase equilibria in question.

	Jag1	Jag2	Jag3	Jag5	Jag10	Magura*	*cohenite*	*cementite*	*Venetia*
Fe	65.43	80.92	88.42	88.41	90.3	91.93	*54.92*	*94.73*	*90.41*
Cr	15.07	8.99	2.04	2.04	0.02	-	-	-	-
Ni	9.32	0.4	0.33	0.33	0.1	6.67	*28.86*	-	*1.61*
Si	0.78	0.55	1.65	1.65	0.78	-	-	-	*0.03*
S	0.14	0.06	0.02	-	0.07	-	-	-	*0.21*
Al	0.43	0.02	0.15	0.14	-	-	-	-	-
O	2.08	1.55	0.97	0.97	3.99	-	-	-	-
C	5.3	6.2	5.9	5.9	4.5	1.40	*6.56*	*5.27*	*6.53*
Co	-	-	-	0.21	0.18	-	*9.66*	-	*0.37*
Totals	98.55	98.69	99.48	99.67	99.94	100.00	*100*	*100*	*99.16*

Table 7.3. Elemental concentrations of various carbides (weight percent). There are 5 analyses from Jagersfontein carbides showing a range of Fe-Cr-Ni with minor but significant Si and O. Data for Cohenite is from Disko Island samples (GOODRICH and BIRD, 1985) and cementite data are theoretical compositions calculated assuming an ideal stoichiometric balance. Data for rare and bizarre-textured Fe-Ni carbide micro-spherules in garnet inclusions from Venetia diamond are from Jacob et al (2004). The data for Magura meteorite is low in nickel compared to actual cohenite, and is taken from a review of the topic by Deines and Wickman (1975). *This composition is for the bulk meteorite and not separates of the cohenite; it therefore represents a solid solution mixture between native iron, nickel-rich phases and cohenite, whose low-T phase relations in meteorites are represented by a complex series of dissolution textures.

7.6.2 Diamond and carbide textures

Secondary ion intensity maps at the nano-scale of the Fe-carbide/diamond textures show the grain contacts to be both irregular and sharp (figure 7.5). There is textural evidence suggestive of synchronous growth for the diamond and Fe-carbide, such as small (<0.5 μm^2) spherical 'blebs' of Fe-carbide within the diamond host (figure 7.5). Because diamond is neither porous nor permeable and no cracks can be identified as feeder networks to these 'blebs' I can find no other explanation for their existence besides liquid/melt immiscibility and therefore synchronous growth.

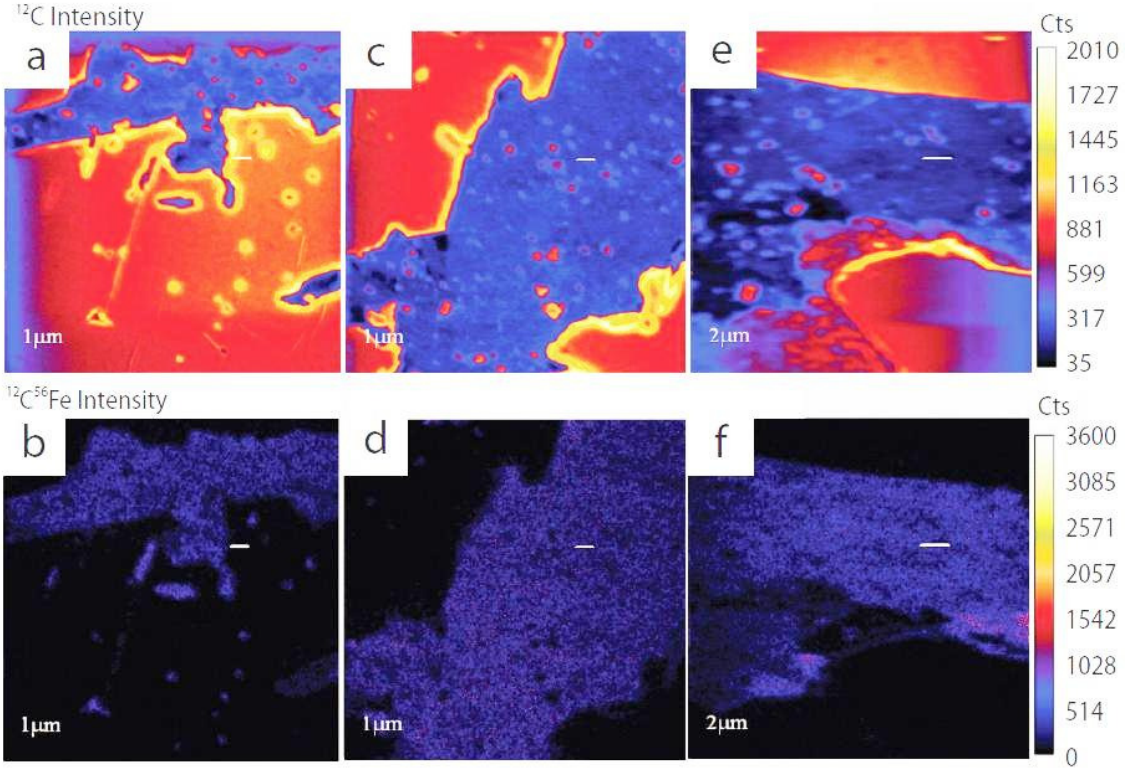

Figure 7.5. Secondary ion intensity maps from Jag5 area F (appendix). The top row is for ^{12}C intensity where the red-orange material is diamond and blue is Fe-carbide. The bottom row is for the coupled $^{12}C^{56}Fe$ intensities where the black area is diamond and the blue is Fe-carbide. Note the small (<0.5 μm^2) spherical 'blebs' of Fe-carbide within the diamond host, more pronounced in the $^{12}C^{56}Fe$ coupled intensity map. The scale bars in a-d are 1 µm and the scale bar in e-f is 2 µm.

7.6.3 $\delta^{13}C$ and $\Delta C_{C\text{-}FeC}$ isotope values

The full data for isotopic values obtained are shown in table 7.4. The $\delta^{13}C$ values for the individual diamonds differ where Jag5 has a mean value of -12.7 ± 1.6 ‰ and Jag10 has a mean value of -17.26 ± 0.59 ‰. Both values fall into the low $\delta^{13}C$ group commonly observed for diamonds from Jagersfontein (Boyd and Pillinger, 1994; Deines et al., 1991; Tappert et al., 2005a; 2005b). The $\delta^{13}C$ values for the individual Fe-carbides also differ where Jag5 has a mean value of -18.6 ± 1.14 ‰ and Jag10 has a mean value of -25.22 ± 2.06 ‰, again these are consistent with the $\delta^{13}C$ range observed in diamond (mantle-sourced carbon) from Jagersfontein (references as above). Irrespective of the differences in the mean $\delta^{13}C$ values, the values for $\Delta C_{C\text{-}FeC}$ are very similar (table 7.4). The overall

mean $\Delta C_{C\text{-}FeC}$ for both samples is +7.2 ± 1.3 ‰. The fractionation factor is expressed using the following equations;

(a) The fractionation factor $\alpha = \frac{\delta^{13}C\,(Phase1) + 1000}{\delta^{13}C\,(Phase2) + 1000}$

(b) $\Delta C_{C\text{-}FeC}$ is defined as $\Delta C = (1000)\cdot \ln\alpha \approx$ parts per mil (‰)

Area (sample)	$\delta^{13}C$ Fe-Carbide	± (1σ)	Area (sample)	$\delta^{13}C$ Diamond	± (1σ)	$\alpha_{Diamond\text{-}FeCarbide}$	$\Delta C_{C\text{-}FeC}$
Area D (Jag 5)			Area D (Jag 5)				
JAG5_D7_1_corr	-20.12	0.68	JAGD3_1809	-12.91	1.60		
JAG5_D7_2_corr	-19.10	0.68	JAGD2_1809_run2	-13.54	1.60		
JAG5_D7_3_	-19.19	0.68	-	-	-		
Area D mean	-19.47	0.68	Area D mean	-13.23	1.60	1.006369	+6.35
Area D Stdev	0.57	-	Area D Stdev	N/A	-		
Area F (Jag 5)			Area F (Jag 5)				
JAG5_F_1	-16.82	1.14	JAG_F3_run2	-11.65	1.54		
JAG5_F2_corr	-18.42	1.14	-	-	-		
JAG5_F3_corr	-17.06	1.14	-	-	-		
JAG5_F_4	-18.77	1.14	-	-	-		
JAG5_F_6	-19.32	1.14	-	-	-		
Area F mean	-18.08	1.14	Area F mean	-11.65	1.54	1.006546	+6.53
Area F Stdev	1.09	-	Area F Stdev	N/A	-		
Area B (Jag10)			Area B (Jag10)				
AreaB4(FeC1)	-23.80	2.06	Area B4 (diamond pt2bis)	-17.05	0.59		
AreaB4(FeC1b)	-27.51	2.06	Area B4 (diamond pt6)	-17.69	0.59		
AreaB4(FeC5)	-24.36	2.06	Area B4 (diamond pt7)	-16.78	0.59		
-	-	-	Area B4 (diamond pt2bis)	-17.22	0.59		
-	-	-	Area B4 (diamond pt6)	-17.85	0.59		
-	-	-	Area B4 (diamond pt7)	-16.95	0.59		
Area B mean	-25.22	2.06	Area B mean	-17.26	0.59	1.008175	+8.14
Area B Stdev	2.00	-	Area B Stdev	0.42	-		
						Total Mean	+7.18
						Total Stdev	1.30

Table 7.4. The full data set for the two samples in this study.

The errors in this study range from ±0.59 to 2.06 ‰ (table 7.4) and is comparable to a recent study of $\delta^{13}C$ values with a resolution of 4 μm^2 (± 1.88 ‰ 2σ) for samples of terrestrial graphite inclusions

in silicates using a facility with the same CAMECA nanoSIMS specification as this study (PAPINEAU et al., 2010).

Regarding the Fe-carbide data there is another issue that must be addressed. Within the Fe-carbides there is an abundance of micron-sized diamonds that probably originated from the diamond polishing process (figure 7.6). These would considerably offset the $^{13}C/^{12}C$ ratio of the Fe-carbide during sputtering owing to their high C concentration (diamond = 100 wt % C whereas Fe-carbide is circa 4-6 wt % C). Where 5 μm^2 intensity maps of ^{12}C were produced, it was noticed that there were no areas of the Fe-carbide where sub-micron-sized diamonds were not present (figure 7.6). Therefore, despite the abundance of Fe-carbide exposed being up to > 5 % of the polished surface, and the majority of the Fe-carbide veins, blebs and platelet features being large enough to measure $^{13}C/^{12}C$ ratios with a 5 μm^2 spots size, acquiring reliable $^{13}C/^{12}C$ ratios from the Fe-carbide was a difficult endeavour. This was due to a combination of several sputter pits containing an abundance of micron-sized diamonds probably sourced from the original polishing material. These areas were avoided by making observations in secondary electron mode prior to $^{13}C/^{12}C$ acquisition.

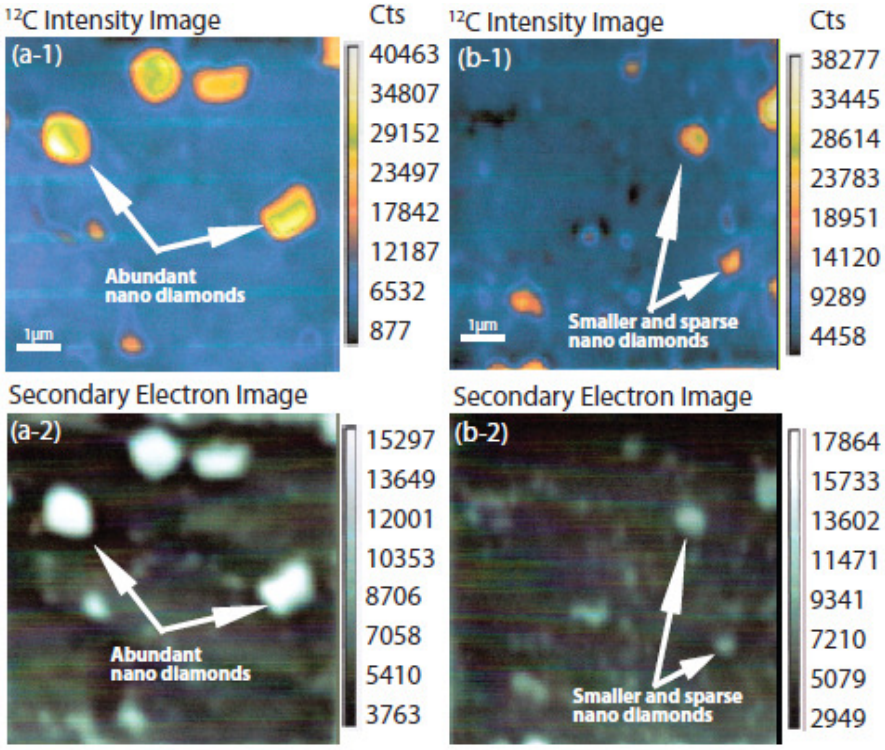

Figure 7.6: Qualitative intensity maps for ^{12}C (a-1 and b1) and secondary electron images (a-2 and b-2) for selected sputter pits on Sample Jag 10 in area B4. The Maps on the left (a1 and a2) exhibit the presence of abundant micron-sized diamonds in the field of view that considerably off set the $^{13}C/^{12}C$ ratio of the Fe-carbide during sputtering. The maps on the right (b-1 and b-2) show less micron-sized diamonds (relatively) but their presence is still visible.

7.7 Discussion

7.7.1 The magnitude of ΔC

The objective of this study is to constrain the ΔC value between the co-existing diamond and the Fe-carbide in these samples. The first point to address in this discussion is the nature of the difference for the $\delta^{13}C$ values for the diamond and the Fe-carbide. There is a near constant difference for the $\delta^{13}C$ values where ΔC = +7.2 ± 1.3 ‰, where the diamond is ^{13}C enriched. What is evident however, is that the error bars are large in some cases (± 2.06 ‰), but the magnitude of the difference in the $\delta^{13}C$ values for each phase is even larger. The consistency in the difference between them and the calculated $\Delta C_{C\text{-}FeC}$ is taken as evidence for an equilibrium fractionation factor, as was seen between

graphite and cohenite in previous studies on iron meteorites (CRAIG, 1953; DEINES and WICKMAN, 1975), which is taken as de-facto evidence for fractionation of ^{13}C in this system, albeit, a poorly constrained one due to the relatively large errors in $^{13}C/^{12}C$ determinations in this study compared to the previous studies on Fe-meteorites that used conventional gas-sourced mass spectrometry (figure 7.7). This means that I cannot state the exact value for $\Delta C_{C\text{-}FeC}$ to better than ~ ± 2 ‰. However, the mean values for the 3 localities on the two samples demonstrate consistency in both scale and direction (table 7.4 and 7.5).

Area	Fe-carbide	Stdev	± ‰ (1σ)	Diamond	Stdev	± ‰ (1σ)	$\Delta C_{C\text{-}FeC}$	Stdev
Jag5 D	-19.47	0.57	0.68	-13.23	-	1.60	+6.35	0.88
Jag5 F	-18.08	1.09	1.14	-11.65	-	1.54	+6.53	1.11
Jag10 B	-25.22	2.00	2.06	-17.26	0.42	0.59	+8.14	2.51
						Overall mean	+7.18	1.30

Table 7.5 Mean values. The standard deviations (Stdev) for multiple analyses expresses the precision on the analysis, where standard deviations are not possible (n = ≤2) I have expressed the precision as the propagated error based on the standard analyses. Both are shown for some areas of the samples to display continuity between both methods.

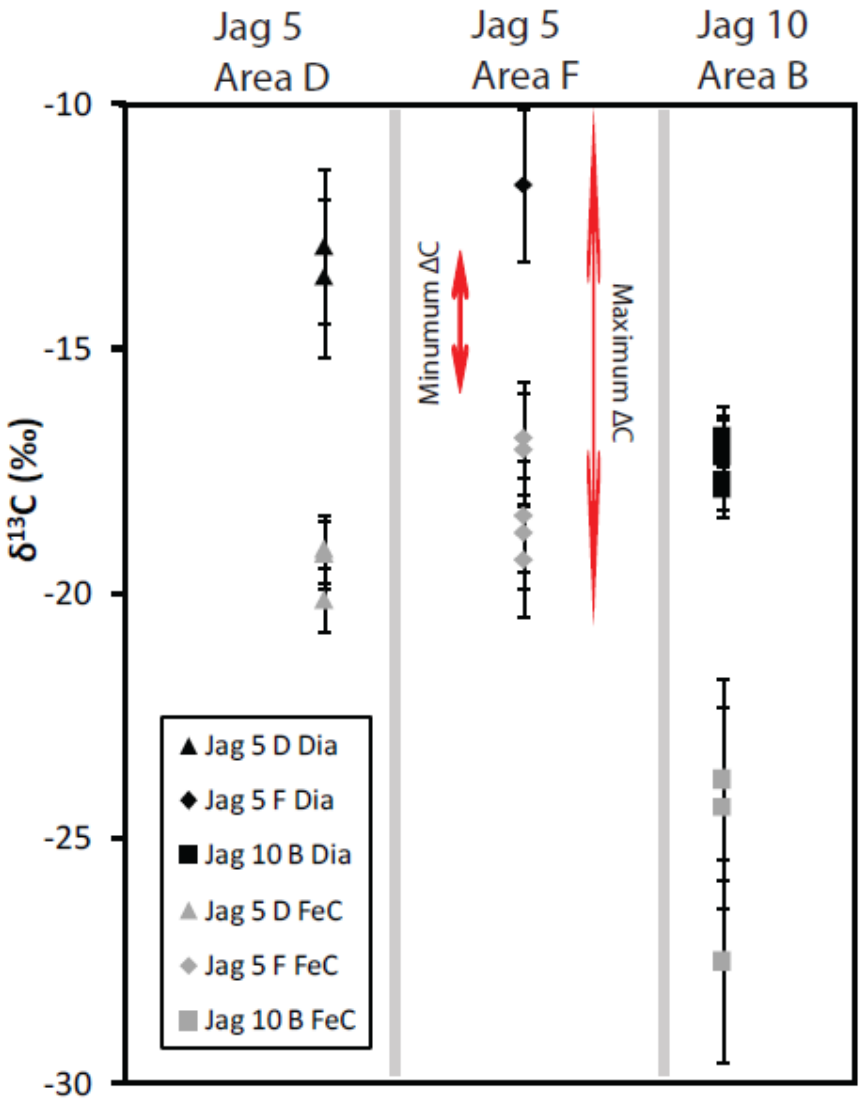

Figure 7.7 Individual $\delta^{13}C$ values for diamond (dia) and Fe-carbide (FeC) with analytical errors shown. This outlines the minimum and maximum that the ΔC value can be in this study, and the significance of the mean values as used subsequently.

7.7.2 Temperature of equilibration

The temperature at which Jag5 and Jag10 equilibrated (crystallised) is unknown. As far as I am aware, there are no known methods to apply, for example, any chemical or crystallographic geo-thermometry for Fe-carbide crystallisation. The diamonds are type II, therefore no apparent temperature constraint using the degree of nitrogen aggregation as a function of time and temperature can be utilised (MENDELSSOHN and MILLEDGE, 1995a; 1995b; TAYLOR et al., 1996).

Another method considered was the Si and O solubility in Fe^0 geobarometry (TAKAFUJI et al., 2005; 2004). This could potentially derive a depth of formation where I could assign a realistic temperature by using the mantle geotherm. The concentrations of Si and O have been show to increase in the Fe^0 as a function of pressure (however the effects of C concentrations on this solubility data are unknown). Figure 7.8 demonstrates that this method fails at placing any constraint upon the pressure of formation because the data in table 7.3 shows large variations in Si and O wt %. The O (wt %) in the 5 of the Jagersfontein Fe-carbides yields a P of < 50 GPa and Si from >80 GPa. Therefore this is not a feasible constraint, especially owing to the fact that such a spread in concentrations is derived from only 5 samples. Therefore I again propose a detailed petrological investigation by using both 2D analysis and depth sections produced by using Focused Ion Beam (FIB) milling in various areas of all the samples available. These polished samples and FIB sections should then be thoroughly studied using nanoSIMS (isotopic variations), WDS (elemental variations) and TEM (crystallography). This would enable better constraints to be placed on the phases present (or lack of) and their spatial distribution, crystal structures, stoichiometric characteristics and relationship with chemical variations (isotopic and elemental). In turn this could yield information regarding their P-T conditions of formation as well as the source of the Fe-carbide (or the Fe^0 that could have been present to react with carbon to form Fe-carbide). Thus far, I do not know the temperature at which Jag5 and Jag10 equilibrated (crystallised).

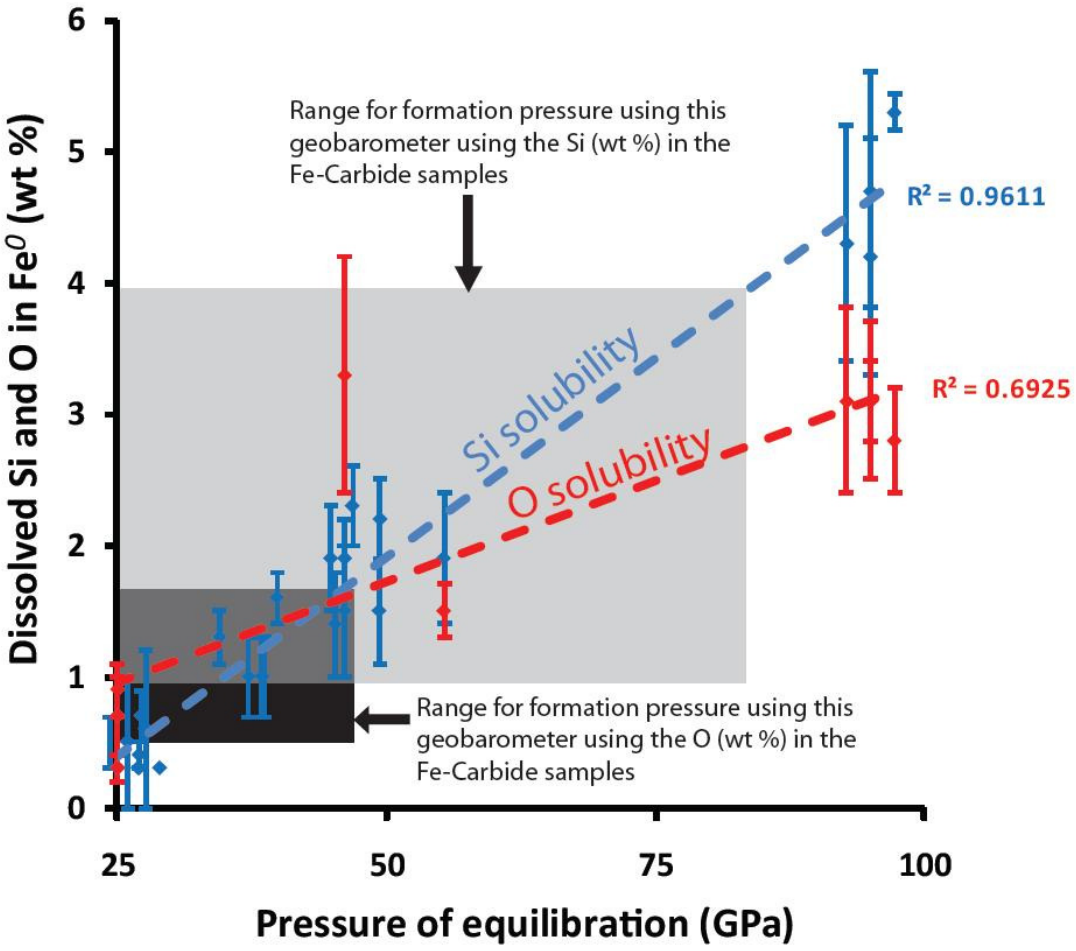

Figure 7.8. Solubility data for Si and O in Fe^0 as a function of pressure between 2000 and 2900 °C (TAKAFUJI et al., 2005; TAKAFUJI et al., 2004). The black and grey boxes represent the range in Si and O concentrations for the Fe-carbide inclusions from the Jagersfontein samples shown in table 7.3. Note the large range in potential P-T conditions one could derive from such a geobarometer, should one be so inclined to propose its use in this study.

7.7.3 Source of the carbon and iron

The origin of the carbon is now interesting to consider. The initial $\delta^{13}C$ value of the carbon is unknown as I do not have a proxy with which to determine the mass of each component and therefore cannot perform a weighted mean calculation, but it is likely that it did not have a $\delta^{13}C$ value consistent with the mean mantle (-5 ± 3 ‰). The initial $\delta^{13}C$ value was more like -20 ‰, which is not uncommon for mantle carbon (diamond) from the Jagersfontein mine (DEINES et al., 1991;

TAPPERT et al., 2005a). It is the origin of low $\delta^{13}C$ values that is the question; however unlike the diamonds with low $\delta^{13}C$ values in chapters 5 and 6, I have no other proxies with which to propose (or eliminate) competing source models.

The origin of the iron is most likely Fe^{0} in the reducing mantle at depths > 250 km (ROHRBACH et al., 2007). The textural evidence (figure 7.5) and near constant difference for the isotopic compositions of the diamond and Fe-carbide (fractionation factor) are suggestive of synchronous growth. But the 'crack-like' macroscopic textures in figure 7.3 seem like the Fe-carbide infiltrated a broken diamond. I propose a working model below;

(1) The diamond was residing in a mantle domain where Fe^{0} is stable (> 250 km).

(2) The diamond and liquid or solid Fe^{0} come into contact causing a chemistry of C + Fe^{0} under mantle pressure and temperature conditions. This is not an equilibrium assemblage (LORD et al., 2009) and so the Fe^{0} begins to react with the diamond.

(3) The first reaction is to dissolve carbon into Fe^{0} whilst infiltrating the diamond along slip planes (or other lines of weakness). This begins to reach a critical point in carbon saturation (pressure and temperature dependant).

(5) This causes the carbon saturated Fe^{0} to precipitate carbide and re-precipitate diamond under isotopic equilibrium. This explains the sharp contact macroscopic textures in figure 7.3 and the spherical blebs that resemble immiscible fluids in figure 7.5 as well as the constant ΔC between the two phases.

7.7.4 The isotopic consequences of $\Delta C_{C\text{-}FeC}$ in the terrestrial mantle

I have demonstrated that careful ion probe analysis of natural complex samples can be used to derive fractionation factors for carbon isotopes between coexisting carbide and diamond with a spatial resolution of 5 μm^2. The fractionation factors for carbon isotopes between coexisting carbide and diamond ($\Delta C_{C\text{-}FeC}$) agree to a first order, with those determined and reviewed in Deines and Wickman (1975) for graphite-carbide-metal systems in meteorites (table 7.1). This congruency of behaviour for carbon isotope fractionation at high P and T (in the mantle) demonstrates a great potential for the generation of distinct $\delta^{13}C$ reservoirs in the Bulk Silicate Earth (BSE). The potential for values of ΔC as large as +7 to +12 ‰ at mantle temperatures can be profound, especially if one applies Rayleigh-type open system fractionation and the stability of Fe^0 in the mantle at depths >250 to ~ 2900 km (ROHRBACH et al., 2007). This $\Delta C_{C\text{-}FeC}$ is large enough at the lower temperature end of the scale to be invoked as an abiogenic, high temperature and solely mantle mechanism (not subduction of organic carbon) to possibly explain mantle materials with low $\delta^{13}C$ values and maybe the existence of isotopic bimodality (for examples see chapter 2, figure 2.11).

There is a conventional thought that fractionation of ^{13}C in the deep Earth (> 200 km) is too small to generate $\delta^{13}C$ values as low as between -15 to -25 ‰ from a starting $\delta^{13}C$ value of circa -5 ‰ (see STACHEL, 2001). This is because CH_4 would be the dominating carbon species (Frost and McCammon, 2008) and the equilibrium isotopic fractionation factor for diamond - CH_4 at upper-most mantle temperatures (1200 °C) is very small, circa +1 ‰ (Richet et al., 1977) and produces ^{13}C-enriched diamond, not depleted. Especially when one considers the smaller fractionation factor alongside the reaction diamond - CO_2 being -3.5 ‰ at 1200 °C (Bottinga, 1969) with the latter reaction dominating only in the upper-most mantle from 100 to 250 km depth (Stagno and Frost, 2011). Therefore the system presented here (diamond + Fe-carbide), does not only seem plausible, but should be expected in the deep Earth so long as carbon-iron ratios are > 0.09 (or 900 ppm for a Fe^0 concentration of 1 wt %) in the region of interest (figure 7.2). This can give rise to two distinct $\delta^{13}C$

reservoirs where one is depleted in ^{13}C (the Fe-carbide relative to diamond). The magnitude of this depletion is dependent upon the initial $\delta^{13}C$ value of the source carbon ($\delta^{13}C_i$), the fractionation factor (α) and the fraction removed (f) according to the equation 1 (below) and graphically demonstrated in shown in figure 7.9.

1. $\delta^{13}C \text{ reservoir} = (\delta^{13}C_i + 1000)f^{(\alpha-1)} - 1000$

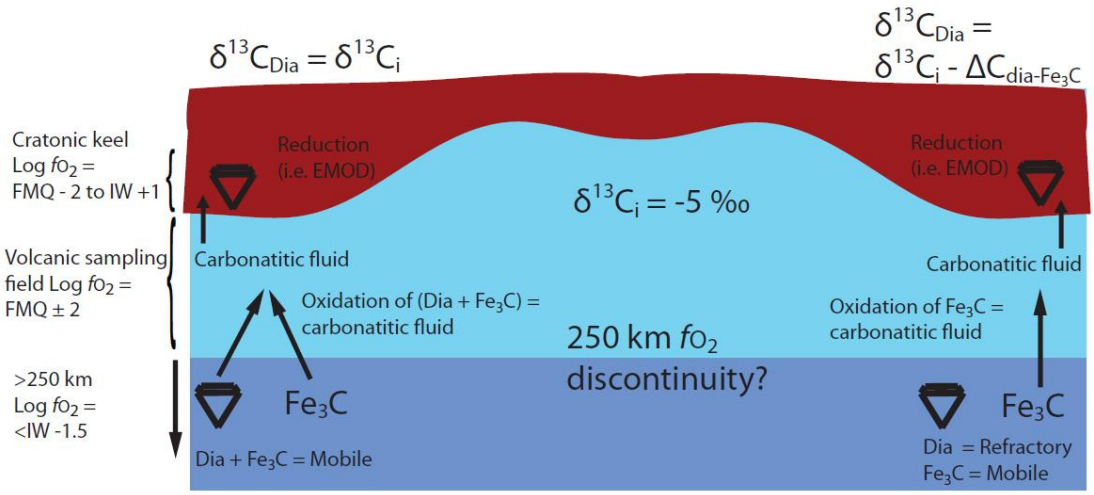

Figure 7.9. This is a cartoon illustrating the possible isotopic consequence of the large ΔC in this system for mantle diamond formation. Whereby diamond (diamond symbol) can form in the cratonic lithosphere from primary mantle carbon with a fractionated $\delta^{13}C$ value, i.e. lower than -5 ± 3 ‰ by roughly 7 ‰ (temperature dependant). Should the diamond-forming carbon in a stable lithospheric craton be sourced from a reducing region of the mantle that is below the IW buffer, then the carbon could be derived from the oxidation of Fe-carbide (FeC), where the diamond is refractory during deep carbon liberation (by convection, melting or otherwise). This would produce ^{13}C depleted carbon in the fluid/melt that precipitates diamonds with low $\delta^{13}C$ values relative to the initial $\delta^{13}C$ value of the source (i.e. mantle -5 ‰). Alternatively, should the diamond-forming carbon be derived from the oxidation of Fe-carbide and diamond in equal proportions the $\delta^{13}C$ values of the diamonds would be equal to the $\delta^{13}C$ value of the mantle source; -5 ± 3 ‰.

Equation 1 also works to calculate the $\delta^{13}C$ value of the second component by the inversion of α or subtracting the $\delta^{13}C$ reservoir from the initial ($\delta^{13}C_i$). However, α is not a constant and is very sensitive to temperature in all systems (SCHAUBLE, 2004; UREY, 1947), pressure in some systems (for a

review see HORITA, 2005) and highly influenced by fO_2 as a variation in speciation changes the nature of the bonding and therefore α.

7.8 Concluding remarks

I have presented an empirical value for $\Delta C_{C\text{-}FeC}$ from mantle-derived samples for the first time. The ΔC of circa +12 ‰ for graphite – cohenite in iron meteorites is almost twice as large as the ΔC for diamond – Fe-carbide in this study, where ΔC = +7.2 ± 1.3 ‰. This could be a consequence of the diamond – Fe-carbide in this study equilibrating at a higher temperature according to the thermodynamics of a reduction of α with increasing temperature (Bottinga, 1969; Hoefs, 2009; Richet et al., 1977; Urey, 1947).

Stable isotope geothermometry using theoretical mass dependant equilibrium stable isotope fractionation factors (Mikhail et al., 2010; Schauble, 2009) yields a temperature of between 1100 and 1300 °C, which equates to a depth of 150-250 km using the mantle geotherm (Brown and Shankland, 1981). This is at the shallowest depths where Fe^0 is thought to be stable in the ambient terrestrial mantle (ROHRBACH et al., 2007), and would explain the source of the carbide-forming iron. This is also consistent with sublithospheric silicate bearing diamonds from the Jagersfontein kimberlite pipe (STACHEL et al., 2005; TAPPERT et al., 2005a).

This has several implications, such as understanding the deep carbon cycle in the mantle as viewed through the $^{13}C/^{12}C$ ratio of mantle samples and volcanic gases and potentially the isotopic effects of carbon incorporation into the core during core formation. But, to understand and predict the effects of this fractionation factor in terms of its cosmochemical and geodynamic implications, one must determine the pressure and temperature effects for α in this system.

Chapter 8

Pressure and temperature constraints on the fractionation of ^{13}C between graphite/diamond and iron carbide at HPHT

8.1 Introduction

The objective of this chapter is to develop a method to quantify the temperature and pressure effects on the magnitude of isotopic fractionation for $^{13}C/^{12}C$ between Gr-Dia and cementite under mantle P-T conditions. This is the first isotopic study in this system using experimental methods; therefore I had to develop a method to resolve the isotopic compositions of the phases in the experimental charges which has been successful.

The field of experimental stable isotope fractionation at high pressure (mantle conditions) is in its infancy relative to low pressure studies (surficial conditions). The main body of work in the field of stable isotope fractionation that is commonly used in the literature to fit empirical data from mantle samples, such as diamonds, comes from thermodynamic calculations performed at 0 GPa (BOTTINGA, 1969; BOTTINGA and CRAIG, 1968; HORITA, 2001; RICHET et al., 1977; SCHAUBLE, 2004; 2009). However the potential effect of pressure on equilibrium isotope fractionation, which is large during subduction zone processes and during mantle differentiation, has been even less constrained to date (for a detailed review see HORITA, 2005).

Mass dependant equilibrium isotopic fractionations are caused by sensitivities of vibrational frequencies to isotopic substitutions (UREY, 1947) and are greater for systems where the percentage

mass difference between the isotopes in question is greater (O'NEIL, 1986). The most important factor that determines the magnitude of the isotopic fractionations is differences in the bond strength in question; in short stiffer bonds concentrate the heavy isotope, also higher oxidation states and lower coordination numbers will both lead to stiffer bonds (SCHAUBLE, 2004). Increasing the pressure in a given system may also stiffen the bonds (SHAHAR et al., 2009). Pressure can decrease the volume of compressible phases and therefore increase the vibrational frequencies of the site of occupation. The previous work investigated the effects of pressure on oxygen and hydrogen isotope partitioning, but pressures in those studies were limited to a ΔP of 1 GPa and contradictory results were obtained; there is no resolvable pressure effect for $^{18}O/^{16}O$ (CLAYTON et al., 1975) or $^{30}Si/^{28}Si$ (SHAHAR et al., 2011) and a large effect for D/H (HORITA et al., 1999). Therefore, the effect of pressure on isotopic partitioning on the systems with masses between oxygen and hydrogen and large mass differences between the isotopes requires an investigation (i.e. carbon). This is an important parameter to consider, especially for environments where ΔP is larger than ΔT with depth, i.e. all planetary interiors.

8.1.1 Potential Implications of this work

There are three main questions that have forged this study;

(1) Is the stable isotope geothermometry in chapter 7 relevant, or does pressure have an effect in the diamond- Fe carbide system?

High pressure experimental constraints will enable the use of stable isotope geothermometry discussed in chapter 7, to be better constrained. This may enable the depth of origin for the two samples from Jagersfontein to be precisely determined.

(2) How much carbon was sequestered into the core during its formation?

High pressure and temperature constraints on stable isotope fractionation are required to better predict the concentration of carbon in the Earth's metallic core. This can be achieved by using an isotopic mass balance, for a similar study involving for silicon isotopes see Shahar et al (2009). There have been several studies that propose carbon as one of the main light elements to offset the observed density deficit of the Earth's metallic core (NAKAJIMA et al., 2009; WOOD, 1993). This is, in part, due to the reactivity of iron and carbon and the stability of iron carbides at all pressures and temperatures akin to the terrestrial mantle before, during and after core formation (Lord et al., 2009). Therefore, an isotopic model could provide a new constraint to this long standing question.

(3) Why does Martian magmatic carbon have a mean $\delta^{13}C$ value of -20 ± 5 and not -5 ‰?

Finally, such a large fractionation factor in a reducing system (< the IW buffer) as discussed in chapter 7 could explain the low $\delta^{13}C$ values recorded in Martian magmatic carbon (-20 ± 5 ‰) relative to Earth (-5 ± 3 ‰) and shown in figure 8.1. An explanation is especially required because both mantle nitrogen isotopes (figure 8.1) and modelled bulk Earth silicon isotopes (SHAHAR et al., 2009) show chondritic values. Therefore the question remains that both planets should share a common primordial value centred at the chondritic value of -5 ‰. The question posed by Wright et al (1992) still stands, *'why does Martian magmatic carbon have a mean $\delta^{13}C$ value of -20 ± 5 and not -5 ‰?'*

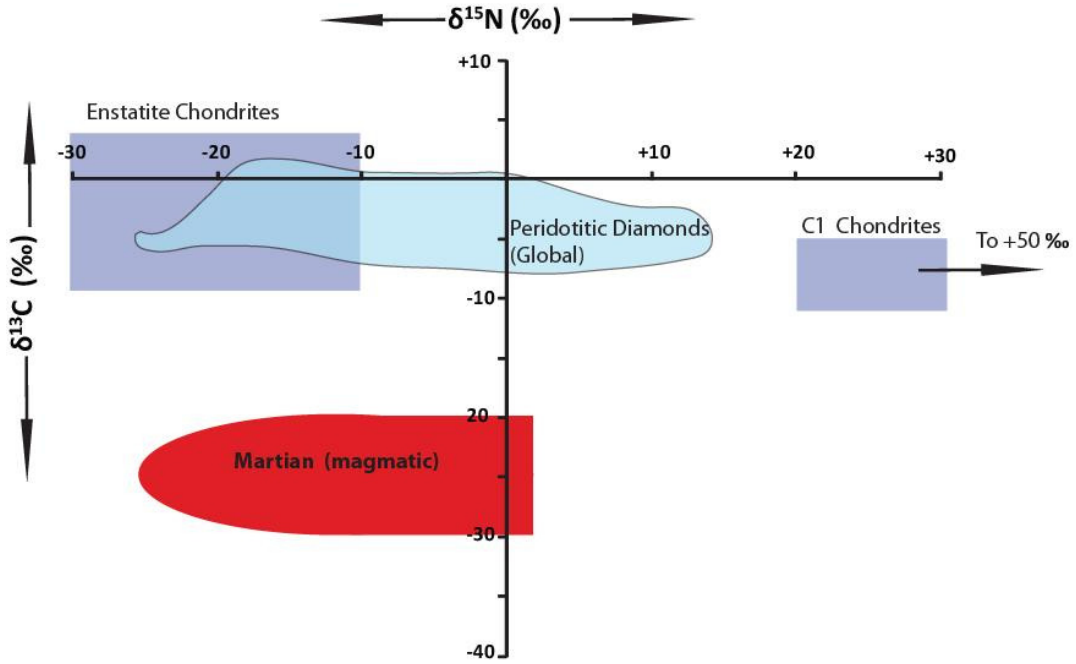

Figure 8.1. This diagram illustrates the similarity for terrestrial mantle nitrogen isotopes with Martian magmatic nitrogen and the carbon isotope discrepancy. The field for peridotitic diamonds is from Cartigny et al (1997); Martian magmatic carbon, C1 and enstatite chondrites are from Grady and Wright (2003 and references therein).

To address these questions I have attempted to determine the temperature effect on the magnitude of the fractionation factor by synthesising Gr-Dia and cementite at different temperatures (1200-1650 °C) and attempted to determine the pressure effect by synthesising diamond and cementite at a constant temperature (1650 °C) and increases pressure (9-25 GPa) from the same carbon source.

8.1.2 Previous isotopic work

There is no experimental data available in the system Gr-Dia and Fe-carbide where the fractionation of the stable isotopes of carbon was the objective. The theoretical work show that there is no predicted difference between graphite -Fe_3C and diamond -Fe_3C or between graphite-Fe_7C_3 and diamond-Fe_7C_3 as a function of temperature (MIKHAIL et al., 2010; SCHAUBLE, 2009 and personal communication 2011). In short, polymorphism between Fe_3C/Fe_7C_3 and Gr-Dia has no effect on the

fractionation factors in this system. Therefore, the discrepancy between the fractionation factor measured in iron meteorites (graphite-cohenite) of ~ +12 ‰ and my own empirical fractionation factor for diamond-Fe carbide of ~ +7 ‰ (chapter 7), may simply be a function of temperature or pressure.

What remains unknown is the exact temperature at which either of these assemblages equilibrated, and determining this with the current data is very difficult. One reason for this is because graphite + cohenite and diamond + Fe carbide can be a thermodynamically stable assemblages over several thousands of degrees Celsius (LORD et al., 2009). Also, the internal mean temperature for the life span of an Fe-meteorite is not well constrained (Goldstein et al., 2009). It is known from HPHT experimental studies that for Fe-carbide and graphite to co-exist between 1 and 5 GPa we would need between 1000 and 1400°C (Tsuzuki et al., 1984). For diamond + Fe-carbide, (in chapter 7, section 7.2) demonstrates that this assemblage can be derived from a large depth (pressure and temperature range) as well as in the lithosphere (according to the model of JACOB et al., 2004). And the diamond mine from which the two samples in chapter 7 originate is known for sourcing diamonds from 150 to > 600 km depth (TAPPERT et al., 2005), which only adds to the unknown variables. However, there is a potential to use stable isotope geothermometry which requires the pressure and temperature effect(s) to be determined.

8.2 HPHT experiments

8.2.1 P-T and C concentration constraints

The aim of these experiments was to produce cementite and Gr or Dia in a solid state reaction from a 1:1 molar mix of powdered graphite and iron powder. Therefore conditions must be recreated in the sample capsule that allows these two phases to be in solid state equilibrium. I must perform the synthesis in the solid state because once the conditions are in the diamond stability field (circa <5

GPa and >1100 °C) elemental C in liquid Fe will lead to rapid diamond formation resulting in dia + Fe^0 and not cementite + Gr-Dia (LORD et al., 2009; NAKAJIMA et al., 2009; REUTSKY et al., 2008; TSUZUKI et al., 1984; WOOD, 1993). I set the limitations on the P-T parameters for my experiments on the phase diagrams published in Lord et al (2009).

My experiments were conducted within the stability field for Fe_3C/Fe_7C_3 and Gr-Dia in accordance, achievable, to the P-T conditions in the terrestrial mantle (Figure 8.2). For example, at 2 GPa the mantle is approximately 900 °C, but at this temperature Fe_3C is stable in equilibrium with α-Fe, not graphite (LORD et al., 2009 and shown in figure 8.3). Therefore my experimental temperature must be above the geotherm and into the field of stability for Fe_3C + graphite (>1000 °C).

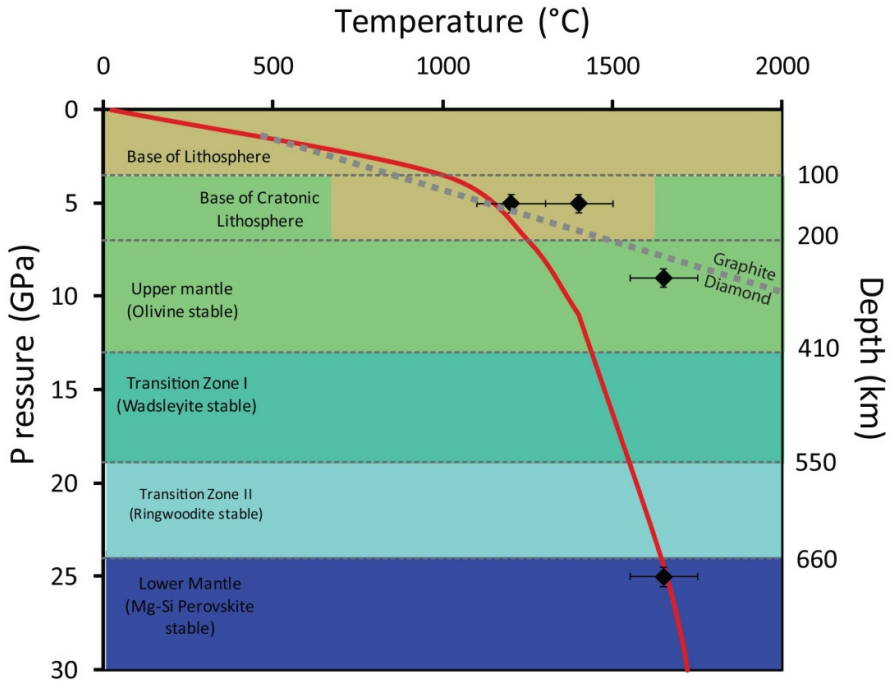

Figure 8.2 The P-T conditions of experiments in this study. Error bars are ± 100 °C and 0.5 GPa . The mantle geotherm of Brown & Shankland (1981) is shown as a red line, where 410 km is 1400 °C and 660 km is 1600 °C. The dashed grey line represents the graphite – diamond phase transition (from Tomlinson (2005).

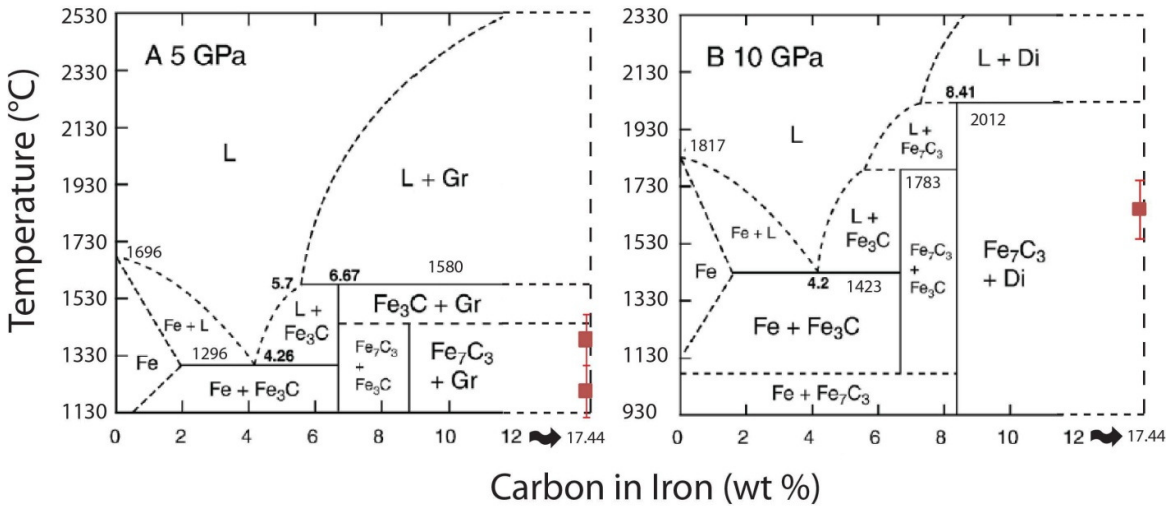

Figure 8.3 Phase diagrams for the iron-rich end of the iron + carbon system from Lord et al (2009) extrapolated to 17.44 wt % carbon. This extrapolation is consistent with the carbon-rich phase diagram of Tzuzuki et al (1984) which used 80 wt % carbon. Error bars are ± 100 °C.

8.2.2 Multi anvil press

A multi-anvil press is a high pressure device used to simulate P-T conditions typically spanning a range of 4 to 30 GPa (static pressure) and a temperature up to circa 2000 °C (furnace material dependant). Confining pressure is generated by applying force to six outer steel anvils which in turn act on a cubic arrangement of eight tungsten carbide inner-anvils (figure 8.4a). The eight inner anvils are each truncated along their three-fold axes (figure 8.4b). The truncations on the anvils are smaller than the edge length of the octahedral pressure-cell so that a force applied to the back of the anvils will be transferred to the pressure cell. The spaces around the octahedra are controlled with gaskets (figure 8.4b), which aid pressure generation by reducing flow of the pressure cell into this space, and help make the pressure cells more stable at high pressure and temperature. The size of anvil truncation and sample octahedron size determine the pressure generated in the cell for a given load from the press (KEPPLER and FROST, 2005). The sizes of cells used are referred to by the edge length of the octahedra and the length of the truncation edges. A sample assembly is shown in figure 8.4c. The high-pressure assembly is an octahedron composed of MgO; the use of soft MgO as the pressure

medium allows the pressure exerted on the sample to be almost hydrostatic. A cylindrical hole is drilled through the octahedron for a tubular resistance heater of graphite, the sample and a thermocouple. The furnace is placed inside a sleeve of ZrO_2 which thermally insulates the octahedra and anvils from the furnace. This minimises heating of the gaskets which would then flow reducing the pressure and stability of the cell.

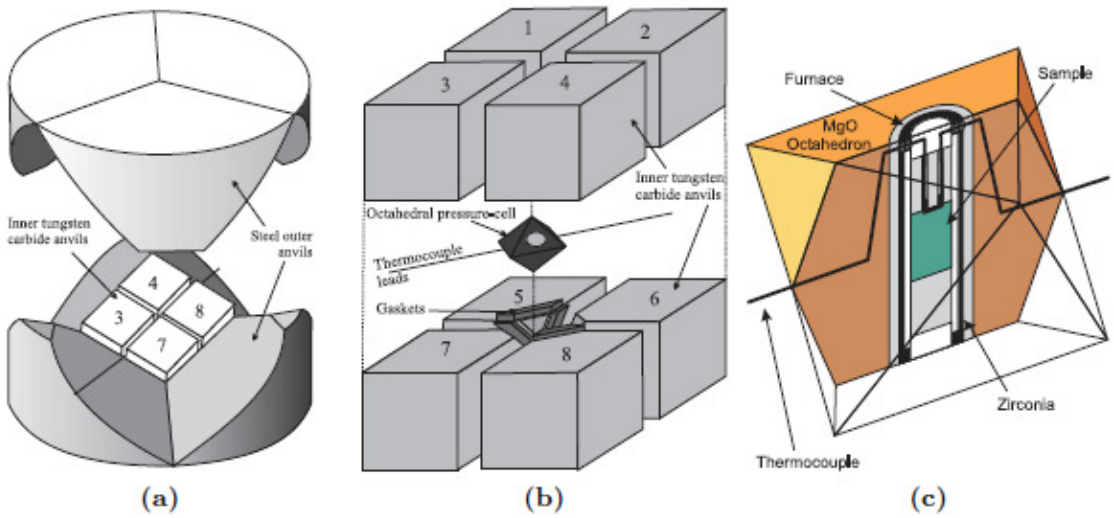

Figure 8.4. The typical 6-8 Kawai-type anvil sets and assembly multi (sourced from HUNT, 2009). The subsystem components are (a) The split-cylinder outer anvils of a Walker cell; (b) The eight inner anvils with the pressure cell and gaskets where the numbered anvils in (a) correspond to the numbers on the anvils in (b); and (c) is an example of a typical high-pressure-cell assembly as used in this work.

8.2.3 Calibration

The pressure exerted by the press on the multi-anvil module is deduced using a hydraulic oil pressure scale. This primary pressure scale was calibrated experimentally on the basis of fixed pressure points caused by identifiable and precisely measurable phase changes whose P-T position is well known. The ideal calibration marker has a polymorphic transformation is in the correct pressure range which is marked by a large change (i.e. resistance, structure); it is chemically pure, stable and easy to handle and has minimal hysteresis and temperature dependence. Pressure was calibrated at

room temperature by measuring the large electrical resistance discontinuity associated with the phase transformations Bi(I)-Bi(II) at 2.55 GPa and Bi(III)-Bi(V) at 7.7 GPa (HUNT, 2009; TOMLINSON, 2005). The pressure calibration for 25 GPa was done using the phase transition of Fe_2SiO_4 to the perovskite structure (Dr S.A. Hunt, pers comm. 2010). Temperatures were estimated from the calibration between applied electrical power and temperature using a W97%Re3%-W75%Re25%. The accuracy of the pressure and temperature determinations was ± 0.5 GPa and ± 100 °C respectively (HUNT, 2009; Dr S A Hunt pers comm. 2010; Dr A Shahar per comm. 2010).

8.2.4 Starting materials

The starting materials used are powdered graphite normally used to construct furnaces. This is of an unknown $^{13}C/^{12}C$ composition with the exception of sample AS1, which used a spiked carbon source (graphite with 10 % ^{13}C spike). After selecting 3 pieces of the un-spiked graphite at random for $\delta^{13}C$ analysis by gas sourced stepped combustion mass spectrometry (according to the methods outlined in chapter 4). The isotopic composition was found to be -25.18 ‰ with a standard deviation of ± 4.13 ‰ (n = 3 samples and 18 individual combustion step analysis). The Fe source was pure Fe^0 powder (99.99 % pure). The two powders were weighed and mixed for 3 hours in iso-propanol in an agate pestle and mortar before being dried overnight and placed in clean glass vial with a plastic screwed top seal. The molar mix of Fe:C was 1:1, which equates to 17.44 wt % C.

8.2.5 Redox conditions

As summarised in figure 8.5, the speciation of C is heavily controlled by variations in the redox state of the system irrespective of the pressure and temperature under mantle conditions. Therefore a mention of the crude redox controls applied in these experiments is required. In short, the experiments are all below IW buffer. This is known because there are no oxides in the sealed sample

capsules. The 5 and 9 GPa experiments used boron nitride (BN) capsule and the 25 GPa experiments was performed in a Re^0 capsule. Any small amounts of O entering the system as a contaminant would be in trace quantities (< ppm), whereas Gr/Dia is 100 wt % C and the wt % for C in Fe_7C_3 and Fe_3C is 8.3 and 6.58 wt % respectively. Therefore any ^{13}C enriched C-O compounds produced by ppm levels of O would not affect the $^{13}C/^{12}C$ of the run products because of their dominance by the mass balance of the system.

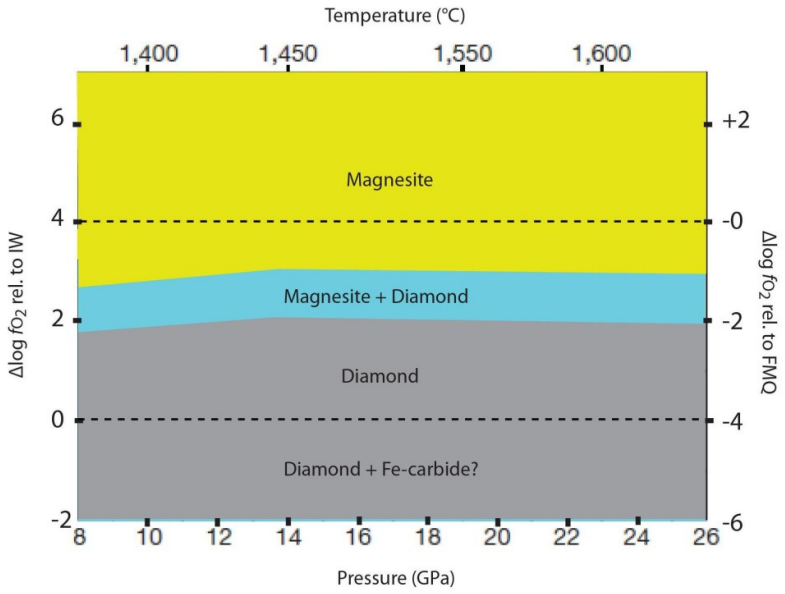

Figure 8.5. Carbon speciation between 8 and 26 GPa and 1350 and 1650 °C as a function of fO_2 in a pyrolitic mantle (modified from ROHRBACH and SCHMIDT, 2011). Note the dependence on fO_2 for speciation across all P-T conditions in this figure.

8.3 Experimental results

Once the samples were removed from the press the octahedron was cut along the axis of the Zr_2O_3 sleeve and broken open manually. The sample capsule was inspected to ensure that there were no re-sealed cracks that may have developed during compression (and re-sealed during heating) that would allow exchange of C between the sample and the graphite furnace. The sealing cap was also

investigated to ensure that the thermocouple wires did not penetrate the sample capsule. Table 8.1 shows the experimental run products that were analysed for their $\delta^{13}C$ values.

Analysis	P (GPa)	T (°C)	Duration
AS1	5	1200	72
CO#2	5	1400*	3
CO#5	9	1650*	3
CO#8	25	1650	3

Table 8.1.Sample names, pressures, temperatures and durations (hours) for experiments in this study. *denotes temperature calculated using a power curve and not measured directly using a thermocouple due to thermocouple failure during pressurisation.

8.3.1 Textural analysis

Upon imaging some of the run products using Scanning Electron Microscopy (SEM) at UCL it was evident that the grain sizes in these samples was variable, but consistently <100 µm. All of these images were taken using a JSM 640 LV SEM at UCL and were performed on uncoated samples.

Figure 8.6 is of experiment CO#2, graphite and cementite at 5 GPa and 1400 °C. What is evident from figure 8.6 is the occurrence of graphite micro grains in the cementite crystals. This is an unavoidable consequence of a solid state reaction as the molar ratio of the powders in the charge do not equate to pure cementite. Therefore, when the Fe^0 is all locked up in the cementite crystals the remaining C^0 will be trapped as an inclusion and either remain as graphite or be converted to diamond (P-T dependant). The rates of diffusion for solid Gr-Dia in cementite of variable size and at any temperature are unknown. This has an effect on the combustion temperature, as samples of a smaller grain size combust at lower temperature (this discussed in section 8.6b).

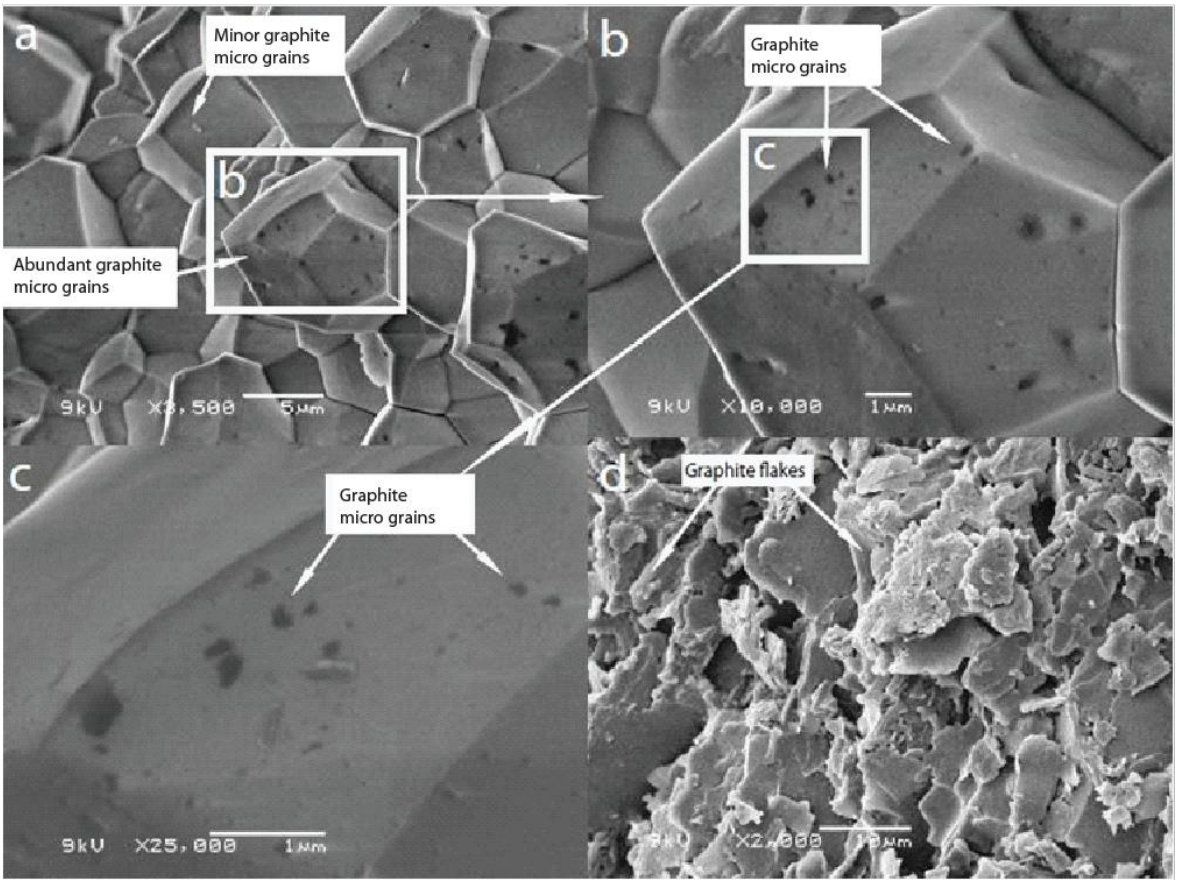

Figure 8.6. SEM images (taken at UCL) of sample CO#2. This sample is representative of samples in this study. (a-c) the occurrence of graphite micro-grains in rhombic cementite; (d) shows detail of the graphite flakes.

8.4 Multi-phase resolution using stepped combustion gas sourced mass spectrometry

To determine the $^{13}C/^{12}C$ ratios of the run products I decided to assess the potential of resolving the isotopic composition of each phase by stepped combustion gas sourced mass spectrometry (outlined in chapter 3). This method has been used for numerous studies to quantify the $\delta^{13}C$ values for multiple components within one sample such as;

- Distinguishing between the contaminant CO_2, degassed CO_2 in basaltic vesicles and finally determining the primary $\delta^{13}C$ values for carbon dissolved into basaltic glasses (EXLEY et al., 1986; MACPHERSON and MATTEY, 1994; MACPHERSON et al., 1999; PINEAU and JAVOY, 1994).

- Distinguishing the isotopic components of various meteorite fractions such as identifying the isotopic composition of magmatic carbon in Martian meteorites (Wright et al., 1992), enstatite chondrites (VERCHOVSKY et al., 2002) and to determine the C, N, and noble gas isotopic compositions of the components within in pre-solar diamonds (VERCHOVSKY et al., 1998) to list a few.
- To quantify the isotopic fractionation factor by determining the $\delta^{13}C$ values for experimental run products between dissolved CO_2 in MORB glasses and degassed CO_2 during basalts crystallisation (MATTEY, 1991) the ΔC between CO_2 vapour and silicate/carbonate melts (MATTEY et al., 1990).
- This method was also used by Boyd et al (1997) to determining the $^{13}C/^{12}C$ ratios of carbonates with varying chemical composition and combustion temperatures (Figure 8.7), for which this study aims to emulate with Gr-Dia + cementite as the carbon phases of interest.

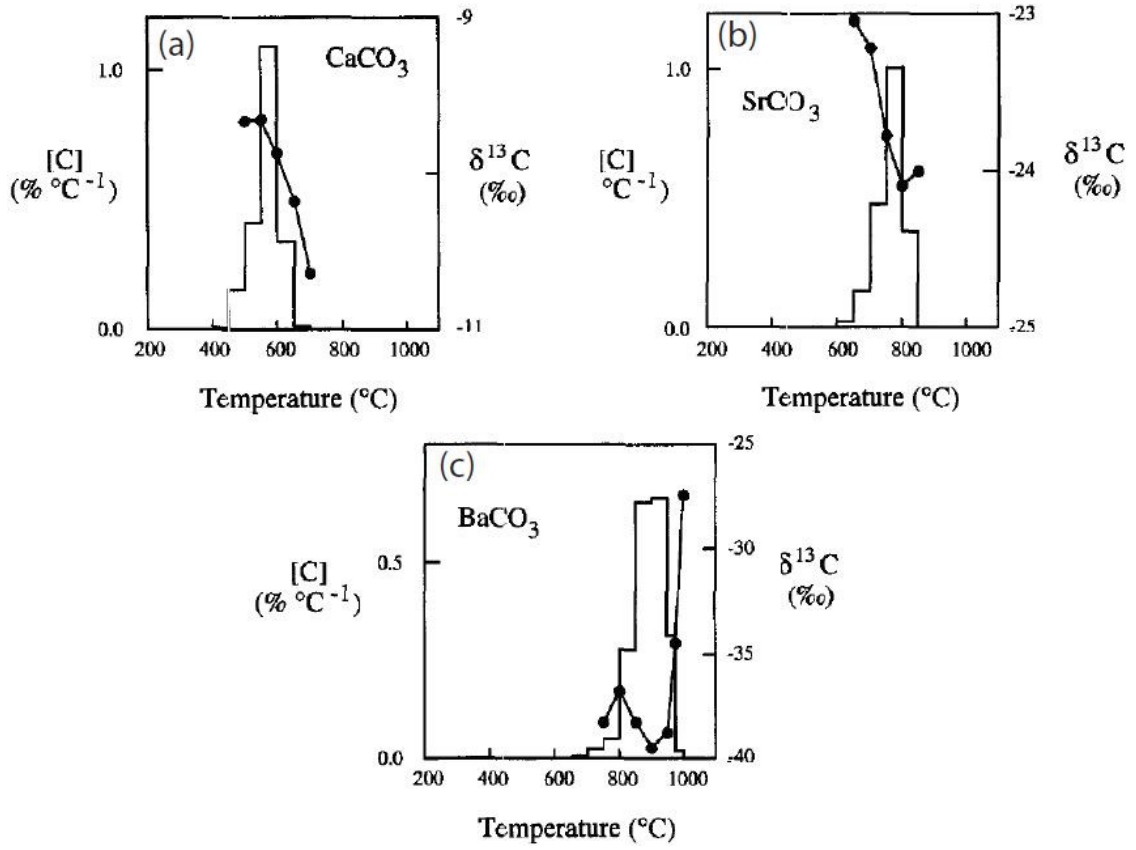

Figure 8.7. Stepped combustion profiles for Ca, Sr and Ba carbonate in Boyd et al (1997). Filled symbols joined by a solid line represent the $\delta^{13}C$ values for each step (right hand axis), the histogram represents the yield at each step. The right hand axis represents the total yield for the percentage carbon released. (a) is calcium carbonate, (b) strontium carbonate and (c) barium carbonate.

Before the task of combusting a composite powder of the two phases was attempted I combusted pure diamond, graphite and cementite (the cementite was a synthetic sample made by multi anvil press experiment with molar mix in a of $Fe_{3.6}$:C_3 at 5 GPa and 1200 °C resulting in $1Fe_3C + 0.6\ Fe^0$) to determine their combustion temperatures and therefore the feasibility that one can use this method (Figure 8.8).

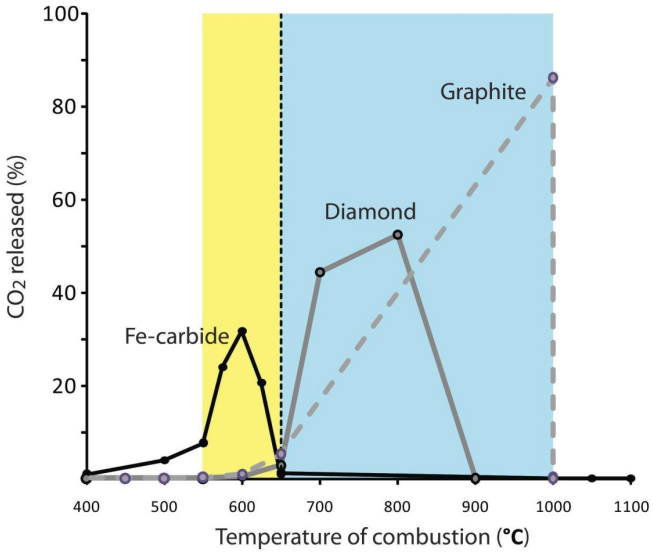

Figure 8.8. Plot of temperature in the furnace vs. the percentage of CO_2 generated relative to the total yield. The relative release temperature for stepped combustion for pure cementite (Fe-carbide), diamond and graphite (all crushed). The vertical dashed line represents the point at which cementite should have been combusted and Gr-Dia begins to combust in vacuo. The yellow and blue fields represent the temperature where one expects to see the $\delta^{13}C$ values for the respective components.

The Fe-carbide combustion temperature is lower than the Gr-Dia combustion temperature with a marked difference of 100 °C. Therefore it seemed feasible that one could simply place a crushed experimental sample (crushed to increase the surface area and expose the internal Fe-carbide) into Pt foil and perform a stepped combustion sequence to resolve the $^{13}C/^{12}C$ ratios for the two phases according to figure 8.8.

8.4.1 Contaminants

External (organic) contamination could be a compromising factor in the determination of the $^{13}C/^{12}C$ ratios of the experimental run products. To minimise this I wash the crushed sample in propanol, by placing the sample powder + propanol in a clean beaker and incubate this in an ultra-sonic bath for 2 hours. Once the sample is wrapped in the Pt foil and loaded into the furnace I perform a pyrolysis step and a subsequent combustion step at 400 or 500 °C in an attempt to remove any residual

contaminants. This has been shown to be effective where pyrolysis in vacuo at only 300 °C (Miller and Pillinger, 1997), I chose a higher temperature to ensure removal. The blank is a negligible contaminant as it is < 50 ng of CO_2.

8.5 Results

(a) Distinguishing the contaminants from the sample $\delta^{13}C$ values

The stepped combustion results are presented in figures 8.9 to 8.11. The first release steps (< 500 °C), implemented to remove organic contaminants, show a variable $\delta^{13}C$ value from -20.3 to -40.5 ‰. This range of ~ 20 ‰ is similar to what was seen for the diamond analysis in the previous chapters where the range for the carbon removed during pyrolysis was from > -10 to < -30 ‰.

The $\delta^{13}C$ values of the release peaks at ≤ 600 °C for sample CO#5 are not considered to represent the $\delta^{13}C$ value of the cementite. This is because they are very similar to the $\delta^{13}C$ value the pyrolysis step (i.e. the contaminant; see figure 8.10). The same is not true for the first release peaks for the samples CO#2 and CO#8 (a) where the first peak is distinct from the pyrolysis step (figure 8.9 and 8.12b respectively). Where the pyrolysis step is assumed to remove contaminant carbon and therefore the associated $\delta^{13}C$ value at this step is inferred to represent this contaminant (MILLER and PILLINGER, 1997).

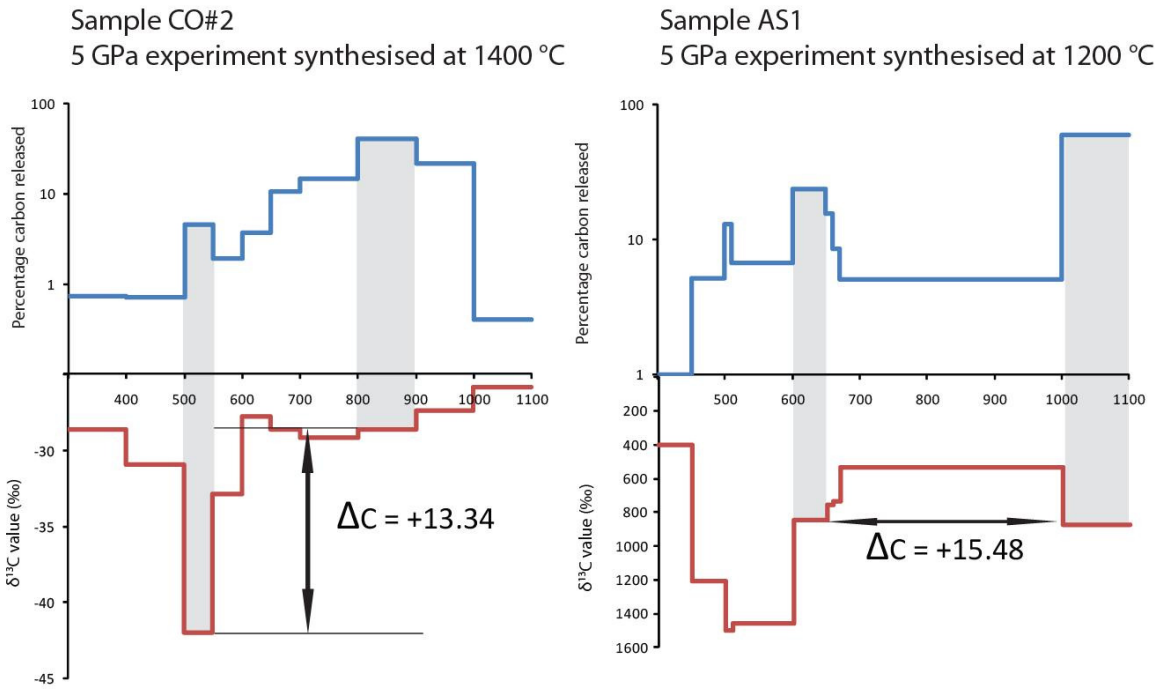

Figure 8.9. Carbon release profile for samples CO#2 and AS1 (left to right). The top graph (blue line) represents the percentage of the total carbon released for the run and the bottom graph (red line) represents the co-determined $\delta^{13}C$ value for the step in question. The grey bands represent the interpreted release that gives the $\delta^{13}C$ values for the components. The x-axis is temperature for the combustion step in degrees Celsius.

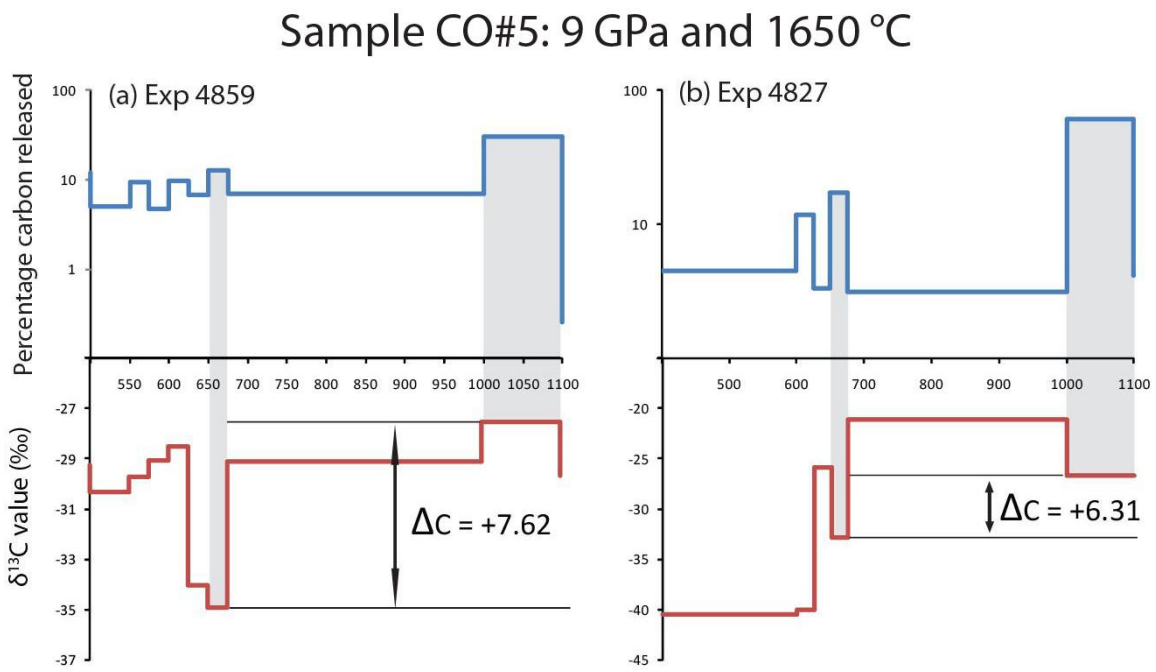

Figure 8.10. The release profile for sample CO#5; description as for figure 8.9.

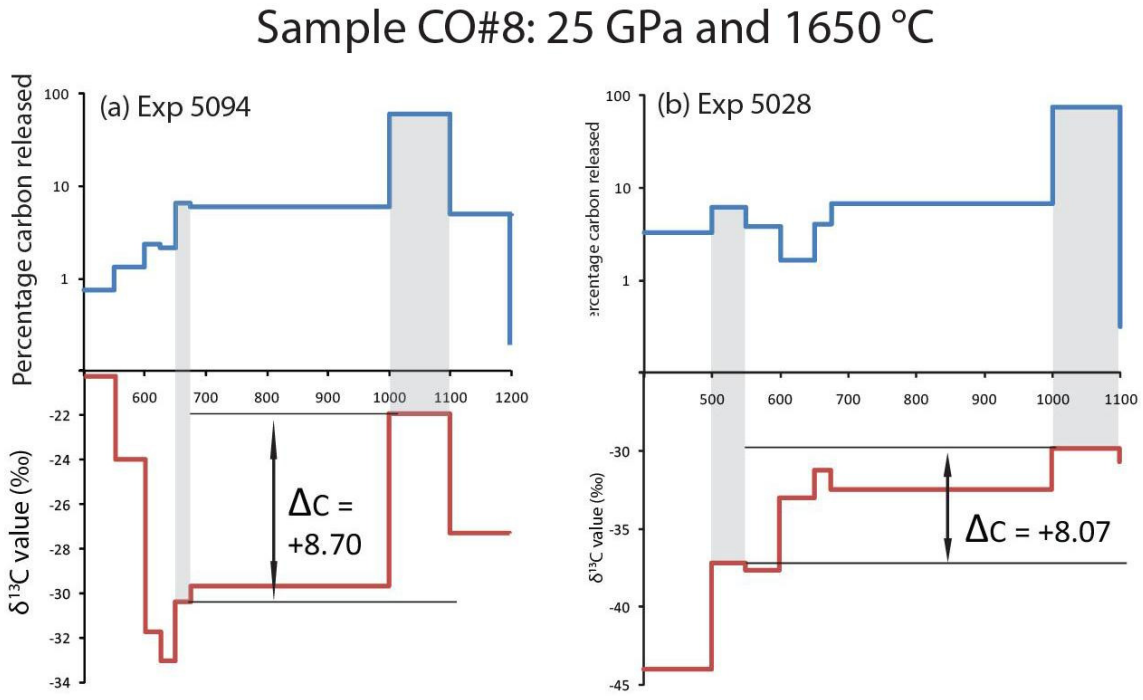

Figure 8.11. The release profile for sample CO#8; description as for figure 8.9.

(b) Distinguishing the phases

For the all of the samples (figures 8.9 to 8.11) the $\delta^{13}C$ value derived from the main release ≤ 650 °C (the largest CO_2 by mass) is considered to represent the $\delta^{13}C$ value of the cementite phase and the main release ≥ 800 °C is considered to represent the $\delta^{13}C$ value of the Gr-Dia phase. The reason for only using the main release peak to determine the $\delta^{13}C$ value of the cementite phase, as opposed to a weighted mean for all steps that are not considered contaminant ≤ 650 °C, is due to the micro-nano inclusions of Gr-Dia within the cementite (figure 8.6). It has been demonstrated that nano diamonds combust at a temperature of up to 400 °C lower than micro diamonds. Therefore, frustratingly, nano diamonds combust at temperatures of between 400 and 600 °C (BOYD et al., 1998). This is a very similar to the temperature of cementite (figure 8.8).

The exact abundance and size distribution of the Gr-Dia micro-nano inclusions cannot be determined. Therefore this is an unknown variable and cannot be mathematically subtracted from the data nor can the effects be predicted. However, using the main cementite release to determine the $\delta^{13}C$ value of the cementite phase can overcome this potential analytical/sample issue. This is assuming a dominance of carbon from the cementite relative to the micro inclusions of Gr-Dia and a mass balance that yields the $\delta^{13}C$ value of the cementite phase.

(c) Calculating the fractionation factor

The fractionation factors (α) are expressed, herein, as ΔC, which is ≈ δ-δ in ‰. These are defined and calculated as follows;

(a) The fractionation factor;

1. $\alpha = \frac{\delta^{13}C\ phase\ 1 + 1000}{\delta^{13}C\ phase\ 2 + 1000}$

(b) The ΔC value for Gr-Dia - cementite

2. $\Delta C = 1000 \cdot \ln(\alpha)$

The fractionation factors, sample names, experimental run numbers, and P-T conditions of the initial synthesis are shown in table 8.2.

Sample	Run number	P (GPa)	T (°C)	1000*ln(α)
AS1	4946	5	1200	15.5
CO#2	4839	5	1400^{+}	13.9
CO#5	4859	9*	1650^{+}	7.6
CO#5	4827	9*	1650^{+}	6.3
CO#8	5094	25*	1650	8.7
CO#8	5028	25*	1650	8.07

Table 8.2. The fractionation factors, sample names, experimental run numbers, and P-T conditions of the initial synthesis. *denotes two analyses of the same experimental sample. $^{+}$denotes the temperature measured using a power curve due to thermocouple failure

8.5.1 Variable release temperature for cementite

The pure cementite in figure 8.10 exhibits a well defined release peak at 600 ± 25 °C, whereas there is variability in the recorded release temperature for cementite of between 500 - 650 °C. Below I explain several reasons that can explain this observation.

(a) Pt foil stacking in the furnace

The variability in the recorded release temperature for cementite may be a function of the recorded temperature using the thermocouple, which is located at the base of the quartz combustion tube. Over time the samples become further away from the thermocouple, thus the thermocouple is not recording the actual temperature of the location where the sample is located. This depends upon the distance of the sample relative to the thermocouple within the quartz furnace and the geothermal gradient, an unknown parameter at present (figure 8.12). This issue arises because the samples are wrapped in Pt foil, therefore post-combustion of the sample there is always a residual component. The Pt foil and the samples in this chapter were analysed intermittently with diamonds from other chapters and studies. These Pt foils builds up over time and are difficult to quantify because the size of the Pt foil (mm^3) is initially an unknown (not measured), and is also not a constant.

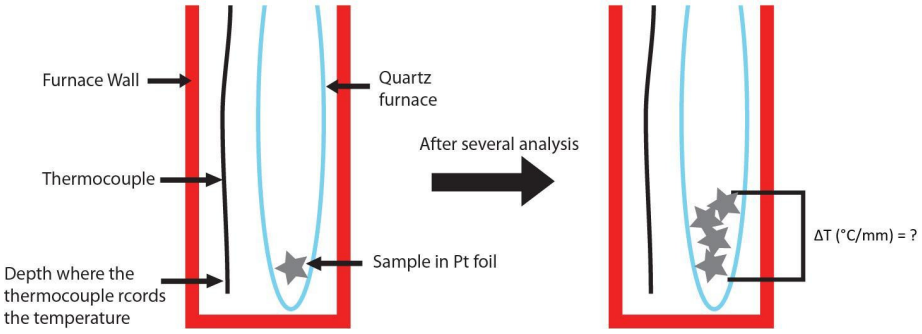

Figure 8.12. Cartoon schematic of the effects that may arise by Pt foil stacking at the base of the furnace. There are several unknown variables, such as ΔT (°C/mm) and, in turn, the amount and size of previous Pt foils in the furnace.

(b) pO_2 in the furnace

As discussed in chapter 3, the oxygen source is CuO powder wrapped in Pt foil within a Pyrex tube that is externally heated and not a pure O_2 gas source. The Cu/CuO ratio of the powder therefore becomes enriched over time (O depleted). As a consequence, the oxygen pressure during combustion decreases over time. This affects the rate of and amount of gas produced during combustion. For example, under optimum conditions 0.2 mg of diamond can be combusted at 1100 °C, whereas when the CuO powder is depleted, at the same temperature only 0.01 is combusted (appendix table A12). This will affect the amount of sample that can be combusted at a given temperature. Because the lower the pO_2 the higher the temperature that is required to combust the phase in question. Therefore the combustion temperature of cementite will be lower for high pO_2 than low pO_2. However, this will still be circa 100 °C lower than Gr-Dia (figure 8.8).

8.6 Discussion

The results are shown in table 8.2. There are some other factors that require discussion before the implications can be discussed with confidence.

8.6.1 Isotopic equilibrium

Regarding the nature of this study there are two meanings for the word equilibrium; thermodynamic phase equilibria and isotopic equilibrium. The thermodynamic phase equilibria are discussed in section 8.2.1. The isotopic equilibrium regards the isotopic exchange towards equilibrium which is the sum of surface exchange and interior exchange over time at a set pressure and temperature. Isotopic re-equilibration within a high pressure cell can take up to 3 days in the system graphite + calcium carbonate between 600 – 1400 °C and at pressures from 1.4 to 2.3 GPa (DEINES and EGGLER, 2009). These experiments differ from my own in that the study placed pre-existing graphite and calcium carbonate with differing $\delta^{13}C$ values into a charge and awaited equilibration.

Surface exchange is not predicted to be a major factor in these experiments. This is because the phases are not present in the initial charge. Therefore I predict that the cementite formation will preferentially partition ^{13}C during the initial synthesis according the to the fractionation factor and will not require isotopic exchange post-synthesis to equilibrate via surface reactions. However, should the internal $^{13}C/^{12}C$ ratios for the two phases have failed to reach equilibrium, then these experiments could be flawed. This is owing to extremely slow rate of ^{13}C self diffusion in diamond (KOGA et al., 2005), and an unknown rate of ^{13}C diffusion in cementite. The interior exchange effect in Deines and Eggler (2009) is a diffusion-controlled process. Diffusion of ^{13}C within the diamonds lattice has been experimentally tested at HPHT and has been shown to be an impractical model to explain any $^{13}C/^{12}C$ variations in diamonds across growth zones identified by CL zonation (Harte et al., 2009; Koga et al., 2005). Koga et al (2005) showed that under mantle PT conditions (circa 1800 °C and 10 GPa) the diffusion data can only constrain the maximum possible age of diamonds. Koga et al

(2005) state that using the empirical (experimental) diffusion data to generate carbon isotopic zonation in the order of 5 to 50 µm only after having been incubated under upper mantle conditions for > $4.5x10^9$ years, older than the Earth itself. Therefore ^{13}C diffusion in the diamond lattice cannot be a factor in my diamond-bearing experiments. This also means that performing time dependant experiments to test for isotopic equilibrium is not a feasible endeavour where diamond is present in the charge. Shahar et al (2009) found that isotopic equilibrium could be attained in 30 mins for $\Delta^{30}Si$ between silicate (pyrolitic) and metal (Fe-Ni alloy) melts at 1800 °C and 1 GPa. These experiments are not directly comparable to my own, but the principle is the same, 2 phases equilibrated from an initial source. And so rapid approach to equilibrium is expected.

8.6.2 Theory vs. experiment

Another way of testing for equilibrium is to compare both theoretical equilibrium fractionation factors (MIKHAIL et al., 2010; SCHAUBLE, 2009) and the experimental fractionation factors in this study at a given temperature. But first I must discuss the accuracy of the theoretical equilibrium fractionation factors (SCHAUBLE, 2009). Equilibrium $^{13}C/^{12}C$ fractionation between iron-carbon alloys and other materials can be calculated thermodynamically, based on the effect of isotope substitution on vibrational frequencies in each substance (e.g., BIGELEISEN and MAYER, 1947; ELCOMBE and HULSTON, 1975). Frequency shifts and the resulting isotope fractionation factors for several crystalline iron-carbide structures have been estimated with density functional theory (MIKHAIL et al., 2010; SCHAUBLE, 2009 and Schauble, personal communication 2011). These can be compared with our experimental results, but one must consider the accuracy of these calculations.

Shahar et al (2009) found that the theoretical equilibrium fractionation factor of Georg et al (2007) required re-scaling to fit the experimental constraints of circa 60 % (figure 8.13). There is a similar difference between theoretical equilibrium fractionation factors (SCHAUBLE, 2009) and the

experimental fractionation factors in this study for a given temperature (MIKHAIL et al., 2010; illustrated in figure 8.13). The best fit is found for the two experiments where a thermocouple was used to measure temperature (AS1 and CO#9), experiments that implemented a power curve to determine the synthesis temperature (after the thermocouple failed; samples CO#2 and CO#5) plot away from the equilibrium values. This may be a function of an incorrect synthesis temperature derived from the power curve. Herein the experiments where a thermocouple was used to measure temperature (AS1 and CO#9) are considered valid and the data from samples CO#2 and CO#5 are omitted.

The reason for the required re-scaling may be due to potential flaws in the calculations that may cause discrepancies between his theoretical ΔC values and empirical ΔC values. These potential flaws would produce a systematic and consistent error for the value of the fractionation factor (α). However the relationship between α and temperature (the slope of α vs. temperature) will be correct, but the value of α may not. These potential flaws are outlined below (from Schauble, 2009):

- Convergence testing for diamond is well known and incorporated, however convergence testing for metallic phases is not yet complete which will have an effect on the electronic structure calculations which in turn can have an effect on the fractionation factor due to the assumed bonding nature of the isotopes;

- Vibrational frequency estimates are critical to estimating isotope fractionation. However, relatively little is known about phonons in light-element inter-metallic phases and interstitials and therefore this can derive errors in the results.

Experiment AS1 was synthesised in 72 hours, and CO#8 in 3 hours. Since both of these experiments plot within error of the theoretical equilibrium fractionation trend (figure 8.13) implies that ≤ 3 hours was sufficient to reach isotopic equilibrium.

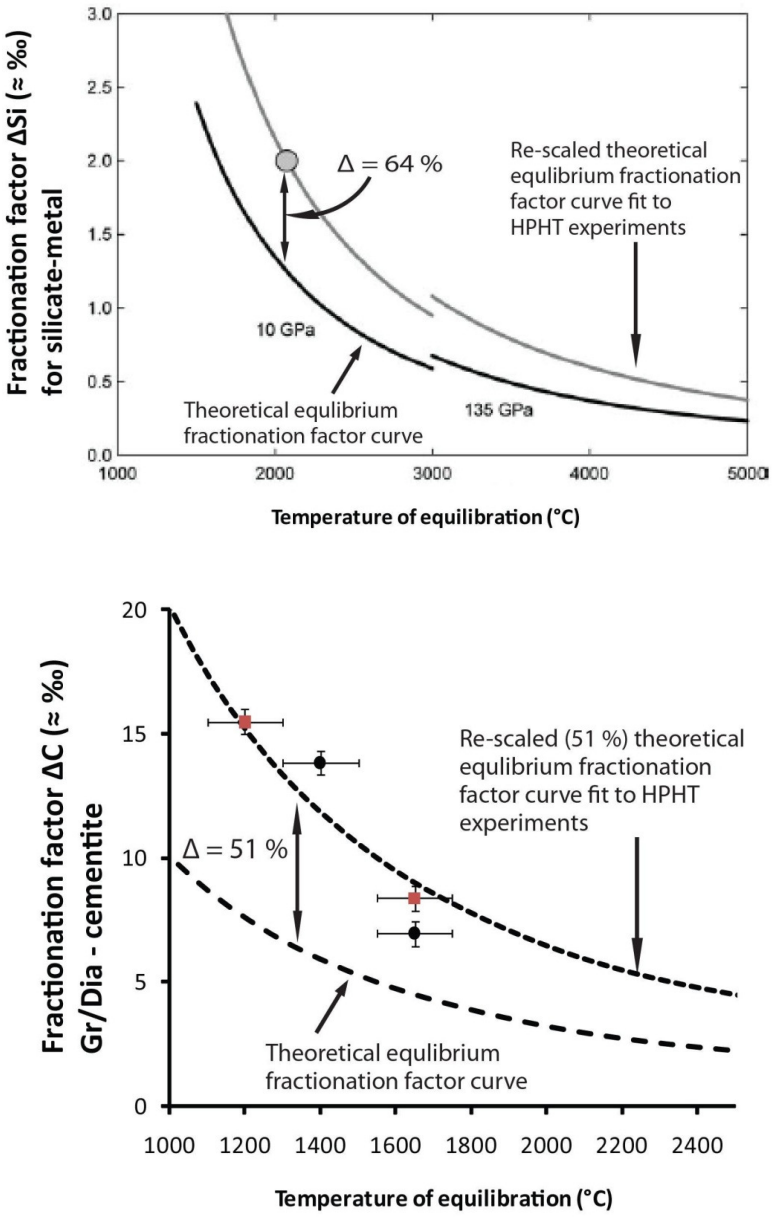

Figure 8.13. Top; The re-scaling of the theoretical equilibrium fractionation factor for Si isotopes between Fe-Ni and silicate melts of Georg et al (2007) to fit the experimental constraints of Shahar et al (2009). Bottom; The black large dashed line is the theoretical equilibrium fractionation factor for $^{13}C/^{12}C$ in the system Gr-Dia – cementite (MIKHAIL et al., 2010; SCHAUBLE, 2009) and the black small dashed line is the re-scaled trend to fit the experimental data. The red squares are the results from samples where the temperature was measured using a thermocouple, and the black circles are where the thermocouple failed and a power curve was used. Note the difference in fit for the experiments where a thermocouple was used compared to the experiments where a power curve was used relative to the trend of the predicted equilibrium fractionation factor.

8.6.3 Theory vs. experiment vs. nature

There are 3 data sets that produce isotope fractionation factors in this system; two have known temperatures of equilibration (experimental data (this study) and theoretical data (SCHAUBLE, 2009)) and one does not, the natural samples (chapter 7). To do this one must assume the temperature of equilibration for the natural samples using circular arguments.

I have attempted this based on the thermodynamic phase equilibria of Fe-C (LORD et al., 2009; TSUZUKI et al., 1984). The phase assemblage in chapter 7 (Fe-carbide + diamond) at 5 - 6 GPa (Lord et al., 2009), one would require a temperature below the mantle geotherm of < 1100 °C for diamond to be stable. For higher pressures, circa 10 GPa, the temperature range is large and crosses the geotherm in both directions for solid state equilibria of diamond + cementite with temperatures of 930 – 2012 °C (LORD et al., 2009 and figure 8.14). I set the temperature range for the diamond samples from the previous chapter from 1200 to 2012 °C for the diamond + Fe-carbide equilibration according to a compromise for the phase equilibria and the position of the mantle geotherm of Brown and Shankland (1981). It is known from HPHT experimental studies that for Fe-carbide and graphite to co-exist between 1 and 5 GPa we would need > 1000 < 1400°C (Tsuzuki et al., 1984). I use these constraints to plot an estimated temperature range for iron meteorite and Jagersfontein fields in figure 8.14, where the range for the fractionation factors for the fields is given by the standard deviation on the determined ΔC values from chapter 7 and Deines and Wickman (1975).

Figure 8.14 demonstrates that the natural and experimental (empirical) fractionation factors corroborate relatively well, albeit with the large assumed temperature ranges for the natural samples (and the use of circular arguments used to produce these temperature ranges). The experimental (empirical) fractionation factors both plot above the theoretical equilibrium fractionation factors shown in figure 8.13. This leads me to question that the theoretical equilibrium fractionation factors may require corrections, most likely arising due to known issues outlined by Schauble's eminent work (shown in figure 8.14).

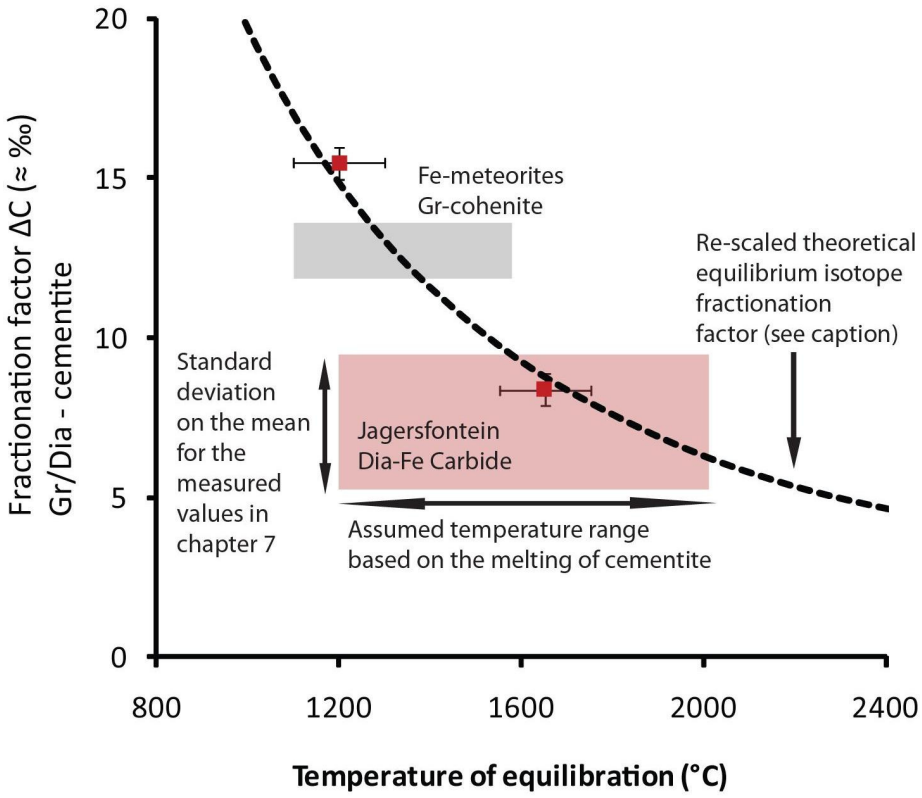

Figure 8.14. The results for the equilibrium fractionation factor for $^{13}C/^{12}C$ in the system Gr-Dia – cementite samples in this study vs. synthesis temperature of the samples. The black dashed line is the re-scaled theoretical equilibrium fractionation factor for $^{13}C/^{12}C$ in the system Gr-Dia – cementite (MIKHAIL et al., 2010; SCHAUBLE, 2009 see section 8.8.3). The errors in synthesis temperature are estimated at ± 100 °C and a maximum error of 0.5 ‰ is placed on the fractionation factors based on the maximum error for the analysis of the individual $\delta^{13}C$ values for the two phases.

8.7 Implications of these new data

8.7.1 A pressure effect?

Diamond is, effectively, an incompressible structure (Harlow and Davies, 2005). Whereas cementite is compressible and shows a volume reduction with pressure increasing from 5 to 30 GPa at room temperature (Li et al., 2002). This, in turn has an effect on the charge and shape of a given occupation site within a crystal lattice (Blundy and Wood, 1994). Should this change effect the relative partitioning of the heavy and light isotopes, then pressure can alter the equilibrium isotope fractionation factor for a given system at a set temperature (Horita, 2005). The implications for a pressure effect could be significant in the deep Earth where ΔT is less than the ΔP with depths > 200 km in the ambient mantle, therefore equilibrium isotope fractionation factors could increase with depth despite an increasing temperature, or decrease greatly (dependent upon the nature of the pressure effect).

This study is based only on a two results, but assuming they are indicative, there is no evidence for a pressure effect in this system under the range of conditions investigated. This is evident from samples at 5 GPa (AS1) and 25 GPa (CO#8) both plotting on the theoretical fractionation curve vs. temperature despite a 20 GPa difference in synthesis pressure. Where the theoretical fractionation factors are calculated at roughly 0 ± 0.05 GPa for 0 K and increase to a what would be comparable of < 5 GPa at 10000 K (SCHAUBLE, 2009 and personal communication 2011).

8.7.2 The depth of origin for the Jagersfontein samples

The near constant fractionation factor of +7.18 ± 1.3 (≈ ‰) for diamond – Fe carbide in chapter 7 requires a temperature of roughly > 1600 and below 2000 °C using the re-scaled curve in figure 8.14. The large range is due to the standard deviation of ± 1.3 ‰ for the measured ΔC. Using the mantle geotherm of Brown and Shankland (1981) I can use stable isotope geothermometry to place these

samples at a depth of > 500 km. This gives a depth range of ~550 to >1500 km (figure 8.2) and is consistent with, or greatly exceeds previous estimates of unusually great depth for diamonds from the Jagersfontein kimberlite pipe ~ 600 km (STACHEL et al., 2005) and the deeper Earth containing Fe^0 (ROHRBACH et al., 2007; STAGNO and FROST, 2011). This is evidence for these samples being transition zone derived diamonds and carbides (and possibly uppermost lower mantle). Better precision on the measured $\delta^{13}C$ values for both the natural diamond and the Fe-carbide for the samples from chapter 7, and further constraints on the experimental fractionation factors here would improve this depth constraint.

8.7.3 The Earth's deep carbon cycle seen through carbon isotopes

The implications of this work can be far reaching in terms of understanding the origin of the carbon in mantle samples using carbon isotopes. In light of this new data I feel that $\delta^{13}C$ values serve as wholly unsatisfactory source indicators without the complements of secondary signals such as nitrogen isotopes in the case of mantle diamonds (chapters 4-6).

Incomplete 'redox freezing', where the Fe^0/CO_3^{2+} ratio is too high to reduce all of the subducted carbonate to diamond according to the experimental constraints in Rohrbach and Schmidt (2011) (discussed in detail in chapter 2 section 2.4.2) could favour diamond and cementite coexisting in thermodynamic equilibrium (LORD et al., 2009). This would cause the two components to be isotopically fractionated, where the cementite ^{13}C depleted relative to diamond (with the magnitude of ^{13}C depletion governed by the temperature of equilibration). Should the cementite become mobile, either by melting or oxidation, and rise to the upper mantle where it later crystallises diamond or forms a carbonatite there is the scope that it would not have the characteristic $\delta^{13}C$ value of pelagic carbonate (0 ± 2 ‰), instead it could have a lower $\delta^{13}C$ value according to the magnitude of isotopic fractionation, so long as the diamond remained in the deep Earth and the

cementite contributed to diamond formation in the lithosphere. This does raise the question as to the behaviour of ^{15}N in this system; i.e. would nitrogen isotopes show similar fractionation, this study is ongoing.

8.7.4 How much carbon is in the Earth's core?

Geophysical observations show that the core has a density deficit 10-15 % should it be a Fe-Ni alloy (LI et al., 2007). This has led to various light elements being proposed to explain this observed deficit (for a review see MCDONOUGH, 2003). The elements most favourable based on their cosmochemical abundances and solubility in Fe-rich liquids are H, C, O, Si, and S or some proportions of each bonded with Fe, Ni or possible each other (MCDONOUGH et al., 2003). Wood (1993) suggested that the density deficit of the core could be offset by the incorporation of Fe_3C in the inner core based on the cosmic abundances, carbon is 4th most abundant element cosmochemically speaking. Yet on Earth carbon is a trace element. Thermodynamic calculations and investigation of the equation of state for Fe_3C at an average inner core pressure (~338 GPa) demonstrated that Fe_3C was a good fit for the density determined from seismic data (WOOD, 1993). Subsequently, Vočadlo et al. (2002) indicated that both the density and incompressibility of Fe_3C differ from the expected values for the inner core observed by seismology. Therefore crystalline Fe_3C could not be the major carbon phase in the core, meaning that '*Fe_3C is unlikely to be the predominant inner core-forming phase*'. However Vočadlo et al. (2002) acknowledge that Fe_3C could make up a smaller proportion of the light element or indeed another carbon phase could be present, such as diamond.

One method used to constrain the concentration of a particular light element in the core is to calculate an isotopic mass balance for the system in question, so long as both the terrestrial mantle and chondritic values are well constrained. The aim is simple, to balance the Earth with chondritic meteorites. For example, the terrestrial and lunar magmatic $\delta^{30}Si$ vs. $\delta^{39}Si$ trend is inconsistent with

chondritic meteorites and Martian samples (Georg et al., 2007). Shahar et al (2009) presented $\Delta^{30}Si$ and $\Delta^{39}Si$ values by HPHT experiment that enabled a mass balance to be calculated that corroborated theoretical calculations and validated the previous model of Georg et al (2007), with up to 5 wt % Si in the Earth's core.

The Earth's mean mantle $\delta^{13}C$ value is consistent with bulk $\delta^{13}C$ values for both enstatite and C1 chondritic meteorites (shown in figure 8.1). During shallow magma ocean metal-silicate partitioning (core formation), the temperature where this partitioning occurred would be highly variable across 1200 to 2500 °C (DASGUPTA and WALKER, 2008), therefore so would the fractionation factor. But I can use the re-scaled thermodynamic calculations at temperatures spanning the likely conditions in the terrestrial magma ocean from 1200 °C at the very top (surface) to 2500 °C (base of the magma ocean) in the system Gr-Dia – cementite (figure 8.14). This demonstrates that a < 5 % of the terrestrial carbon budget (mantle + core) could have been incorporated into the core before the modal $\delta^{13}C$ value would be fractionated away from the observed modal $\delta^{13}C$ value of -5 ‰, for all temperatures listed above (figure 8.15).

The results are for 500 ppm carbon in the core, would require 10000 ppm carbon in the mantle and a mantle to core ratio of 20. This would result, according to my isotopic mass balance model, of a modal mantle $\delta^{13}C$ value of -4.77 ‰, a reasonable value when compared to the observed modal value of - 5 ‰ (CARTIGNY, 2005). The lower end of the model would be 5 ppm the core for a mantle with 100 ppm carbon. This is a very interesting result. There is a big discrepancy between this model and the geophysical models. The geophysical models (DASGUPTA and WALKER, 2008; LORD et al., 2009; MCDONOUGH, 2003; NAKAJIMA et al., 2009; VOCADLO and GERALD, 2007; WOOD, 1993) all predict the core to be enriched in carbon relative to the mantle, making the core the dominant terrestrial carbon reservoir. Whereas the isotopic constraints implemented in this chapter require the mantle to be the dominating reservoir for carbon, by a considerable amount (> 95 %). This is however, wholly inconclusive in terms of the concentrations. It is not inconceivable to assume that no solid

phases were involved during metal-silicate partitioning in the terrestrial magma ocean (core formation). And there would be a difference in the fractionation factor for CO_3^{2+} or CO-CO_2 dissolved in silicate (or most likely CH_4), in isotopic equilibrium with cementite or carbon dissolved in Fe^0, and not solid Gr-Dia. One can predict that the fractionation factor would be different in these reactions owing to the effect of isotope substitution on vibrational frequencies in each substance which is a function of the atomic bonding within the phase in question (O'NEIL, 1986). Therefore, this system may not reflect the magnitude of isotopic fractionation that would have occurred during carbon incorporation into the core. Nonetheless, this study does demonstrate the following important point regarding the carbon concentration in the core and the core/mantle carbon ratio. The mantle must have more carbon than the core. This is because carbon bonding with Fe alloys will be ^{13}C depleted relative to CO_3^{2+}, CO-CO_2, CH compounds and Gr-Dia, and the model and mean mantle $\delta^{13}C$ values remain chondritic.

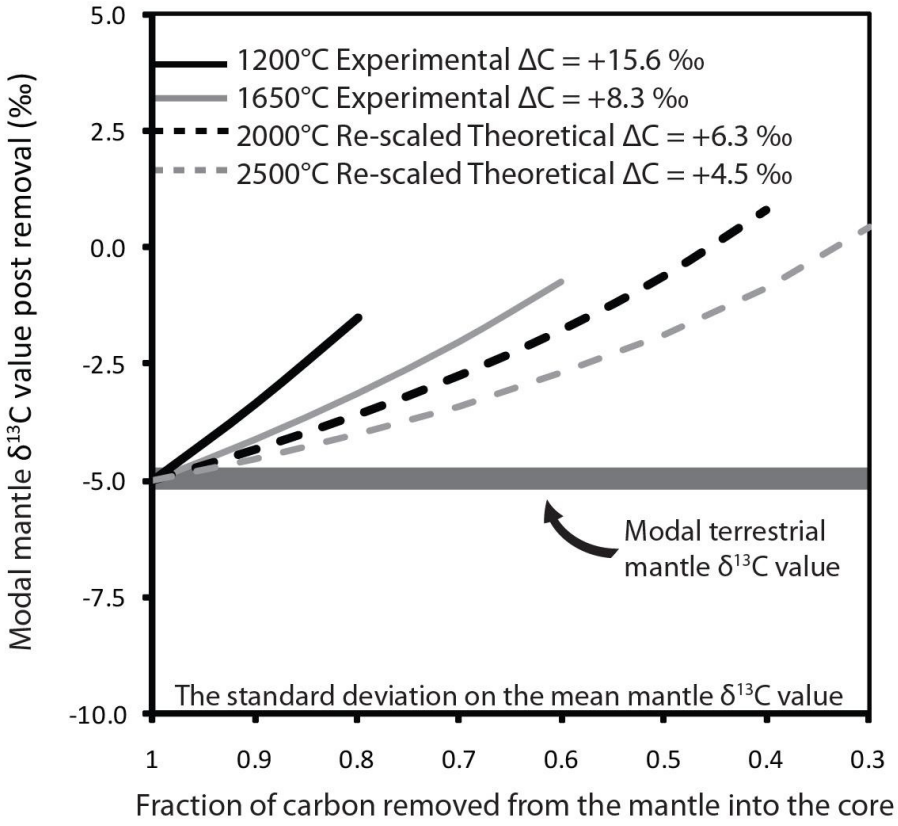

Figure 8.15. Results from a model of isotopic fractionation of carbon incorporation into the core using the lowest round number for the fractionation factor in this study, +7 ‰ where the reaction is diamond – cementite. The curves show the evolution of the mantle $\delta^{13}C$ value (y-axis) vs. the percentage of carbon in the core on the (x-axis). The model was calculated a closed system (solid line; steady-state) and open system (dashed line; Rayleigh-type). The grey bar -5 ‰ represents the observed mean $\delta^{13}C$ value of the mantle (CARTIGNY, 2005).

8.7.5 Martian magmatic carbon

The range of $\delta^{13}C$ values for *magmatic* carbon in Martian meteorites (SNC) is comparable to that of biogenic carbon on Earth and is distinct from the mean $\delta^{13}C$ values for terrestrial magmatic carbon and chondritic meteorites (GRADY and WRIGHT, 2003; GRADY et al., 2004; WRIGHT and PILLINGER, 1994 and shown in figure 8.1). This means one of these planets are not exhibiting a primordial value, although they should. This is because both planets formed from the same proto planetary-disk at

roughly the same distance from the sun and at the same time, geologically speaking and therefore should have chondritic primordial compositions (WRIGHT and PILLINGER, 1994).

The two celestial bodies do appear to have undergone similar differentiation processes, i.e. metal-silicate separation to form a core (BERTKA and FEI, 1997). However this rationale cannot explain the $\delta^{13}C$ values. Especially when one considers silicon isotopes, where the terrestrial and lunar magmatic $\delta^{30}Si$ vs. $\delta^{39}Si$ trend is inconsistent with chondritic meteorites and Martian samples (Georg et al., 2007). This demonstrates that no or negligible Si could have partitioned into the Martian core, otherwise the $\delta^{30}Si$ vs. $\delta^{39}Si$ trend of SNC meteorites would not be chondritic. As figure 8.1 demonstrates, C1 and enstatite chondrites do not have bulk (mean) $\delta^{13}C$ values of -20 ± 5 ‰, and are similar to that of the Earth (-5 ± 3 ‰). Therefore, unlike in the case for the stable isotopes of Si, the Martian mantle is the isotopic outlier. Carbon incorporation into the Martian metallic core should increase the $\delta^{13}C$ value of the silicate proportion of Mars (section 8.9.4), where the carbon in the core (probably carbides) would be ^{13}C depleted. Therefore this cannot be proposed to explain why Martian magmatic carbon is lower than the Earth by circa -15 ‰. Below I propose a working model to explain this isotopic discrepancy in light of this new data.

The lack of dominant Mg,Si-perovskite in the Martian mantle (because the maximum pressure in the Martian mantle is roughly 25 GPa FEI and BERTKA, 2005) means that during a closed system scenario for core formation there will be no 'self-oxidation' (according to the model of WADE and WOOD, 2005). This would result in a more reduced Martian mantle relative to Earth, this is observed with SNC meteorites (HERD et al., 2002; MCSWEEN et al., 2007). Additionally, the Martian mantle has a FeO concentration more than double the Earth's mantle (~18 to ~8 wt % respectively). This is not a consequence of a different primordial composition, and can be explained by the solubility of O in Fe melts as a function of temperature (FEI and BERTKA, 2005). The relatively low temperatures of a Martian magma ocean (to Earth) resulted in less FeO extraction to the core from the mantle, which thus remains FeO-rich relative to the Earth (RUBIE et al., 2004). This has led to the Martian mantle

being a more reducing environment that the Earth's mantle by at least 2 log units (HERD et al., 2002). In short, in the upper mantle of the Earth carbonates are likely the dominant carbon phase (circa IW +2 to +4) and in the lower terrestrial mantle as well as the Martian mantle reduced carbon should dominate where the fO_2 is ~ IW -2 to +1 . Under such reducing conditions carbonates are not a stable carbon bearing phases (ROHRBACH and SCHMIDT, 2011; SIEBERT et al., 2005). Experimental studies demonstrate that Fe-carbide would be the preferred solid phase < 6 wt % carbon in Fe^0, and would coexist with Gr-Dia in the system Fe-C above 6 wt % of carbon in Fe^0 (LORD et al., 2009). Because the assumed maximum Martian mantle fO_2 is governed by the IW buffer, but only +1 log units above it (HERD et al., 2002; HIRSCHMANN and WITHERS, 2008), the Gr-Dia will remain stable and the Fe-carbide will be the most thermodynamically unstable of the two. Therefore, the magmatic carbon in SNC meteorites can be dominated by 'isotopically lighter' carbon (low $\delta^{13}C$) from the Fe-carbide due to the low fO_2 enabling the 'isotopically heavier' graphite to remain in the residual.

This would produce highly fractionated carbon in the melt and produce magmatic carbon in SNC meteorites with low $\delta^{13}C$ values on Mars, but is not practical for the upper mantle on Earth as carbonate is the dominant carbon phase (FROST and MCCAMMON, 2008; STAGNO and FROST, 2011). According to the fractionation factors determined in this study, and assuming the isotopic equilibration occur in the upper-most Martian mantle at < 1200 °C, one would expect to see an isotopic shift between graphite and Fe-carbide in excess of +16 ‰ (table 8.2). The region of melting to produce Martian basalts (SNC meteorites) would be at temperature comparable to that of OIB and MORB on Earth (900 – 1200 °C). According to this new data, and modelling a 1:1 ratio of graphite to cementite from an initial $\delta^{13}C$ value of -5 ‰, with an associated fractionation factor of +16 ‰ (for 1200 °C) one produces carbide with a $\delta^{13}C$ value of -15 ‰ for closed system (steady state) and -24 ‰ for an open system (Rayleigh-type) using equation 3. This produces a good fit to the mean $\delta^{13}C$ value of Martian magmatic carbon, which is -20 ± 5 ‰ (GRADY et al., 2004).

3. $\delta^{13}C \text{ reservoir} = (\delta^{13}C_i + 1000)f^{(\alpha-1)} - 1000$

In equation 3 $\delta^{13}C_i$ is the $\delta^{13}C$ value of the source carbon, α is the fractionation factor and *f* is the fraction removed. For lower temperatures the fractionation factor would be larger and the effects greater, thus possibly deriving the mean $\delta^{13}C$ value of Martian magmatic carbon without the need for an open system (Rayleigh-type fractionation). This model is can explain the low '*Organic*-looking' $\delta^{13}C$ values observed in SNC meteorites by solely abiogenic processes. It also assumes that nitrogen isotopes are not significantly fractionated in this process, as both celestial bodies exhibit comparable $\delta^{15}N$ values (figure 8.1).

8.8 Concluding remarks

The scale of $^{13}C/^{12}C$ isotopic fractionation for the system Gr-Dia - cementite is larger than any other system under mantle temperature conditions. The ΔC at 1200 °C of roughly + 16 ‰ for Gr-Dia – cementite is much larger than the ΔC at 1200 °C for diamond – CH_4 of +1 ‰ for (BOTTINGA, 1969) and roughly -3.5 ‰ for diamond – CO_3^{2+} or CO-CO_2 (RICHET et al., 1977).

Using this new data it is required that the Earth's mantle is host to a larger proportion of the terrestrial carbon budget than the core, possibly by a factor of 20 or more. This is because the modal mantle $\delta^{13}C$ value is chondritic, and the iron-bonded carbon is strongly ^{13}C depleted at the high temperature (by - 4.5 ‰ relative to diamond at 2500 °C). Therefore, extraction of carbon into the core during metal silicate partitioning in a Hadean magma ocean (core formation) would and should have left an isotopic fingerprint. For a situation where the mantle dominates the carbon budget the fingerprint is a chondritic modal $\delta^{13}C$ value in mantle samples, as is seen. For a situation where the core dominates the carbon budget this would have been manifest in the form of a ^{13}C enriched mantle relative to chondritic values, which is not seen today.

The lack of a pressure effect in this system, based on the 5 GPa experiment and 25 GPa experiment both plotting on the same re-scaled thermodynamic fractionation trend vs. temperature, makes it

possible to use stable isotope geothermometry to revise the depth constraint for the samples Jag5 and Jag10 (from chapter 7). The new perspective requires that they must have equilibrated at above 1600 °C, or > 500 km depth using the mantle geotherm (BROWN and SHANKLAND, 1981), and not 150-250 km as was deduced in chapter 7. This is still consistent with silicate bearing diamonds from the Jagersfontein kimberlite pipe as the Jagersfontein pipe samples the mantle from 150 to > 600 km (STACHEL et al., 2005; TAPPERT et al., 2005). However, my new data extends the potential depth range to > 1000 km, which would make these samples the deepest known terrestrial materials to have been documented. This also places a constraint on the equilibration temperature for the graphite + cohenite in the Fe meteorites, Canyon Diablo (CRAIG, 1953) and Magura (DEINES and WICKMAN, 1975). The observed ΔC of +12 ± 1 ‰ requires a temperature of about 1400 °C.

This new data, in turn, demonstrates a great potential to produce low $\delta^{13}C$ reservoirs in the deep Earth, isotopically akin to organic carbon. The abiogenic and inorganic high temperature equilibrium isotopic fractionation factors in this study are as large as the equilibrium isotopic fractionation factors between organic carbon (i.e. hydrocarbons) and carbonates of circa 20 ‰, a near constant through time on Earth (SHIELDS and VEIZER, 2002; THOMAZO et al., 2009). Such low $\delta^{13}C$ values have been interpreted as evidence of life on Earth > 3700 Ma, with the low $\delta^{13}C$ values as the only constraint (Rosing, 1999) and as evidence of life on Mars through the study of a single Martian meteorite (Wright et al., 1989). This assumption is based on two related paradigms. The near constant fractionation factor of ≥ 20 ‰ though time for biogenic processes on Earth (Shields and Veizer, 2002; Thomazo et al., 2009), and the relatively small (< 4 ‰) fractionation factors for carbon isotopes at mantle temperatures (Bottinga, 1969; Richet et al., 1977).

I propose that the reason for Martian magmatic carbon exhibiting $\delta^{13}C$ values between -10 and -20 ‰ lower than terrestrial mantle samples/melts is a consequence of the fractionation factor in this study. The reason it is active in Martian magmatism is because the Martian mantle is buffered below or a maximum of 1 log unit above the IW system (HERD et al., 2002). This enables the graphite to

remain in the residual during melting and carbide to potentially co-exist in the initial, thus giving rise to Fe-carbide sourced low ^{13}C depleted carbon in Martian lavas.

Chapter 9

Stable isotope fractionation and the Earth's deep carbon cycle: Conclusions and discussion

9.1 Introduction

The overall aim of this work was to apply new constraints on the origins of low $\delta^{13}C$ values in mantle diamond. In the simplest sense I can conclude that using carbon isotopes to constrain the origins of low $\delta^{13}C$ values in mantle diamond remains as it was prior to this work; i.e. without the use of another primary source indicator in the diamond lattice itself, any conclusions are still ambiguous. Any study using carbon isotopes in the host diamond as the sole source indicator can conclude any of the following models: that the ^{13}C depleted diamond-forming carbon was derived from unconstrained primordial heterogeneities (Deines, 2002), it can reflect re-cycled (subducted) crustal organic carbon (Bulanova et al., 2010) or high temperature isotopic fractionation in the mantle prior to diamond formation (Maruoka et al., 2004). However, what can be concluded from this study is listed below;

1. Very small fragments (< 0.1 mg) of Type II diamond can routinely be analysed for their coupled $\delta^{15}N$ and $\delta^{13}C$ values simultaneously with enough precision to resolve the main terrestrial reservoirs using a fully automated facility (the Finesse Machine, The Open University).

2. The effectiveness of coupled $\delta^{13}C$-$\delta^{15}N$ data to further constrain which of the three models is the most feasible to explain the origins of low $\delta^{13}C$ values in mantle diamond. This has

provided evidence of crust-mantle carbon recycling to depths > 150 km (the diamond stability field) through plate tectonic processes > 2.11 Ga using Type II mantle diamond.

3. Peridotitic diamondites show ^{13}C depletion and ^{15}N enrichment; this is contrary to peridotitic monocrystalline diamond that do typically exhibit mantle-like ^{13}C and ^{15}N concentrations. This is best explained by subducted organic carbon becoming oxidised and mobile and initiating redox melting and harzburgite depletion in the sub-continental lithospheric mantle.

4. Isotopic fractionation of carbon during diamond formation is larger under reducing conditions than under oxidising conditions, contrary to the previous data.

5. This work may also have identified the deepest samples of the Earth's interior to date with a depth potentially in excess of 1000 km using stable isotope geothermometry.

6. The consistency for Martian magmatic carbon to exhibit low $\delta^{13}C$ values which is akin to biogenic (and abiogenic organic) carbon on Earth can be explained by abiogenic mantle processes.

7. The mantle, and not the core, may potentially be the largest carbon reservoir on Earth.

9.1.1 Layout of this chapter

To discuss these seven conclusions in a concise manner and avoid overlapping and repeating of principles, I have grouped some of them. I have devised four essays to expand on the above list and discuss the geodynamic implications and potentials of each, the essay titles are followed by the relevance to the particular conclusion (by number) shown in red text. These are listed below;

- The usefulness of coupled $\delta^{13}C$-$\delta^{15}N$ data to establishing the origins of low $\delta^{13}C$ values in type II mantle diamond (conclusions 1 and 2)

- The origin of low $\delta^{13}C$ values and positive $\delta^{15}N$ values in peridotitic diamondites (conclusion 3)
- The largest high temperature isotopic fractionation of carbon isotopes where Fe^0 is a stable phase in a silicate mantle (conclusions 4, 5 and 6)
- The mantle may potentially be the largest carbon reservoir on Earth; implications for mass extinction events induced by volcanism (conclusion 7)

9.2 The usefulness of coupled $\delta^{13}C$-$\delta^{15}N$ data to establishing the origins of low $\delta^{13}C$ values in type II mantle diamond

As stated above, conclusions derived from the use carbon isotopes to constrain the origins of low $\delta^{13}C$ values in mantle diamond without the use of another primary source indicator in the diamond lattice itself, are ambiguous. If one observed the distribution of the carbon isotope values for the eclogitic Dachine diamonds (chapter 5) that are sourced from a volcaniclastic host rock > 2 Ga (Capdevila et al., 1999) it is apparent that they do not match the mean mantle by about -20 ‰ (chapter 5, figure 5.2, page 107). This data can lead to two equally plausible conclusions;

(1) They are sourced from a relic primordial heterogeneity. This can be deduced as the insoluble fraction of C1 chondrites, extraterrestrial organic carbon that displays a range in $\delta^{13}C$ values from -20 to -30 ‰ (Grady and Wright, 2003).

(2) The $\delta^{13}C$ distribution also corroborates well with pre-Cambrian terrestrial organic carbon (Shields and Veizer, 2002) and the silicate and sulphide inclusions are eclogitic (SMITH et al., In Prep 2011), therefore one could deduced that these samples formed by subducted organic carbon.

This is where nitrogen isotopes can further constrain the origins of this ^{13}C depleted carbon. But, before determining and interpreting the $\delta^{15}N$ values for the diamonds from Dachine, one must first determine the $\delta^{15}N$ values for Type II diamond (in general) with mean mantle $\delta^{13}C$ values, because

the Dachine diamond population is 97 % Type II (n = ~ 200; Cartigny, 2010 and chapter 5). This has been achieved in the work presented in chapter 4. The results show that for Type II diamonds with mean mantle $\delta^{13}C$ values, the $\delta^{15}N$ values cover a range indistinguishable from the field derived from Type I peridotitic diamond that define the mean mantle (chapter 4, figure 4.8 page 101). The $\delta^{15}N$ values for the insoluble fraction of C1 chondrites, extraterrestrial organic carbon is > +20 ‰, whereas the $\delta^{15}N$ values for the pre-Cambrian terrestrial organic carbon has a range of -4 to + 30 ‰ with a definitive peak at +6 ‰. Additionally, ~ 80 % of mantle phases have negative $\delta^{15}N$ values (for a review see Cartigny, 2005 shown in chapter 2 figure 2.13 page 49). As shown in chapter 5, the Dachine diamonds have a mean $\delta^{15}N$ value of +6.6 ‰, indistinguishable from pre-Cambrian terrestrial organic carbon (chapter 5, figure 5.12, page 122). Therefore, the ^{13}C depletion is coupled with ^{15}N enrichment relative to the mean mantle. This is unlike various monocrystalline diamond with ^{13}C depletion is correlate with progressive ^{15}N enrichment and N/C depletion, concluded to be a product of isotopic fractionation (Cartigny, 2005; Cartigny et al., 1998a; 1999; 1998b). The results in chapter 5 show that the diamonds from Dachine, French Guyana are indistinguishable in carbon and nitrogen isotope space from Pre-Cambrian crustal organic carbon being ^{13}C depleted and ^{15}N enriched relative to the mean mantle and distinct from several main chondritic components (i.e. such as the insoluble organic carbon in C1 chondrites- shown in chapter 5 figure 5.18 page 132). These observations are best explained whereby the origins of the low $\delta^{13}C$ values in the diamond are derived from subducted crustal organic carbon. The ^{15}N enrichment (relative to the mantle) is not consistent with low nitrogen concentrations for the Dachine diamonds being derived by extensive ^{14}N loss from the source during crystallisation of the mostly Type II diamonds. I base this statement on the $\delta^{15}N$ values for the type II diamonds in chapter 4 that exhibit a range for their $\delta^{15}N$ values that is consistent with Type I diamonds (roughly +10 to -10 ‰ chapter 4, figure 4.7 page 101). The Type II samples in chapter 4 also having $\delta^{13}C$ values in the mean mantle range imply that both Type I and Type II diamonds with mean mantle $\delta^{13}C$ values can, and maybe do, also reflect the mantle in $\delta^{15}N$ space. Therefore, I conclude that the carbon and nitrogen isotope compositions of the Dachine

diamonds are evidence of carbon recycling via subduction zone plate tectonics to the depths of diamond stability > 2.11 Ga.

9.3 The origin of low $\delta^{13}C$ values and positive $\delta^{15}N$ values in peridotitic diamondites

The best explanation of the origin of the diamond-forming carbon in diamondites based on coupled carbon and nitrogen isotope constraints from the samples in this study is the same as for the Dachine diamonds, one of subducted organic carbon (chapter 6, figure 6.11, page 168). There is however, evidence of a mantle component in both carbon and nitrogen isotope space and some evidence for mixing dominated by the subducted organic carbon (chapter 6, figure 6.13, page 175). Also, as for several monocrystalline diamond populations (i.e. Jwaneng, Botswana- Cartigny et al, 1998a discussed in chapter 2, section 2.8.1), the diamonds and silicates can be completely un-related in terms of geochemical origins. Where, in the case of diamondites, the silicates are sourced from peridotitic mantle and the diamonds sourced mainly from subducted crustal pelagic (organic) carbon and nitrogen. Noteworthy is that there are no garnets in these diamondites that plot as eclogitic. Based on the major element geochemistry they all instead plot as peridotitic (lherzolitic), and are mostly websteritic (chapter 6, figure 6.4, page 156). Websteritic garnets are more akin to a Cr-poor peridotites that has had chromite or ilmenite removed, rather than an eclogite (Dobosi and Kurat, 2010). Therefore it has been proposed that this sample suite should be viewed as peridotitic as a whole (Dobosi and Kurat, 2002; Dobosi and Kurat, 2010; Rege et al., 2008), this opinion is followed here.

The most important observation that this study provides is low $\delta^{13}C$ values and positive $\delta^{15}N$ values in peridotitic diamondites relative to the mean mantle (chapter 6, figure 6.11 page 168). This is a very interesting and an extremely un-usual observation in light of the carbon isotope distribution for diamond globally. It has long been known that peridotitic diamond does not regularly show ^{13}C

depletion based on the analysis of > 5000 individual inclusion-bearing diamonds of eclogitic and peridotitic affinity (for a review see Cartigny, 2005). This notion is now only true for monocrystalline and coated diamonds as peridotitic diamondites from this work do unequivocally show ^{13}C depletion (chapter 6, figure 6.5 on page 158). The question is now 'why do peridotitic diamondites show ^{13}C depletion?'. Below I outline a model that admittedly requires a study of the coupled $\delta^{13}C$ and $\delta^{15}N$ values for diamondites *globally* to test it. Therefore I propose the following as a working model.

The mass of carbon is in the mantle is considered by all the studies I can find to dwarf the crustal reservoirs by several orders of magnitude (for a review see DASGUPTA and HIRSCHMANN, 2010). However the carbon in the mantle may not be as concentrated, whereas subducted crustal carbon in oceanic sediments could be relatively more concentrated (spatially). This model then requires that the subducted carbon and nitrogen become mobile and migrate into a peridotite; otherwise one may expect eclogitic garnets to be present, which is not the case (chapter 6, figure 6.4, page 156). This can be explained possibly as an oxidised carbonatitic COHN-rich fluid, where the low viscosity enables extreme grain boundary mobility (Dobson et al., 1996). The $H_2O + CO_2$ rich fluid can induced redox melting of mantle harzburgite, resulting in a siliceous carbonatitic melt (Dasgupta and Hirschmann, 2010). This later precipitates a mostly diamond-rich mantle rock consisting of polycrystalline diamonds with low $\delta^{13}C$ values and positive $\delta^{15}N$ values akin to crustal organic carbon (with minor mixing with mantle carbon and nitrogen) and euhedral intergrowths of peridotitic to websteritic garnet ± pyroxene, defined as diamondite. This would not precipitate monocrystalline diamonds, due to carbon oversaturation leading to rapid nucleation and polycrystalline growth (Litvin, 2006). This model explains the occurrence of low $\delta^{13}C$ peridotitic polycrystalline diamonds in diamondites and predicts that some subduction-derived diamonds could be polycrystalline, and not of a gem quality monocrystalline morphology.

9.4 The largest high temperature isotopic fractionation of carbon isotopes where Fe^0 is a stable phase in a silicate mantle

The Fe-carbide bearing mantle diamonds that were available to study in chapter 7 have enabled an assessment of the magnitude and direction of carbon isotope fractionation in the system diamond + Fe-carbide, which in light of recent experimental studies appears to be the dominant solid assemblage for carbon in the deep Earth > 250 km, where Fe^0 is stable (Lord et al., 2009; Rohrbach and Schmidt, 2011a; 2011b) and where carbon concentrations are > 300 ppm (DASGUPTA and HIRSCHMANN, 2010). The results showed that the diamond would be depleted in ^{13}C relative to Fe-carbide by +7.2 ± 1.3 ‰ (chapter 7, table 7.5, page 200). This fractionation factor is from samples derived from an unknown depth and therefore no temperature constraints can be applied. To make a comparison with the thermodynamic data one must constrain the temperature effect in this system. This was achieved by high pressure high temperature experiments (chapter 8). It can be concluded that the magnitude of $^{13}C/^{12}C$ isotopic fractionation for the system Gr/Dia - cementite is larger than any other system under mantle temperature conditions. The ΔC at 1200 °C of roughly + 16 ‰ for Gr-Dia – cementite (chapter 8, figure 8.14, page 235) is much larger than the ΔC at 1200 °C for diamond – CH_4 of +1 ‰ (Bottinga, 1969) and roughly -3.5 ‰ for diamond – CO_3^{2+} or CO-CO_2 (Richet et al., 1977). This demonstrates that carbon isotope fractionation in this system is larger than between diamond and either CO_2 or CH_4. Where the latter was previously regarded as the dominating reaction in the lower mantle, thus ruling out carbon isotope fractionation in the deeper mantle as a mechanism to explain diamonds from the transition zone and below exhibiting low $\delta^{13}C$ values (Stachel, 2001). There are two main implications for this work discussed in more detail below:

(a) Applying stable isotope geothermometry to ascertain a depth of origin for the samples in chapter 7.

(b) The generation of distinct isotopic carbon reservoirs in the deep terrestrial and everywhere in the Martian mantle.

(a) Applying stable isotope geothermometry to ascertain a depth of origin for the Fe-carbide bearing diamonds from the Jagersfontein kimberlite

The temperature relationship for the magnitude of $^{13}C/^{12}C$ isotopic fractionation for the system Gr/Dia – cementite (chapter 8) has enabled me to place depth constraints on the origin of the natural samples in chapter 7 using stable isotope geothermometry. Diamond from the Jagersfontein kimberlite pipe are known to be derived from depths of 150 to > 600 km (Stachel et al., 2005; Tappert et al., 2005). This new data potentially extends the depth range to > 1000 km, which would make these samples the deepest known terrestrial materials documented.

(b) The generation of distinct isotopic carbon reservoirs

This new data also demonstrates a great potential to produce low $\delta^{13}C$ reservoirs in the reduced silicate mantle, isotopically akin to organic carbon. The abiogenic and inorganic high temperature equilibrium isotopic fractionation factors in this study are as large as the low temperature equilibrium isotopic fractionation factors between organic carbon (i.e. hydrocarbons) and carbonates of circa 20 ‰, a near constant through time on Earth (Horita, 2005; Shields and Veizer, 2002; Thomazo et al., 2009).

How applicable this model is to terrestrial mantle diamonds that exhibit low $\delta^{13}C$ values is not fully understood. There are issues regarding the distance in the terrestrial mantle that the ^{13}C depleted

carbon (from the carbides) could have to travel, without mixing with normal mantle carbon, before forming diamonds in the cratonic lithosphere. The Fe-carbide + diamond assemblage is stable where the fO_2 is buffered < IW, which is at depths of ~ > 250 km (Rohrbach et al., 2007), and the vast majority of diamond formation occurs in the cratonic lithosphere at a depth of circa 150 km (Gurney et al., 2010). Therefore, should this ^{13}C depleted carbon from the carbides enter the oxidising shallow mantle, it *could* mix with mantle carbon that exhibits a mean mantle $^{13}C/^{12}C$ ratio. The final $\delta^{13}C$ value of this hybrid fluid would then be governed by the proportional mass ratio of the ^{13}C depleted carbon from the carbides, and the carbon from the mantle with a mean mantle $^{13}C/^{12}C$ ratio. I.e. the hybrid fluid could exhibit a $\delta^{13}C$ value of the mean mantle despite entraining some ^{13}C depleted carbon from the deep mantle carbides. The reaction diamond + Fe-carbide should also produce ^{13}C enriched carbon in the deep mantle (diamond), which may not manifest in the sampled mantle rock/mineral record due to the same *travelling* issue raised above.

There is a planet where the long distance of travel from liberated ^{13}C depleted carbon from the carbides to emplacement in the lithosphere is not a problem, this planet is Mars. Martian magmatic carbon consistently exhibits low $\delta^{13}C$ values relative to the Earth's mantle and akin to organic carbon on Earth with $\delta^{13}C$ values of -20 ± 5 ‰ (Grady et al., 2004). The Martian mantle redox state is buffered 2 log units *below* or to a maximum of 1 log unit above the IW system (Herd et al., 2002). This enables graphite and Fe-carbide to co-exist in the upper Martian mantle, the high melting temperature of carbon (EGGERT et al., 2010) means that the relatively ^{13}C enriched graphite will remain residual during partial melting and melt extraction. Therefore the carbon in the melt should be derived from the ^{13}C depleted Fe-carbide, producing low $\delta^{13}C$ values in Martian basalts (SNC meteorites). This is not seen in the upper mantle of the Earth because the redox state is buffered 4 ± 2 log units *above* the IW buffer where carbonates dominate (Stagno and Frost, 2011). I propose that the reason for Martian magmatic carbon exhibiting $\delta^{13}C$ values of -20 ± 5 ‰ (Grady et al., 2004) is a consequence of the fractionation factor in this study (chapter 8, figure 8.14, page 234) and the P-T-fO_2 stability of graphite in the Martian mantle relative to Fe-carbides. This means that the carbon in

Martian mantle melts is derived from ^{13}C depleted Fe-carbide, where the Fe is incorporated into ferromagnesian silicates that crystallise from the Martian basaltic melts.

9.5 The mantle may potentially be the largest carbon reservoir on Earth: implications for mass extinction events induced by volcanism

The core is considered by most geophysical studies in the literature to be the largest terrestrial carbon reservoir (Dasgupta and Walker, 2008; Lord et al., 2009; Nakajima et al., 2009; Vocadlo et al., 2002; Wood, 1993), thus, the majority of the terrestrial carbon budget would be *removed* from chemical geodynamic mantle processes such as mantle convection and volcanic degassing.

The data in this thesis suggest that the Earth's mantle is host to a larger proportion of the terrestrial carbon budget and not the core, possibly by a factor of 20 or more (chapter 8, figure 8.15, page 241). This is because the modal mantle $\delta^{13}C$ value is chondritic (C1 and enstatite), and the iron bonded carbon is strongly ^{13}C depleted at the high temperature (by - 4.5 ‰ relative to diamond at 2500 °C- chapter 8, figure 8.14, page 234). Therefore, extraction of carbon into the core during metal silicate partitioning in a Hadean magma ocean (core formation) would and should have left an isotopic fingerprint, where the $\Delta^{13}C$ between the mantle and chondrite (enstatite or C1) being above or below 0, as is the case for $\Delta^{57}Fe$ and $\Delta^{29}Si$ (Rumble et al., 2011). For a situation where the mantle dominates the carbon budget, the fingerprint is a chondritic modal $\delta^{13}C$ value in mantle samples, as is seen (Cartigny, 2005). For a situation where the core dominates the carbon budget, this would manifest in the form of a ^{13}C enriched mantle relative to chondritic values, which is not seen. Therefore, the majority of the terrestrial carbon budget *is not removed* from chemical geodynamic mantle processes such as mantle convection and volcanic degassing.

This raises the potential for large volumes of volcanic CO_2 emissions during anomalously large and short (< 10 Ma) periods of volcanic activity that are termed large igneous provinces (LIPs; Bryan and

Ernst, 2008). If the majority of the terrestrial carbon budget was in the core it would not have a direct route to the atmosphere, but with mantle as the main host for the terrestrial carbon budget enables the mantle to transfer this climate shifting gas (carbon dioxide ± carbonyl sulphide) to the atmosphere from deep in the Earth via mantle plumes and LIPs in a short time span < 5 Ma (Bryan and Ernst, 2004).

Some LIPs correlate with minor mass extinctions as well as the largest mass extinction events (SAUNDERS, 2005), for example the Siberian traps which correlate with the Permo-Triassic mass extinction, and the Deccan Traps which correlate with the Cretaceous-Tertiary mass extinction (SAUNDERS, 2005). In fact, every LIP in the last 300 Ma correlates with a mass extinction event (WIGNALL, 2001). Noteworthy is that neither the total eruption volume nor the duration of volcanism of LIPs are related to the extinction intensity (Wignall, 2001), but the 'greenhouse gas' budget, and therefore to some extent the CO_2 concentration in the mantle, could explain the correlation for LIPs of variable size and duration correlating with mass extinctions (SAUNDERS, 2005). This is because the amount of volatiles degassed during an eruption is not comparable to the size or duration of the eruption (SAUNDERS, 2005; WALLACE, 2005), but to the volatile content of the source (WIGNALL, 2001).

Studying this in situ is impossible, because any direct determinations of the amounts of CO_2 degassed during the eruption of any LIP flood are not available (SELF et al., 2006). Several studies point to the depletion of CO_2 in the upper-most mantle (SAAL et al., 2002) as evidence that LIPs could only emit a maximum amount of CO_2 comparable to the current anthropogenic releases today (SELF et al., 2006). However should the LIP be sourced from a thermo-chemical plume sourced from the deep mantle (< 250 km) and the mantle dominate the terrestrial carbon budget this may not be the case. One mechanism for large scaled CO_2 release from LIP formation could be related to an abundance of carbon in the deep and reducing Earth being dominated by diamond. The diamond, through mechanical convection, could concentrate within the mantle due to the density contrast between diamond and mantle silicates and produce diamondiferous deep mantle reservoirs that are

'frozen' in the deep Earth (Rohrbach and Schmidt, 2011b). These diamondiferous horizons would remain residual over geological time, even during partial melting events with the governing parameter being the redox conditions; i.e. so long as the fO_2 remains below IW +3, diamond is stable in the mantle (FROST and MCCAMMON, 2008; STAGNO and FROST, 2011; WOOD et al., 1990) and immobile (ROHRBACH and SCHMIDT, 2011b). A deep mantle plume could transport these diamonds from the reducing deep mantle (< IW) into the oxidising shallow mantle (IW +4 ± 2 log units). This would convert the diamond to carbonate or CO_2, which in turn would lower the solidus of the surrounding peridotite and could cause widespread redox melting (Dasgupta and Hirschmann, 2010; Rohrbach and Schmidt, 2011b) and eventually large volume CO_2 degassing from the LIP due to the low solubility of CO_2 in basalts (Mattey, 1991) and associated mineral phases (Shcheka et al., 2006). The result would be a LIP that releases vast amounts of CO_2 (figure 9.1). Alternatively, should the plume be either from shallower depths or pass through diamond-depleted mantle, the CO_2 budget would be less and would result in a LIP with less of an environmental impact, i.e. the difference between a major and minor impact.

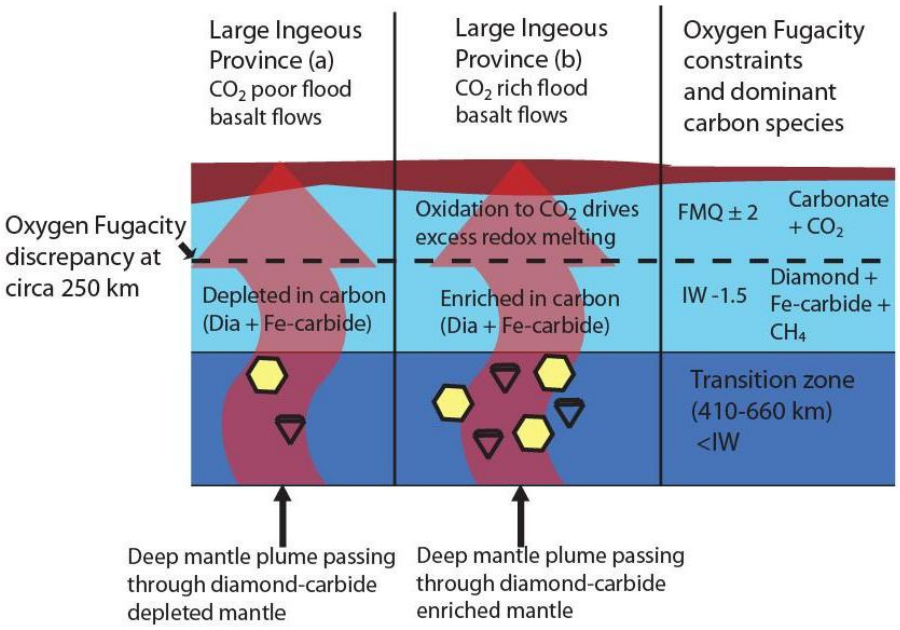

Figure 9.1. A cartoon illustrating the potential for a plume to transport reduced carbon (diamond and Fe-carbide) to the surface and oxidise it en route. This causes CO-CO_2 formation and can increase melting in the upper mantle (DASGUPTA and HIRSCHMAN, 2010) should the plume pass through a reduced carbon-poor environment one would expect a lower CO_2 budget (a) whereas should there be a more reduced carbon to oxidise this would lead to a volcanic province with elevated CO_2 emissions (b). Therefore the environmental impact would be reduced.

9.6 Limitations; a prelude to some proposed further work

This thesis proposes deep subduction and deep mantle-crustal carbon recycling before 2 Ga, extreme mobility of subducted volatiles that metasomatise and induce melting of stable mantle, a very high mantle/core ratio for carbon and possibly evidence for two diamonds from > 1000 km depth; but not without caution. I acknowledge that there are several unknown parameters in these models that are detailed in each chapter's discussion section. There are various poorly-constrained parameters that require further work to enable better testing on scientific theories in this thesis and the peer-reviewed scientific literature.

9.7 Further work

This study has provided many more questions than answers. There are several studies required to test the theories discussed within this thesis, and I shall outline the most pressing below. There are three sections relating to terrestrial samples, extraterrestrial samples and experimental samples.

9.6.1 Studies related to terrestrial samples

(a) A study of the stable isotopes of Diamondites globally

There are only 20 samples of known paragenesis in my study of diamondites and 20 of unknown paragenesis from the literature that demonstrate distinctively low $\delta^{13}C$ and high $\delta^{15}N$ values akin to organic components (see section 9.3 and chapter 6). What is required to better understand the origin of diamondite-forming carbon is a detailed global study of the garnet and diamond geochemistry alongside monocrystalline diamonds from the same locality. Also required are time constraints such as; (1) direct dating of the syngenetic intergrowths and (2) the degree of nitrogen aggregation to address the amount of diamondite-forming events at a given locality, and the relationship or lack of with proto-kimberlite fluids/melts (phenocrystic vs. xenocrystic). A detailed study for the $\delta^{15}N$ values for populations of diamondites that lie at each end of the global $\delta^{13}C$ bimodality (chapter 2, figure 2.11) would also be required to test the above model further.

(b) Utilising the Finesse machine for mantle geochemistry

The ability to accurately determine the coupled $\delta^{13}C$-$\delta^{15}N$ values in spectral type II diamonds with a mass of < 0.1 mg using the Finesse machine (Open University- with a blank routinely < 0.5 ng of nitrogen) makes it possible to perform a detailed study of the coupled $\delta^{13}C$-$\delta^{15}N$ values in (i) sublithospheric diamonds, (ii) Type II megacryst suites and (ii) potentially in mantle silicates, described below:

(i) Sublithospheric diamonds

Sublithospheric diamonds are all eclogitic and mostly type II, where 88.99 % (n = 109) of the lower mantle-derived diamonds and 50 % (n = 26) of the transition zone diamonds (majoritic) are both type II (Bulanova et al., 2010; Hutchison et al., 1997; Kaminsky et al., 2001; 2009; Stachel et al., 2002) as opposed to 2 % of cratonic diamonds (CARTIGNY, 2010). This can enable a better understanding of both the carbon and nitrogen cycles as seen through diamond formation with depth, as well as probe the potential depths of carbon transport from the ocean floor to the lower mantle during subduction, should some of the eclogitic diamonds be subduction related.

(ii) Type II megacryst suites

Noteworthy is that megacryst diamonds, diamonds larger than 4 cm^2, tend to be Type II (Moore, 2009), and polishing of diamond (from rough to gem quality) results in the loss of more than double the original mass (Dr G Bulanova pers comm. 2009). Therefore, a detailed study of the coupled $\delta^{13}C$-$\delta^{15}N$ values in megacryst samples from a given mine where the macro diamonds have been studied for coupled $\delta^{13}C$-$\delta^{15}N$ values (i.e. several southern African mines including Orapa- the world's most productive diamond mine) is overdue from an exploration point of view. Especially as this study demonstrates that the amount of sample required to determine the coupled $\delta^{13}C$-$\delta^{15}N$ values in Type II diamonds can be < 0.1 mg.

(iii) Mantle silicates

Peridotite xenoliths and individual mineral separates exhibit mantle-like homogeneous $\delta^{18}O$ values (Mattey et al., 1994) and $\delta^{13}C$ values (Deines, 2002), as do peridotitic diamonds and their silicate inclusions (Cartigny, 2005). However the $\delta^{15}N$ values for peridotitic diamonds have a much wider

range than they do for $\delta^{13}C$ values, with a range from -30 to + 15 ‰ (chapter 2, figure 2.16, page 53). The reason for the $\delta^{15}N$ variability alongside such a restricted range for $\delta^{13}C$ (± 5 ‰) is not well constrained. Several models exist to explain this, from a isotopically heterogeneous accretion of nitrogen (Javoy et al., 1986) and nitrogen isotope fractionation during diamond formation (Boyd et al., 1988; Reutsky and Palyanov, 2008; Thomassot et al., 2007). Therefore an investigation of the $\delta^{15}N$ variability in peridotite xenoliths determined by high temperature stepped pyrolysis (see chapter 3) and can enable a better understanding of the isotopic range for mantle nitrogen. This can be achieved whilst simultaneously measuring the $\delta^{13}C$ values in the same samples from the same gas extraction stage, thus enabling constraints to be placed whilst using a well constrained system (C isotopes) to test for how representative the sample is for mantle volatiles. This could also been conducted whilst measuring several noble gas isotope ratios such as Xe, Ne and Ar in mantle peridotite (see Verchovsky et al., 1998 for a study looking at meteoritic diamonds). This could place further constraints on the origins of mantle nitrogen, Xe, Ne and Ar.

9.6.2 Studies related to extra-terrestrial samples

As stated in chapter 2; '*for the context of this thesis, the beginning of time is regarded as the formation of the solar system*', and understanding the isotopic partitioning between the silicate and metallic proportions of the Earth can enable a mass balance model to be made to estimate the composition of the Earth's inaccessible core, but we can access and sample the metallic cores of asteroids, Fe meteorites. As discussed in chapter 7 (section 7.3) carbon isotope fractionation (by ~ 12 ‰) in the system cohenite and graphite from Fe meteorites was observed by Craig (1953) and Deines and Wickman (1975). Therefore I am suggesting that one could use Fe-meteorites as laboratories that have conducted isotopic fractionation experiments at high temperatures and search for more fractionation factors within them. They are known to contain several mineral phases such as graphite, cohenite, troilite and ferromagnesian silicates grains all within a Fe-Ni alloy

(Goldstein et al., 2009). Using these previous studies as a foundation, the diversity of the mineral phase chemistry within the Fe-meteorites and the high precision now available using modern analytical facilities with small sample sizes, one could study various mineral separates and the Fe-Ni host matrix from Fe-meteorites and test for isotopic and elemental fractionation factors applicable to core formation in various isotopic systems, such as Fe, Si, S, N, C and O.

9.6.3 Experimental studies

The experiments in chapter 8 should be performed in the graphite stability field and analysed by nanoSIMS to ensure that the $^{13}C/^{12}C$ ratios measured are of the phases in question. The reason for doing the experiments in the graphite stability field is that one could use Al_2O_3 as a polishing powder to avoid carbon contamination in the form of micro-diamonds (chapter 7, figure 7.6, page 198). Then one can determine the temperature effect with a better spatial resolution. There are also two additional experimental studies that I feel are required to fully constrain the meaning of observed light element stable isotope ratios measured in mantle samples, such as diamond.

(a) The behaviour of carbon and nitrogen during subduction

The discussions in chapter 5, section 5.9.3 and chapter 6 section 6.9 demonstrates that there is a huge need for further experimental constraints to be placed on the behaviour of both carbon and nitrogen, both in terms of isotopic fractionation and the partitioning and speciation of stable phases to better understand the in-gassing of the mantle during subduction of oceanic sediments. The study of the ratios of volatiles such as He, C, N and Ar in arc basalts can produce contrasting results. Such as global estimates of 50 % (WALLACE, 2005) to zero sedimentary carbon contribution to the arc basalts at the Mariana Trough (MACPHERSON et al., 2010). Fischer et al (2002) studied the N and He isotopic and relative abundance characteristics of volatiles emitted from two segments of the

Central American volcanic arc, and concluded that globally the recycling of subducted nitrogen to the surface via arc volcanism is an extremely efficient process. There is experimental evidence for N-H compounds decoupling from Ar and partitioning into silicate melts at high pressure and temperature (MYSEN et al., 2009; ROSKOSZ et al., 2006) and clinopyroxene potentially acting as a store for nitrogen in the deep Earth (WATENPHUL et al., 2010); these studies demonstrate a mechanism for both ingassing and degassing during subduction zone metamorphism and arc magmatism. Therefore it is clear that more work is required to constrain the partition coefficients and isotopic fractionation factors for carbon and nitrogen devolatilisation during subduction along various P-T-fO_2-fH_2 conditions to better understand the cycling of these elements into and out of the mantle during subduction, which will place constraints on the C/N ratio of subducted organic carbon predicted to form some diamonds.

(b) The behaviour of nitrogen during diamond formation

There are several mentions in this thesis to the value of ^{13}C fractionation factors during diamond growth from thermodynamic calculations (Bottinga, 1969; Richet et al., 1977; Schauble, 2009) and empirical determinations using natural samples (chapter 7) and experiments (chapter 8). However, there is very little mention of $^{15}N/^{14}N$ fractionation factors. There is also no experimental work that aims to determine the partition coefficient for nitrogen between diamond and various potential mantle melts/fluids that vary in composition and P-T-fO_2 conditions. Ironic as it may seem, but the actual K value for diamonds most common impurity is inferred and not quantified (for for a review that infers N as incompatible see CARTIGNY et al., 2001; and for a review that infers N as compatible see STACHEL et al., 2009). There are also several mentions in this thesis of speciation of carbon as a function of P-T-fO_2 conditions. There is however, as above, very little work on nitrogen speciation in the mantle available in the literature (Watenphul et al., 2010). I feel these topics should be addressed at the same time by experiment, especially as the facilities required are all in existence

and well understood techniques (multi anvil and pistol cylinder press, single crystal and powder X-ray diffraction, Infra red absorption spectroscopy, scanning electron microscopy, gas sourced mass spectrometry and secondary ionisation mass spectrometry).

(c) Isotopic fractionation factors applicable to core formation

Using the proposed study in section 9.6.2 using separates from Fe-meteorite as a first principle, one could follow up any potential fractionation factors observed between the phases in Fe meteorites and apply temperature and pressure constraints using multi-anvil and pistol cylinder press experiments (that are then analysed using an applicable multi collector mass spectrometer). Also, for any light element isotopic ratio (i.e. elements between H and Fe) where the mean mantle and chondritic ratios are defined and relatively constant, one can conduct first principle isotope fractionation experiments between Fe-Ni alloys and pyrolitic silicate melts as a function of high pressure and high temperature. Before quantifying the fractionation factors, the time dependence on isotopic equilibration during synthesis and the temperature effect of isotope fractionation must be investigated using low pressure (i.e. 2 GPa) using piston cylinder experiments. This is owing to the relatively larger sample size acquired at lower pressures making multiple analyses of run products a simpler endeavour to fully constrain these effects. Once these constrains are in place for the low pressure system the same experiments can be performed at 5, 15, and 25 GPa for at least two temperatures each (the range of temperatures to be investigated depends upon the temperature dependency shown in the 2 GPa experiments) to test the coupled pressure and temperature effects in the system under investigation. This can enable one to decipher the amount of or lack any of these light elements in the Earth's core (or the core of related planetary bodies, such as Mars and the Moon).

Appendices

Section A1: Standards and Blanks

This section lists the data for the accuracy on the measured mass of carbon using the microbalance and the Baratron®, the methods used for the analysis of the nitrogen references gasses, the carbon isotope standards and the mass and isotopic composition for nitrogen blanks, as cited in chapter 3.

Date	Exp #	Sample	Mg (Scales)	Mg (Bara)
28/04/2010	4713	WA5	0.65	0.67
31/03/2010	4656	WA1	0.20	0.22
31/03/2010	4657	Prem22d	0.46	0.48
27/03/2010	4651	Prem22c	0.29	0.30
10/04/2010	4680	Mir3	0.28	0.27
27/04/2010	4712	Mir2	0.34	0.35
02/04/2010	4662	Prem173f	0.29	0.19
26/03/2010	4649	Prem173a	0.22	0.24
24/04/2010	4706	JUC4	0.25	0.19
26/04/2010	4711	JUA3	0.38	0.31
12/04/2010	4683	J(BZ270)	0.61	0.65
15/04/2010	4691	JUC35	0.20	0.19
14/04/2010	4689	JUC7	0.20	0.18
26/04/2010	4710	JUC5	0.65	0.61
14/04/2010	4690	JUC6	0.34	0.32
07/04/2010	4675	DAC101 y1	0.55	0.54
12/04/2010	4684	Koma101W	0.77	0.80
06/04/2010	4674	DAC102	0.49	0.51
30/03/2010	4655	DAC103	0.31	0.34
09/04/2010	4679	DAC103'2	0.65	0.62
11/04/2010	4681	DAC104	0.46	0.47
08/04/2010	4677	DAC105	0.50	0.52
13/04/2010	4688	DAC45-2	0.69	0.71
24/04/2010	4707	DAC45-3	0.31	0.23
06/08/2010	4774	DAC45-6	0.39	0.37
05/08/2010	4772	DAC45-9	0.36	0.32
09/08/2010	4783	DAC45-7	0.49	0.48
10/08/2010	4784	DAC-BS-4A-12	0.04	0.04
11/08/2010	4788	DAC-JR-A01-4	0.27	0.28
13/08/2010	4791	DAC45-8	0.60	0.64
14/08/2010	4792	DAC106'1	0.19	0.18
15/08/2010	4795	DAC106'2	0.18	0.16
15/08/2010	4798	DAC107	0.22	0.24
16/08/2010	4800	DAC-BS-4B-N3	0.29	0.31
08/08/2010	4777	DAC101 y2	0.20	0.19
23/08/2010	4811	Prem173(8)	0.35	0.38

25/08/2010	4813	WA3	0.59	0.62
07/08/2010	4775	DAC-JR-405-5	0.12	0.12

Table A1: The data for the mass of carbon in mg (determined as diamond weight), determined by using using the microbalance (scales) and then after combustion using the capacitance manometer (Baratron®) for 38 diamonds. The sample names reflect the geographical origin of the samples as follows: WA is West Africa; Prem is Cullinan, SA; JU is Juina, Brazil; Mir is Mir, Siberia (all from chapter 4) and DAC is Dachine French Guyana (chapter 5).

Int28	±	28/29	±	29/30	±	BAR P	K (ng/v)	Int14
3.8732	0.0011	140.01	0.03	0.003893	5.00E-05	0.00233	0.508	65641
2.4099	0.0006	139.86	0.03	0.004954	8.40E-05	0.00468	0.515	127240
3.5944	0.0010	140.06	0.03	0.003757	5.90E-05	0.00702	0.518	187130

Table A2: The intensities of mass 28 ($^{14}N_2$) and the ratios of mass intensities 28/29 ($^{14}N_2/^{14+15}N$) and the intensities of mass 29/30 ($^{14+15}N/^{15}N_2$) with the measured voltage in the baratron (BAR P), K (ng/v) determined using the N MS and the intensities of mass 14 (^{14}N) determined using the quadrupole MS.

Time (seconds)	Int28	Time (Seconds)	Intensity M14
10	0.74104	50	21536
20	1.2218	100	31691
30	1.7182	150	41809
40	2.2212	200	52050
50	2.7345	250	61286
60	3.2257	300	71371
70	3.7541	350	81524
80	4.2627	400	91229
90	4.8002	450	97698
100	5.3108	500	1.08E+05

Table A3: Intensities for the measured intensity of mass 28 ($^{14}N_2$ as int28) in the N MS and mass 14 (^{14}N) in the quadrupole MS for the Air reference gas (M14) against bleed time.

Sample	Experiment #	$\delta^{13}C$ measured	$\delta^{13}C$ true	Δ	σ
St. diamond	4065	-5.39	-9.70	-4.31	0.58
-"-	4066	-4.62	-9.70	-5.08	
-"-	4078	-4.49	-9.70	-5.21	
-"-	4079	-5.85	-9.70	-3.85	
-"-	4084	-5.45	-9.70	-4.25	
NBS 18	4067	0.11	-5.01	-5.12	1.12
-"-	4068	1.69	-5.01	-6.70	
NBS 19	4074	6.10	1.95	-4.15	0.50
-"-	4075	5.39	1.95	-3.44	
St Graphite	4077	-21.70	-24.50	-2.80	0.15
-"-	4081	-21.43	-24.50	-3.07	
-"-	4082	-21.69	-24.50	-2.81	
				Average	0.59
				σ	0.40

Table A4: $\delta^{13}C$ standards. The standards used are two International standards NBS 18 and NBS 19, and two internal standards St Diamond and St Graphite. The method for analysis is stepped combustion as detailed in chapter 3.

Date	Exp#	T (°C)	mass (ng)	$\delta^{15}N$	± ‰	Mean Mass	σ mass	Average $\delta^{15}N$	σ ± ‰
24/03/2010	4644	1000	0.20	-11.92	1.85	0.22	0.03	-16.64	3.19
24/03/2010		1200	0.20	-18.21	1.86				
24/03/2010		1300	0.21	-18.83	1.76				
24/03/2010		1400	0.26	-17.59	1.53				
27/03/2010	4650	800	0.55	-1.94	0.82	0.59	0.27	-7.06	7.12
27/03/2010		1000	1.10	1.22	0.41				
27/03/2010		1200	0.67	-1.76	0.68				
27/03/2010		1300	0.42	-10.29	1.03				
27/03/2010		1400	0.41	-15.36	1.06				
27/03/2010		1400	0.38	-14.23	1.19				
28/03/2010	4652	500	0.24	-22.42	1.72	0.27	0.06	-15.01	5.04
28/03/2010		700	0.21	-13.63	1.86				
28/03/2010		900	0.23	-17.30	1.69				
28/03/2010		1100	0.35	-12.39	1.15				
28/03/2010		1300	0.34	-9.30	1.19				
29/03/2010	4653	800	0.22	-16.16	1.87	0.47	0.17	-8.00	5.05
29/03/2010		1000	0.44	-5.04	1.45				
29/03/2010		1200	0.68	-3.49	0.68				
29/03/2010		1300	0.55	-5.92	0.75				

29/03/2010		1400	0.44	-9.38	0.95				
30/03/2010	4654	800				0.42	0.07	-7.39	3.38
30/03/2010		1000	0.41	-9.41	2.14				
30/03/2010		1200	0.50	-2.36	0.82				
30/03/2010		1300	0.45	-8.51	0.93				
30/03/2010		1400	0.34	-9.27	1.33				
01/04/2010	4661	800	0.31	-10.86	1.27	0.44	0.17	-9.45	3.52
01/04/2010		1000	0.44	-6.38	0.90				
01/04/2010		1200	0.73	-5.03	0.56				
01/04/2010		1300	0.36	-12.68	1.16				
01/04/2010		1400	0.37	-12.30	1.77				
04/04/2010	4671	800	0.17	-11.92	1.87	0.32	0.10	-11.28	3.08
04/04/2010		1000	0.31	-11.06	1.17				
04/04/2010		1200	0.46	-8.05	0.81				
04/04/2010		1300	0.35	-9.27	1.11				
04/04/2010		1400	0.32	-16.08	3.48				
08/04/2010	4676	800	0.20	-15.11	1.83	0.32	0.08	-13.97	4.16
08/04/2010		1000	0.30	-19.99	1.30				
08/04/2010		1200	0.41	-9.23	0.95				
08/04/2010		1300	0.35	-10.97	1.06				
08/04/2010		1400	0.33	-14.54	1.17				
11/04/2010	4682	800	0.31	-13.18	1.24	0.40	0.08	-7.64	3.35
11/04/2010		1000	0.42	-8.06	0.89				
11/04/2010		1200	0.53	-4.47	0.71				
11/04/2010		1300	0.37	-6.55	1.09				
11/04/2010		1400	0.35	-5.95	1.16				
25/04/2010	4708	800	0.54	-2.22	0.64	0.92	0.45	-1.38	5.26
25/04/2010		1100	*1.58*	*4.37*	*0.27*				
25/04/2010		1200	0.73	-8.15	0.50				
25/04/2010		1400	0.84	0.47	0.48				
28/04/2010	4709	800	0.34	-12.48	1.03	0.49	0.22	-5.92	5.89
28/04/2010		1100	0.81	1.69	0.47				
28/04/2010		1200	0.43	-5.32	0.85				
28/04/2010		1300	0.36	-7.58	0.94				
04/08/2010	4770	1200	0.36	-5.32	1.10	0.68	0.27	-5.74	3.00
04/08/2010		1200	0.55	-5.05	0.77				
04/08/2010		1200	0.95	-2.71	0.45				

04/08/2010		1400	0.57	-10.77	0.76				
04/08/2010		1400	0.97	-4.84	0.43				
07/08/2010	4776	800	0.40	-8.60	1.03	0.54	0.17	-12.97	5.37
07/08/2010		1000	0.50	-11.36	0.82				
07/08/2010		1200	0.72	-18.96	0.60				
07/08/2010		1400	1.14	-28.88	0.40				
13/08/2010	4790	1100	0.17	-12.46	3.04	0.46	0.22	-5.67	4.34
13/08/2010		1100	0.46	-3.37	0.91				
13/08/2010		1100	0.49	-3.54	0.89				
13/08/2010		1100	0.79	-1.62	0.83				
13/08/2010		1100	0.41	-7.34	1.41				
14/08/2010	4796	1100	0.50	0.88	0.84	0.58	0.12	1.58	1.07
14/08/2010		1100	0.44	1.59	1.44				
14/08/2010		1100	0.69	3.08	1.20				
14/08/2010		1100	0.68	0.77	0.69				
15/08/2010	4797	1100	0.60	0.00	0.61	0.54	0.04	-1.23	1.66
15/08/2010		1100	0.53	-2.06	0.66				
15/08/2010		1100	0.54	0.31	0.68				
15/08/2010		1100	0.51	-3.15	0.92				
20/08/2010	4807	1100	0.52	-1.66	0.76	0.49	0.04	-1.58	3.10
20/08/2010		1100	0.45	1.11	0.78				
20/08/2010		1100	0.45	0.12	1.63				
20/08/2010		1100	0.52	-5.90	0.69				
20/08/2010									
24/08/2010	4812	1100	1.41	4.20	0.39	0.89	0.31	1.23	1.92
24/08/2010		1100	0.89	1.92	0.60				
24/08/2010		1100	0.82	-0.73	2.88				
24/08/2010		1100	0.67	0.17	0.74				
24/08/2010		1100	0.65	0.57	1.91				

Table A5: The mass and isotopic compositions for nitrogen blanks for the clean platinum foil.

Section A2: Type II diamonds

This section lists the stepped and bulk data for the type II samples in chapter 4. The term 'stepped' refers to individual combustion steps (amount of diamond in mg combusted at a given step) and 'bulk' as weighted means for each sample (this terminology is used herein). The errors shown for $\delta^{13}C$ (± ‰) are calculated using the reference gas and no blank correction was required. The errors for $\delta^{15}N$ (± ‰) are blank-corrected according to the equations 1-6 in chapter 4.

Sample	T	C mg	N ppm	$\delta^{13}C$	± ‰	$\delta^{15}N$	± ‰	% blank N
WA5	800	0.10	12	-3.28	0.84	-3.42	2.73	29
	1100	0.21	14	-0.57	0.65	-4.16	1.14	14
	1200	0.17	24	-3.94	0.45	-8.62	0.90	11
	1250	0.14	25	-4.07	0.53	-9.02	1.05	12
	1300	0.05	21	-3.33	0.66	-7.72	3.62	33
WA1	800	0.10	2	-6.47	0.46	-14.72	7.71	64
	1000	0.13	7	-4.67	1.03	-4.86	1.70	32
Prem22d	800	0.19	2	-7.38	0.68	2.55	4.57	56
	1000	0.20	3	-5.55	0.62	-0.24	2.42	40
	1200	0.09	6	-5.03	0.78	0.82	2.65	43
Prem22c	800	0.06	32	-8.11	0.84	1.59	2.48	24
	1000	0.07	65	-8.31	0.69	11.19	1.28	12
	1200	0.13	32	-6.41	0.75	2.01	1.09	12
	1300	0.05	8	-5.75	0.93	9.69	15.41	63
Mir3	800	0.16	30	-8.82	0.76	10.43	0.35	7
	1000	0.10	44	-8.14	1.47	-0.34	0.32	8
Mir2	800	0.11	3	-5.09	0.75	6.57	9.84	58
	1100	0.19	2	-5.60	0.46			52
	1200	0.04	B.Q	-5.15	0.76			106
Prem173f	800	0.19	5	-5.79	0.60	7.90	1.72	24
Prem173a	800	0.06	6	-0.52	1.24	8.95	14.68	62
	1000	0.07	28	-4.94	0.77	2.44	2.33	23
	1200	0.07	42	-4.49	0.83	4.59	1.68	17
	1300	0.05	8	-3.29	1.24			62
JUC4	800	0.16	13	-6.71	0.36	3.26	0.41	10
	1100	0.03	40	-5.12	0.25	4.09	0.83	18

JUA3	800	0.18	3	-8.80	0.44	4.02	7.98	50
	1100	0.13	9	-8.85	0.64	-0.75	3.87	33
J(BZ270)	800	0.22	3	-7.73	0.71	4.34	2.18	36
	1000	0.22	4	-7.91	0.64	6.18	1.89	32
	1200	0.03	61	-6.52	0.86	-2.46	0.79	17
JUC35	800	0.15	B.Q	-7.55	1.02			114
	1000	0.04	B.Q	-7.44	0.37			99
JUC7	800	0.15	12	-6.57	0.92	-6.83	0.90	18
	1000	0.04	10	-6.47	0.41	-4.62	4.37	53
JUC5	800	0.19	B.Q	-8.44				148
	1100	0.24	B.Q	-7.48				63
	1250	0.17	1	-8.44				75
JUC6	800	0.19	B.Q	-9.07	0.65			135
	1000	0.13	B.Q	-7.88	1.21			93
Prem173(8)	1100	0.24	2	-5.28	0.11	-7.26	4.76	60
	1100	0.14	3	-4.92	0.14			72
WA3	1100	0.26	5	-4.43	0.14	-3.95	1.70	41
	1100	0.25	24	-4.45	0.15	-11.77	0.65	13
	1100	0.11	47	-3.98	0.23	-11.55	0.81	15

Table A6: Stepped data for the spectral type II samples in chapter 4. Where WA is samples from West African, Prem is samples from Cullinan, SA, Mir is samples from Mir, Siberia and JU is samples from Juina, Brazil. B.Q refers to below quantification (circa 1-2 ppm) and C mg refers to the mass of carbon (as CO_2) was derived by combustion ≈ to the sample size for the step in question.

Sample	Locality	N ppm	$\delta^{13}C$	± ‰	$\delta^{15}N$	± ‰
WA1	West Africa	5	-5.45	0.78	-6.88	4.78
WA3	West Africa	20	-4.36	0.16	-10.89	1.47
WA5	West Africa	19	-2.78	0.62	-7.17	1.48
Prem22c	Cullinan, SA	36	-7.06	0.64	5.87	2.80
Prem22d	Cullinan, SA	3	-6.18	0.67	0.76	5.99
Prem173a	Cullinan, SA	23	-3.46	0.75	4.72	3.48
Prem173f	Cullinan, SA	5	-5.79	0.60	7.90	0.99
Prem173(8)	Cullinan, SA	2	-5.15	0.12	-7.26	8.08
Mir2	Mir, Siberia	2	-5.38	0.59	6.57	9.21
Mir3	Mir, Siberia	36	-8.56	1.04	5.19	0.61
JUC4	Juina, Brazil	16	-6.50	0.35	3.53	0.79
JUA3	Juina, Brazil	6	-8.82	0.52	0.83	5.23
J(BZ270)	Juina, Brazil	7	-7.73	0.67	5.34	2.35
JUC35	Juina, Brazil	B.Q	-7.53	0.89		
JUC7	Juina, Brazil	12	-6.55	0.83	-6.47	1.74
JUC5	Juina, Brazil	B.Q	-8.06	0.12		
JUC6	Juina, Brazil	B.Q	-8.58	0.88		

Table A7: Bulk data for the type II samples in chapter 4. Abbreviations are as in table A3.

Section A3: Dachine diamond and inclusion data

There are three sub-sections in this section. There is data for the diamond themselves as stepped and bulk N/C (N ppm), $\delta^{13}C$ and $\delta^{15}N$ (sub-section i); the methods used to produce the cathode luminescence images (sub-section ii) and the methods used and data for the major and trace element data for the three garnets (sub-section iii).

(i)Diamond stable isotope data

Sample	T (°C)	C mg	N ppm	$\delta^{13}C$	± ‰	$\delta^{15}N$	± ‰	% blank
DAC-JR-405-5	800	0.07	3	-20.96	0.48			76.85
	1000	0.06	8	-20.34	0.51	4.19	8.16	56.76
DAC101 y1	800	0.22	37	-2.91	0.58	8.62	0.23	3.78
	1000	0.23	59	0.74	1.07	4.28	0.13	2.27
	1200	0.09	51	-1.32	0.67	3.85	0.40	6.79
DAC101 y2	800	0.09	13	2.89	0.35	3.32	3.19	34.05
	1000	0.10	10	2.78	0.30	4.28	3.70	37.27
DAC101W	800	0.23	20	-0.36	0.94	0.86	0.32	7.99
	1000	0.23	21	-0.56	0.73	1.99	0.30	7.41
	1200	0.24	37	-0.10	0.83	3.58	0.16	4.15
	1250	0.10	19	-2.08	0.52	4.47	0.82	17.54
DAC102	800	0.20	7	-28.10	0.57	7.44	1.26	19.28
	1000	0.23	6	-24.55	0.82	7.52	1.22	18.75
	1200	0.08	22	-25.48	0.66	5.24	0.89	15.04
DAC103	800	0.12	2	-31.29	0.92	-1.73	7.77	68.43
	1000	0.13	4	-31.13	1.06	-2.03	3.28	47.72
	1200	0.09	10	-28.97	0.49	-4.44	1.72	32.06
DAC103'2	800	0.22	9	-29.79	1.10	1.92	0.88	13.92
	1000	0.23	3	-29.79	0.85	0.60	2.59	32.26
	1200	0.17	19	-30.02	0.73	0.55	0.55	9.14
DAC104	800	0.22	15	-20.36	0.45	10.35	0.54	11.13
	1000	0.22	21	-18.43	0.83	-0.11	0.32	7.89
	1200	0.03	32	-10.17	0.30	5.56	1.59	28.89
DAC105	800	0.22	5	-30.85	0.65	15.28	1.77	21.01
	1000	0.23	5	-26.84	1.00	3.98	1.51	21.42

	1200	0.08	26	-24.75	0.81	2.85	0.86	13.63
DAC45-2	800	0.22	1	-28.76	0.98			64.21
	1000	0.23	2	-30.56	0.91	6.06	3.12	44.22
	1200	0.25	10	-29.23	0.76	5.29	0.60	13.28
DAC45-3	1150	0.23	53	-28.12	0.58	8.33	0.30	3.81
DAC45-6	800	0.12	5	-27.88	0.43	23.30	8.51	49.76
	1200	0.14	64	-29.50	0.41	7.46	0.43	6.26
	1400	0.11	27	-30.28	0.30	-5.32	1.32	17.37
DAC45-9	1200	0.32	110	-24.06	0.21	17.15	0.13	1.71
DAC45-4	1000	0.14	3	-30.90	0.43			58.61
DAC45-7	900	0.15	2	-35.74	0.16			66.53
	1000	0.15	9	-35.94	0.23	2.01	2.78	31.15
	1100	0.18	14	-36.44	0.18	33.27	2.46	18.88
DAC-BS-4A-12	800	0.03	B.Q	-25.86	0.15			120.68
	1000	0.01	B.Q	-26.18	0.17			123.66
DAC-JR-A01-4	900	0.14	1	-25.84	0.29			82.54
	1000	0.14	2	-25.70	0.33			65.68
	1100	0.01	38	-23.51	0.65			62.34
DAC45-8	1100	0.25	13	-31.69	0.17	5.40	0.82	12.49
	1100	0.24	8	-32.58	0.21	3.03	1.28	19.39
	1100	0.16	13	-32.55	0.29			18.74
DAC106'1	1100	0.18	4	-32.55	0.27			43.08
DAC106'2	1100	0.16	3	-28.54	0.31			56.50
DAC107	1100	0.22	3	-27.81	0.21	-3.94	1.46	51.00
	1100	0.02	7	-27.81	0.33			81.63
DAC-BS-4B-N3	1100	0.26	15	-23.85	0.15	3.91	0.23	11.96
	1100	0.05	19	-23.61	0.29	15.00	1.15	36.61

Table A8: Stepped data for the type II samples from Dachine, French Guyana in chapter 5. The errors shown for $\delta^{13}C$ (± ‰) are calculated using the reference gas and no blank correction was required. The errors for $\delta^{15}N$ (± ‰) are blank-corrected according to the equations 1-6 in chapter 4.

Sample	N ppm	$\delta^{13}C$	± ‰	$\delta^{15}N$	± ‰
DAC-JR-405-5	5	-20.67	0.49	4.19	8.16
DAC101Y	39	-0.04	0.68	5.41	0.46
DAC101W	26	-0.55	0.80	2.67	0.29
DAC102	9	-26.07	0.70	6.59	1.10
DAC103	5	-30.59	0.85	-3.38	2.94
DAC103'2	9	-29.85	0.91	1.02	0.90
DAC104	19	-18.78	0.62	4.30	0.20
DAC105	8	-28.23	0.82	6.54	1.28
DAC106	3	-30.66	0.29		
DAC107	3	-27.81	0.22	-3.94	1.46
DAC45-2	5	-29.52	0.88	5.79	1.46
DAC45-3	53	-28.12	0.58	8.33	0.30
DAC45-4	3	-30.90	0.43	4.79	8.84
DAC45-6	34	-29.21	0.38	5.30	0.42
DAC45-7	9	-36.07	0.19	21.93	3.37
DAC45-8	11	-32.23	0.21	15.01	2.06
DAC45-9	110	-24.06	0.21	17.15	0.13
DAC-BS-4A-12	B.Q	-25.93	0.15		
DAC-JR-A01-4	2	-25.70	0.32	11.59	13.18
DAC-BS-4B-N3	16	-23.81	0.18	6.02	0.40

Table A9: Bulk data for the type II samples from Dachine, French Guyana in chapter 5.

(ii) *Cathode luminescence*

Cathodoluminescence images were taken with a JSM-35 scanning electron microscope (I = 3 nA, U = 20 kV) at the University of Bristol. These images were used for the study of internal crystal growth.

(iii)Mineral inclusion data

Sample	DACBS 4A-5	DACBS 4A-11	DACBS 4B-2
Mineral	Garnet	Garnet	Garnet
SiO_2	37.60	38.51	39.89
TiO_2	0.62	0.85	0.60
Al_2O_3	20.08	20.39	20.49
Cr_2O_3	0.05	0.06	0.08
FeO^T	12.51	6.68	8.01
MnO	15.11	18.77	12.78
MgO	4.99	5.98	6.90
CaO	7.67	8.64	10.15
Na_2O	0.03	0.03	0.12
K2O	0.00	0.01	0.00
NiO	0.00	0.00	
ZnO	0.01	0.06	
Total	98.66	99.97	99.01

Table A10: Electron microprobe analyses of syngenetic mineral inclusions from Dachine diamonds. Electron microprobe analysis of exposed and polished garnet inclusions in diamonds was made at the University of Bristol with a Cameca SX100 using a beam current of 20 nA at 15 kV voltage, and a spot size of ~1 micron at the surface. Silicate and oxide standards with conventional PAP data reduction techniques were employed, and replicate analysis of standards yields uncertainties at the 2 and 5% level, respectively, for major and minor elements (SMITH et al., In Prep 2011).

Sample	D-BS4A-5	D-BS4A-11	D-BS4B-2 g
Si	175740.85	179988.01	186480.51
Ca	57190.97	62421.31	71983.94
Ti	3585.42	4706.86	3667.77
Sr	1.69	0.78	0.82
Y	61.41	98.75	104.05
Zr	12.69	30.62	30.19
Nb	0.04	0.15	0.23
Ba	0.08	0.38	0.58
La	nd	0.06	0.01
Ce	0.04	0.11	0.12
Pr	nd	0.05	0.03
Nd	0.31	1.56	0.67
Sm	0.59	1.14	0.91
Eu	0.23	0.75	0.44
Gd	2.72	3.79	3.10
Tb	0.78	1.09	1.06
Dy	7.25	10.17	12.47

Ho	2.10	2.70	3.69
Er	7.10	9.96	11.27
Tm	0.99	1.77	1.81
Yb	7.90	12.13	12.87
Lu	1.22	1.97	2.01
Hf	1.25	1.34	0.72
Ta	nd	0.44	0.02
Th	0.03	nd	0.02
U	nd	0.02	nd
Li	1.99	2.89	3.20
Na	567.07	363.93	725.74
Mg	34027.79	40009.06	48199.93
Si	175740.85	179988.01	186480.51
P	83.96	9.72	10.77
K	30.32	73.47	44.73
Sc	57.00	68.31	65.23
V	448.02	533.82	352.77
Cr	431.61	421.08	458.13
Mn	119925.68	128669.78	89597.75
Fe	97354.04	48586.49	60791.42
Ni	1492.96	775.65	956.66
Co	85.16	46.13	44.52
Ga	79.25	87.14	77.20
Rb	<3	<3	<1.5
Mo	<0.07	<0.14	<0.06
Sn	4.59	16.05	4.48
Cs	0.00	0.05	0.02

Table A11: SIMS trace element analyses of syngenetic garnet inclusions from Dachine diamonds. Notes: values are in ppm. Nd - not determined. Trace element concentrations in garnet inclusions were determined using a Cameca IMS-4f ion-microprobe at the Edinburgh Ion Microprobe Facility (EIMF). The primary beam was ~11 keV 16O- ions (~15 keV net impact energy), with a sample current of 2 nA that corresponds to a spatial resolution of ~15 µm at the sample surface. The secondary ion accelerating voltage of 4,500 V was offset by 75 eV (energy window of 40 eV) to reduce molecular ion transmission. Calibration was performed on glass standards under identical operating conditions. Statistical precision at concentrations [1 ppm is better than 10% relative for all isotopes. Accuracy is better than 10% relative for the rare-earth elements (REE), Ba, Sr, Nb, Zr and Y. Hf, Rb, Th and U are accurate to within 30% relative (SMITH et al., In Prep 2011).

Section A3: Polycrystalline diamond data

This section lists the stepped and bulk data for the diamonds from Diamondite samples in chapter 6. The errors shown for $\delta^{13}C$ (± ‰) are calculated using the reference gas and no blank correction was required. The errors for $\delta^{15}N$ (± ‰) are blank-corrected according to the equations 1-6 in chapter 4.

Exp #	Sample	T (°C)	C mg	N ppm	$\delta^{13}C$	± ‰	$\delta^{15}N$	± ‰	% blank
4318	Dia061a	900	0.09	1377.76	-13.90	0.48	15.54	0.07	0.38
		1000	0.08	1485.02	-14.60	0.59	15.65	0.07	0.38
		1100	0.07	1423.43	-12.86	0.27	14.67	0.09	0.50
4410	Dia063	800	0.08	412.61	-19.63	0.24	22.29	0.37	1.42
		1000	0.08	452.54	-19.54	0.45	24.76	0.35	1.24
		1400	0.09	514.97	-18.24	0.41	20.83	0.25	1.04
4408	Dia068	800	0.08	208.39	-5.46	0.41	0.87	0.26	2.63
		1000	0.10	278.97	-6.36	0.31	5.28	0.19	1.64
		1400	0.03	368.40	-3.02	0.18	-0.74	0.09	3.58
4531	Dia001	700	0.05	44.50	-18.45	0.53	2.23	2.11	17.39
		900	0.07	52.89	-17.84	0.32	-5.53	1.46	11.37
		1100	0.08	77.85	-19.79	0.24	-8.72	1.00	6.97
		1300	0.06	30.50	-19.40	0.31	-5.39	2.74	19.54
4312	Dia005	900	0.01	287.74	-18.97	0.49	26.97	4.99	14.26
		1100	0.02	482.70	-22.01	0.25	25.31	1.66	5.53
		1200	0.02	538.29	-22.82	0.18	22.31	1.29	4.83
		1300	0.02	503.33	-19.58	0.24	21.99	1.42	5.35
		1400	0.02	461.49	-22.15	0.23	22.96	1.36	4.96
		1400	0.02	444.42	-21.16	0.16	21.86	1.24	4.71
		1400	0.02	453.64	-20.62	0.20	23.08	1.26	4.60
		1400	0.02	497.00	-21.31	0.22	22.49	1.22	4.56
		1450	0.03	423.60	-20.03	0.15	18.80	0.72	3.14
		1450	0.03	403.73	-25.43	0.66	18.67	0.89	3.88
		1450	0.02	454.56	-22.07	0.53	23.15	1.21	4.39
		1450	0.02	525.76	-21.55	0.20	20.99	1.10	4.34
		1450	0.02	412.83	-21.79	0.19	21.06	1.69	6.51
		1450	0.01	344.82	-20.47	0.31	20.87	2.27	8.64
4328	Dia006	900	0.07	33.67	-19.41	0.30	4.77	2.20	16.71
		1000	0.09	28.19	-19.37	0.36	-3.89	1.94	15.46
		1100	0.10	23.43	-19.16	0.46	-1.18	1.97	16.71

4524	Dia019	700	0.07	147.03	-19.41	0.26	7.28	0.57	4.39
		900	0.09	227.83	-19.37	0.17	8.84	0.31	2.21
		1100	0.10	231.59	-19.16	0.45	8.47	0.27	1.99
		1300	0.03	200.85	-16.84	0.95	10.63	1.30	8.05
4311	Dia020 3rd	700	0.06	241.51	-11.81	0.24	16.70	0.68	3.25
		900	0.06	351.57	-10.59	0.23	20.21	0.50	2.08
		1000	0.07	371.34	-11.23	0.19	19.09	0.41	1.82
		1100	0.05	415.91	-10.82	0.29	17.78	0.47	2.19
4305	Dia020 1st	700	0.03	197.12	-9.12	0.35	13.81	1.45	7.65
		900	0.03	485.28	-8.07	0.28	6.85	0.43	3.40
		1100	0.03	436.59	-8.99	0.28	9.98	0.52	3.53
		1100	0.04	152.81	-10.98	0.36	13.75	1.39	7.37
		1200	0.07	468.77	-8.58	0.60	8.60	0.20	1.51
		1300	0.08	476.94	-9.05	0.48	12.85	0.21	1.26
		1400	0.09	386.72	-8.27	0.33	-4.48	0.06	1.34
		1400	0.07	315.33	-10.05	0.16	12.03	0.37	2.26
		1400	0.06	543.26	-9.06	0.17	5.11	0.18	1.56
4307	Dia020 2nd	700	0.01	384.77	-4.58	0.43	9.49	1.61	10.31
		900	0.01	709.31	-9.38	0.27	4.61	0.63	5.48
		1100	0.01	676.95	-8.93	0.19	7.81	0.61	4.59
		1200	0.02	310.54	-9.84	0.15	-15.22	0.31	6.63
		1300	0.02	605.76	-9.27	0.53	1.27	0.36	3.48
		1400	0.02	728.44	-9.05	0.16	-4.66	0.15	3.47
		1400	0.01	432.83	-7.55	0.24	11.15	1.13	6.91
		1400	0.02	394.51	-8.90	0.22	16.15	1.23	5.93
		1400	0.02	869.87	-9.77	0.19	9.15	0.42	2.97
		1450	0.02	520.72	-10.12	0.12	16.90	0.88	4.17
		1400	0.01	538.02	-10.68	0.28	7.38	0.85	6.35
		1400	0.01	723.16	-10.25	0.28	12.66	0.92	5.27
4513	Dia022	700	0.06	1959.04	-22.59	0.35	7.52	0.05	0.39
		900	0.11		-23.81	0.18			
		1100	0.15	2826.16	-19.51	0.17	11.35	0.02	0.11
		1200	0.04	1108.32	-19.61	0.50	-13.38	0.04	1.01
4331	Dia030	900	0.13	13.35	-15.00	0.35	6.01	3.13	21.23
		1000	0.16	7.31	-18.19	0.32	6.97	4.95	28.84
		1100	0.08	0.00	-14.86	0.67			
		1200	0.00	0.00	-12.02	0.40			
4313	Dia050	700	0.03	244.61	-24.84	0.56	17.86	1.50	6.61

		800	0.08	351.10	-23.95	0.83	21.45	0.40	1.58
		900	0.08	300.19	-24.11	0.64	22.46	0.52	1.99
		1000	0.01	296.62	-22.83	0.21	23.39	7.00	20.90
4521	Dia052	700	0.07	59.81	-16.25	0.28	6.37	1.32	10.03
		900	0.11	25.49	-15.52	0.31	0.57	1.73	15.06
		1100	0.10	18.81	-16.15	0.33	5.49	2.88	20.25
		1300	0.00	164.98	-15.41	0.13	11.50	13.53	46.54
4515	Dia053	700	0.11	46.04	-20.56	0.25	0.81	0.88	8.25
		900	0.14	64.17	-21.47	0.19	2.72	0.56	5.19
4324	Dia054	900	0.11	170.42	-15.47	0.39	11.74	0.39	2.43
		1000	0.11	185.69	-16.05	0.58	12.08	0.39	2.37
		1100	0.16		-17.67	0.33		0.00	
		1200	0.10	244.43	-16.19	0.45	11.90	0.31	1.88
		1300	0.01	88.43	-14.88	0.30	16.88	7.98	28.26
4523	Dia059	700	0.07	13.62	-23.00	0.23	3.80	4.99	32.10
		900	0.08	15.22	-22.79	0.23	4.82	4.36	28.38
		1100	0.09	11.18	-23.16	0.22	6.92	5.61	31.55
		1300	0.02	14.68	-21.10	0.27	6.64	18.98	61.26
4411	Dia066 2nd	800	0.07	209.92	-25.424	0.25	22.47	0.84	3.17
		1000	0.08	134.77	-25.062	0.24	33.75	1.68	4.36
		1200	0.10	378.01	-27.234	0.34	19.69	0.30	1.29
		1400	0.07	276.05	-24.564	0.21	24.28	0.64	2.27
		1400	0.02	133.67	-22.743	0.21	43.72	8.34	15.06
4325	Dia066	900	0.05	497.46	-23.248	0.44	18.97	0.39	1.71
		1000	0.08	492.85	-23.943	0.35	20.25	0.30	1.27
		1100	0.10	536.63	-24.821	0.68	21.25	0.22	0.90
		1200	0.11	699.87	-24.845	0.38	17.49	0.13	0.60
		1300	0.07	569.49	-19.544	0.24	21.33	0.31	1.23
4516	Dia073	700	0.03	2156.83	-16.956	0.24	5.16	0.07	0.63
		900	0.10	4067.09	-18.405	0.19	6.22	0.01	0.12
		1100	0.11	3736.25	-16.978	0.27	7.74	0.02	0.12
		1300	0.00	3171.30	-16.694	0.15	10.09	0.57	3.77
4319	Dia074	900	0.08	68.81	-5.128	0.21	5.77	1.01	8.06
		1000	0.08	52.66	-4.476	0.24	3.98	1.24	10.49
		1100	0.08	25.62	-4.08	0.23	6.07	2.76	19.11
4321	Dia078	900	0.16	73.85	-28.247	0.28	7.09	0.48	3.80

		1000	0.16	91.48	-29.073	0.32	5.68	0.36	3.09
		1100	0.07	102.50	-27.616	0.28	7.50	0.78	5.86
4332	Dia018	900	0.08	21.30	-18.201	0.29	11.76	4.57	22.49
		1000	0.09		-17.995	0.53			
		1100	0.12	22.88	-18.99	0.42	5.35	1.91	14.52
		1200	0.06	15.76	-17.409	0.34	0.61	2.28	32.45

Table A12: Stepped data for the diamondite samples in chapter 6.

Paragenesis	Sample	N ppm	$\delta^{13}C$	± ‰	$\delta^{15}N$	± ‰
P	Dia061a	1428	-13.85	0.46	15.34	0.08
P	Dia063	462	-19.11	0.37	22.53	0.32
P	Dia068	266	-5.49	0.33	2.66	0.25
P	Dia001	54	-18.93	0.34	-5.70	2.80
P	Dia005	449	-21.59	0.29	21.76	1.33
P	Dia006	28	-19.30	0.51	-0.22	2.03
P	Dia019	207	-19.07	0.36	8.59	0.43
P	Dia020	437	-9.78	0.28	10.66	0.73
W	Dia022	1635	-21.33	0.24	8.58	0.04
W	Dia030	8	-16.28	0.41	6.39	3.86
W	Dia050	314	-24.10	0.70	21.50	0.76
W	Dia052	34	-15.93	0.31	4.83	2.46
W	Dia053	56	-21.05	0.22	1.99	0.68
W	Dia054	130	-16.45	0.42	12.00	0.50
W	Dia059	13	-22.85	0.23	5.29	6.14
W	Dia066	412	-24.55	0.39	21.67	0.56
W	Dia073	3635	-17.55	0.24	6.87	0.03
W	Dia074	59	-4.56	0.23	5.19	1.40
W	Dia078	76	-28.47	0.30	6.57	0.50
W	Dia018	15	-22.23	0.42	6.42	2.78

Table A13: Bulk data for the diamondite samples in chapter 6. For the paragenesis P refers to peridotitic and W to websteritic.

Section A4: nanoSIMS carbon isotope data

This section lists the sample and standard data acquired using the Ion Probe (nanoSIMS) at the Open University from chapter 7. The errors and counting statistics were determined using the methods of Fitzsimons et al (2000). The information about the standards is given in chapter 7 section 7.5.2. I also show 4 graphs for the intensities of $^{13}C/^{12}C$ vs. ^{16}O, ^{28}Si and $^{12}C^{14}N$ that were measured simultaneously on the same 5 μm^2 spot (qualitative data). These were used to demonstrate a lack of a matrix effects between the standard and the sample carbides based on the Si, O and N concentrations of the samples being greater than the standards, these demonstrate the lack of correlations as discussed in chapter 7 section 7.5.3.

Diamond	Position	$^{13}C/^{12}C$	$\delta^{13}C_{PDB}$	± (‰)	Mean $^{13}C/^{12}C$	σ
	Jag5					
Standard	DRUKER4_1809_run2_1	0.011038	-4.95	1.88	0.011028	0.000017
Standard	DRUKER4_1809_run2_2	0.011037	-5.04			
Standard	DRUKER4_1809_run2_3	0.011008	-7.65			
Sample	JAGD3	0.010951	-12.91	1.60	0.010948	0.000005
Sample	JAGD2	0.010944	-13.54			
Sample	JAG_F3 Dia	0.010965	-11.65			
Standard	DRUKER4_1809_1	0.011014	-7.23	1.88	0.011026	0.000012
Standard	DRUKER4_1809_2	0.011027	-6.06			
Standard	DRUKER4_1809_3	0.011038	-5.07			
	Jag10					
Sample	Area B4 (pt2bis)	0.0108720	-17.05	0.59	0.010871	0.000005
Sample	Area B4 (pt6)	0.0108650	-17.69			
Sample	Area B4 (pt7)	0.0108750	-16.78			
Standard	CVD_Top_27JUL10_1	0.0103670	-62.60	0.59	0.010370	0.000004
Standard	CVD_Top_27JUL10_2	0.0103680	-62.51			
Standard	CVD_Top_27JUL10_3	0.0103750	-61.87			
Standard	CVD_Top_27JUL10_4	0.0103670	-62.60			
Standard	CVD_Top_27JUL10_5	0.0103620	-63.05			
Sample	Area B4 (pt2bis)	0.0108720	-17.22	0.59	0.010871	0.000005
Sample	Area B4 (pt6)	0.0108650	-17.85			
Sample	Area B4 (pt7)	0.0108750	-16.95			

Table A14: Diamond analyses from chapter 7 for the samples and the standards.

Fe-Carbide	Position	$^{13}C/^{12}C$	$\delta^{13}C_{PDB}$	± (‰)	Mean $^{13}C/^{12}C$	σ
	Jag5					
Sample	JAG5_D7	0.010538	-20.12	0.68	0.010545	0.000006
Sample	JAG5_D7_2	0.010549	-19.10			
Sample	JAG5_D7_3	0.010548	-19.19			
Standard	DISKO_DC6_30	0.010504	-24.71	0.88	0.010502	0.000004
Standard	DISKO_DC6_31	0.010497	-25.36			
Standard	DISKO_DC6_32	0.010504	-24.71			
Standard	DISKO_DC6_1308_1	0.010529	-20.96	0.88	0.010517	0.000009
Standard	DISKO_DC6_1308_2	0.010517	-22.07			
Standard	DISKO_DC6_1308_3	0.010510	-22.73			
Standard	DISKO_DC6_1308_4	0.010512	-22.54			
Sample	JAG5_E2_4	0.010576	-18.05	0.89	0.010573	0.000005
Sample	JAG5_E2_6_corr	0.010569	-18.64			
Standard	DISKO_DC6_1408_1	0.010525	-22.76	0.50	0.010522	0.000004
Standard	DISKO_DC6_1408_2	0.010518	-23.41			
Standard	DISKO_DC6_1408_3	0.010523	-22.94			
Sample	JAG5_F_1	0.010594	-16.82	1.14	0.010580	0.000012
Sample	JAG5_F2_corr	0.010577	-18.42			
Sample	JAG5_F3_corr	0.010591	-17.06			
Sample	JAG5_F_4	0.010573	-18.77			
Sample	JAG5_F_6	0.010567	-19.32			
	Jag10					
Standard	Disko_Shoe_29JUL10_1	0.01052	-23.87	0.77	0.010520	0.000005
Standard	Disko_Shoe_29JUL10_2	0.01052	-24.15			
Standard	Disko_Shoe_29JUL10_3	0.01053	-23.31			
Standard	Disko_Shoe_29JUL10_4	0.01052	-24.43			
Sample	AreaB4(FeC1)	0.0105170	-23.80	2.06	0.010502	0.000022
Sample	AreaB4(FeC1b)	0.010477	-27.51			
Sample	AreaB4(FeC5)	0.010511	-24.36			

Table A15: Fe-carbide analyses from chapter 7 for the samples and the standards.

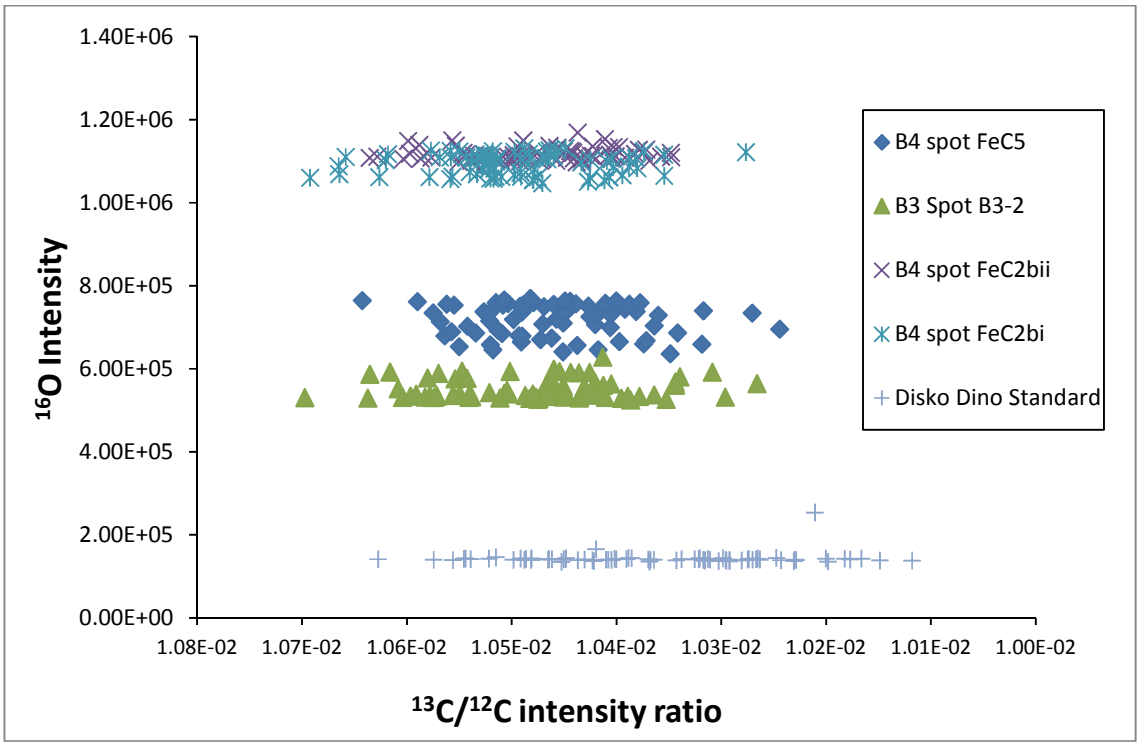

Graph A1: A variation diagram for the intensities of $^{13}C/^{12}C$ vs. ^{16}O (qualitative data). Disko Dino standard is the data from the standard of Disko cohenite from Disko Island and the other 4 symbols represent 4 points in sample Jag10.

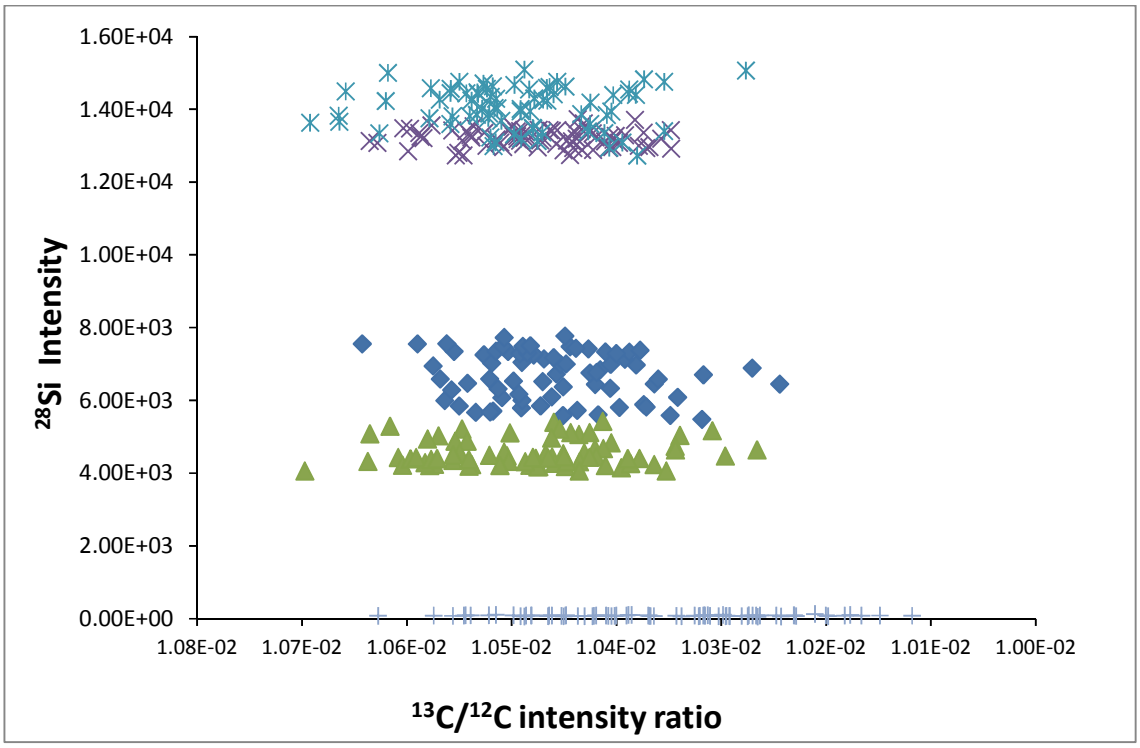

Graph A2: A variation diagram for the intensities of $^{13}C/^{12}C$ vs. ^{28}Si (qualitative data). Symbols as in graph A2.

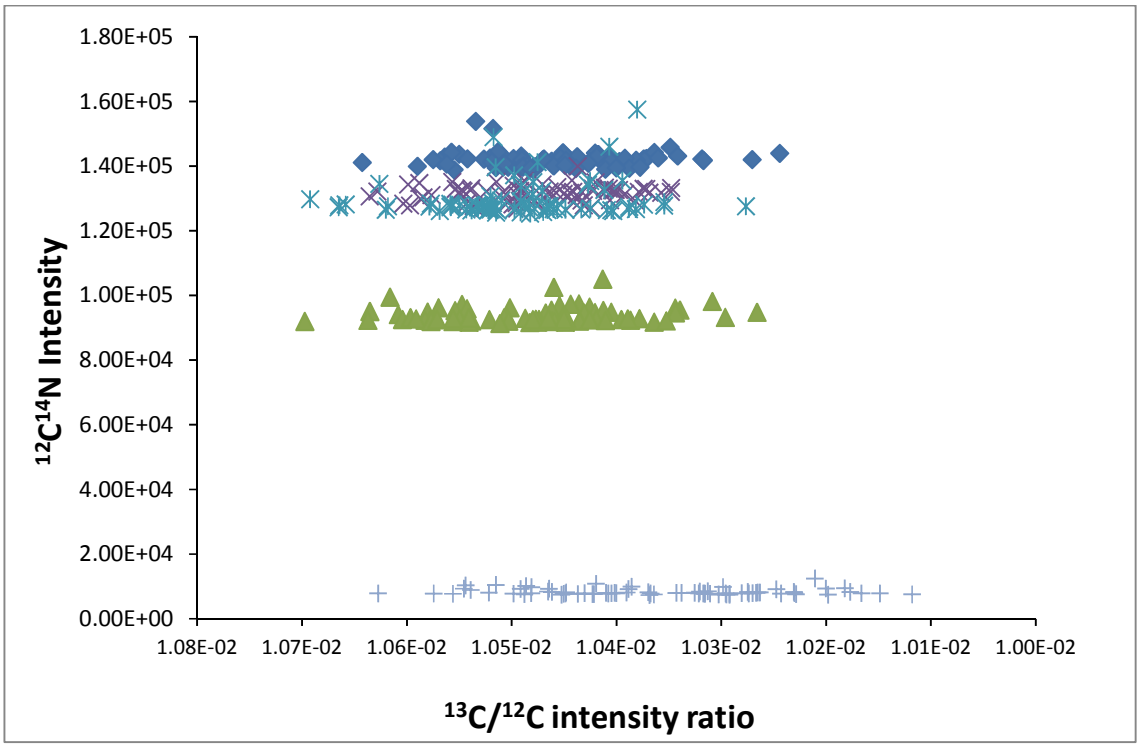

Graph A3: A variation diagram for the intensities of $^{13}C/^{12}C$ vs. $^{12}C^{14}N$ (qualitative data). Symbols as in graph A2.

Section A5: HPHT data

This section lists the stepped combustion data for the experimental samples of Gr-Dia and cementite in chapter 8. The synthesis pressures and temperatures are shown. The Comb T refers to the temperature of combustion with the mass of carbon released (C ng), carbon isotope composition and standard error using the reference gas and the percentage of carbon released relative to the total release with the exception of the first step which is a pyrolysis step (heating without O_2).

Exp	Pressure	Temperature		
4946	5	1200		
Comb T	C ng	$\delta^{13}C$	±‰	%C
400	911	402.42	0.48	-
450	770	1210.10	0.30	5.11
500	1955	1501.90	0.29	12.98
500	996	1459.30	0.65	6.61
600	3508	843.06	0.42	23.28
650	2302	756.82	0.34	15.28
650	1272	732.06	0.39	8.44
650	755	535.29	0.27	5.01
1000	8860	871.81	0.25	58.80
1010	401	549.09	0.14	2.66
1020	223	360.90	0.31	1.48
1030	156	228.40	0.26	1.04
1040	127	203.05	0.36	0.85
Total C	15067			

Table A16: The data from sample AS1.Note, this experiment was performed using ^{13}C spiked graphite (1 %).

Exp	Pressure	Temperature		
4839	5	1400		
Comb T	C ng	$\delta^{13}C$	±‰	%C
300	1014	-28.65	0.27	
400	1006	-30.97	0.28	0.72
500	6495	-41.98	0.10	4.66
550	2675	-32.88	0.36	1.92
600	5245	-27.79	0.14	3.76
650	14669	-28.63	0.20	10.52
700	20961	-29.12	0.11	15.03
800	57023	-28.64	0.22	40.89
900	30730	-27.40	0.26	22.04
1000	564	-25.80	0.10	0.40
1100	89	-21.90	0.33	0.06
Total C	139457			

Table A17: The data from sample CO#2.

Exp	Pressure	Temperature		
5028	25	1650		
Comb T	C ng	$\delta^{13}C$	±‰	%C
400	1091	-44.05	0.22	3.36
500	2049	-37.22	0.28	6.31
600	1271	-37.69	0.20	3.92
600	545	-33.00	0.14	1.68
650	1340	-31.28	0.21	4.13
650	2238	-32.48	0.34	6.90
1000	24874	-29.89	0.12	76.66
1100	104	-30.73	0.33	0.32
1150	25	-31.42	0.30	0.08
Total C	32446			

Table A18: The data from sample CO#8.

Exp	Pressure	Temperature		
5094	25	1650		
Comb T	C ng	$\delta^{13}C$	±‰	%C
500	157	-27.28		
500	1465	-20.28	0.79	0.73
550	2628	-23.99	1.68	1.32
600	4565	-31.75	0.91	2.29
600	4194	-33.05	1.12	2.10
650	12793	-30.40	0.54	6.40
650	11590	-29.68	0.20	5.80
1000	117090	-21.92	0.14	58.61
1100	9666	-27.28	0.21	4.84
1200	29515	-29.99	0.34	14.78
1250	1019	-25.88	0.12	0.51
1300	5237	-29.78	0.47	2.62
Total C	199762			

Table A19: A second run of sample CO#8.

Exp	Pressure	Temperature		
4859	9	1650		
Comb T	C ng	$\delta^{13}C$	±‰	%C
500	210	-30.25	0.93	
500	978	-29.27	0.96	12.31
510	411	-30.33	0.79	5.17
550	776	-29.73	1.68	9.76
560	385	-29.09	0.91	4.84
600	784	-28.50	1.12	9.87
600	544	-34.06	0.54	6.85
650	1036	-34.93	0.96	13.03
650	572	-29.11	0.42	7.20
1000	2441	-27.54	0.68	30.71
1100	21	-29.67	1.57	0.26
Total C	7949			

Table A20: The data from sample CO#5.

Exp	Pressure	Temperature		
4827	9	1650		
Comb T	C ng	$\delta^{13}C$	±‰	%C
400	90	-40.52	0.59	
600	236	-40.09	0.91	11.82
600	67	-25.87	1.00	3.36
650	342	-32.82	0.65	17.14
650	63	-21.16	0.96	3.13
1000	1207	-26.69	1.20	60.42
1100	82	-39.81	0.61	4.13
Total C	1998			

Table A21: A second run of sample CO#5.

References

Alexander, C. M. O. D., Grossman, J. N., Ebel, D. S., and Ciesla, F. J., 2008. The Formation Conditions of Chondrules and Chondrites. *Science* **320**, 1617-1619.

Aulbach, S., O/'Reilly, S. Y., Griffin, W. L., and Pearson, N. J., 2008. Subcontinental lithospheric mantle origin of high niobium/tantalum ratios in eclogites. *Nature Geosci* **1**, 468-472.

Aulbach, S., Stachel, T., Viljoen, K. S., Brey, G. P., and Harris, J. W., 2002. Eclogitic and websteritic diamond sources beneath the Limpopo Belt-is slab-melting the link? *Contrib. Mineral. Petrol.* **143**, 56.

Bailey, L. M., 1999. An unusual diamond-bearing talc schist from the Dachine Area of French Guiana. M.Sc. Thesis, Queen's University, Canada.

Bebout, G. E. and Fogel, M. L., 1992. Nitrogen-isotope compositions of metasedimentary rocks in the Catalina Schist, California: Implications for metamorphic devolatilization history. *Geochimica Et Cosmochimica Acta* **56**, 2839-2849.

Berry, A. J., Danyushevsky, L. V., St C. O'Neill, H., Newville, M., and Sutton, S. R., 2008. Oxidation state of iron in komatiitic melt inclusions indicates hot Archaean mantle. *Nature* **455**, 960-963.

Bertka, C. M. and Fei, Y., 1997. Mineralogy of the Martian interior up to core-mantle boundary pressures. *J. Geophys. Res.* **102**, 5251-5264.

Best, M. G., 2003. *Igneous and metamorphic petrology 2nd Edition* Wiley-Blackwell

Bibby, D. M., 1982. Impurities in natural diamond. *Phys. Chem. Carbon* **18**, 3.

Blundy, J. and Wood, B., 1994. Prediction of crystal–melt partition coefficients from elastic moduli. *Nature* **372**, 452-454.

Blundy, J. D., Brodholt, J. P., and Wood, B. J., 1991. Carbon Fluid Equilibria and the Oxidation-State of the Upper Mantle. *Nature* **349**, 321-324.

Bostick, B. C., Jones, R. E., Ernst, W. G., Chen, C., Leech, M. L., and Beane, R. J., 2003. Low-temperature microdiamond aggregates in the Maksyutov Metamorphic Complex, South Ural Mountains, Russia. *American Mineralogist* **88**, 1709-1717.

Bottinga, Y., 1969. Calculated fractionation factors for carbon and hydrogen isotope exchange in the system calcite-carbon dioxide-graphite-methane-hydrogen-water vapor. *Geochimica Et Cosmochimica Acta* **33**, 49-64.

Bottinga, Y. and Craig, H., 1968. Oxygen isotope fractionation between CO2 and water, and the isotopic composition of marine atmospheric CO2. *Earth and Planetary Science Letters* **5**, 285-295.

Bouvier, A. and Wadhwa, M., 2010. The age of the Solar System redefined by the oldest Pb-Pb age of a meteoritic inclusion. *Nature Geosci* **3**, 637-641.

Boyd, S., R, Wright, I., P, Alexander, M., O'D, and Pillinger, C., T, 1998a. High Resolution Stepped-Combustion Mass Spectrometry: Application to the Detection and Analysis of Fine-Grained Diamond in Meteorites and Rocks. *Geostandards and Geoanalytical Research* **22**, 71-83.

Boyd, S., R, Wright I, P., Franchi, I. A., and Pillinger C, T., 1988a. Preparation of sub-nanomole quantities of nitrogen gas for stable isotopic analysis. *Journal of Physics E: Scientific Instruments* **21**, 876.

Boyd, S., Wright, I. P., and Pillinger, C. T., 1997. Stepped-heating of carbonates and carbon-bearing quartz grains. *Chemical Geology* **134**, 303-310.

Boyd, S. R., 2001. Ammonium as a biomarker in Precambrian metasediments. *Precambrian Research* **108**, 159-173.

Boyd, S. R. and Pillinger, C. T., 1994. A preliminary study of 15N/14N in octahedral growth form diamonds. *Chemical Geology* **116**, 43-59.

Boyd, S. R., Pillinger, C. T., Milledge, H. J., Mendelssohn, M. J., and Seal, M., 1988b. Fractionation of nitrogen isotopes in a synthetic diamond of mixed crystal habit. *Nature* **331**, 604-607.

Boyd, S. R., Pillinger, C. T., Milledge, H. J., and Seal, M. J., 1992. C and N isotopic composition and the infrared absorption spectra of coated diamonds: evidence for the regional uniformity of CO2F---H2O rich fluids in lithospheric mantle. *Earth and Planetary Science Letters* **108**, 139-150.

Boyd, S. R., Pineau, F., and Javoy, M., 1994. Modelling the growth of natural diamonds. *Chemical Geology* **116**, 29-42.

Boyd, S. R., Wright, I. P., Alexander, C. M., and Pillinger, C., 1998b. High Resolution Stepped-Combustion Mass Spectrometry: Application to the Detection and Analysis of Fine-Grained Diamond in Meteorites and Rocks. *Geostandards and Geoanalytical Research* **22**, 71-83.

Brett, R. and Higgins, G. T., 1969. Cliftonite: A proposed origin, and its bearings on the origin of diamonds in meteorites. *Geochimica Et Cosmochimica Acta* **33**, 1473-1484.

Brown, J. M. and Shankland, T. J., 1981. Thermodynamic parameters in the Earth as determined from seismic profiles. *Geophysical Journal of the Royal Astronomical Society* **66**, 579-596.

Bryan, S. E. and Ernst, R. E., 2008. Revised definition of Large Igneous Provinces (LIPs). *Earth-Science Reviews* **86**, 175-202.

Bulanova, G. P. and Zayakina, N. V., 1991. Graphite – iron – cohenite assemblage in the central zone of diamond from 23rd Party Congress kimberlite. *Dokl. Aka. Nauk SSSR*, 706-709 (in Russian).

Bulanova, G. P., 1995. The formation of diamond. *J. Geochem. Exp.* **53**, 1-23.

Bulanova, G. P., Pearson, D. G., Hauri, E. H., and Griffin, B. J., 2002. Carbon and nitrogen isotope systematics within a sector-growth diamond from the Mir kimberlite, Yakutia. *Chemical Geology* **188**, 105-123.

Bulanova, G., Walter, M., Smith, C., Kohn, S., Armstrong, L., Blundy, J., and Gobbo, L., 2010. Mineral inclusions in sublithospheric diamonds from Collier 4 kimberlite pipe, Juina, Brazil: subducted protoliths, carbonated melts and primary kimberlite magmatism. *Contributions to Mineralogy and Petrology*. **160**, 489-510

Burgess, R., Johnson, L. H., Mattey, D. P., Harris, J. W., and Turner, G., 1998. He, Ar and C isotopes in coated and polycrystalline diamonds. *Chemical Geology* **146**, 205-217.

Busigny, V., Cartigny, P., Philippot, P., Ader, M., and Javoy, M., 2003. Massive recycling of nitrogen and other fluid-mobile elements (K, Rb, Cs, H) in a cold slab environment: evidence from HP to UHP oceanic metasediements of the Schistes Lustres nappe (western Alps, Europe). *Earth and Planetary Science Letters* **215**, 27-42.

Capdevila, R., Arndt, N., Letendre, J., and Sauvage, J.-F., 1999. Diamonds in volcaniclastic komatiite from French Guiana. *Nature* **399**, 456-458.

Cartigny, P., Boyd, S. R., Harris, J. W., and Javoy, M., 1997. Nitrogen isotopes in peridotitic diamonds from Fuxian, China: the mantle signature. *Terra Nova* **9**, 175-179.

Cartigny, P., Harris, J. W., and Javoy, M., 1998a. Eclogitic Diamond Formation at Jwaneng: No Room for a Recycled Component. *Science* **280**, 1421-1424.

Cartigny, P., Harris, J. W., Phillips, D., Girard, M., and Javoy, M., 1998b. Subduction-related diamonds? The evidence for a mantle-derived origin from coupled $\delta^{13}C$-$\delta^{15}N$ determinations. *Chemical Geology* **147**, 147-159.

Cartigny, P., Harris, J. W., and Javoy, M., 1999. Eclogitic, Peridotitic and Metamorphic diamonds and the problems of carbon recycling—the case of Orapa (Botswana). *7th International Kimberlite Conference Extended Abstract*, 117– 124.

Cartigny, P., De Corte, K., Shatsky, V. S., Ader, M., De Paepe, P., Sobolev, N. V., and Javoy, M., 2001a. The origin and formation of metamorphic microdiamonds from the Kokchetav massif, Kazakhstan: a nitrogen and carbon isotopic study. *Chemical Geology* **176**, 265-281.

Cartigny, P., Harris, J. W., and Javoy, M., 2001b. Diamond genesis, mantle fractionations and mantle nitrogen content: a study of $\delta^{13}C$-N concentrations in diamonds. *Earth and Planetary Science Letters* **185**, 85-98.

Cartigny, P., Harris, J. W., Taylor, A., Davies, R., and Javoy, M., 2003. On the possibility of a kinetic fractionation of nitrogen stable isotopes during natural diamond growth. *Geochimica Et Cosmochimica Acta* **67**, 1571-1576.

Cartigny, P., Chinn, I., Viljoen, K. S., and Robinson, D., 2004a. Early Proterozoic Ultrahigh Pressure Metamorphism: Evidence from Microdiamonds. *Science* **304**, 853-855.

Cartigny, P., Stachel, T., Harris, J. W., and Javoy, M., 2004b. Constraining diamond metasomatic growth using C- and N-stable isotopes: examples from Namibia. *Lithos* **77**, 359-373.

Cartigny, P., 2005. Stable isotopes and the origin of diamond. *Elements* **1**, 79-84.

Cartigny, P., Farquhar, J., Thomassot, E., Harris, J. W., Wing, B., Masterson, A., McKeegan, K., and Stachel, T., 2009. A mantle origin for Paleoarchean peridotitic diamonds from the Panda kimberlite, Slave Craton: Evidence from 13C-, 15N- and 33,34S-stable isotope systematics. *Lithos* **112**, 852-864.

Cartigny, P., 2010. Mantle-related carbonados? Geochemical insights from diamonds from the Dachine komatiite (French Guiana). *Earth and Planetary Science Letters* **296,** 329-339

Chrenko, R. M., 1973. Boron, Dominant Acceptor in Semiconducting Diamond. *Physical Review B* **7**, 4560-4567.

Clayton, R. N., Goldsmith, J. R., Karel, K. J., Mayeda, T. K., and Robert C, N., 1975. Limits on the effect of pressure on isotopic fractionation. *Geochimica Et Cosmochimica Acta* **39**, 1197-1201.

Craig, H., 1953. The geochemistry of the stable carbon isotopes. *Geochimica Et Cosmochimica Acta* **3**, 53-92.

Dasgupta, R. and Hirschmann, M. M., 2010. The deep carbon cycle and melting in Earth's interior. *Earth and Planetary Science Letters* **298**, 1-13.

Dasgupta, R. and Walker, D., 2008. Carbon solubility in core melts in a shallow magma ocean environment and distribution of carbon between the Earth's core and the mantle. *Geochimica Et Cosmochimica Acta* **72**, 4627-4641.

Dauphas, N. and Marty, B., 1999. Heavy Nitrogen in Carbonatites of the Kola Peninsula: A Possible Signature of the Deep Mantle. *Science* **286**, 2488-2490.

Davis, W. J., Jones, A. G., Bleeker, W., and Grutter, H., 2003. Lithosphere development in the Slave craton: a linked crustal and mantle perspective. *Lithos* **71**, 575-589.

De Corte, K., Cartigny, P., Shatsky, V. S., Sobolev, N. V., and Javoy, M., 1998. Evidence of fluid inclusions in metamorphic microdiamonds from the Kokchetav massif, northern Kazakhstan. *Geochimica et Cosmochimica Acta* **62**, 3765-3773.

De Stefano, A., Kopylova, M., Cartigny, P., and Afanasiev, V., 2009. Diamonds and eclogites of the Jericho kimberlite (Northern Canada). *Contributions to Mineralogy and Petrology* **158**, 295-315.

Deines, P. and Wickman, F. E., 1975. A contribution to the stable carbon isotope geochemistry of iron meteorites. *Geochimica Et Cosmochimica Acta* **39**, 547-557.

Deines, P., 1980. The carbon isotopic composition of diamonds: relationship to diamond shape, colour, occurrence and vapour composition. *Geochimica Et Cosmochimica Acta* **44**, 943-961.

Deines, P., Harris, J. W., and Gurney, J. J., 1987. Carbon Isotopic Composition, Nitrogen-Content and Inclusion Composition of Diamonds from the Roberts Victor Kimberlite, South-Africa - Evidence for C-13 Depletion in the Mantle. *Geochimica Et Cosmochimica Acta* **51**, 1227-1243.

Deines, P., Harris, J. W., Spear, P. M., and Gurney, J. J., 1989. Nitrogen and 13C content of Finsch and Premier diamonds and their implications. *Geochimica Et Cosmochimica Acta* **53**, 1367-1378.

Deines, P. and Wickman, F. E., 1985. The stable carbon isotopes in enstatite chondrites and Cumberland Falls. *Geochimica Et Cosmochimica Acta* **49**, 89-95.

Deines, P., Harris, J. W., and Gurney, J. J., 1991a. The carbon isotopic composition and nitrogen content of lithospheric and asthenospheric diamonds from the Jagersfontein and Koffiefontein kimberlite, South Africa. *Geochimica Et Cosmochimica Acta* **55**, 2615-2625.

Deines, P., Harris, J. W., Robinson, D. N., Gurney, J. J., and Shee, S. R., 1991b. Carbon and oxygen isotope variations in diamond and graphite eclogites from Orapa, Botswana, and the nitrogen content of their diamonds. *Geochimica Et Cosmochimica Acta* **55**, 515-524.

Deines, P., Harris, J. W., and Gurney, J. J., 1993. Depth-Related Carbon-Isotope and Nitrogen Concentration Variability in the Mantle Below the Orapa Kimberlite, Botswana, Africa. *Geochimica Et Cosmochimica Acta* **57**, 2781-2796.

Deines, P., Harris, J. W., and Gurney, J. J., 1997. Carbon isotope ratios, nitrogen content and aggregation state, and inclusion chemistry of diamonds from Jwaneng, Botswana. *Geochimica Et Cosmochimica Acta* **61**, 3993-4005.

Deines, P., Viljoen, F., and Harris, J. W., 2001. Implications of the carbon isotope and mineral inclusion record for the formation of diamonds in the mantle underlying a mobile belt: Venetia, South Africa. *Geochimica Et Cosmochimica Acta* **65**, 813-838.

Deines, P., 2002. The carbon isotope geochemistry of mantle xenoliths. *Earth-Science Reviews* **58**, 247-278.

Deines, P. and Harris, J. W., 2004. New insights into the occurrence of 13C-depleted carbon in the mantle from two closely associated kimberlites: Letlhakane and Orapa, Botswana. *Lithos* **77**, 125-142.

Deines, P. and Eggler, D. H., 2009. Experimental determination of carbon isotope fractionation between CaCO3 and graphite. *Geochimica Et Cosmochimica Acta* **73**, 7256-7274.

Dobosi, G. and Kurat, G., 2002. Trace element abundances in garnets and clinopyroxenes from diamondites - a signature of carbonatitic fluids. *Mineralogy and Petrology* **76**, 21-38.

Dobosi, G. and Kurat, G., 2010. On the origin of silicate-bearing diamondites. . *Mineralogy and Petrology* **99**, 29–42.

Dobrzhinetskaya, L. F., Green, H. W., Mitchell, T. E., and Dickerson, R. M., 2001. Metamorphic diamonds: Mechanism of growth and inclusion of oxides. *Geology* **29**, 263-266.

Dobrzhinetskaya, L. F., Wirth, R., Yang, J., Hutcheon, I. D., Weber, P. K., and Green, H. W., 2009. High-pressure highly reduced nitrides and oxides from chromitite of a Tibetan ophiolite. *Proceedings of the National Academy of Sciences* **106**, 19233-19238.

Dobson, D. P., Jones, A. P., Rabe, R., Sekine, T., Kurita, K., Taniguchi, T., Kondo, T., Kato, T., Shimomura, O., and Urakawa, S., 1996. In-situ measurement of viscosity and density of carbonate melts at high pressure. *Earth and Planetary Science Letters* **143**, 207-215.

Eggert, J. H., Hicks, D. G., Celliers, P. M., Bradley, D. K., McWilliams, R. S., Jeanloz, R., Miller, J. E., Boehly, T. R., and Collins, G. W., 2010. Melting temperature of diamond at ultrahigh pressure. *Nat Phys* **6**, 40-43.

Ehleringer, J. R., Cooper, D. A., Lott, M. J., and Cook, C. S., 1999. Geo-location of heroin and cocaine by stable isotope ratios. *Forensic Science International* **106**, 27-35.

Evans, T. and Harris, J. W., 1989. Nitrogen aggregation, inclusion equilibration temperatures and the age of diamonds. *Special Publication Geological Society of Australian Journal of Earth Sciences* **14**, 1001-1006.

Evans, T. and Qi, Z., 1982. The Kinetics of the Aggregation of Nitrogen-Atoms in Diamond. *Proceedings of the Royal Society of London Series a- Mathematical Physical and Engineering Sciences* **381**, 159-&.

Exley, R. A., Mattey, D. P., Clague, D. A., and Pillinger, C. T., 1986. Carbon Isotope Systematics of a Mantle Hotspot - a Comparison of Loihi Seamount and Morb Glasses. *Earth and Planetary Science Letters* **78**, 189-199.

Fei, Y. and Bertka, C., 2005. The Interior of Mars. *Science* **308**, 1120-1121.

Fischer, T. P., Hilton, D. R., Zimmer, M. M., Shaw, A. M., Sharp, Z. D., and Walker, J. A., 2002. Subduction and Recycling of Nitrogen Along the Central American Margin. *Science* **297**, 1154-1157.

Fitzsimons, I. C. W., Harte, B., Chinn, I. L., Gurney, J. J., and Taylor, W. R., 1999. Extreme chemical variation in complex diamonds from George Creek, Colorado: a SIMS study of carbon isotope composition and nitrogen abundance. *Mineralogical Magazine* **63**, 857.

Fitzsimons, I. C. W., Harte, B., and Clark, R. M., 2000. SIMS stable isotope measurement: counting statistics and analytical precision. *Mineralogical Magazine* **64** 59-83.

French, B. M. and Rosenberg, P. E., 1965. Siderite (FeCO3): Thermal Decomposition in Equilibrium with Graphite. *Science* **147**, 1283-1284.

Frost, B. R., 1991. Introduction to oxygen fugacity and its petrologic importance. *Reviews in Mineralogy and Geochemistry: Oxide Minerals: Petrologic and Magnetic Significance* **25** 1–9

Frost, D. J., Liebske, C., Langenhorst, F., McCammon, C. A., Tronnes, R. G., and Rubie, D. C., 2004. Experimental evidence for the existence of iron-rich metal in the Earth's lower mantle. *Nature* **428**, 409-412.

Frost, D. J., Mann, U., Asahara, Y., and Rubie, D. C., 2008. The redox state of the mantle during and just after core formation. *Philosophical Transactions of the Royal Society A: Mathematical, Physical and Engineering Sciences* **366**, 4315-4337.

Frost, D. J. and McCammon, C. A., 2008. The Redox State of Earth's Mantle. *Annual Review of Earth and Planetary Sciences* **36**, 389-420.

Galimov, E. M., 1984. Variations of Isotopic Composition of Diamonds and Their Relation to Conditions of Diamond Formation. *Geokhimiya*, 1091-1118.

Galimov, E. M., 1991. Isotope fractionation related to kimberlite magmatism and diamond formation. *Journal Name: Geochimica et Cosmochimica Acta* **55***,* 697-1708.

Garai, J., Haggerty, S. E., Rekhi, S., and Chance, M., 2006. Infrared absorption investigations confirm the extraterrestrial origin of Carbonado diamonds. *The Astrophysical Journal* **653**, L153-L156.

Gardiner, L. R. and Pillinger, C. T., 1979. Static mass spectrometry for the determination of active gases. *Anal. Chem.* **51**, 1230-1236.

Gautheron, C., Cartigny, P., Moreira, M., Harris, J. W., and Allègre, C. J., 2005. Evidence for a mantle component shown by rare gases, C and N isotopes in polycrystalline diamonds from Orapa (Botswana). *Earth and Planetary Science Letters* **240**, 559-572.

Gautheron, C., Cartigny, P., Moreira, M., Harris, J. W., and Allègre, C. J., 2006. Reply to: "Recycled" volatiles in mantle-derived diamonds--Evidence from nitrogen and noble gas isotopic data. *Earth and Planetary Science Letters* **252**, 220-222.

Georg, R. B., Halliday, A. N., Schauble, E. A., and Reynolds, B. C., 2007. Silicon in the Earth's core. *Nature* **447**, 1102-1106.

Goldschmidt, V. M., 1954. *Geochemistry* Clarendon Press, Oxford.

Goldstein, J. I., Scott, E. R. D., and Chabot, N. L., 2009. Iron meteorites: Crystallization, thermal history, parent bodies, and origin. *Chemie der Erde - Geochemistry* **69**, 293-325.

Goodrich, C. A. and Bird, J. M., 1985. Formation of Iron-Carbon Alloys in Basaltic Magma at Uivfaq, Disko Island: The Role of Carbon in Mafic Magmas. *The Journal of Geology* **93**, 475-492.

Grady, M. and Wright, I., 2003. Elemental and Isotopic Abundances of Carbon and Nitrogen in Meteorites. *Space Science Reviews* **106**, 231-248.

Grady, M. M., Verchovsky, A. B., and Wright, I. P., 2004. Magmatic carbon in Martian meteorites: attempts to constrain the carbon cycle on Mars. *International Journal of Astrobiology* **3**, 117-124.

Gurney, J. J., Helmstaedt, H. H., Richardson, S. H., and Shirey, S. B., 2010. Diamonds through Time. *Economic Geology* **105**, 689-712.

Haendel, D., Mühle, K., Nitzsche, H.-M., Stiehl, G., and Wand, U., 1986. Isotopic variations of the fixed nitrogen in metamorphic rocks. *Geochimica Et Cosmochimica Acta* **50**, 749-758.

Haggerty, S. E., 1986. Diamond genesis in a multiply-constrained model. *Nature* **320**, 34-38.

Haggerty, S. E., 1998. Diamond-Carbonado: Geological Implications and Research-Industrial Applications*5th NIRIM International Symposium on Advanced Materials*. National Institute for Research in Inorganic Materials, Tsukuba, Japan.

Haggerty, S. E., 1999. A Diamond Trilogy: Superplumes, Supercontinents, and Supernovae. *Science* **285**, 851-860.

Harlow, G. E. and Davies, R. M., 2005. Diamonds. *Elements* **1**, 67-70.

Harte, B., Taniguchi, T., and Chakraborty, S., 2009. Diffusion in diamond. II. High-pressure-temperature experiments. *Mineral Mag* **73**, 201-204.

Hauri, E. H., Wang, J., Pearson, D. G., and Bulanova, G. P., 2002. Microanalysis of delta C-13, delta N-15, and N abundances in diamonds by secondary ion mass spectrometry. *Chemical Geology* **185**, 149-163.

Hayes, J. M. and Waldbauer, J. R., 2006. The carbon cycle and associated redox processes through time. *Philosophical Transactions of the Royal Society B: Biological Sciences* **361**, 931-950.

Hayman, P. C., Kopylova, M. G., and Kaminsky, F. V., 2005. Lower mantle diamonds from Rio Soriso (Juina area, Mato Grosso, Brazil). *Contrib. Mineral. Petrol.* **149**, 430-445.

Heaney, P. J., Vicenzi, E. P., and De, S., 2005. Strange Diamonds: The Mysterious Origins of Carbonado and Framesite. *Elements* **1**, 85-89.

Herd, C. D. K., Borg, L. E., Jones, J. H., and Papike, J. J., 2002. Oxygen fugacity and geochemical variations in the martian basalts: implications for martian basalt petrogenesis and the oxidation state of the upper mantle of Mars. *Geochimica Et Cosmochimica Acta* **66**, 2025-2036.

Hilton, D. R., Fischer, T. P., and Marty, B., 2002. Noble Gases and Volatile Recycling at Subduction Zones. *Reviews in Mineralogy and Geochemistry* **47**, 319-370.

Hirschmann, M. M. and Withers, A. C., 2008. Ventilation of CO2 from a reduced mantle and consequences for the early Martian greenhouse. *Earth and Planetary Science Letters* **270**, 147-155.

Hoefs, J., 2009. *Stable Isotope Geochemistry*. Springer.

Holzheid, A., Sylvester, P., O'Neill, H. S. C., Rubie, D. C., and Palme, H., 2000. Evidence for a late chondritic veneer in the Earth's mantle from high-pressure partitioning of palladium and platinum. *Nature* **406**, 396-399.

Honda, M., Phillips, D., Harris, J. W., and Yatsevich, I., 2004. Unusual noble gas compositions in polycrystalline diamonds: preliminary results from the Jwaneng kimberlite, Botswana. *Chemical Geology* **203**, 347-358.

Horita, J., Driesner, T., and Cole, D. R., 1999. Pressure Effect on Hydrogen Isotope Fractionation Between Brucite and Water at Elevated Temperatures. *Science* **286**, 1545-1547.

Horita, J., 2001. Carbon isotope exchange in the system CO2-CH4 at elevated temperatures. *Geochimica Et Cosmochimica Acta* **65**, 1907-1919.

Horita, J., 2005a. Some perspectives on isotope biosignatures for early life. *Chemical Geology* **218**, 171-186.

Horita, J., 2005b. Stable isotope thermometry: There is more to it than temperature. *Geochemical Journal* **39**, 481-496.

Hunt, S., A, 2009. Deforming the Earth: An experimental study of subduction-zone rheology, Ph.D thesis, University of London.

Hunter, R. H. and McKenzie, D., 1989. The equilibrium geometry of carbonate melts in rocks of mantle composition.. *Earth Planet. Sci. Lett.* **92** 347–356

Hutchinson, M. T., Cartigny, P., and Harris, J. W., 1997. Carbon and Nitrogen Compositions and Physical Characteristics of Transition Zone and Lower Mantle Diamonds from Sao Luiz, Brazil. In: Gurney, J. J., Gurney, J. L., Pascoe, S. H., and Richardson, S. H. Eds.), *Proceedings of the VII International Kimberlite Conference*. Red Roof Design, Cape Town.

Hutchison, M. T., Cartigny, P., and Harris, J. W., 1997. Carbon and Nitrogen Compositions and Physical Characteristics of Transition Zone and Lower Mantle Diamonds from Sao Luiz, Brazil. In: Gurney, J. J., Gurney, J. L., Pascoe, S. H., and Richardson, S. H. Eds.), *Proceedings of the VII International Kimberlite Conference*. Red Roof Design, Cape Town.

Jackson, M. G., Carlson, R. W., Kurz, M. D., Kempton, P. D., Francis, D., and Blusztajn, J., 2011. Evidence for the survival of the oldest terrestrial mantle reservoir. *Nature* **466**, 853-856.

Jacob, D. E., Kronz, A., and Viljoen, K. S., 2004. Cohenite, native iron and troilite inclusions in garnets from polycrystalline diamond aggregates. *Contributions to Mineralogy and Petrology* **146**, 566-576.

Jacob, D. E., Viljoen, K. S., Grassineau, N., and Jagoutz, E., 2000. Remobilization in the Cratonic Lithosphere Recorded in Polycrystalline Diamond. *Science* **289**, 1182-1185.

Javoy, M., 1995. The integral enstatite chondrite model of the Earth. *Geophys. Res. Lett.* **22**, 2219-2222.

Javoy, M., Kaminski, E., Guyot, F., Andrault, D., Sanloup, C., Moreira, M., Labrosse, S., Jambon, A., Agrinier, P., Davaille, A., and Jaupart, C., 2009. The chemical composition of the Earth: Enstatite chondrite models. *Earth and Planetary Science Letters* **293**, 259-268.

Javoy, M., Pineau, F., and Delorme, H., 1986. Carbon and nitrogen isotopes in the mantle. *Chemical Geology* **57**, 41-62.

Jones, A. P., 2002. Komatiites: new information on the type locality (Barberton), and some new ideas. *Geology Today* **18**, 23-25.

Jones, A. P., Dobson, D. P., Wood, I., Beard, A. D., Verchovsky, A. B., and Milledge, H. J., 2008. Iron carbide and metallic inclusions in diamonds from Jagersfontein, *Ninth International Kimberlite Conference Extended Abstract*, Frankfurt, Germany.

Jones, A. P., Kearsley, A. T., Friend, C. R. L., Robin, E., Beard, A., Tamura, A., Trickett, S., and Claeys, P., 2005. Are there signs of a large Paleocene impact, preserved around Disko Bay, West Greenland? Nuussuaq spherule beds origin by impact instead of volcanic eruption? *Geological Society of America Special Papers* **384**, 281-298.

Jones, A. P., Milledge, H. J., and Beard, A. D., 2006. New nitride minerals in carbonado diamond. *Eighth International Kimberlite Conference Abstracts, Victoria, Canada, availible at http://www.venuewest.com/8IKC/s3post.htm#3.24.*

Kaminsky, F., Zakharchenko, O., Davies, R., Griffin, W., B., Khachatryan-Blinova, G., Shiryaev, A., 2001a. Superdeep diamonds from the Juina area, Mato Grosso State, Brazil. *Contributions to Mineralogy and Petrology* **140**, 734-753.

Kaminsky, F. V., Khachatryan, G. K., Andreazza, P., Araujo, D., and Griffin, W. L., 2009. Super-deep diamonds from kimberlites in the Juina area, Mato Grosso State, Brazil. *Lithos* **112**, 833-842.

Kaminsky, F. V. and Wirth, R., 2011. Iron carbide incluisons in lower-mantle diamond from Juina, Brazil. *Can Mineral* **49**, 555-572.

Kaminsky, F. V., Zakharchenko, O. D., Davies, R., Griffin, W. L., Khachatryan-Blinova, G. K., and Shiryaev, A. A., 2001b. Superdeep diamonds from the Juina area, Mato Grosso State, Brazil. *Contributions to Mineralogy and Petrology* **140**, 734-753.

Kaminsky, F. V., Zakharchenko, O. D., Griffin, W. L., Channer, D. M., and Khachatryan, G. K., 2000. Diamond from the Guaniamo area, Venezuela. *Canadian Mineralogist* **38**.

Keppler, H. and Frost, D. J., 2005. Introduction to minerals under extreme conditions. In: Miletich, R. (Ed.), *Mineral behaviour at extreme conditions*. Eotvos University Press, Budapest.

Keshav, S., Gudfinnsson, G., and Presnall, D., 2006. Majoritic-garnets and clinopyroxenes in cratonic diamonds: Precipitates from CO2-rich melts. *Proc. 11th Int. Conf. EMPG*.

Kirkley, M. B., Gurney, J. J., Otter, M. L., Hill, S. J., and Daniels, L. R., 1991a. The application of C isotope measurements to the identification of the sources of C in diamonds: a review. *Appl. Geochem.* **6**, 477-494.

Kirkley, M. B., Gurney, J. J., and Rickard, R. S., 1991b. Jwaneng Framesites: Carbon Isotopes and Intergrowth Composition, *5th International Kimberlite Conference*.

Klein-BenDavid, O., Izraeli, E. S., Hauri, E., and Navon, O., 2004. Mantle fluid evolution--a tale of one diamond. *Lithos* **77**, 243-253.

Klein-BenDavid, O., Izraeli, E. S., Hauri, E., and Navon, O., 2007. Fluid inclusions in diamonds from the Diavik mine, Canada and the evolution of diamond-forming fluids. *Geochimica Et Cosmochimica Acta* **71**, 723-744.

Koga, K. T., Walter, M. J., Nakamura, E., and Kobayashi, K., 2005. Carbon self-diffusion in a natural diamond. *Physical Review B* **72**, 024108.

Koziol, A. M., 2004. Experimental determination of siderite stability and application to Martian Meteorite ALH84001. *American Mineralogist* **89**, 294-300.

Kurat, G. and Dobosi, G., 2000. Garnet and diopside-bearing diamondites (framesites). *Mineralogy and Petrology* **69**, 143-159.

Lee, C.-T. A., Luffi, P., Hoink, T., Li, J., Dasgupta, R., and Hernlund, J., 2010. Upside-down differentiation and generation of a `primordial' lower mantle. *Nature* **463**, 930-933.

Li, J., Fei, Y., Heinrich, D. H., and Karl, K. T., 2007. Experimental Constraints on Core Composition, *Treatise on Geochemistry*. Pergamon, Oxford. **2.14**, 1-31

Li, J., Mao, H. K., Fei, Y., Gregoryanz, E., Eremets, M., and Zha, C. S., 2002. Compression of Fe_3C to 30 GPa at room temperature. *Phys. Chem. Miner.* **29**, 166-169.

Li, L., Cartigny, P., and Ader, M., 2009. Kinetic nitrogen isotope fractionation associated with thermal decomposition of NH3: Experimental results and potential applications to trace the origin of N2 in natural gas and hydrothermal systems. *Geochimica Et Cosmochimica Acta* **73**, 6282-6297.

Litvin, Y. A., 2006. High-pressure mineralogy of diamond genesis. In: Ohtani, E. (Ed.), *Advances in High-Pressure Mineralogy*. GSA.

Litvin, Y. A., Chudinovskikh, L. T., and Zharikov, V. A., 1997. Crystallization of diamond and graphite in the mantle alkaline-carbonate melts in the experiments at pressure 7-11 GPa. *Doklady Akademii Nauk* **355**, 669-672.

Lord, O. T., Walter, M. J., Dasgupta, R., Walker, D., and Clark, S. M., 2009. Melting in the Fe-C system to 70 GPa. *Earth and Planetary Science Letters* **284**, 157-167.

Luth, R. W., 1993. Diamonds, Eclogites, and the Oxidation State of the Earth's Mantle. *Science* **261**, 66-68.

Mackenzie, F. T. and Morse, J. W., 1992. Sedimentary carbonates through Phanerozoic time. *Geochimica Et Cosmochimica Acta* **56**, 3281-3295.

Macpherson, C. and Mattey, D., 1994. Carbon-Isotope Variations of CO_2 in Central Lau Basin Basalts and Ferrobasalts. *Earth and Planetary Science Letters* **121**, 263-276.

Macpherson, C. G., Hilton, D. R., and Hammerschmidt, K., 2010. No slab-derived CO2 in Mariana Trough back-arc basalts: Implications for carbon subduction and for temporary storage of CO2 beneath slow spreading ridges. *Geochem. Geophys. Geosyst.* **11**, Q11007.

Macpherson, C. G., Hilton, D. R., Newman, S., and Mattey, D. P., 1999. CO2, 13C/12C and H2O variability in natural basaltic glasses: a study comparing stepped heating and ftir spectroscopic techniques. *Geochimica Et Cosmochimica Acta* **63**, 1805-1813.

Magee, C. W., 2001. Geologic, microstructural, and spectroscopic constraints on the origin and history of carbonado diamond, Australian National University.

Magee, C. W. and Taylor, W. R., 1999. Diamond and chromite geochemical constraints on the nature of the Dachine complex, French Guiana. *Research School of Earth Sciences, Australian National University, Annual Report* 85.

Malkovets, V. G., Griffin, W. L., O'Reilly, S. Y., and Wood, B. J., 2007. Diamond, subcalcic garnet, and mantle metasomatism: Kimberlite sampling patterns define the link. *Geology* **35**, 339-342.

Maruoka, T., Kurat, G., Dobosi, G., and Koeberl, C., 2004. Isotopic composition of carbon in diamonds of diamondites: record of mass fractionation in the upper mantle. *Geochimica Et Cosmochimica Acta* **68**, 1635-1644.

Mattey, D., Lowry, D., and Macpherson, C., 1994. Oxygen isotope composition of mantle peridotite. *Earth and Planetary Science Letters* **128**, 231-241.

Mattey, D. P., 1991. Carbon-Dioxide Solubility and Carbon Isotope Fractionation in Basaltic Melt. *Geochimica Et Cosmochimica Acta* **55**, 3467-3473.

Mattey, D. P., Taylor, W. R., Green, D. H., and Pillinger, C. T., 1990. Carbon Isotopic Fractionation between CO_2 Vapor, Silicate and Carbonate Melts - an Experimental-Study to 30 Kbar. *Contributions to Mineralogy and Petrology* **104**, 492-505.

McCammon, C., 2001. Deep Diamond Mysteries. *Science* **293**, 813-814.

McCammon, C., 2005. The Paradox of Mantle Redox. *Science* **308** 807-808.

McCandless, T. E., Letendre, J., and Eastoe, C. J., 1999. Morphology and carbon isotope composition of microdiamonds from Dachine, French Guiana. . In: Gurney, J. J., Gurney, J. L., Pascoe, M. D., and Richardson, S. H. Eds.)*Proceedings of the 7th International Kimberlite Conference.* . Red Roof Design, Cape Town, pp. 550–557.

McDonough, W.F., 2003, Compositional Model for the Earth's Core, in Heinrich, D.H., and Karl, K.T., eds., Treatise on Geochemistry: Oxford, Pergamon, p. 547-568

McDonough, W. F. and Sun, S. s., 1995. The composition of the Earth. *Chemical Geology* **120**, 223-253.

McNeill, J., Pearson, D. G., Klein-BenDavid, O., Nowell, G. M., Ottley, C. J., and Chinn, I. L., 2009. Quantitative analysis of trace element concentrations in some gem-quality diamonds. *Journal of Physics Condensed Matter* **21**, 364207.

McSween Jr, H. Y., Heinrich, D. H., and Karl, K. T., 2007. Mars, *Treatise on Geochemistry*. Pergamon, Oxford. **1**, 1-27

Mendelssohn, M. J. and Milledge, H. J., 1995a. Geologically significant information from routine analysis of the mid-infrared spectra of diamonds. *International Geology Review* **37**, 95-110.

Mendelssohn, M. J. and Milledge, H. J., 1995b. Morphological characteristics of diamond populations in relation to temperature-dependent growth and dissolution rates. *International Geology Review* **37**, 285-312.

Menneken, M., Nemchin, A. A., Geisler, T., Pidgeon, R. T., and Wilde, S. A., 2007. Hadean diamonds in zircon from Jack Hills, Western Australia. *Nature* **448**, 917-920.

Meyer, H. O. A., 1987. Inclusions in diamond. In: Nixon, P. H. (Ed.), *Mantle xenoliths*. John Wiley and Sons Ltd, Chichester.

Mikhail, S., Jones, A. P., Basu, S., Milledge, H. J., Dobson, D. P., Wood, I., Beard, A., Guillermier, C., Verchovsky, A. B., and Franchi, I. A., 2010. Carbon isotope fractionation between natural Fe-carbide and diamond; a proxy for the Earth's core? *AGU 2010 Abstract*.

Milledge, H. J., Mendelssohn, M. J., Seal, M., Rouse, J. E., Swart, P. K., and Pillinger, C. T., 1983. Carbon isotopic variation in spectral type II diamonds. *Nature* **303**, 791-792.

Milledge, H. J. and Meyer, H. O. A., 1962. Nitrogen-14 in Natural Diamonds. *Nature* **195**, 171-172.

Miller, M. F. and Pillinger, C. T., 1997. An appraisal of stepped heating release of fluid inclusion CO2 for isotopic analysis: A preliminary to [delta]13C characterisation of carbonaceous vesicles at the nanomole level. *Geochimica Et Cosmochimica Acta* **61**, 193-205.

Minarik, W. G. and Watson, E. B., 1995. Interconnectivity of carbonate melt at low melt fraction. . *Earth Planet. Sci. Lett.* **133**, 423–437

Mitchell, E. C., Fischer, T. P., Hilton, D. R., Hauri, E. H., Shaw, A. M., de Moor, J. M., Sharp, Z. D., and Kazahaya, K., 2010. Nitrogen sources and recycling at subduction zones: Insights from the Izu-Bonin-Mariana arc. *Geochem. Geophys. Geosyst.* **11**, Q02X11.

Mohapatra, R. K. and Honda, M., 2006. "Recycled" volatiles in mantle-derived diamonds-- Evidence from nitrogen and noble gas isotopic data. *Earth and Planetary Science Letters* **252**, 215-219.

Moore, A. E., 2009. Type II diamonds: Flamboyant Megacrysts? *South African Journal of Geology* **112**, 23-38.

Murakami, M., Hirose, K., Kawamura, K., Sata, N., and Ohishi, Y., 2004. Post-Perovskite Phase Transition in MgSiO3. *Science* **304**, 855-858.

Mysen, B. O., Fogel, M. L., Morrill, P. L., and Cody, G. D., 2009. Solution behavior of reduced COH volatiles in silicate melts at high pressure and temperature. *Geochimica Et Cosmochimica Acta* **73**, 1696-1710.

Nakajima, Y., Takahashi, E., Suzuki, T., and Funakoshi, K.-i., 2009. "Carbon in the core" revisited. *Physics of the Earth and Planetary Interiors* **174**, 202-211.

Navon, O., Hutcheon, I. D., Rossman, G. R., and Wasserburg, G. J., 1988. Mantle-derived fluids in diamond micro-inclusions. *Nature* **335**, 784-789.

O'Neil, J. R., 1986. Theoretical and experimental aspects of isotopic fractionation. *Reviews in Mineralogy and Geochemistry* **16**, 1-40.

Oganov, A. R. and Ono, S., 2004. Theoretical and experimental evidence for a post-perovskite phase of MgSiO3 in Earth's D'' layer. *Nature* **430**, 445-448.

Oganov, A. R., Ono, S., Ma, Y., Glass, C. W., and Garcia, A., 2008. Novel high-pressure structures of MgCO3, CaCO3 and CO2 and their role in Earth's lower mantle. *Earth and Planetary Science Letters* **273**, 38-47.

Ogasawara, Y., 2005. Microdiamonds in ultrahigh-pressure metamorphic rocks. *Elements* **1**, 91-96.

Oppenheimer, C., Kyle, P., Eisele, F., Crawford, J., Huey, G., Tanner, D., Kim, S., Mauldin, L., Blake, D., Beyersdorf, A., Buhr, M., and Davis, D., 2010. Atmospheric chemistry of an Antarctic volcanic plume. *J. Geophys. Res.* **115**, D04303.

Palot, M., Cartigny, P., and Viljoen, F., 2009. Diamond origin and genesis: A C and N stable isotope study on diamonds from a single eclogitic xenolith (Kaalvallei, South Africa). *Lithos* **112**, 758-766.

Papineau, D., De Gregorio, B. T., Stroud, R. M., Steele, A., Pecoits, E., Konhauser, K., Wang, J., and Fogel, M. L., 2010. Ancient graphite in the Eoarchean quartz-pyroxene rocks from Akilia in southern West Greenland II: Isotopic and chemical compositions and comparison with PaleoProterozoic banded iron formations. *Geochimica Et Cosmochimica Acta* **74**, 5884-5905.

Pearson, D. G., Canil, D., Shirey, S. B., Heinrich, D. H., and Karl, K. T., 2003. Mantle Samples Included in Volcanic Rocks: Xenoliths and Diamonds, *Treatise on Geochemistry*. Pergamon, Oxford. **2**, 171-175

Pell, J. A., 1998. Lamproite-Hosted Diamonds, *Geological Fieldwork 1997*. British Columbia Ministry of Employment and Investment.

Pillinger, C. T., 1992. New technologies for small sample stable isotope measurement: static vacuum gas source mass spectrometry, laser probes, ion probes and gas chromatography-isotope ratio mass spectrometry. *International Journal of Mass Spectrometry and Ion Processes* **118-119**, 477-501.

Pineau, F. and Javoy, M., 1994. Strong degassing at ridge crests: The behaviour of dissolved carbon and water in basalt glasses at 14°N, Mid-Atlantic Ridge. *Earth and Planetary Science Letters* **123**, 179-198.

Rayleigh, L., 1902. On the distillation of binary mixtures. *Phil. Mag.* **4**, 521–537.

Rege, S., Griffin, W. L., Kurat, G., Jackson, S. E., Pearson, N. J., and O'Reilly, S. Y., 2008. Trace-element geochemistry of diamondite: Crystallisation of diamond from kimberlite-carbonatite melts. *Lithos* **106**, 39-54.

Reutsky, V. N., Borzdov, Y. M., and Palyanov, Y. N., 2008a. Carbon isotope fractionation associated with HPHT crystallization of diamond. *Diamond and Related Materials* **17**, 1986-1989.

Reutsky, V. N., Harte, B., Eimf, Borzdov, Y. M., and Palyanov, Y. N., 2008b. Monitoring diamond crystal growth, a combined experimental and SIMS study. *European Journal of Mineralogy* **20**, 365-374.

Richet, P., Bottinga, Y., and Javoy, M., 1977. A Review of Hydrogen, Carbon, Nitrogen, Oxygen, Sulphur, and Chlorine Stable Isotope Fractionation Among Gaseous Molecules. *Annual Review of Earth and Planetary Sciences* **5**, 65-110.

Rohrbach, A., Ballhaus, C., Golla-Schindler, U., Ulmer, P., Kamenetsky, V. S., and Kuzmin, D. V., 2007. Metal saturation in the upper mantle. *Nature* **449**, 456-458.

Rohrbach, A., Ballhaus, C., Ulmer, P., Golla-Schindler, U., and Schanbohm, D., 2010. Experimental Evidence for a Reduced Metal-saturated Upper Mantle. *J. Petrol.* **52***, 717-731*

Rohrbach, A. and Schmidt, M. W., 2011a. Redox-freezing and -melting of carbonates in the deep mantle and the role of transient carbides *Goldschmidt*. Mineralogical Magazine, Prague

Rohrbach, A. and Schmidt, M. W., 2011b. Redox freezing and melting in the Earth/'s deep mantle resulting from carbon-iron redox coupling. *Nature* **advance online publication**.

Rosing, M. T., 1999. C-13-depleted carbon microparticles in > 3700-Ma sea-floor sedimentary rocks from west Greenland. *Science* **283**, 674-676.

Roskosz, M., Mysen, B. O., and Cody, G. D., 2006. Dual speciation of nitrogen in silicate melts at high pressure and temperature: An experimental study. *Geochimica Et Cosmochimica Acta* **70**, 2902-2918.

Rouquette, J., Dolejs, D., Kantor, I. Y., McCammon, C. A., Frost, D. J., Prakapenka, V. B., and Dubrovinsky, L. S., 2008. Iron-carbon interactions at high temperatures and pressures. *Appl. Phys. Lett.* **92**, 121912-3.

Rubie, D. C., Gessmann, C. K., and Frost, D. J., 2004. Partitioning of oxygen during core formation on the Earth and Mars. *Nature* **429**, 58-61.

Rumble, D., III, Young, E. D., Shahar, A., and Guo, W., 2011. Stable Isotope Cosmochemistry and the Evolution of Planetary Systems. *Elements* **7**, 23-28.

Saal, A. E., Hauri, E. H., Langmuir, C. H., and Perfit, M. R., 2002. Vapour undersaturation in primitive mid-ocean-ridge basalt and the volatile content of Earth's upper mantle. *Nature* **419**, 451-455.

Saunders, A. D., 2005. Large Igneous Provinces: Origin and Environmental Consequences. *Elements* **1**, 259-263.

Schauble, E. A., 2004. Applying stable isotope fractionation theory to new systems. *Reviews in Mineralogy and Geochemistry* **55** 65-111.

Schauble, E. A., 2009. Equilibrium carbon and hydrogen (and oxygen, nitrogen and sulfur) isotope fractionation in iron. *AGU 2009 Abstract*.

Scott-Smith, B. H., Danchin, R. V., Harris, J. W., and Stracke, K. J., ,, 1984. Kimberlites near Orroroo, South Australia. In: Kornprobst, J. (Ed.), *Kimberlites I: Kimberlites and related rocks*. Elsevier, Amsterdam.

Self, S., Widdowson, M., Thordarson, T., and Jay, A. E., 2006. Volatile fluxes during flood basalt eruptions and potential effects on the global environment: A Deccan perspective. *Earth and Planetary Science Letters* **248**, 518-532.

Shahar, A., Hillgren, V., Young, E., Deng, L., Fei, Y., Marcris, C., and Georg, R. B., 2011. High Pressure and Temperature Silicon Isotope Fractionation between Metal and Silicate, *Goldschmidt conference*. Mineralogical Magazine, Prague, Czech Republic.

Shahar, A., Ziegler, K., Young, E. D., Ricolleau, A., Schauble, E. A., and Fei, Y., 2009. Experimentally determined Si isotope fractionation between silicate and Fe metal and implications for Earth's core formation. *Earth and Planetary Science Letters* **288**, 228-234.

Sharp, W. E., 1966. Pyrrhotite: a Common Inclusion in South African Diamonds. *Nature* **211**, 402-403.

Shcheka, S. S., Wiedenbeck, M., Frost, D. J., and Keppler, H., 2006. Carbon solubility in mantle minerals. *Earth and Planetary Science Letters* **245**, 730-742.

Shelkov, D., Verkhovsky, A. B., Milledge, H. J., and Pillinger, C. T., 1997. Carbonado: A comparison between Brazilian and Ubangui sources with other forms of microcrystalline diamond based on carbon and nitrogen isotopes. *Geol. Geofiz.* **38**, 315-322.

Shelkov, D. A., 1997. N and C isotopic composition of different varieties of terrestrial diamond and carbonado, The Open University.

Shields, G. and Veizer, J., 2002. Precambrian marine carbonate isotope database: Version 1.1. *Geochem. Geophys. Geosyst.* **3**, 1031.

Shimizu, N. and Sobolev, N. V., 1995. Young peridotitic diamonds from the Mir kimberlite pipe. *Nature* **375**, 394-397.

Shirey, S. B., Harris, J. W., Richardson, S. H., Fouch, M., James, D. E., Cartigny, P., Deines, P., and Viljoen, F., 2003. Regional patterns in the paragenesis and age of inclusions in diamond, diamond composition, and the lithospheric seismic structure of Southern Africa. *Lithos* **71**, 243-258.

Shirey, S. B., Harris, J. W., Richardson, S. H., Fouch, M. J., James, D. E., Cartigny, P., Deines, P., and Viljoen, F., 2002. Diamond Genesis, Seismic Structure, and Evolution of the Kaapvaal-Zimbabwe Craton. *Science* **297**, 1683-1686.

Shirey, S. B. and Richardson, S. H., 2011. Start of the Wilson Cycle at 3 Ga Shown by Diamonds from Subcontinental Mantle. *Science* **333**, 434-436.

Siebert, J., Guyot, F., and Malavergne, V., 2005. Diamond formation in metal-carbonate interactions. *Earth and Planetary Science Letters* **229**, 205-216.

Smith, B. H. S. and Skinner, E. M. W., 1984. Diamondiferous Lamproites. *J Geol* **92**, 433-438.

Smith, C. B., 1983. Pb, Sr and Nd isotopic evidence for sources of southern African Cretaceous kimberlites. *Nature* **304**, 51-54.

Smith, C. B., Bulanova, G. P., Walter, M., Kohn, S. C., Mikhail, S., Gobbo, L., and Eimf, In Prep 2011. The origin of diamonds from the Dachine ultramafic pyroclastic, French Guiana.

Sobolev, N. V., 1977. Deep seated inclusions in kimberlites and the problem of the composition of the upper mantle (English translation of Russian edition 1974 by Brown DA). *American Geophysical Union, Washington, DC,*, 279 pp.

Spanu, L., Donadio, D., Hohl, D., Schwegler, E., and Galli, G., 2011. Stability of hydrocarbons at deep Earth pressures and temperatures. *Proceedings of the National Academy of Sciences*. **108**, 6843-6846

Stachel, Stachel, T., Harris, Harris, J., Aulbach, Aulbach, S., Deines, and Deines, P., 2002. Kankan diamonds (Guinea) III: d13C and nitrogen characteristics of deep diamonds. *Contributions to Mineralogy and Petrology* **142**, 465-475.

Stachel, T., 2001. Diamonds from the asthenosphere and the transition zone. *Eur. J. Mineral.* **13**, 883-892.

Stachel, T., Aulbach, S., Brey, G. P., Harris, J. W., Leost, I., Tappert, R., and Viljoen, K. S., 2004. The trace element composition of silicate inclusions in diamonds: a review. *Lithos* **77**, 1-19.

Stachel, T., Brey, G. P., and Harris, J. W., 2005. Inclusions in Sublithospheric Diamonds: Glimpses of Deep Earth. *Elements* **1**, 73-78.

Stachel, T., Harris, J. W., and Brey, G. P., 1998. Rare and unusual mineral inclusions in diamonds from Mwadui, Tanzania. *Contributions to Mineralogy and Petrology* **132**, 34-47.

Stachel, T., Harris, J. W., and Muehlenbachs, K., 2009. Sources of carbon in inclusion-bearing diamonds. *Lithos*.

Stachel, T., R. and Harris, J., W. , 2009. Formation of diamond in the Earth's mantle. *Journal of Physics: Condensed Matter* **21**, 364206.

Stagno, V. and Frost, D. J., 2011. Carbon speciation in the asthenosphere: Experimental measurements of the redox conditions at which carbonate-bearing melts coexist with graphite or diamond in peridotite assemblages. *Earth and Planetary Science Letters* **300**, 72-84.

Strasser, M., Weissert, H., Bernasconi, S. M., and 2006. Data report: Carbon and oxygen isotope geochemistry along a subducting pelagic section offshore Costa Rica (ODP Legs 170 and 205). In: Morris, J. D., Villinger, H. W., and Klaus, A. Eds.), *Proceedings of the Ocean Drilling Program, Scientific Results Volume 205*.

Takafuji, N., Hirose, K., Mitome, M., and Bando, Y., 2005. Solubilities of O and Si in liquid iron in equilibrium with (Mg,Fe)SiO3 perovskite and the light elements in the core. *Geophys. Res. Lett.* **32**, L06313.

Takafuji, N., Hirose, K., Ono, S., Xu, F., Mitome, M., and Bando, Y., 2004. Segregation of core melts by permeable flow in the lower mantle. *Earth and Planetary Science Letters* **224**, 249-257.

Tappert, R., Foden, J., Stachel, T., Muehlenbachs, K., Tappert, M., and Wills, K., 2009. Deep mantle diamonds from South Australia: A record of Pacific subduction at the Gondwanan margin. *Geology* **37**, 43-46.

Tappert, R., Stachel, T., Harris, J., Muehlenbachs, K., Ludwig, T., and Brey, G., 2005a. Diamonds from Jagersfontein (South Africa): messengers from the sublithospheric mantle. *Contributions to Mineralogy and Petrology* **150**, 505-522.

Tappert, R., Stachel, T., Harris, J. W., Muehlenbachs, K., Ludwig, T., and Brey, G. P., 2005b. Subducting oceanic crust: The source of deep diamonds. *Geology* **33**, 565-568.

Taylor, W. R., Canil, D., and Judith Milledge, H. H., 1996. Kinetics of Ib to IaA nitrogen aggregation in diamond. *Geochimica Et Cosmochimica Acta* **60**, 4725-4733.

Thomassot, E., Cartigny, P., and Harris, J. W., 2008. Metasomatic Processes in the Cratonic Lithosphere: the case of Polycrystalline Diamonds. *9th International Kimberlite Conference Extended Abstract*, No. 9IKC-A-00313.

Thomassot, E., Cartigny, P., Harris, J. W., Lorand, J. P., Rollion-Bard, C., and Chaussidon, M., 2009. Metasomatic diamond growth: A multi-isotope study (13C, 15N, 33S, 34S) of sulphide inclusions and their host diamonds from Jwaneng (Botswana). *Earth and Planetary Science Letters* **282**, 79-90.

Thomassot, E., Cartigny, P., Harris, J. W., and Viljoen, K. S., 2007. Methane-related diamond crystallization in the Earth's mantle: Stable isotope evidences from a single diamond-bearing xenolith. *Earth and Planetary Science Letters* **257**, 362-371.

Thomazo, C., Ader, M., and Philippot, P., 2011. Extreme 15N-enrichments in 2.72-Gyr-old sediments: evidence for a turning point in the nitrogen cycle. *Geobiology* **9**, 107-120.

Thomazo, C., Pinti, D. L., Busigny, V., Ader, M., Hashizume, K., and Philippot, P., 2009. Biological activity and the Earth's surface evolution: Insights from carbon, sulfur, nitrogen and iron stable isotopes in the rock record. *Comptes Rendus Palevol* **8**, 665-678.

Tomlinson, E., De Schrijver, I., De Corte, K., Jones, A. P., Moens, L., and Vanhaecke, F., 2005. Trace element compositions of submicroscopic inclusions in coated diamond: A tool for understanding diamond petrogenesis. *Geochimica Et Cosmochimica Acta* **69**, 4719-4732.

Tomlinson, E. L., 2005. The role of fluid in the growth of fibrous diamond: a study of African and Canadian coated diamonds, PhD thesis, University of London.

Tomlinson, E. L., Müller, W., and Eimf, 2009. A snapshot of mantle metasomatism: Trace element analysis of coexisting fluid (LA-ICP-MS) and silicate (SIMS) inclusions in fibrous diamonds. *Earth and Planetary Science Letters* **279**, 362-372.

Tsuzuki, A., Sago, S., Hirano, S.-I., and Naka, S., 1984. High temperature and pressure preparation and properties of iron carbides Fe7C3 and Fe3C. *J. Mater. Sci.* **19**, 2513-2518.

Urey, H. C., 1947. The thermodynamic properties of isotopic substances. *Journal of the Chemical Society (Resumed)*, 562-581.

Verchovsky, A. B., Fisenko, A. V., Semjonova, L. F., Wright, I. P., Lee, M. R., and Pillinger, C. T., 1998. C, N, and Noble Gas Isotopes in Grain Size Separates of Presolar Diamonds from Efremovka. *Science* **281**, 1165-1168.

Verchovsky, A. B., Sephton, M. A., Wright, I. P., and Pillinger, C. T., 2002. Separation of planetary noble gas carrier from bulk carbon in enstatite chondrites during stepped combustion. *Earth and Planetary Science Letters* **199**, 243-255.

Viljoen, K. S., Dobbe, R., Smit, B., Thomassot, E., and Cartigny, P., 2004. Petrology and geochemistry of a diamondiferous lherzolite from the Premier diamond mine, South Africa. *Lithos* **77**, 539-552.

Vocadlo, L., Brodholt, J., Dobson, D. P., Knight, K. S., Marshall, W. G., Price, G. D., and Wood, I. G., 2002. The effect of ferromagnetism on the equation of state of Fe3C studied by first-principles calculations. *Earth and Planetary Science Letters* **203**, 567-575.

Vocadlo, L. and Gerald, S., 2007. Mineralogy of the Earth - The Earth's Core: Iron and Iron Alloys, *Treatise on Geophysics*. Elsevier, Amsterdam. **2**, *91-120*

Wade, J. and Wood, B. J., 2005. Core formation and the oxidation state of the Earth. *Earth and Planetary Science Letters* **236**, 78-95.

Wallace, P. J., 2005. Volatiles in subduction zone magmas: concentrations and fluxes based on melt inclusion and volcanic gas data. *J. Volcanol. Geotherm. Res.* **140**, 217-240.

Walter, M. J., Bulanova, G. P., Armstrong, L. S., Keshav, S., Blundy, J. D., Gudfinnsson, G., Lord, O. T., Lennie, A. R., Clark, S. M., Smith, C. B., and Gobbo, L., 2008. Primary carbonatite melt from deeply subducted oceanic crust. *Nature* **454**, 622-625.

Watenphul, A., Wunder, B., Wirth, R., and Heinrich, W., 2010. Ammonium-bearing clinopyroxene: A potential nitrogen reservoir in the Earth's mantle. *Chemical Geology* **270**, 240-248.

Wignall, P. B., 2001. Large igneous provinces and mass extinctions. *Earth-Science Reviews* **53**, 1-33.

Wood, B. J., 1993. Carbon in the core. *Earth and Planetary Science Letters* **117**, 593-607.

Wood, B. J., Bryndzia, L. T., and Johnson, K. E., 1990. Mantle Oxidation State and Its Relationship to Tectonic Environment and Fluid Speciation. *Science* **248**, 337-345.

Wood, B. J., Walter, M. J., and Wade, J., 2006. Accretion of the Earth and segregation of its core. *Nature* **441**, 825-833.

Wright I, P. and Pillinger C, T., 1994. On the isotopic chemistry of carbon at the Martian surface. *Phil. Trans. R. Soc. Lond*, 309-321.

Wright, I. P., Boyd, S. R., Franchi, I. A., and Pillinger, C. T., 1988. High-precision determination of nitrogen stable isotope ratios at the sub-nanomole level. *Journal of Physics E: Scientific Instruments* **21**, 865.

Wright, I. P., Grady, M. M., and Pillinger, C. T., 1989. Organic materials in a Martian meteorite. *Nature* **340**, 220-222.

Wright, I. P., Grady, M. M., and Pillinger, C. T., 1992. Chassigny and the nakhlites: Carbon-bearing components and their relationship to Martian environmental conditions. *Geochimica Et Cosmochimica Acta* **56**, 817-826.

Wyman, D. A., Ayer, J. A., Conceição, R. V., and Sage, R. P., 2006. Mantle processes in an Archean orogen: evidence from 2.67 Ga diamond-bearing lamprophyres and xenoliths. *Lithos* **89**, 300-328.

Wyman, D. A., O'Neill, C. O., and Ayer, J. A., 2008. Evidence for modern-style subduction to 3.1 Ga: A plateau–adakite–gold (diamond) association. In: Condie, K. C. and Pease, V. Eds.), *When Did Plate Tectonics Begin on Planet Earth?* The Geological Society of America Special Paper, **440**, 129